Carbon dioxide removal from natural and potential enhanced silicate weathering in the UK



Kirsty Harrington

St-Anne's College

Michaelmas 2023

Supervisors: Gideon M Henderson

Robert G Hilton

A thesis submitted for the degree of Doctor of Philosophy

Department of Earth Sciences

Mathematical, Physical and Life Sciences Division

University of Oxford

Statement of originality

I confirm that the work submitted here is my own and has not been submitted to any other degree awarding institution. Whilst this thesis is my own work, parts were written in collaboration with Gideon Henderson and Robert Hilton, the specifics of which are outlined below.

Chapter 3 and 4 are currently being drafted to be published. For these Chapters, I undertook the field sampling, collection of data, modelling using MEANDIR and PHREEQC, and wrote the initial drafts of the manuscript. Gideon assisted with the initial conceptualisation of the study and helped to facilitate and support the fieldwork. Gideon and Bob both provided help with interpreting the data and developing the themes of the chapters. They also both provided much appreciated edits to the manuscripts.

Chapter 5 was published in Applied Geochemistry:

Harrington, K.J., Hilton, R.G., and Henderson, G.M. (2023) 'Implications of the Riverine Response to Enhanced Weathering for CO2 removal in the UK', *Applied Geochemistry*, 152(March), p. 105643. Available at: https://doi.org/10.1016/j.apgeochem.2023.105643.

Conceptualisation of the study was undertaken with Gideon at the outset. I undertook the lab work, mass balance calculations, and PHREEQC modelling, and Gideon supported the interpretation of the results. I wrote the initial draft manuscript, and Bob and Gideon provided edits to this, as well as helpful discussion of ideas and developing the themes and structure of the paper.

The theme of Chapter 6 was developed with both Bob and Gideon. I developed the initial draft, and Bob and Gideon helped with subsequent development of ideas and edits.

Acknowledgements

There have been so many people that have shaped the last few years and have made the research in this thesis possible. I am hugely indebted to the following people:

Firstly, I would like to thank my supervisors Gideon Henderson and Robert Hilton for sharing their scientific and professional knowledge with me. I feel extremely lucky to have been able to work with both of you- you have taught me so much about what it means to be a scientist. Gideon, thank you for all your help and support over the last five years. Your genuine love of science and problem solving is extremely inspiring, and I have learnt so much from the many discussions we have had. Bob, thank you for bringing more river geochemistry to the department! I am very grateful all the interesting discussions about river carbon chemistry, and for all your thoughtful support with my research and writing.

I would also like to thank many other people within the Oxford Earth Science Department who have helped shape my research project over the years. Thank you to Gail, Martha, and David for helping to put through all my finance requests and for nice conversations. To that end, thanks should also go to Elizabeth, Asheigh, Cornelius and Jeanette for many more great chats. I am grateful to Phil Holdship for his support with ICP- MS analyses, Katherine Clayton for assisting with XRD analysis, and Jane Barling and Steve Wyatt for help within the clean lab and for helpful conversations. I am also extremely appreciative for the group members within the Isotope and Climate Research group, as well as the Carbon Coffee group, for providing lots of stimulating discussions about all things related to carbon, climate, and environmental geochemistry. Finally, I particularly want to thank Frankie for being my Enhanced Weathering 'partner in crime' and being so encouraging and helpful over the years.

I am grateful for the funding I have received from the Oxford NERC DTP studentship (NE/L002612/1), which enabled me carry out this research, and has given me this wonderful opportunity in the first place. I especially thank Victoria Forth for her hard work in putting together DTP training and events. I had been initially nervous when arriving at Oxford, and her welcoming spirit put me at ease almost immediately.

I am hugely grateful to all the friends I have made throughout my time in Oxford. Thanks go to my pals in the Oxford University Underwater Exploration Group (OUUEG), who provided so much patient training while I was learning to dive and gave me a window into the world

under the sea. I am thankful for my time with the ‘Vicaroo’s- what a wonderful group of people to be locked away with for many months during a global lockdown! To the other ~30 people in my DTP 2018 cohort, thanks for all the laughs over the years and for making the first Michaelmas so brilliant!

To the Addison Parker gang: Annika, Ben, David, Ian, Laura, Matthew, Nacho, Roberta and Anna. I feel so blessed to have had the chance to share the ups and downs of the last five years with you. For all the dinners and drinks and chats and cries and laughs, it’s been a beautiful time of my life that I will treasure.

Thank you to my family who have been very supportive from a far. I will definitely make up for a lack of visits in 2024!

And then finally, I thank my partner David. He has been endlessly patient with my countless requests for ‘help- desk’ sessions. For all the cheeky quick pub visits after work, for fun food sessions and for just being generally supportive and caring over the years.

I feel very lucky for this period in Oxford, which will remain one of the best times of my life.

Thesis Abstract

The UK's route to net zero relies on employing carbon dioxide removal (CDR) strategies to offset hard-to-abate emissions from sectors such as transport and agriculture. Enhanced Weathering (EW) has emerged as a promising CDR technique that involves applying crushed alkaline silicate minerals onto agricultural land. Chemical weathering reactions involving these minerals within the soil transform atmospheric C to a dissolved ionic form, which is subsequently transported to the ocean via river systems for storage. It is essential to evaluate the feasibility of EW for CDR, both globally and in the UK, and a critical area of uncertainty concerns the role of rivers in transporting the atmospheric carbon removed via EW reactions. This thesis focuses on two key factors crucial to understand impacts of the widespread implementation of EW in the UK: i) the baseline CDR of natural silicate and carbonate weathering in the UK; ii) the potential release of CO_2 resulting from secondary carbonate precipitation during the river transport of EW products.

To quantify the baseline flux of weathering across the UK, two approaches have been applied in this thesis that combine river geochemical data and modelling. First, an intensive spatial river sampling campaign was completed over two years in the Severn and Thames catchments. These two large rivers have contrasting bedrock geology and land use, providing a focused study on the spatial variations in natural silicate and carbonate weathering-based CDR at a catchment scale (Chapter 3). Second, the longer-term temporal variation in natural silicate and carbonate weathering CDR for 52 UK catchments was for the first time assessed using historical records from the Environmental Agency (Chapter 4). Building on these, the geochemical modelling results were compared alongside statistical methods to explore the relationship between weathering fluxes and various environmental drivers (Chapter 6).

The outcomes indicate that in the UK, natural weathering removes up to 6.3 Mt CO_2 yr^{-1} of CO_2 from the atmosphere. Approximately 79% of this removal is attributed to the dissolution of carbonate minerals. CDR by carbonate weathering increases towards the southeast, which is spatially linked to the large presence of carbonate rich bedrock. Conversely, silicate weathering yields are greatest in the midlands and in northern regions. The factors influencing silicate weathering rates are difficult to deconvolve in UK catchments, but likely involve a combination of lithology and water availability. Midlands regions exhibiting the highest silicate weathering yields are characterised by an optimal water supply; sufficient to sustain weathering reactions

and permit the removal of dissolved products before reaching equilibrium in water. Additionally, in the rivers of most catchments, the proportion of solutes from silicates increases in the drier summer months which is presumed to be due to the increased contribution of groundwater to river water. This underscores the significance of prolonged water residence time in influencing natural silicate weathering fluxes in the UK. Finally, I account for the roles of strong acid weathering, secondary carbonate formation and cation exchange to decrease CDR by natural weathering. Only sulphuric acid- driven weathering may have the potential to significantly reduce the CDR resulting from natural weathering: from 6.3 to 4.9 Mt CO_2 yr^{-1}. However, further research is necessary to better understand sources of sulphate in UK catchments, and the potential role of sulphuric acid as a weathering agent.

The baseline quantity of CO_2 removed through natural weathering in the UK calculated in this thesis is lower than the removal achievable through enhanced weathering in some previous studies (6-30 Mt CO_2 yr^{-1}). To address whether UK rivers can accommodate this extra EW derived influx on top of their baseline natural weathering flux (the second thesis objective), I estimated alterations in river chemistry of 36 major UK catchments by simulating the complete dissolution of 10-50 t ha^{-1} yr^{-1} of silicate rock within each catchment's arable cropland (Chapter 5). Results indicated that if all this material dissolved and entered the river, most rivers would experience considerable changes in the dissolved inorganic carbon (DIC), causing most rivers to surpass calcite saturation. This indicates a high likelihood of carbonate precipitation, and I show that this riverine process has the potential to reduce the CDR potential of EW in the UK by up to 16% (10 t ha^{-1}), 21% (20 t ha^{-1}) and 27% (50 tha^{-1}). If the flux carried by rivers is additionally constrained by silicate saturation, reductions in maximum CDR potential is decreased significantly further. Catchments in the southeast of England, characterised by extensive arable land and low river water flows, are likely to experiment higher influxes of DIC from EW, leading to increased carbonate precipitation.

This thesis contributes to understanding of the potential for EW by emphasizing the heterogenous nature of natural weathering in UK catchments and delineating specific zones which may be better placed for the adoption of EW. The southeast exhibits high natural weathering rates, alongside abundant arable land, seemingly making it an optimal location for EW. However, my research demonstrates that the high weathering rate in these regions causes higher chemical fluxes in rivers which drives waters to be saturated with respect to calcite naturally. Therefore, these rivers are unlikely to be able to transport the excess material. Consequently, caution is advised regarding EW application in southeastern catchments due to

their limited water supply and the potential for substantial changes to river chemistry due to the significant portions of arable land. Conversely, the midlands regions, characterised by an optimal water availability, emerge as the most suitable areas for EW implementation. Based on the thesis findings a uniform spreading rate across all arable land may not be optimal, and a catchment- specific approach to EW implementation would be beneficial.

This work presents a first estimate for CO_2 naturally consumed due to weathering in the UK, highlights the need for a catchment specific approach to determining suitable regions for employing enhanced weathering, and provides new scientific insights into the feasibility of EW for CDR in the UK.

Table of Contents

1 Introduction 23
1.1 General overview and motivation 23
1.2 Extent of anthropogenic emissions and remaining CO_2 budget 25
1.3 The carbon cycle 26
1.4 Natural rock weathering 28
1.4.1 Oceanic inorganic carbon system 29
1.5 Calculating the amount of carbon dioxide removed via natural weathering 32
1.6 Controls on weathering rates 35
1.6.1 Temperature 35
1.6.2 Geological heterogeneity/ mineral composition 37
1.6.3 Supply of fresh minerals 38
1.6.4 Water availability and the residence time of this water within the catchment 39
1.6.5 Arable land 40
1.6.6 Other weathering drivers 41
1.7 Enhanced Weathering (EW) 42
1.7.1 Enhancing weathering reactions 43
1.7.2 Carbon dioxide removal potential for EW 46
1.7.3 Uncertainties and research needs 47
1.8 Thesis Research Objectives 49
2 Extended Methodology 51
2.1 Introduction to the methods utilized in this thesis 51
2.2 Geochemical analytical methods 52
2.2.1 Sample collection and preservation 52
2.2.2 Alkalinity 53
2.2.3 Ion Chromatography 54
2.2.4 ICP-MS 55
2.2.5 Carbonate precipitation experiments 55
2.3 PHREEQC 57
2.4 MEANDIR 58
2.4.1 Introduction to the model 59
2.4.2 Solute chemical data for UK rivers 62
2.4.3 Model Selections 62
2.4.3.1 Cost function 63
2.4.4 Summary of other parameter choices 73

3 The origin and fate of dissolved inorganic carbon in the Rivers Severn and Thames, UK.....75
3.1 Introduction.....77
3.1.1 Study catchments and strong acid sources.....78
3.2 Calculating the maximum and net carbon dioxide removal from natural weathering.....80
3.3 Catchment Characteristics for the Severn and Thames Basins.....84
3.3.1 Geology and topography of the basins.....84
3.3.2 Hydrology and Land Use.....86
3.4 Chemistry of the Severn and Thames waters.....88
3.4.1 Sampling methods.....88
3.4.2 DIC and cation chemistry.....89
3.5 Inverting the chemistry to assess silicate and carbonate weathering.....93
3.5.1 Results from the Inversion (sources of solutes).....96
3.5.2 Temporal variation in the weathering source of cations.....96
3.5.3 The annual Carbon Dioxide Removal in the Thames and Severn catchments.....100
3.6 Riverine processes which may reduce the maximum CDR.....101
3.6.1 Cation Exchange.....101
3.6.2 Riverine Secondary Carbonate Precipitation.....104
3.6.3 Sulphuric acid weathering from sulphides.....108
3.6.4 Nitric Acid.....116
3.6.5 Overall reduction to CDR via riverine processes and comparison to other UK and global basins.....121
3.7 Conclusions.....122
4 Atmospheric carbon dioxide removal due to chemical weathering processes in the UK.....123
4.1 Introduction.....125
4.2 Summary of the approach.....128
4.3 UK catchment characteristics.....129
4.3.1 River chemistry.....129
4.3.2 Geology and topography.....135
4.3.3 Hydrology.....137
4.3.4 Land Use.....138
4.4 Dissolved Inorganic Carbon (DIC) in UK rivers.....140
4.5 Inverting chemistry to assess the sources of solutes.....143
4.5.1 MEANDIR inversion.....143
4.5.2 Sources of solutes.....146
4.6 Annual CDR from natural weathering in the UK (Maximum).....147
4.6.1 Calculating weathering fluxes and CO_2 removed.....147
4.6.2 Maximum CDR for UK.....149
4.7 Factors that may make the maximum CDR value an over-estimate.....154

4.7.1 Variations in how the sequestered CO_2 speciates in solution (w value) 154
4.7.2 Sulphuric acid mediated weathering 154
4.7.3 Nitric acid weathering from fertilizers 162
4.8 Overall Carbon Dioxide Removal due to Natural Weathering in the UK 163
4.8.1 Implications for carbon dioxide removal (CDR) utilizing Enhanced Weathering in the UK 164
4.9 Conclusions 164
5 Riverine Response, and Limitation to, Enhanced Weathering for Negative Emissions in the UK 167
5.1 Introduction 169
5.2 Predicting the impact of carbonate precipitation and silica saturation on EW CO_2 sequestration 173
5.3 Scenarios for alkalinity release from applied basalt to fluvial systems 176
5.3.1 Scenario one: The maximum alkalinity released to rivers due to EW (FEW) 176
5.3.2 Scenario two: The reduced EW alkalinity released to rivers due to limitations by silica saturation ($FEW - silc$) 178
5.4 Determining the saturation state required for carbonate precipitation ($SIthreshold$) 179
5.4.1 $SICalcite$ of global rivers 179
5.4.2 River water carbonate precipitation experiments to assess precipitation 181
5.5 The impact of Scenario 1 (maximum alkalinity release) on UK river chemistry and the potential for CO_2 removal 182
5.6 Impact on riverine pH 188
5.7 The impact of Scenario 2 (limitations caused by silica saturation) on UK river chemistry and EW CDR 190
5.8 Conclusions 192
6 General Discussion on Natural and Enhanced Weathering in the UK 195
6.1 Introduction 195
6.2 How does UK weathering compare to other global catchments? 196
6.3 What drives high weathering rates in the UK? 199
6.3.1 UK nationwide relationships between drivers and weathering 201
6.3.2 Natural variables that may influence UK weathering 204
6.3.3 Impacts of Anthropogenic land use on UK weathering rates 216
6.3.4 Summary of main drivers for silicate and carbonate weathering 221
6.4 What are the best UK locations for the adoption of EW? 222
6.4.1 Southeastern catchments: Ely Ouse, Welland, Hull, Nene, Test, Stour, Arun, Avon (Bath), Avon (Hampshire), Chelmer 222
6.4.2 Midlands- northeastern catchments: Severn, Trent, Wear, Wharfe, Ouse, Coquet, Tees, Ribble, Mersey, Clyde, Annan, Eden (Kemback) 223
6.4.3 Cornish: Exe, Tamar, Taw; northeastern: Tweed, Tyne; highlands: Don, Tay, Dee ..223

6.5 Future Research Opportunities 225
7 Thesis Conclusions 2299
8 Appendices 244
8.1 Appendix A- Appendices for Chapter 2 244
8.1.1 Auto titrator Precision Testing 244
8.1.2 The volume of concentrated alkalinity added to Thames River water (for carbonate precipitation experiments) 244
8.1.3 The volume of concentrated alkalinity added to the Severn River 245
8.2 Appendix B- Appendices for Chapter 3 2455
8.2.1 Flow rate histograms for the two catchments 245
8.2.2 Historical DIC concentration and flux in the Severn and Thames Catchments 246
8.2.3 Historic chemical variations implying changes in source endmembers. 247
8.2.4 Variations in the fraction of solutes from each endmember (MEANDIR results) 247
8.2.5 Variation in source of solutes across the River Severn 248
8.2.6 Longer term changes in Qsil and Qcarb in the Severn and Thames catchments 248
8.2.7 Historic $SIcalc$ 249
8.2.8 Historic sulphate trends 249
8.2.9 Changes to overall fertilizer application in the UK (NO_3^-, PO_4^{3-}, K) 250
8.2.10 Spatial NO3/Cl varations across the Thames and Severn Catchments 250
8.3 Appendix C- Appendices for Chapter 4 251
8.3.1 Catchment characteristics 251
8.3.2 Sulphate variability across UK catchments 254
8.3.3 Percentage reduction in CDR due to nitrate from fertiliser 255
8.4 Appendix D- Appendices for Chapter 5 255
8.4.1 Arable land and annual discharge in each catchment 256
8.4.2 UK baseline river chemical data 258
8.4.3 Composition of basalt used for the EW calculations. 261
8.4.4 Ranges of natural pCO2 in UK rivers 262
8.4.5 Temperature and pressure dependence on the saturation concentration of silica (Deriving the saturation concentration of silica in UK soils) 264
8.4.6 Sampling localities for beaker experiments 265
8.4.7 Experimental methodology 265
8.4.8 Composition of the precipitate collected from the beaker experiments. 267
8.4.9 Chemistry changes during beaker precipitation experiments. 268
8.4.10 PHREEQC predicted the proportion of Ca removed in secondary carbonates in all catchments in the study under scenario 1. 269
8.5 Appendix E- Appendices for Chapter 6 270
8.5.1 Silicate yield vs calcite saturation index 270

8.5.2 $Xsil$ and average flow and permeability.....271
8.5.3 The degree of seasonal variability in $Xsil$ and permeability and silicate yield.....271
8.5.4 Suspended sediment yield and %arable and runoff.....272
8.5.5 Relationship between riverine nitrate concentration and the concentration of cations from carbonates 273

Table of Figures

Figure 1.1 From State of Carbon Dioxide Removal Report, i.e. Smith et al., (2023)- Three different emissions reductions scenarios featured in the Carbon Dioxide Removal Report, 2023, all of which meet the Paris Temperature Goals. All three scenarios rely on both emissions reductions, and substantial carbon dioxide removal (CDR). 'Conventional CDR' includes methods such as reforestation, and soil carbon sequestration, while 'novel CDR' includes methods such as Enhanced Weathering, Bioenergy for Carbon Capture and Storage (BECCS), Direct Air Carbon Capture and Storage (DACCS). _____ *24*

*Figure 1.2- (a) (from Friedlingstein et al., 2022) represents the main sinks of carbon and shows the degree that these sinks are perturbed on an annual basis by anthropogenic emissions. (b) (From Hilton and West, 2020). The long-term inorganic carbon cycle. Note the difference between the magnitude fluxes between the anthropogenic emissions (a) in Gt C and the inorganic natural long term carbon fluxes (b) in Mt C. Figure 1.2 presents fluxes in C rather than CO_2, the latter which is the preferred flux in text to compare with following chapters.*_____ *27*

Figure 1.3 (from Zeebe and Wolf-Gladrow, 2001).- The seawater dissolved inorganic carbon system. The relative proportions of each carbonate species (CO_2, $HCO3-$ and $CO32-$) will determine the pH of the solution. $pK1*$ and $pK2*$ are the pH values when the concentration of CO_2 equals the concentration of $HCO3-$ ($pK1*$), and when the concentration of $HCO3-$ equals the concentration of $CO32-$ ($pK2*$). These are temperature and salinity dependent constants which can be calculated using equations discussed in detail within Zeebe and Wolf-Gladrow, (2001). The range in pH observed in UK rivers is also included within the figure. This range is based on the mean pH of the 52 UK rivers included in this thesis (Chapter 4). Mean taken from geochemical river data from the Harmonised Monitoring Scheme (DEFRA, 2013) which will be introduced in Chapter 2. _____ *32*

Figure 1.4 (from Chapter 4)- Simplified geological map of the UK from (BGS, 2023a). The large variation in lithology across the UK suggests that weathering fluxes will be variable _____ *34*

Figure 1.5 (Taken from Gaillardet et al., 2019)- The temperature dependence of Ca and Mg in solution from rivers draining carbonate lithologies. Solid and dashed lines represent the theoretical concentrations given thermodynamic theory and equations discussed in text. The impact of variable pCO2 concentrations to the theoretical concentrations of Ca and Mg with temperature is also given, represented by 1 AL, 10 AL, and 100 AL- equivalent to 1, 10 and 100 x atmospheric pCO_2 levels. The plotted data within the bell-shaped curve are river concentrations collected from the GLORICH database. The actual relationship between carbonate flux and temperature is shown to be a boomerang shape, which is suggested to be controlled by changing pCO2 concentrations within soils. _____ *37*

*Figure 1.6- The Goldich Dissolution series (Figure from (Renforth, 2012) and originally reported by (Goldich, 1938) shows the order of reactivity of different silicate minerals. Order of reactivity is mainly related to silica content- an increase in strong Si=Si double bonds within the mineral lattice will decrease the mineral weathering intensity. For example, silica content of quartz can be greater than 60%, while silica content of olivine is typically <45% (Renforth, 2012).*_____ *38*

*Figure 1.7 Taken from Hangx and Spiers, (2009)- the importance of grain size in determining the time needed to fully dissolve olivine. Using grain sizes 10-1000 um. At a T= 25°C and typical pH of seawater (given in paper as pH= 8.2)*_____ *45*

Figure 2.1- Variations in Cl/Na ratios of the River Severn and Thames to assess anthropogenic input of Cl. _ *68*

Figure 2.2- Using the chemistry of rivers that drain silicate lithologies to derive the silicate end-member. Histograms represent the chemical range of four UK catchments (Fal, Fowey, Carnon, Wick). The median and standard deviation were used in MEANDIR. _____ *70*

Figure 3.1- Catchment geology of the River Severn (c) and River Thames (b) catchments. (a) is the insert map to show location of catchments in the UK. Main river is coloured darker and bolder to differentiate between main river and tributaries. Sampling locations are highlighted by red stars for main body and tributaries. Geological map was simplified from the British Geological Survey 625k Geological map (BGS, 2023a). Catchment boundaries were collated from NRFA who derived these using the Centre of Ecology and Hydrology's Hydrological Digital Terrain Model (IHDTM) (Morris and Flavin, 1990; NRFA, 2023). _____ *85*

Figure 3.2-Average flow rate per month for the period between the start of the historic chemical measurements (1974) and the end of the timeseries sampling period (2021) for the Severn catchment (a), and the Thames (b). Flow rate data was obtained from the NRFA (NRFA, 2023). _____ *87*

Figure 3.3- land use variations in the Severn (a) and Thames (B). Catchment boundaries taken from the National River Flow Archive (NRFA, 2023), and catchment land use data from the Centre of Ecology and Hydrology Land Cover Map 2021 (Marston et al., 2022). _____ *87*

Figure 3.4- Geochemical differences between dominating cations in the River Severn and the Thames. Crosses denote historic data (Appendix A5- Severn, Appendix A6- Thames). Diamonds represent the concentrations from field sampling sites (Appendix A7). Note that y- axis is different for each plot, and that Li concentrations are in nmol L^{-1}. _____ *90*

*Figure 3.5- Ca/(Na+K) molar ratio variations in (a) the River Severn mainstem, (b) River Thames mainstem, (c) the main tributaries of the River Severn (V= Vyrnwy, Tn= Tern, Te= Teme, A= Avon), and (d) the main tributaries of the Thames (Ch= Cherwell, Tm= Thame, Pg= Pand, Kt= Kennet, Ld= Loddon, Ct= The Cut). Symbols represent measurements taken at the sampled locations on x-axis. And separated into year by symbol type and colour for season. In (a) Plyn= Plynlimon, Ldloes =Llanidloes, Cgn= Crewgreen, Atc= Atcham, Hl= Hampton Loade, Wor= Worcester, UonS= Upton on Severn, Mme= Maisemore. Flow direction is from left to rightIn b) Cklde= Cricklade, Bcot= Buscot, Fmr= Farmoor, Wall=Wallingford, Pbne= Pangbourne, Mhd= Maidenhead, Win= Windsor, Walk= Walton and KonT= Kingston on Thames. Flow direction is left to right*_____ *92*

Figure 3.6- Results from the inversion. Average percentage of each cation from each source endmember (silicate, carbonate, evaporite and rain) in the Severn and Thames catchments. Total= the total percentage flux of major cations from each endmember. Values were normalised to 100% where they did not equal 100% _____ *98*

Figure 3.7- Monthly average of the fraction of cations (Ca, Mg, Na) sources from silicates and carbonates (Xsil and Xcarb) for the River Severn and Thames (from HMS data). _____ *99*

Figure 3.8- Relationship between Sr/Ca and Na/Ca in the River Thames and Severn and their main tributaries. Line A-B indicates the line of best fit through a global carbonate endmember (A) and silicate endmember (B). Values for the global endmembers are taken from Bufe et al., (2021). In the mentioned study, they use a carbonate 1000 Sr/Ca of 1-1.5. This study assigns the value of carbonate 1000*Sr/Ca at 1.5. The four points lying above the A-B endmember line are all the River Avon, which had consistently high Sr/Ca, despite flowing over carbonate rich lithologies.* _____ *105*

Figure 3.9- Saturation Index variations along stream in (a) Severn and (b) Thames. (c) and (d) show the saturation indexes of the main tributaries to enter (c) the Severn and (d) the Thames. Dashed lines indicate the saturation of secondary carbonates under ideal conditions, while full black horizontal line at SI=1 shows the threshold index used in Chapter 5 to account for suppression of precipitation due to inhibitant ions in solution. Sampling periods are categorised into summer months (Apr- Sept) and winter months (Oct- Mar) to show any seasonal variation in saturation index. Tributaries in (c) A= Avon, Te= Teme, Tn= Tern, Vr= Vyrnwy. Tributaries in (d) R= Ray, Ch= Cherwell, Th= Thame, O= Ock, Pg= Pang, Kt= Kennet, Ld= Loddon, Ct= The Cut. Sampling Locations in (a) Plyn=Plynlimon, Ldloes= Llanidloes, Cgn= Crew Green, Atc= Atcham, HL= Hampton Loade, Wor= Worcester, UonS= Upton on Severn, MM= Maisemore. Sampling locations in (b) Cklde= Cricklade, Bcot= Bscot, Fmr= Farmoor, Wall= Wallingford, PBne= Pangbourne, Mhd= Maidenhead, Win= Windsor, Walt= Walton, KonT= Kingston upon Tha 107

Figure 3.10-Flux of excess riverine sulphate ($Xexcess\ SO42-$) which has not been sourced from the four end member sources (carbonate, evaporite, rain, and silicates (not including sulphides)). Results collated from the historic dataset. Comparing seasonal trends in the River Severn and the Thames (a), along with the monthly flux of $Xexcess\ SO42-$, calculated by upscaling from monthly averages. Error bars represent the range using 25-75 percentile results of $Xexcess\ SO42-$. 111

Figure 3.11- The variation in excess SO_4^{2-} along the mainstem of the river (a) Severn and (b) Thames, as well as the Severn's tributaries (c) and Thames tributaries (d). Sampling periods are defined into summer months (Apr-Sept) and winter months (Oct- Mar), and year of sampling. Severn sampling localities: Plyn= Plynlimon, Ldloes= Llanidloes, Cgn= Crewgreeen, Atc= Atcham, HL= Hampton Loade, Wor= Worcester, UonS= Upton on Severn, MM= Maisemore. Thames sampling localities: Cklde= Cricklade, Fmoor= Farmoor, Wall= Wallingford, PBne= Pangbourne, Mhd= Maidenhead, Win= Windsor, Walt= Walton, KonT= Kingston upon Thames. Severn tributaries: V= Vyrnwy, Tn= Tern, Te= Teme, A= Avon. Thames tributaries: R= Ray, Ch= Cherwell, Th= Thame, O= Ock, Pg= Pangboune, Kt= Kennet, Ld= Loddon, Ct= Cut. 112

Figure 3.12- Historic NO_3^-/Cl in rivers Severn and the Thames. For both rivers, the historical annual quantity of samples collected was variable, with some years having extensive records while others had fewer. The x-axis of the graphs therefore represents individual sampling dates organised chronologically (See datasheets in supporting information). Random data points were highlighted in both plots to illustrate seasonal variations. 119

Figure 4.1-UK Catchments included in this study. Catchment boundaries were supplied from the National River Flow Archive, by the Centre of Ecology and Hydrology's Integrated Hydrological Digital Terrian Model (IHDTM) (Morris and Flavin, 1990; NRFA, 2023). For specific catchment details see Table 4.4.1 (for area, flow, land use variables and chemistry), and for data used in model see datasheets with supporting informat 131

Figure 4.2 (a) UK geology (simplified from the British Geological Survey) (BGS, 2023a), (b) Topography (LIDAR Composite 10m DTM) (DEFRA, 2022b) 136

Figure 4.3- Land use variations within the UK. QGIS shapefile is the Land Cover Map 2021(Marston et al., 2022), from the Centre of Ecology and Hydrology) 139

Figure 4.4- DIC concentrations ($\mu mol\ L^{-1}$) (a) and DIC yields per hectare ($kg\ CO_2\ ha^{-1}\ yr^{-1}$) (b) across the catchments within the study area. 141

Figure 4.5- Comparing the annual yield of Ca^{2+} and HCO_3^- (a) and the ratio of Ca/Na and HCO3/Na (b) of UK rivers. Both can be used to infer the increased contribution of carbonates. Each datapoint represents an individual river within the study and was calculated using average concentrations (Table 4.4.1). 142

Figure 4.6- Results of the inversion showing the fraction of total major cations (Ca^{2+}, Mg^{2+}, and Na^+) from each source endmember I (where i= silicate, carbonate, evaporite and rain) in UK rivers, following (Gaillardet et al., 1999). Rivers are ranked in ascending order of silicate %. H'shre = Hampshire, B'mnt= Beaumont, G'lcr = Glenlochar 147

Figure 4.7- The potential maximum quantity of CDR due to natural (a) silicate and (b) carbonate weathering in the UK catchments within the study. (c) is the total combined CDR for natural weathering. Given in CO_2 yield (kg CO_2 ha^{-1} yr^{-1}). Yields are calculated from the median fraction of ions from silicate and carbonate sources as predicted by the inversion results (supporting information). 151

Figure 4.8- A medium positive correlation can be between carbonate yield and (a) the percentage of high permeable lithology within the catchment, while a medium negative correlation can be seen between carbonate yield and (b) the maximum elevation. In contrast, no correlation can be seen between silicate yield and (c) permeable lithology, and (d) the maximum elevation. 152

Figure 4.9- Correlations between catchment parameters and weathering yields. First three plots show medium correlations between carbonate yield (kgCO_2 ha^{-1} yr^{-1}) and (a) Percentage arable land, (b) percentage grassland and (c) Catchment runoff (mm yr^{-1}). Last three show no correlation in silicate yield vs (d) percentage arable land, (e) percentage grassland and (f) Runoff (mm yr^{-1}). 153

Figure 4.10- Presents the contrast in (a) sulphate yields (mol ha^{-1} yr^{-1}) and (b) the amount of total sulphate from excess (µmol L^{-1}) for the catchments in the study. 157

Figure 4.11- The potential maximum reduction to the net quantity of CO_2 consumed due to sulphide produced sulphuric acid weathering of (a) silicates and (b) carbonates in the catchments studied. In percentage reduction from the maximum total CO_2 removed per catchment (given in Mt CO_2 yr^{-1} per catchment). 160

Figure 4.12- Riverine nitrate flow weighted flux versus the flux of sulphate from excess sources (mol s^{-1}), showing that for catchments with high agriculture, excess sulphate and nitrate are very highly correlated. Column one in the figure are catchments with high expected sulphide weathering due to presence of Mesozoic shales within catchment lithology- (a) Tyne, (d) Tees, (g) Wear); column two are catchments with a high percentage of arable land (High Agriculture- (b) Ely Ouse, (e) Nene, (h) Chelmer); column 3 are a subset of catchments which have very little agriculture and minimal expected sulphide weathering (Low Agriculture- (c) Conon, (f) Annan, (i) Leven H. 161

Figure 5.1 (a) Average annual discharge per catchment studied (10^{12} L yr^{-1}). (b) Percentage of arable land within each catchment. >90% of all UK arable land is housed within the 36 catchments shaded in figures (a) and (b). Numbered catchments in (b) will be compared in detail within the results and discussion, chosen due to their differences in arable land%, discharge and bedrock lithology. (1= Ancholme, 2= Great Ouse, 3= Hull, 4= Ouse, 5= Severn, 6= Tay, 7= Thames) 174

Figure 5.2- A summary of the variables and terms used in the study. Input variables are obtained from natural catchment data, as discussed in the main text. Outputs are the variables derived in this study: FEW and $FEW - silc$ are terms describing the flux of ions released from the applied basalt, which will be dependent on limitations by silica saturation ($FEW - silc$) or carbonate saturation (FEW) as discussed in Section 5.3. $RCO2$ is the

maximum CO_2 drawdown expected from EW, and $RCO2-net$ is the CO_2 drawdown once carbonate precipitation and silicic acid saturation are considered (Section 5.7). 175

Figure 5.3- Global river saturation index data obtained from the GLORICH database. Bottom plot represents the interquartile range of the global river calcite saturation indexes (median = -0.59, 25 percentile= -2.21, 75 percentile = 0.47) Database from Hartmann et al., (2019). 180

Figure 5.4- Experimental confirmation that a threshold saturation index of 1.0 is realistic for carbonate precipitation in UK rivers. The figure compares the predicted amount of carbonate precipitation for a given saturation index, with those of the river water carbonate precipitation experiments of this study 182

Figure 5.5- Derived EW initial alkalinity changes in UK catchments due to spreading scenarios 10 and 50 t ha^{-1} under scenario 1 in the absence of secondary carbonate precipitation and kinetic limitations. For comparison, the median natural alkalinity is 1.9 mmol L^{-1}. Alkalinity increase is calculated under the assumption that 10 and 50 t of basalt is applied to half of the available arable land in the catchment and that all the mobile cations Ca, Mg, Na and K within the basalt reach the river. River water flux used is the average discharge in each catchment (L yr^{-1}). 183

Figure 5.6- Catchment calcite saturation indexes for the 10 t ha^{-1} and the 50 t ha^{-1} application rates under scenario 1 in the absence of calcite precipitation. Saturation Index values were obtained using PHREEQC, and the alkalinity and chemistry were calculated using assumptions discussed in (section 3). Brown colours on this figure represent catchments in which riverine carbonate precipitation is expected (i.e. SI >1). 184

Figure 5.7-Total CO_2 drawdown due to EW. (a) Without carbonate precipitation= the total quantity of CO_2 which could be sequestered due to the application of basalt onto 50% of the arable land of 36 UK catchments. (b) The revised quantity which includes secondary carbonate precipitation in the calculations. Both (a) and (b) are without secondary limitations on weathering by silicic acid saturation 186

Figure 5.8- Maximum alkalinity increase in 5 example UK rivers, with and without secondary carbonate precipitation, due to the dissolution of 20 t ha^{-1} over half of the available land in the catchment. Values represent scenario 1 whereby all cations released reach the rivers. Alkalinity is compared to present-day average natural seawater levels (dashed line). Error bars represent the predicted amounts of carbonate precipitation, depending on the initial pCO_2 (see Section 5.6). 188

Figure 5.9- Modelled pH change in 7 UK catchments as a function of basalt dissolution rate (10-50 t $ha^{-1}yr^{-1}$). (a) prior to carbonate precipitation, (b) post precipitation. Maximum is compared with the minimum $Silimitation$. Error bars are associated with the natural range in pCO2, upper bound = 95 percentile, lower bound= 5 percentile. Ecosystem pH limit line (pH >9) based on values reported by the US Environmental Protection Agency (USEPA, 2022). 189

Figure 5.10- Ca/Si ratio of basalt vs Ca/Si of the river water that flowed over it. Basalt composition from Reunion Island was taken from Fretzdorff and Haase, (2002), other basalt compositions came from Das et al., (2005) (Deccan Traps) and Georg et al., (2007) (Iceland). The concentration of Ca was corrected for other sources of Ca (carbonate, cyclic, evaporites), so that the Ca/Si corrected represented the Ca/Si in the water which came from basalt. 192

Figure 6.1– Comparing the average silicate yield in the UK (kg CO_2 ha^{-1} yr^{-1}) with averages from global catchments calculated from Moon et al 2014. 198

Figure 6.2 (From Chapter 4)- The potential maximum quantity of CDR due to natural (a) silicate and (bcarbonate weathering in the UK catchments within the study. (c) is the total combined CDR for natural weathering. Given in CO_2 yield (kg CO_2 ha^{-1} yr^{-1}). Yields are calculated from the median fraction of ions from silicate and carbonate sources as predicted by the inversion results (data within datasheets in supporting information). _____ *201*

Figure 6.3 (From Chapter 4)- A medium positive correlation can be between carbonate yield and (a) the percentage of high permeable lithology within the catchment, while a medium negative correlation can be seen between carbonate yield and (b) the maximum elevation. In contrast, no correlation can be seen between silicate yield and (c) permeable lithology, and (d) the maximum elevation. _____ *202*

Figure 6.4 (From Chapter 4)- Correlations between catchment parameters and weathering yields. First three plots show medium correlations between carbonate yield (kgCO_2 ha^{-1} yr^{-1}) and (a) Percentage arable land, (b) percentage grassland and (c) Catchment runoff (mm yr^{-1}). Last three show no correlation in silicate yield vs (d) percentage arable land, (e) percentage grassland and (f) Runoff (mm yr^{-1}). _____ *203*

*Figure 6.5- The relationship between saturation index in UK rivers and the CO_2 yield due to carbonate weathering. 5(a) is the trend seen in all UK rivers. The highlighted area in Figure 6.5(a) is shown in Figure 6.5(b). In general, 6.5 (a) shows that carbonate yield increases with saturation index until ~SI= 0.4, then any further increase in saturation index tends to drive lower yields. 5(b) shows this negative relationship in the calcite oversaturated rivers. For catchments of similar saturation indexes, increasing the runoff increases yield, suggesting water availability/ runoff does play a role in increasing carbonate yields in UK catchments.*____ *205*

Figure 6.6- Seasonal trend in the portion of solutes from silicates ($Xsil$) and carbonates ($Xcarb$) for a selection of UK river. ($Xsil$) and ($Xcarb$) were calculated based on the inversion results from Chapter 4 for each datapoint. For each river, data was then collated into months, and the average ($Xsil$) and ($Xcarb$) for each month was taken. In the majority of UK catchments, $Xsil$ increases in summer months compared to carbonates, however the extent of this variation is heterogeneous across catchments: in rivers such as the River Ribble, large variations are observed, whilst the River Tweed sees comparatively minor seasonal variations. _____ *208*

*Figure 6.7- Average monthly $Xsil$ vs average monthly runoff for a few select catchments. Plot highlights that some rivers (Trent, Ribble, Coquest, Thames, and Wear) have a strong negative correlation between Average monthly $Xsil$ vs average monthly runoff, while others (Ely Ouse, Forth, and Tweed) do not have the same trend . (T-tests for these catchments are >0.05 and therefore statistically significant).*_____ *211*

Figure 6.8 (a) Catchment scale annual carbonate derived CO_2 yield vs suspended sediment yield. Suspended sediment data is taken from the Harmonised Monitoring Scheme dataset used within Chapter 3 and 4 (DEFRA, 2013). Note the lack of correlation (R= 0.11) between carbonate yield and SSY for the catchments in general. Figure 6.8(b) shows SSY and carbonate yield for rivers with high runoff. For these rivers, a medium strength positive relationship (R= 0.62) exists between carbonate yield and SSY (b). These areas are typically have limited carbonate lithology, and this positive relationship may suggest an erosional control to weathering fluxes in these catchments, possibly due to a lack of mineral supply and abundant water supply. _____ *214*

*Figure 6.9- No correlation exists between (a) the suspended sediment yield and the silicate yield when assessing all the studied catchments together. (b) 10 catchments with the least suspended sediment yield- plot of the SSY vs silicate yield shows no correlation. (c) The top 10 catchments with the most suspended sediment yield. A weak negative relationship between silicate yield and SSY suggests possibility that high erosion rates decrease silicate yield in certain UK catchments.*_____ *215*

Figure 6.10- Investigating the potential causes of high sediment yield in UK rivers to discover whether arable land may impact erosion. Colours indicate positive (green), negative (red) , weak negative (orange) or no (grey) trend. Figures (a- c) represent the relationship between suspended sediment and (a) the percentage of arable land in a catchment, (b) the maximum elevation (metres above sea level) and (c) the average annual runoff (mm yr-1) for the whole 52 catchments studied in Chapter 4. Figures (d-f) are a sub-set of the 15 most low- lying catchments (defined as those with a maximum elevation no greater than 330 m . Figures (g-i) represent the same trends for the top 15 highland catchments (defined here as those with a maximum elevation of greater than 850m. ___ 218

Figure 6.11- Meandir calculated flux weighted Ca from carbonates (mol s-1) in a subsection of UK rivers with highest carbonate flux. DL= Decreased Lime (production) in the UK, which decreased by ~1.5 Mt CaO in 1995. DL is the first sample date from 01/01/1996 _____ 220

List of Tables

Table 1.1- A variety of methods of carbon dioxide removal exist and have been split into 'Conventional' and ''Novel'. Conventional methods are those already used, while novel methods are still being assessed for their feasibility for implementation. The values for the global potential of CO_2 removed due to utilizing these methods is taken from (Fuss et al 2018), unless otherwise specified. Current deployment of all novel CDR methods combined is 0.002 Gt CO_2 yr^{-1}. (Smith et al., 2023) 25

*Table 1.2- Key core and pot EW trials aimed to test the dissolution rate and CDR potential of EW. Bracketed values are the quoted CDR potentials given in the literature, which have been converted here to t CO_2 ha^{-1} yr^{-1} for easier comparison between studies. (Renforth et al., 2015) quoted a likely amount of olivine dissolution per hectare given the results of their core trial which have been converted into CO_2 t ha^{-1} here, using RCO_2 value of Olivine of 0.93 (From Renforth 2012). *Based on calculations from the Mg concentration in outflow solution- however, they also noted significant Mg accumulation in topsoil layers, which were not accounted for in the values provided in this table.....47*

Table 2.1- (From Kemeny et al 2021). Given the river observation Ca/Na and K/Na and the results from two hypothetical runs (Run 1 and Run 2), Table 2.3 demonstrates the difference between how absolute and relative cost functions would assign cost. 63

Table 2.2- Shows the difference in the overall calculated CO_2 consumed due to natural silicate and carbonate weathering in the Severn catchment due to changing the cost function used in the MEANDIR inversion. The chemical dataset used for both runs was the historical dataset for the River Severn (provided in the supporting information). Run 1 was run using a relative cost function, and is the default used in this study. Run 2 was run using an absolute cost function. All other parameters were kept constant. CDR was calculated using methods described in Chapters 3 and 4. 64

Table 2.3- End members used in the inversion calculations. Silicate endmembers were derived from UK silicate draining rivers (Figure 2.2). Carbonate and evaporate endmembers are global endmembers from Gaillardet et al., (1999) and Moon et al., (2014). The rain endmember represents the average composition of the 'cyclic' endmember- the average composition of rain, which is derived entirely from sea salts, taken from Moon et al., (2014). It is assumed that any other dissolved Ca, Mg and Na present in rain other than this cyclic endmember will be derived from weathering. 65

Table 2.4- Rainfall data and catchment characteristics from the Severn and the Thames- used to equate the $Clcritical$. Average discharge and annual precipitation were taken from the National River Flow Archive (NRFA, 2023). Chemical data was obtained from the Environmental Change Network (ECN, 2015). $Clcritical$ values given in table are then used in the inversion for both the River Severn and Thames. 67

Table 2.5- Outcomes of sensitivity tests for using different endmembers. 72

Table 2.6- MEANDIR inversion parameter choices used in this study, and the justification for each choice 73

Table 3.1- Processes which add and remove cations and anions to the river water column. 82

Table 3.2- Average dissolved inorganic carbon fluxes in the River Severn and Thames. The average historic values (Severn: 1974-1992, Thames: 1976-2003) compared to those within this study (Severn: Dec 2019- Nov 2021, Thames: Apr 2021- Nov 2021). Maisemore and Kingston upon Thames are the closest sampling points to the tidal reach.....89

Table 3.3- Average Historic Chemical Data for the River Severn and the Thames from the Harmonised Monitoring Scheme (DEFRA, 2013). Severn data is taken from Haw Bridge, Thames data is from Kingston on Thames. DIC and SI calcite for each chemical sample were calculated using PHREEQC (version 3 Parkhurst and Appelo, 2013) and the average is given here.....90

Table 3.4-Seasonal variations in DIC flux and concentrations. Values given in table are averages taken from historic dataset. DIC calculated using PHREEQC, as discussed in text.....91

Table 3.5- (From Chapter 2) Endmember compositions used throughout the study. Rain endmember is determined from the average composition of sea-salts and was taken from Gaillardet et al., (1999), SO4/Na from Moon et al., (2014). Carbonate and evaporite endmembers from Gaillardet et al., (1999).....95

Table 3.6- Example table of a selection of the results from the MEANDIR inversion of River Severn Historic Data (for Ca only). Full results also include fractions for riverine Mg and Na, and 237 individual samples for the Severn, and 168 for the Thames. The full results can be found in datasheets within supporting information.....98

Table 3.7 Maximum potential CDR due to natural weathering in the Severn and the Thames catchments (for w= 1.7). Given in annual flux (Mt $CO_2 yr^{-1}$) and yield (kg CO_2 ha^{-1} yr^{-1}). The latter of these is useful when comparing weathering rates between catchments of different sizes. 100

Table 3.8- Potential Impact of cation exchange on the CDR for the Severn and the Thames.....103

Table 3.9- Average concentration and flux of riverine sulphate in the river Severn and Thames taken from the historic datasets. Overall (yearly average) compared to average in winter months (Oct- Mar) and summer months (Apr- Sept), show that the flux of sulphate is significantly higher in winter for both rivers.....108

Table 3.10- Average fraction of riverine sulphate from excess sources in the River Severn and Thames. Overall is the overall average over the historic sampling period. Average taken for all data sampled in summer months (Apr- Sept) and winter months (Oct-Dec) to assess for possible seasonal trends.....111

Table 3.11- The maximum estimated CO_2 consumption due to silicate and carbonate weathering in the Severn and the Thames, compared to the possible reduction in efficiency due to sulphuric acid weathering.....115

Table 3.12- Seasonal variation in nitrate concentrations and flux. Data split into summer months (Apr- Sept) and winter months (Oct- Mar). 118

Table 3.13- Potential impact of nitric acid on the CDR budget of natural weathering in the Severn and the Thames. In (Mt $CO_2 yr^{-1}$).....120

Table 3.14- Maximum potential CDR due to natural weathering in the Severn and the Thames catchments, assuming that all weathering derived cations are balanced in the river by HCO_3^-. Given in annual flux (Mt CO_2 yr^{-1}) and yield (kg CO_2 ha^{-1} yr^{-1}). Compared to the reduced CDR due to correcting for the river cations derived from sulphide and nitric weathering, as well as for carbonate precipitation and cation exchange.....121

Table 4.1- Average chemical composition of the UK rivers within the study. Data collated from the Harmonised Monitoring Scheme dataset (DEFRA, 2013) 132

Table 4.2- Top ten UK rivers in terms of DIC flux (in Mt CO_2 yr^{-1}). Compared to the total of the 52 catchments within this study, as well as accounting for the whole UK land mass. 140

Table 4.3- Endmember compositions used throughout the study. Ca/Na, Mg/Na and Cl/Na are used in the main inversion, whilst SO_4/Na is used in post-inversion mixing equations to derive $XSO4excess$. Values for carbonates are derived from Gaillardet et al., (1999). Silicates are derived from UK small sub-catchments draining silicates (described in Chapter 2). The evaporite end-member was taken from (Moon et al 2014).....144

Table 4.4- Maximum consumed CO_2 due to silicate and carbonate weathering in the catchments studied, and upscaled to include the whole UK landmass. Implied C flux from carbonates= DIC flux- CDR total 150

Table 4.5- Comparing the total cation flux from silicate and carbonate weathering of four different catchments within the study. The median value for each variable is given in each column.....158

Table 4.6- Maximum potential CDR due to natural weathering in the UK catchments, and upscaled to account for UK landmass. Given in annual flux (Mt CO_2 yr^{-1}). Compared to the reduced CDR due to sulphide weathering, nitrate weathering, carbonate precipitation and cation exchange. 163

Table 6.1- Comparison between the CO_2 consumed due to silicate and carbonate weathering in the UK, and the global estimates for silicate weathering from Hilton and West (2020), carbonate weathering (Zeng et al., 2019), Silicate CO_2 yields from Moon et al., (2014) and carbonate CO_2 yields from Zeng et al., (2019). Estimates were reported in Mt C yr^{-1} but converted to Mt CO_2 yr^{-1} for easier comparison with results here. 197

*Table 6.2- Example catchments split into two groups. In the first group of catchments, termed 'hydrologically influenced' catchments in the table, the variations in $Xsil$ appear to be influenced by variations in hydrology. In the second group of catchments, termed 'non- hydrologically influenced', there is no discernible relationship between $Xsil$ and hydrology in the table, and other parameters must have a greater influence on silicate weathering. Catchment parameters are compared to the average for the catchments within the study. *Variability in flow rate is the 5-95 percentile range in flow rate over the sampling period for each catchment (m^3 s^{-1}). $Xsil - JJA$ is the average X_{sil} for summer months, and therefore the ratio $Xsil - JJAXsil$ refers to the seasonal variability in X_{sil} within a catchment. The higher the value, the greater seasonal variability. 209*

Table 6.3- Comparison of the natural average riverine calcite saturation index (calculated using natural river chemistry from HMS dataset and carbonate equations via PHREEQC. See Chapter 4) for different catchment zones across the UK. HL= Highland, NE= northeastern, C= Cornish. This is compared to the estimated proportion of alkalinity derived from EW (utilising a 20 t ha^{-1} spreading rate and assuming 100% dissolution and complete transfer to the river) expected to precipitate as CaCO3. This is the median calculated using the median pCO2 in calculations (see Chapter 5 for further information). 225

Chapter 1

1 Introduction

1.1 General overview and motivation

The correlation between global climate change and atmospheric carbon dioxide (CO_2) concentration is well established (Manabe and Wetherald, 1967). Over the last century, human activity, particularly the burning of fossil fuels, has elevated atmospheric CO_2 from 278 ppm in preindustrial periods (Friedlingstein *et al.*, 2022) to 421 ppm (on 12/11/2023). To mitigate the potential negative impacts of resulting warming temperatures on human health and on the environment, the objectives of the Paris Agreement and subsequent IPCC reports have centred on limiting global temperature rise to within 1.5 °C above pre-industrial levels and well below 2 °C (IPCC, 2023). However, the current trajectory indicates an imminent likelihood of surpassing these prescribed limits, with projections within the IPCC 2018 report suggesting an overshooting of the 1.5 °C threshold between 2030-2052 (IPCC, 2018). In 2023, reports indicate that numerous global regions are already experiencing temperatures above this threshold in at least one annual season (Jones, 2023).

To halt further temperature rise and reach targets set by the Paris Agreement requires ambitious reductions in greenhouse gas emissions, as well as the removal of between 100-1000 Gt of atmospheric CO_2 over the coming century (or between 2-14 Gt CO_2 yr^{-1} dependent on the emission reduction scenario, Figure 1.1) (Smith *et al.*, 2023). A portfolio of carbon dioxide removal (CDR) strategies currently exists (Table 1.1). However most require further research to validate the achievable quantity of proposed CDR for each strategy, and to assess whether there would be any potential negative environmental or social impacts upon either regional or global implementation. This thesis aims to investigate the validity of one such CDR strategy, Enhanced Weathering (EW, Section 1.7). EW exploits a component of the long- term carbon cycle (Section 1.3) thought to regulate climate over geological timescales.

This thesis assesses unknown components of this process (Section 1.7.3), with the goal to advance knowledge for the potential application of EW as a CDR strategy. While the research is largely focused on EW adoption in the UK, the findings aim to have broader applicability and can be used for comparisons with other regions sharing similar climatic conditions and land use management practices to the UK.

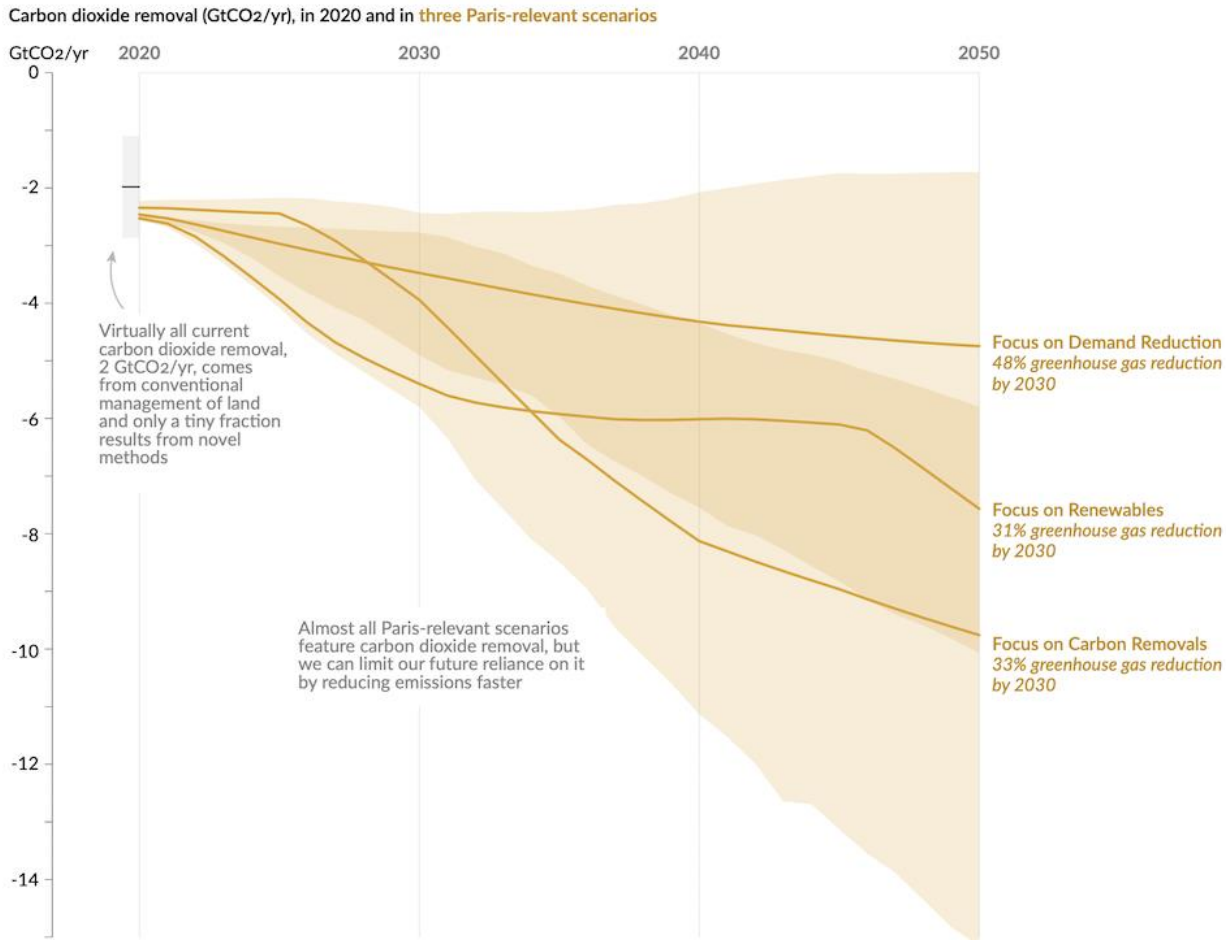

Figure 1.1 From the State of Carbon Dioxide Removal Report, i.e. Smith *et al.*, (2023)- *Three different emissions reductions scenarios featured in the Carbon Dioxide Removal Report, 2023, all of which meet the Paris Temperature Goals. All three scenarios rely on both emissions reductions and substantial carbon dioxide removal (CDR). 'Conventional CDR' includes methods such as reforestation, and soil carbon sequestration, while 'novel CDR' includes methods such as Enhanced Weathering, Bioenergy for Carbon Capture and Storage (BECCS), Direct Air Carbon Capture and Storage (DACCS).*

Table 1.1- A variety of methods of carbon dioxide removal exist and have been split into 'Conventional' and ''Novel'. Conventional methods are those already used, while novel methods are still being assessed for their feasibility for implementation. The values for the global potential of CO_2 removed due to utilizing these methods is taken from (Fuss et al 2018), unless otherwise specified. Current deployment of all novel CDR methods combined is 0.002 Gt CO_2 yr^{-1}. (Smith *et al.*, 2023)

CDR Method	Potential global (Gt CO_2 yr^{-1})	Potential UK (Mt CO_2 yr^{-1})
Conventional CDR		
Reforestation/ afforestation	0.5-3.6	3 (CCC, 2020a)
Peatland restoration	0.5-2.1	5 (CCC, 2020a)
Soil carbon sequestration	Up to 5	1-31 (Royal Society, 2018)
Novel CDR		
BECCS (Bioenergy with carbon capture and storage)	0.5-5	13 (CCC, 2020a)
DACCS (Direct air carbon capture and storage)	0.5-5	5 (CCC, 2020b)
Enhanced Weathering	2-4 (Fuss) 0.5-4 (RS, Beerling)	6-30 (Kantzas *et al.*, 2022)
Ocean alkalinity enhancement	1-100	n.a
Biochar	0.5-2 (Fuss) 1.8-4.8 (RS)	6-41 (Royal Society, 2018)

1.2 Extent of anthropogenic emissions and remaining CO_2 budget

Globally, CO_2 emissions increased in 2022 relative to 2021 from 40.2 to 40.5 Gt CO_2 yr^{-1} (Friedlingstein *et al.*, 2022). Of this, fossil fuels contributed the majority (89%, 36.3 $\pm$1.8 Gt CO_2 yr^{-1}) and emissions due to land use change contributed the remainder (4.5 $\pm$ 2.6 Gt CO_2 yr^{-1}) (Friedlingstein *et al.*, 2022). In the United Kingdom, there was a 2.4% decrease in CO_2 emissions in 2022 compared to 2021 (to 331.5 Mt CO_2 in 2022), and overall greenhouse gas emissions also dropped by 2.2% (417.1 Mt CO_{2eq}) (DESNZ, 2023). These reductions were primarily attributed to warmer weather, leading to decreased reliance on gas-based heating systems. Major contributing UK sectors included transport (112.5 Mt CO_2), energy (82.2 Mt

CO_2), business (61.9 Mt CO_2), public sector (7.6 Mt CO_2), residential (56.4 Mt CO_2) and other sectors, mainly associated with emissions via land use (10.9 Mt CO_2) (DESNZ, 2023).

For a 50% chance of limiting global warming to 1.5 °C and 2 °C, the remaining global carbon budget reduced to 380 Gt CO_2 and 1230 Gt CO_2 respectively from the beginning of 2023, equating to approximately 9 and 30 years of maintaining global emissions levels consistent with 2022 (Friedlingstein *et al.*, 2022). This limited remaining budget underscores the critical significance of investigating CDR methods.

1.3 The carbon cycle

Naturally, carbon dioxide undergoes exchange between the atmosphere and various natural sinks, such as the ocean, biosphere, soils, permafrost, and the lithosphere (Figure 1.2a, b). Human activities have significantly disrupted these natural processes (Figure 1.2a). Some of the surplus CO_2 emitted via fossil fuel use and alterations to land use (40.5 Mt CO_2 yr^{-1}) is mitigated by increased absorption into the ocean (10.6 Gt CO_2 yr^{-1} in 2021), and enhanced uptake by land (11.4 Gt CO_2 yr^{-1} in 2021, Figure 1.2a) (Friedlingstein *et al.*, 2022). Consequently, the net increase to atmospheric CO_2 concentration is ~19.1 Gt CO_2 yr^{-1} due to anthropogenic activity (Relative to 2022 emissions, Figure 1.2a).

Over long timescales, CO_2 exchange is mainly facilitated by geologic processes which transfer CO_2 between the lithosphere and the other sinks. The main long- term natural sinks for atmospheric CO_2 are the weathering of silicate minerals by carbonic acid (Section 1.3, Equation 1.1 and 1.2) and the burial of organic carbon (OC), preventing the return of the CO_2 to the atmosphere due to decomposition (Hilton and West, 2020). The main long- term sources of CO_2 to the atmosphere are volcanic degassing, the weathering of carbonates by sulphides (Equation 1.9), and the oxidation of petrogenic OC in sedimentary rocks (For annual flux estimates in Mt C, see Figure 1.2b) (Hilton and West, 2020). These various lithospheric processes broadly offset one another, maintaining relatively stable atmospheric CO_2 levels, and regulating Earth's climate over geological timescales (Berner and Berner, 1996).

Significantly, these natural lithospheric CO_2 fluxes are substantially smaller than those released through human activities (compare Figure 1.2a to Figure 1.2b). For instance, natural silicate weathering removes 0.3-0.5 Gt atmospheric CO_2 yr^{-1}: far less than the annual increase (19.1 Gt

CO_2 yr^{-1}). Hence, to achieve effective removal of sufficient CO_2 through silicate weathering within the required short- term intervention timescales (e.g. for CDR) demands a notable increase in the annual CO_2 flux from silicate weathering.

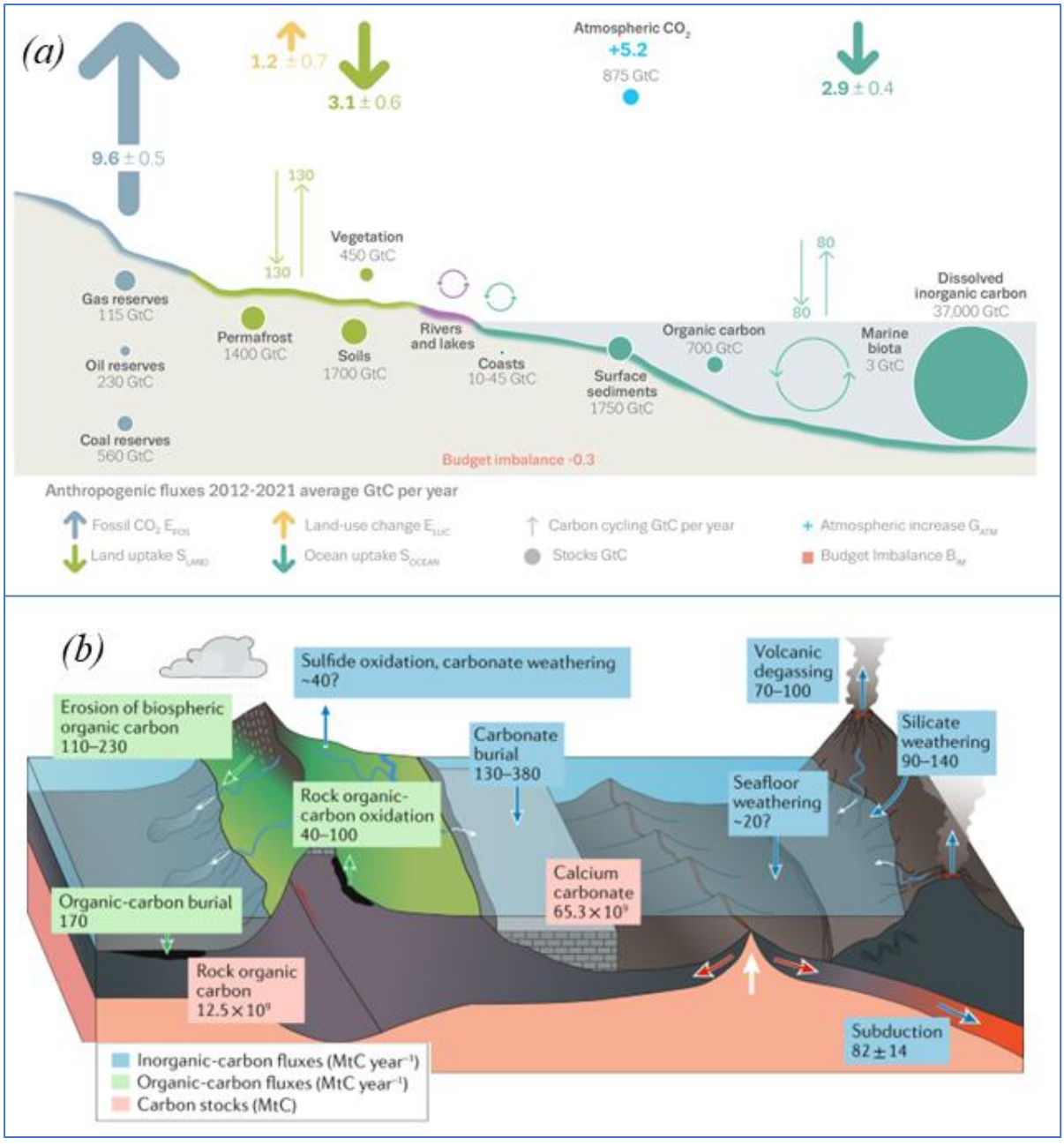

Figure 1.2- (a) (from Friedlingstein *et al.*, 2022) *represents the main sinks of carbon and shows the degree that these sinks are perturbed on an annual basis by anthropogenic emissions. (b) (From* Hilton and West, 2020). *The long-term inorganic carbon cycle. Note the difference between the magnitude of fluxes in (a) anthropogenic emissions (in Gt C) and (b) the inorganic natural long term carbon fluxes (in Mt C). Also note that Figure 1.2 presents fluxes in C rather than CO_2 - the latter of which is used in text to compare with the following chapters in this thesis.*

1.4 Natural rock weathering

The chemical breakdown of silicate and carbonate minerals in soils or at bedrock surfaces releases cations into solution and can convert atmospheric CO_2 into bicarbonate (Equation 1.1-1.3). The products of weathering reactions are transferred via runoff or groundwater to rivers and are eventually discharged into the ocean, increasing the alkalinity of fresh and oceanic water (Box 1, Total alkalinity, carbonate alkalinity and conservative alkalinity, Equation 1.6-1.8).

Examples of silicate dissolution reactions via carbonic acid:

Olivine (Forsterite): $$Mg_2SiO_4 + 4CO_2 + 4H_2O \rightarrow 2Mg^{2+} + 4HCO_3^- + H_4SiO_4 \quad (1.1)$$

Plagioclase (Anorthite): $$CaAl_2Si_2O_8 + 2CO_2 + 3H_2O \rightarrow Ca^{2+} + 2HCO_3^- + H_4SiO_4 \quad (1.2)$$

Carbonate weathering via carbonic acid:

$$CaCO_3 + CO_2 + H_2O \rightarrow Ca^{2+} + 2HCO_3^- \quad (1.3)$$

The dissolved products of weathering can persist in the oceanic water column for approximately 10 ka (Renforth and Henderson, 2017). Eventually, the DIC will form carbonate minerals and be buried on the ocean shelf, and in doing so, one mole of CO_2 will be re- released into the atmosphere per mole of carbonate formed (Equation 1.4). Consequently, the net removal and subsequent re-release of CO_2 from carbonate weathering balance out (Equation 1.3 and 1.4 combined), and it is silicate weathering only that influences the carbon cycle over geological timescales.

Carbonate precipitation and burial:

$$Ca^{2+} + 2HCO_3^- \rightarrow CaCO_3 + CO_2 + H_2O \quad (1.4)$$

1.4.1 Oceanic inorganic carbon system

Because CO_2 is re-released during carbonate formation in the ocean (Equation 1.4), the maximum removal of atmospheric CO_2 due to weathering occurs while the products of weathering remain dissolved in the water column. Therefore, understanding the mechanisms that retain this carbon within the water column is essential in establishing the upper threshold for storing excess CO_2 derived from weathering processes.

The current reservoir of carbon dioxide in the ocean is substantial (140,000 Gt CO_2) (Renforth and Henderson, 2017). Approximately 10.6 Gt CO_2 yr^{-1} of anthropogenic CO_2 is transferred from the atmosphere to the ocean, driven by a concentration gradient between the two sinks, whereby $pCO_{2\ atmosphere} > pCO_{2\ ocean}$ (Grace, 2004). Previous research suggests that the ocean can absorb significantly more CO_2 (>Gt C) than it currently holds without significantly increasing surface ocean calcite saturation levels (Renforth and Henderson, 2017). Some CDR approaches, such as ocean alkalinity enhancement and EW, aim to leverage this potential (Section 1.6 and 1.7).

Upon transfer into water, CO_2 reacts with water to form weak carbonic acid, which dissociates into bicarbonate (HCO_3^-) and carbonate (CO_3^{2-}) according to the dynamic carbonate equilibrium that exists in the water column (the carbonate buffer system, Equation 1.5).

The carbonate buffer system (from Zeebe and Wolf-Gladrow, 2001)

$$CO_{2(g)} \rightarrow CO_{2(g)} + H_2O_{(aq)} = H_2CO_{3(aq)} = HCO^-_{3(aq)} + H^+_{(aq)} = CO^{2-}_{3(aq)} + 2H^+_{(aq)} \quad (1.5)$$

The speciation of dissolved inorganic carbon (CO_2, HCO_3^-, CO_3^{2-}) upon entry into the ocean system is governed by water alkalinity, temperature, and salinity (Figure 1.3) (Zeebe and Wolf-Gladrow, 2001). Alkalinity has been defined in various ways (Box 1), but essentially represents a solution's ability to counteract acidity (or excess protons ($H^+_{(aq)}$)). Higher alkalinity, as observed in seawater relative to most waters on land (alkalinity ~2.5 mEql/L) (Renforth and Henderson, 2017), results in more DIC speciating as $CO^{2-}_{3(aq)}$, which neutralises extra protons

(Equation 1.2). In seawater with a T = 25 °C, and S = 35, the ratio of CO_2: HCO_3^-: CO_3^{2-} is approximately 0.5%: 86.5%: 13% (Zeebe and Wolf-Gladrow, 2001).

The speciation of carbon in the ocean will also determine the maximum amount of CO_2 that will be removed by natural (and enhanced) weathering reactions. When the cations are initially released into freshwater system, at close to neutral pH and lower alkalinity, most of the CO_2 will form bicarbonate and two moles of CO_2 will be needed to balance one mole of divalent cation (mainly calcium (Ca^{2+}) and magnesium (Mg^{2+})) released from the rock. In the seawater ratio given above, more of the DIC will form CO_3^{2-} and therefore the total amount of CO_2 per divalent cation is lowered to 1.4-1.7 (Renforth and Henderson, 2017). The exact amount of DIC for every mole of cation dissolved is termed the w value, which is used to calculate a rocks ability to remove CO_2 upon dissolution (the RCO_2 value) (Renforth, 2019). This concept is considered within many studies of enhanced weathering (i.e. Renforth, 2012, 2019; Renforth and Henderson, 2017), as well as throughout the thesis, as it is integral in calculating the amount of carbon dioxide removed due to enhanced weathering (Section 1.7).

It is hard to constrain the relative proportions of each species of DIC using routine measurement techniques. However, the 6 carbonate system variables- dissolved inorganic carbon (DIC), CO_2, HCO_3^-, CO_3^{2-}, pH and Total Alkalinity- can be determined using equations defined in Zeebe and Wolf-Gladrow, (2001), as long as 2 out of 6 are known. pH and alkalinity are usually the easiest to constrain via routine field measurements.

Total alkalinity (TA)- is defined as the amount of excess base within a solution (Equation 1.6):

$$TA = \left[HCO_{3(aq)}^{-}\right] + 2\left[CO_{3(aq)}^{-}\right] + \left[B(OH)_{4(aq)}^{-}\right] + [OH^{-}] + [HPO_4^{-}] + 2[PO_4^{2-}] + [H_3SiO_4^{-}] + [HS^{-}] + 2[S^{2-}] + [NH_3^{-}] - [H^{+}] - [HSO_4^{-}] - [HF] - [H_3PO_4] \quad (1.6)$$

Carbonate alkalinity (CA)- Given the significantly higher proportion of carbonate species relative to the other ions in Equation 1.5, carbonate alkalinity (Equation 1.7) can serve as an approximation for alkalinity:

$$CA = \left[HCO_{3(aq)}^{-}\right] + 2\left[CO_{3(aq)}^{-}\right] + [OH^{-}] - [H^{+}] \quad (1.7)$$

C*onservative Alkalinity (CsA)*- as ionic charge equilibrium must be maintained, the difference between conservative cations and anions (Equation 1.8) can be utilized to estimate alkalinity, as total alkalinity must equal conservative alkalinity.

$$CsA = \sum[cations - anions] \quad (1.8)$$

$$\boldsymbol{where\ TA = CsA \approx CA}$$

Box 1: Different definitions of alkalinity. A full discussion is given in Zeebe and Wolf-Gladrow, (2001).

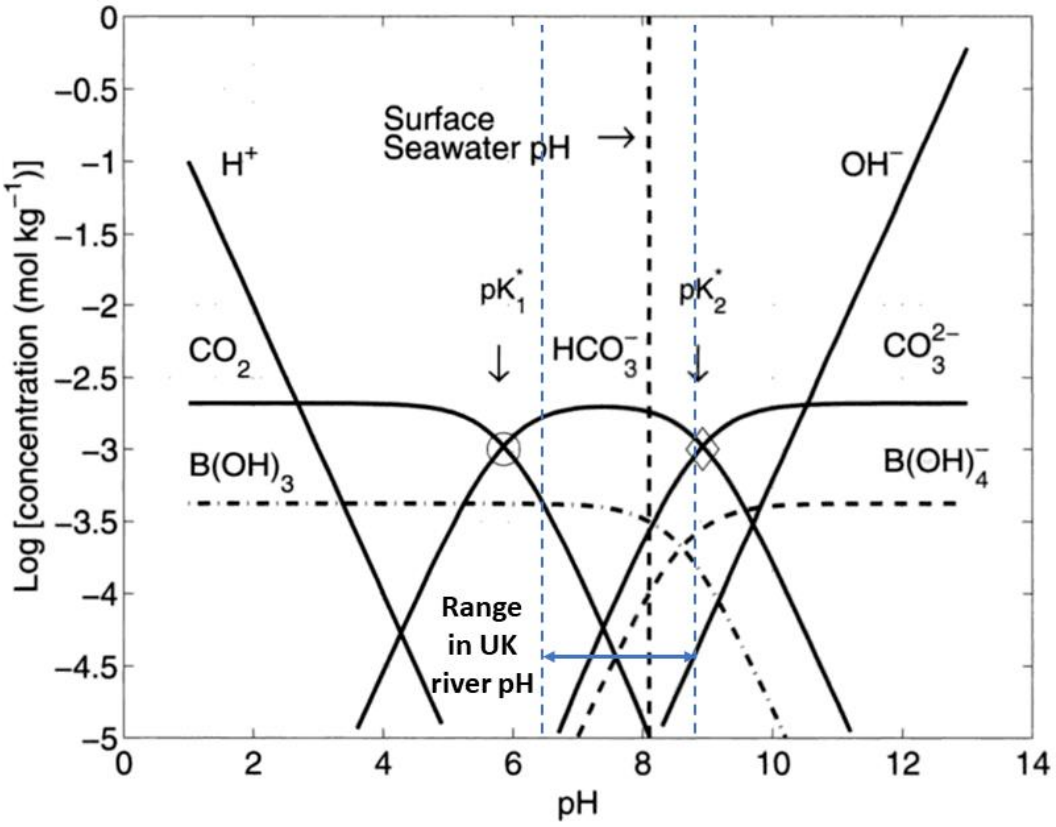

Figure 1.3 (from Zeebe and Wolf-Gladrow, 2001).- The seawater dissolved inorganic carbon system. The relative proportions of each carbonate species (CO_2, HCO_3^- and CO_3^{2-}) will determine the pH of the solution. pK_1^* and pK_2^* are the pH values when the concentration of CO_2 equals the concentration of HCO_3^- (pK_1^*), and when the concentration of HCO_3^- equals the concentration of CO_3^{2-} (pK_2^*). These are temperature and salinity dependent constants which can be calculated using equations discussed in detail within Zeebe and Wolf-Gladrow, (2001). The range in pH observed in UK rivers is also included within the figure. This range is based on the mean pH of the 52 UK rivers included in this thesis (Chapter 4). This mean is taken from geochemical river data from the Harmonised Monitoring Scheme (DEFRA, 2013) *which will be introduced in Chapter 2.*

1.5 Calculating the amount of carbon dioxide removed via natural weathering

Weathering products are conveyed to the ocean through river systems. Quantifying weathering fluxes in a catchment area therefore relies on measuring dissolved solutes (usually Ca^{2+}, Mg^{2+}, Na^+ and K^+) in river water. These solute concentrations can be linked back to their sources by using either forward mass balance calculations (i.e. Galy and France-Lanord, 2001; Jacobson and Blum, 2003; Chetelat *et al.*, 2008) or inverse geochemical mixing models (Such as in Gaillardet *et al.*, 1999; Moon *et al.*, 2014; Burke *et al.*, 2018) provided the chemical composition of the source endmember is known.

Calculating the CO_2 removed from weathering reactions also requires an understanding of the acids responsible for weathering. Silicate and carbonate weathering via carbonic acid leads to CO_2 removal (Equations 1.1-1.3). However, if other acids dissolve the rocks instead, then CO_2 removal may not occur. Two strong acids involved in some weathering environments are sulphuric acid (from the oxidative weathering of sulphide minerals) and nitric acid (derived from fertilisers). When these acids weather silicates, no atmospheric CO_2 is consumed (Equation 1.9 and 1.11). Conversely, if these acids weather carbonates, CO_2 is released. (Equations 1.10 and 1.12).

Sulphuric acid weathering of wollastonite (Equation 1.9) and carbonate (Equation 1.10)

$$CaSiO_3 + H_2SO_4 + H_2O \rightarrow Ca^{2+} + H_4SiO_4 + SO_4^{2-} \quad (1.9)$$

$$CaCO_3 + H_2SO_4 \rightarrow CO_2 + H_2O + Ca^{2+} + SO_4^{2-} \quad (1.10)$$

Nitric acid weathering of wollastonite (Equation 1.11) and carbonate (Equation 1.12)

$$CaSiO_3 + 2HNO_3 + H_2O \rightarrow 2NO_3^- + Ca^{2+} + H_4SiO_4 \quad (1.11)$$

$$CaCO_3 + 2HNO_3 + 2O_2 \rightarrow Ca^{2+} + 2NO_3^- + H_2O + CO_2 \quad (1.12)$$

Accurately estimating the proportion of weathering via carbonic acid versus strong acids is thus important when assessing the CDR potential resulting from natural (and enhanced) weathering.

Globally, geochemical modelling of riverine solute fluxes has helped to constrain the CO_2 removal via natural silicate and carbonate weathering to between 330-510 Mt $MtCO_2$ yr^{-1} and 730-2570 $MtCO_2$ yr^{-1} respectively (Gaillardet *et al.*, 1999; Moon *et al.*, 2014; Zeng *et al.*, 2019). Furthermore, river chemistry has been instrumental in elucidating the primary weathering drivers at the catchment level (e.g., (Jacobson and Blum, 2003; Tipper *et al.*, 2006) and discussed further in Section 1.5). Nevertheless, silicate and carbonate fluxes in the UK remain understudied.

The estimated annual dissolved inorganic carbon (DIC) flux from land to ocean in the UK ranges between 7.3-11 Mt CO_2 yr^{-1} (Bell *et al.*, 2021). Riverine DIC concentrations display

significant variation across the UK, with a previous study indicating an order of magnitude increase in DIC concentrations from northwest to southeast regions (Jarvie *et al.*, 2017). This increase coincides with carbonate rich regions (Figure 1.4), implying a potential dominance of carbonate weathering over silicates in contributing to the overall annual DIC flux exported to the ocean. However, the distinction between DIC originating from carbonate and silicate sources has not been attempted. This differentiation is crucial for accurately measuring the quantity of atmospheric CO_2 removed through weathering. DIC incorporates carbon from the rock itself, and therefore DIC does not equal CDR, plus silicates and carbonates consume different amounts of C in the first place (Equation 1.1-1.3) Additionally, discerning this difference contributes to our comprehension of the carbon cycle- as only silicate weathering contributes to the long- term removal of CO_2.

This thesis will adopt a geochemical inversion approach following methods by Gaillardet *et al.*, (1999) and Kemeny and Torres, (2021) and using chemical data for the UK to calculate annual weathering fluxes.

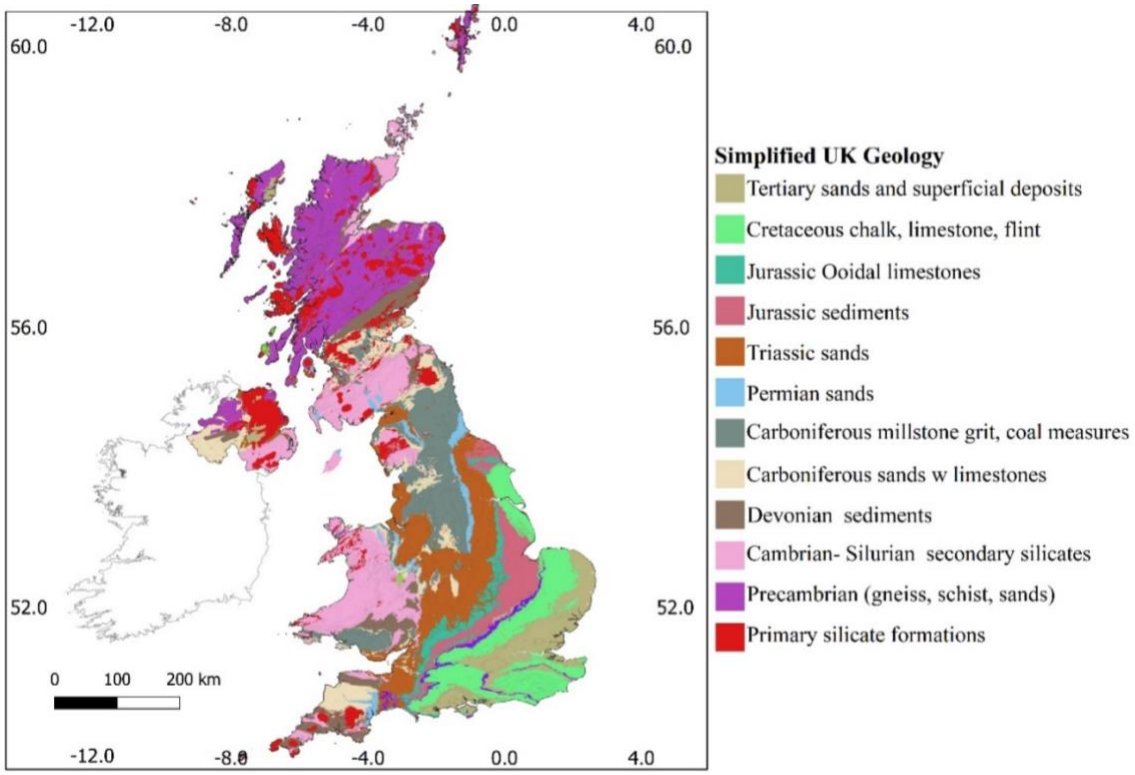

Figure 1.4 (from Chapter 4)- Simplified geological map of the UK from (BGS, 2023a). *The large variation in lithology across the UK suggests that weathering fluxes will be variable.*

1.6 Controls on weathering rates

The environmental drivers which are known to influence weathering reactions include those discussed below. Their specific influence on the weathering fluxes in the UK will be considered throughout this thesis (Chapter 6). Examining these factors is crucial for a complete understanding of UK-specific weathering and for pinpointing ideal locations for EW.

1.6.1 Temperature

The rate that a mineral dissolves over time ($^{dm}/_{dt}$) is temperature dependent and can be characterised following Lasaga, (1984) (Equation 1.13):

$$^{dm}/_{dt} = -SA * Ae^{(-^{Ea_{dissolution}}/_{RT})} * f(a_i) * (1 - \Omega) \quad (1.13)$$

Where A is the Arrehenis pre- exponential factor, $Ea_{dissolution}$ is the activation energy of the reaction, R is the gas constant, T is in (K), SA is the specific surface area, f(a_i) is a function that describes the activities of the elements within the reaction and Ω is the saturation state of the solution. $^{dm}/_{dt}$ is negative to reflect the dissolution of the material: thus, a more negative $^{dm}/_{dt}$ signifies increased dissolution. The full term $Ae^{(-^{Ea_{dissolution}}/_{RT})}$ describes the kinetic rate constant of the reaction, (i.e., $k_{dissolution}$).

Equation 1.13 demonstrates that, given a constant Ω, f(a_i) and SA, an increase in temperature will lead to an increase in the rate constant ($k_{dissolution}$) and therefore, to an increase in reaction rate ($^{dm}/_{dt}$). Soley focusing on the kinetic term suggests that silicate and carbonate weathering would increase in regions with increasing temperatures. However, this may not be observed at catchment scale.

For silicates, under laboratory conditions increasing the temperature increases weathering rates. For instance, at pH = 2, increasing the temperature from 25°C to 35°C, increases the

$k_{dissolution}$ of dissolving olivine (with a forsterite content of 91%) from between $10^{-7.92}$-$10^{-7.87}$ to $10^{-7.58}$(Lasaga, 1984). However, at catchment scale, Brantley *et al.*, (2023) demonstrated that other influencing factors, such as mineral supply (discussed in point iii) or water availability (point iv), may overshadow the influence of temperature on silicate weathering fluxes. Consequently, the relationship between temperature and silicate weathering appears to be limited across global catchments (Brantley *et al.*, 2023).

Despite the temperature influence on $k_{dissolution}$, the rate of carbonate dissolution decreases with an increase in temperature. This occurs because the dissolution rate ($^{dm}/_{dt}$) is not solely governed by the kinetic rate constant $k_{dissolution}$, but also by the equilibrium reactions within the reacting fluids, impacting the $(1 - \Omega)$ term in Equation 1.13.

The dissolution of carbonate (Equation 1.14) introduces Ca^{2+} and CO_3^{2-} ions into solution and impacts (Ω) by Equation 1.15.

$$CaCO_3 \rightarrow Ca^{2+} + CO_3^{2-} \quad (1.14)$$

$$\Omega = \frac{\gamma_{Ca} * \gamma_{CO3}}{K_{sp}} \quad (1.15)$$

Where γ_{Ca} and are activities of Ca^{2+} and CO_3^{2-} ions respectively. Note that Ω is the calcite saturation state rather than calcite saturation index (SI_{calc}). The two terms are related: SI_{calc} is the log of Ω. SI_{calc} is mainly used throughout the thesis.

K_{sp} is the thermodynamic constant of carbonate dissolution, which is temperature dependent and decreases as temperatures rise. Consequently, elevated temperatures increase the saturation state of the solution (Ω), and cause the term $(1 - \Omega)$ in Equation 1.13 to approach 0. Overall, this causes $^{dm}/_{dt}$ to decrease. Effectively, higher temperatures therefore decrease carbonate dissolution rates, and elevate the likelihood of carbonate precipitation due to the increased Ω.

Considering the thermodynamics governing carbonate precipitation/dissolution, it might be assumed that colder regions would be optimal for carbonate weathering. However, the temperature dependency of carbonate weathering follows a more boomerang-shaped curve, which Gaillardet *et al.*, (2019) attribute to variable pCO_2 levels in soils supplied by respiration

(Figure 1.5). Soil pCO_2 exhibits a temperature dependency; higher temperatures lead to increased rates of respiration and therefore of soil pCO_2, crucial for carbonate dissolution. An optimal temperature for carbonate weathering (~11 °C) is proposed which allows sufficient pCO_2 concentrations for weathering reactions, without significantly reducing K_{sp}. Notably, this is approximately the average surface temperature in the UK (10 °C) (Worrall *et al.*, 2022), hinting at the potential optimal conditions for carbonate weathering in this region.

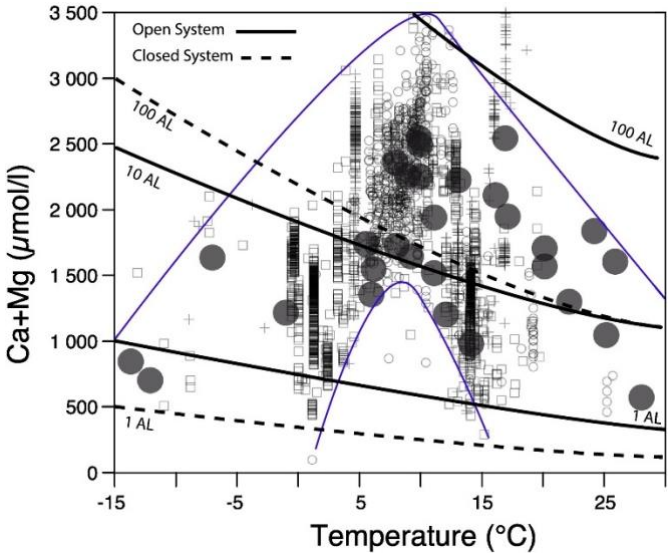

Figure 1.5 (Taken from Gaillardet *et al.*, 2019)- *The temperature dependence of Ca^{2+} and Mg^{2+} in solution from rivers draining carbonate lithologies. Solid and dashed lines represent the theoretical concentrations given thermodynamic theory and equations discussed in text. The impact of variable pCO_2 concentrations to the theoretical concentrations of Ca^{2+} and Mg^{2+} with temperature is also given, represented by 1 AL, 10 AL, and 100 AL- equivalent to 1, 10 and 100 x atmospheric pCO_2 levels. The plotted data within the bell-shaped curve are river concentrations collected from the GLORICH database. The actual relationship between carbonate flux and temperature is shown to be a boomerang shape, which is suggested to be controlled by changing pCO2 concentrations within soils.*

1.6.2 Geological heterogeneity/ mineral composition

The rate at which a mineral dissolves depends on the strength of the chemical bonds within their lattice structure (Lasaga, 1984). Silicate minerals possessing strong silica double bonds tend to exhibit very slow dissolution rates, leading to a decrease in rate with increasing silica content (Figure 1.6) (Goldich, 1938). Conversely, carbonate minerals containing weaker Ca^{2+}-CO_3^{2-} ionic bonds dissolve orders of magnitude faster than silicates (dependent on the specific silicate mineral) (Palandri and Kharaka, 2004). For instance, according to Lasaga *et al.*, (1994), at a constant temperature (T= 25 °C) and pH (pH = 5), complete dissolution of a spherical 1mm

calcite mineral occurs within 10 years, while the silicate mineral anorthite dissolution takes approximately 100 years.

Various studies have determined the dissolution rates for individual minerals, the results of which were consolidated into a comprehensive report by (Palandri and Kharaka, 2004). The Goldich series expresses this graphically for a few of the common silicate minerals (Figure 1.6) (Goldich, 1938; Renforth, 2012).

As mineral composition impacts weathering rate, bedrock geology becomes important in determining the rate of weathering occurring within the catchment. In the UK, high riverine DIC concentrations observed in southeastern carbonate rich regions imply that lithology may be a primary driver of the variations in weathering derived DIC observed (Jarvie *et al.*, 2017).

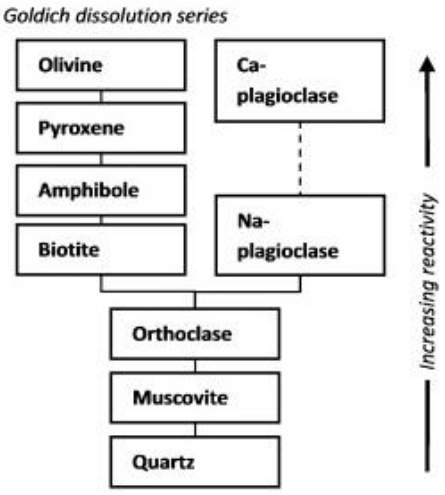

Figure 1.6- The Goldich Dissolution series (Figure from (Renforth, 2012) *and originally reported by* (Goldich, 1938) *shows the order of reactivity of different silicate minerals. Order of reactivity is mainly related to silica content- an increase in strong Si=Si double bonds within the mineral lattice will decrease the mineral weathering intensity. For example, silica content of quartz can be greater than 60%, while silica content of olivine is typically <45%* (Renforth, 2012).

1.6.3 Supply of fresh minerals

Variations in physical erosional processes can significantly influence chemical weathering fluxes within a catchment, impacting silicate and carbonate reactions differently. Increased erosion supplies fresh mineral surfaces and given the fast dissolution kinetics of carbonate weathering, will typically increase carbonate weathering fluxes (Gaillardet *et al.*, 1999). Typically, erosion has a limited impact on silicate weathering fluxes due to slow kinetics of dissolution (West *et al.*, 2005; Hilton and West, 2020; Bufe *et al.*, 2021). However, when

mineral supply is low, increasing erosion rates can increase silicate weathering (West *et al.*, 2005; Hilton and West, 2020).

The relationship between erosion and silicate and carbonate weathering has been observed within various global catchments. For instance, in rivers draining New Zealand's Southern Alps, erosion enhances the overall weathering flux, however highly erosive terrains tend to elevate the proportion of solutes from carbonates compared to silicates (Jacobson and Blum, 2003; Hilton and West, 2020). It has been proposed that within stable geomorphic zones with reduced physical erosion, silicate weathering chemical reactions are allowed more time to proceed, leading to a higher proportion of silicate weathering in these regions. Geochemical modelling of catchments across southern Taiwan with varying erosional gradients showed similar results- with carbonate weathering increasing with erosion, while silicate weathering either remained constant or decreased (Bufe *et al.*, 2021). This indicated that erosion has a limited impact on silicate weathering processes, and that other environmental parameters which influence reaction kinetics (such as temperature and pH) may play a more important role in silicate weathering rates in these catchments.

1.6.4 Water availability and the residence time of this water within the catchment

Hydrology is an important factor in determining weathering rates. In general, the removal of solutes from the site of weathering by aqueous transport can reduce the likelihood of porewaters and river waters reaching equilibrium, which would otherwise slow chemical reactions (Maher, 2011). This is particularly important for carbonate weathering, where mineral kinetics allow fast accumulation of solutes in waters. For silicate weathering, transport of products away from site of weathering is still important, however a longer water-rock interaction time is needed to allow the slower reaction processes to proceed. Silicate dissolution may be enhanced within groundwater aquifers for example, where water may interact with mineral surfaces over substantial periods ranging from 0-1Ma (Gleeson *et al.*, 2016).

These contrasting relationships between water supply and silicate and carbonate weathering were observed in seasonal variations in riverine chemistry in the Marsyandi catchment, Nepal (Tipper *et al.*, 2006). After correcting for cyclic and hydrothermal inputs and using typical

forward mixing equations to attribute solutes to endmember sources (as introduced in Section 1.5), Tipper *et al.*, (2006) found that the proportion of solutes sourced from carbonates increased during the monsoonal high discharge event, while the relative contribution of silicate ions increased in periods of low flow. Additional studies, such as Ohrui and Mitchell, (1999) and Rademacher *et al.*, (2001), have also demonstrated an increase in silicate cation content with age of the water within the river. These observations suggest the significance of residence time within the catchment in facilitating silicate weathering reactions.

1.6.5 Arable land

One potential driver for natural weathering considered in this thesis is anthropogenic activity, via agricultural land use. The UK landscape has been extensively altered by human activity over the last century. The use of land for agricultural purposes has been suggested to modify silicate (Fortner *et al.*, 2012) and carbonate (Raymond and Oh, 2009) weathering rates, via the following mechanisms:

i) Clearing forested areas for agriculture exposes soil to hydrological erosional processes, supplying more fresh mineral surfaces to the weathering zone (Woodward and Foster, 1997; Walling, 1999).

ii) Catchment hydrologic pathways are altered due to forest felling: trees can draw rainwater to deep soil zones via large root systems, thus increasing water infiltration and soil moisture, while reducing direct runoff (Fohrer *et al.*, 2001; Fortner *et al.*, 2012).

iii) The practise of agricultural tilling overturns soils and breaks up mineral aggregates, which exposes fresh mineral surfaces to the weathering environment.

iv) The application of organic fertilizer adds nitrogen to soils, which on nitrification, produces acids (nitric acid, HNO_3^-) which can act as the reagents for weathering (i.e., via Equations 1.9-1.12) (Perrin *et al.*, 2008).

v) Arable crops release organic acids and CO_2 into soil porewater, increasing soil pCO_2 and decreasing the pH of the weathering zone (Raymond and Cole, 2003; Fortner *et al.*, 2012). Further, microbial activity surrounding the root systems of crops can promote the enhanced breakdown of minerals (Raymond and Cole, 2003)

All these factors can potentially alter the rates of rock weathering. In the United States, for example, there has been a significant increase in agricultural development since the 1950's, and estimates suggest that ~40% of the suspended sediment in US rivers is now agriculturally derived (Woodward and Foster, 1997). In the UK, with substantial area utilized for arable croplands and grasslands (4.9 and 12.2 Mha respectively in 2021) (Marston *et al.*, 2022), there is considerable potential for natural weathering rates to be enhanced.

Additionally, the application of lime to soils to buffer acidification may also supply HCO_3^- to rivers. The significant increase in bicarbonate concentrations in the Mississippi River from the 1950's is suggested to be primarily derived from agricultural lime (Raymond and Oh, 2009). In the UK, although lime was applied to less than 9% of the total arable land between 2006-2016 (Defra, 2022), this still equated to 1.5-2 Mt $CaCO_3$ per year (Holland *et al.*, 2018). If this HCO_3^- were to be transported to riverine waters, then this could significantly impact the dissolved inorganic carbon in UK rivers.

1.6.6 Other weathering drivers

Other environmental conditions which may impact weathering rates in the UK include the variability in porosity, permeability, aquifer content, type of vegetation and biotic activity, and anthropogenic factors, such as percentage urban cover or pollutive sources (Brantley *et al.*, 2023). Additionally, the presence of additional strong acids from sulphide oxidation and fertilisers (H_2SO_4 and HNO_3 respectively) can enhance weathering reactions.

Understanding the contribution of each of these drivers to silicate and carbonate weathering fluxes in the UK is key to elucidate the mechanisms of weathering in the UK and to identify suitable locations for the employment of enhanced weathering technologies.

1.7 Enhanced Weathering (EW)

Enhanced Weathering is a CDR method that accelerates the natural dissolution of silicate and carbonate rocks (Equations 1.1-1.3). While both carbonates and silicate rocks can be used in EW, alkaline silicates, such as olivine, basalt and wollastonite, are favoured in the literature (e.g. Peters *et al.*, 2004; Köhler, Hartmann and Wolf-Gladrow, 2010; Hartmann *et al.*, 2013; Kantzas *et al.*, 2022). This is due to their capacity to remove more CO_2 per cation released from the rock, (Section 1.4), and because only silicates play a role in the long-term carbon cycle (Equations 1.1-1.4). Natural silicate weathering reactions occur slowly, impacting atmospheric carbon concentrations over geological timescales. Accelerating the process for relevant CO_2 removal over human timescales involves exposing the rock to optimal environmental conditions conducive to weathering reactions (Section 1.6). Crushing the rock to increase the specific surface area (SSA) of the mineral (see discussion in Section 1.7.1), and applying this to acidic farmland soils, has been proposed as a method to achieve complete dissolution within decades (Beerling *et al.*, 2018). Fast dissolution facilitates the increased transfer of CO_2 from the atmosphere to the weathering zone: where it is converted to HCO_3^- and assumed to be ultimately exported, via rivers, to the ocean.

The CDR potential of EW across a specific land area relies on three main factors: the quantity of rock applied to the area, the rate at which the rock dissolves, and the rock's composition (Strefler *et al.*, 2018). Typical application rates found in literature range between 10-50 t ha^{-1} (Renforth, 2012; Beerling *et al.*, 2018; Kantzas *et al.*, 2022), although higher rates (100-150 t ha^{-1}) have been considered in some EW modelling and core studies (Strefler *et al.*, 2018; Amann *et al.*, 2020; Buckingham, 2022). The dissolution rate is influenced by multiple factors including temperature, pH, mineral saturation, and the grain size and composition of the rock (Palandri and Kharaka, 2004). EW employs some of these factors to enhance the dissolution rate (Section 1.7.1). Additionally, the chemical composition of the rock dictates the maximum potential amount of atmospheric CO_2 removal per tonne of silicate applied to the soil and is referred as the R_{CO_2} value. It can be quantified by Equation 1.16 (Following Renforth, 2019):

$$R_{CO_2\,i} = \left(\frac{\%CaO}{M_{CaO}} + \frac{\%MgO}{M_{MgO}} + \frac{\%Na_2O}{M_{Na_2O}} + \frac{\%K_2O}{M_{K_2O}} + \frac{\%SO_3}{M_{SO_3}} + \frac{\%P_2O_5}{M_{P_2O_5}}\right) * w \quad (1.16)$$

Where M_x is the molar mass of each oxide and $\%x$ is the weight percentage of each oxide in one tonne of rock. w is the factor that accounts for the carbonate speciation in seawater, i.e. $w = 1.4 - 1.7$ (see discussion in Section 1.4.1) (Renforth and Henderson, 2017)

Equation 1.16 emphasises that silicate rocks with higher cation content possess increased CDR potential per tonne. Rocks that demonstrate the highest CDR potential are olivine rich varieties like dunite and harzburgite, with R_{CO_2} values ranging between 0.8-1 (Renforth, 2012). Due to this high R_{CO_2}, olivine has been preferred in early modelling assessments to predict EW's CDR potential (i.e. Köhler, Hartmann and Wolf-Gladrow, 2010; Strefler *et al.*, 2018), and in bench scale EW dissolution experiments (i.e. Renforth, Pogge von Strandmann and Henderson, 2015; Amann *et al.*, 2020). However, olivine typically contains high concentrations of Cr and Ni, with one bench dissolution study revealing Ni levels in leachate solutions exceeding safe drinking water limits (Amann *et al.*, 2020). In contrast, although basalt possesses a lower R_{CO_2}- a typical flood basalt typically has an R_{CO_2} values of around 0.3 (Renforth, 2012)- it contains fewer hazardous trace elements. Additionally, the application of basalt to farmland has been shown to provide a further added benefits of providing nutrients (i.e. P, K, Fe) for the crops and mitigating soil acidification (Beerling *et al.*, 2018). Therefore, in widespread implementation, basalt is more likely to be employed for EW initiatives.

1.7.1 Enhancing weathering reactions

As the dissolution rate of a given mineral relies on the available surface area for mineral reactions (Equation 1.13), the choice of grain size of the applied silicate is important. The theoretical time required for complete dissolution of a spherical mineral with an initial grain size (d_0-as a diameter (m)), can be calculated by the Shrinking Core Model (Equation 1.17, discussed in Hangx and Spiers, (2009):

$$X(t)_i = \frac{d_0^3 - (d_0 - 2 * Wr_i * V_m t)^3}{d_0^3} * 100 \quad (1.17)$$

Where d_0 is the initial grain size (m), $X(t)_i$ is the percentage of material (i) left at any time (t), V_m is the molar volume of mineral (i) and Wr_i is the weathering rate of mineral (i). The full term within the equation $(2 * Wr_i * V_m t)$ accounts for the change in particle size with time.

The time taken for complete mineral dissolution significantly decreases with smaller grain sizes (Figure 1.7). Therefore, reducing grain size can notably enhance the CDR potential of EW. However, very small grain sizes (~10 μm) lead to a substantial increase in the energy needed for crushing (Lefebvre *et al.*, 2019). Additionally, these small grain sizes pose a human risk due to potential dust inhalation (Beerling *et al.*, 2018). Therefore, a balance is necessary: the grain size should facilitate dissolution within timescales needed for CO_2 removal without excessive energy demand or jeopardizing human health. Kantzas *et al.*, (2022) propose that basalt grain sizes of 100 μm could be utilised for EW implementation in the UK without the need for excess energy consumption.

A potential alternative that would reduce the energy requirements of EW involves utilising pre-existing crushed alkaline silicate rock resources- such as mine waste rock, or artificial material such as concrete and demolition waste, and steel slag (Renforth *et al.*, 2009, 2011; Renforth, 2012). By eliminating the need for crushing, and minimising reliance on new rock extractions, this approach could effectively support EW implementation at regional or national scales.

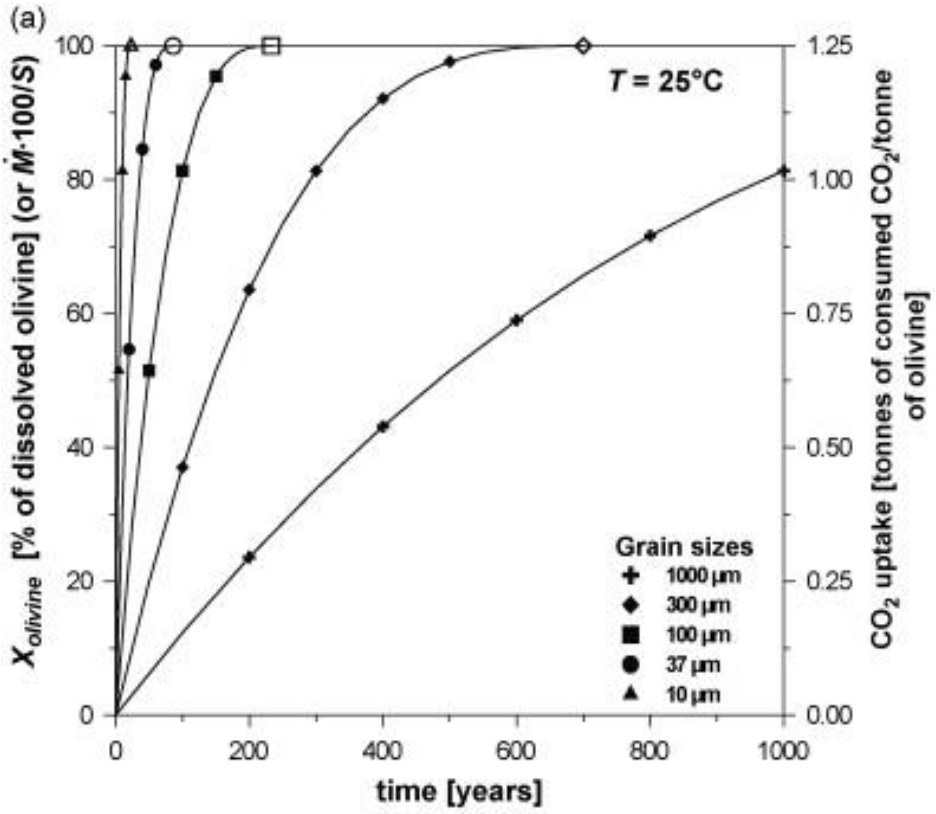

Figure 1.7 Taken from Hangx and Spiers, (2009)- *the importance of grain size in determining the time needed to fully dissolve olivine. Using grain sizes 10-1000 µm. At a T= 25°C and typical pH of seawater (given in paper as pH= 8.2)*

Temperature also influences the rates at which silicate dissolution reactions occur (Equation 1.13), making equatorial regions, with warm climates and abundant water supply, ideal locations for EW (Beerling *et al.*, 2018; Strefler *et al.*, 2018). Strefler *et al.*, (2018) assessed the global CDR potential of spreading 150 t ha^{-1} of both basalt and dunite (with particle size of 20 µm) over 50% of global arable land (7.8×10^8 ha). Their findings suggest that dunite could potentially sequester up to 95 Gt CO_2 yr^{-1}, whereas basalt may remove up to 4.9 Gt CO_2 yr^{-1}. Moreover, they indicate that 75% of the total annual CDR drawdown would be attributed to warmer equatorial regions (Strefler *et al.*, 2018). The UK sits outside this zone, and with lower average temperatures (10 °C) may not be the most conducive environment for implementing EW. Nevertheless, a recent sophisticated modelling study indicates that the application of crushed basalt to arable croplands in the UK could potentially remove up to 45% of the atmospheric carbon dioxide required for the UK to achieve its net zero targets by 2050 (6-30 Mt CO_2 yr^{-1}) (Kantzas *et al.*, 2022).

1.7.2 Carbon dioxide removal potential for EW

Considerable uncertainties remain regarding the CDR potential of EW. A preliminary estimate indicated that spreading 10-30 t ha^{-1} of crushed basalt over 9×10^8 ha of global arable land under optimal weathering conditions could potentially lead to a CDR of between 0.5-4 Pg CO_2 yr^{-1} by 2100 (Beerling *et al.*, 2018). However, the global study by Strefler *et al.*, (2018) suggests that the CDR may be much lower (4.9 Gt CO_2 yr^{-1} for spreading basalt over 7.8 x 10^8 ha), even at a higher spreading rate (150 t ha^{-1}), due to the impact of dissolution rate on CDR over a range of global climates. Other studies suggest CDR ranges of between 0.5-5 Gt CO_2 yr^{-1}, dependent on utilised rock type, spreading rate, initial grain size, as well as economic assumptions (Fuss *et al.*, 2018; Beerling *et al.*, 2020; Goll *et al.*, 2021).

The global CDR reported in Strefler *et al.*, (2018) might serve as an upper boundary due to several factors. Their applied spreading rate of 150 t ha^{-1} represents the upper limit of what is considered feasible for EW (Kelland *et al.*, 2020). Additionally, they used previously established dissolution rates for individual minerals that were determined under laboratory ideal conditions (from Palandri and Kharaka, 2004). Dissolution rates often differ between laboratory settings and natural environments due to various factors operating often simultaneously in the soil zone and at catchment scale. These factors, such as pH variations, temperature fluctuations, microbial activity, soil structure, water availability, and mineral saturation can significantly influence weathering processes (Strefler *et al.*, 2018; Vicca *et al.*, 2022). Further, catchment scale environmental drivers, such as hydrology and water availability, erosion, topography, underlying rock properties, and climate, can vary temporally and spatially (see Section 1.6), indicating that weathering rates for the same applied crushed rock might significantly differ even at catchment scale.

Due to limitations in the ability of modelling studies to fully encompass the dynamic nature of the soil system, core and pot soil experiments are conducted to bridge the gap between modelling and real-world conditions. These studies often vary in their initial experimental conditions- such as the initial soil composition, rock type, grain size of added silicate, application rate, incorporation of plants, etc- making direct comparisons challenging (Table 1.2). Nonetheless, these investigations generally indicate significantly lower dissolution rates compared to those derived from laboratory settings. These reduced rates can lead to significant variations in the estimated CDR potential calculated between modelling and core studies,

emphasising the need for further investigation into the primary factors influencing dissolution rate within soils, as well as on a catchment scale (Section 1.6)

*Table 1.2- Key core and pot EW trials aimed to test the dissolution rate and CDR potential of EW. Bracketed values are the quoted CDR potentials given in the literature, which have been converted here to t CO_2 ha^{-1} yr^{-1} for easier comparison between studies. *Based on calculations from the Mg^{2+} concentration in outflow solution- however, they also noted significant Mg^{2+} accumulation in topsoil layers, which were not accounted for in the values provided in this table.* ** (Renforth *et al.*, 2015) *quoted a likely amount of olivine dissolution per hectare given the results of their core trial which have been converted into CO_2 t ha^{-1} here, using RCO_2 value of Olivine of 0.93 (From Renforth 2012).*

Study	Spreading rate (t ha^{-1})	Particle size (µm)	Type of rock	CDR potential (t CO_2 ha^{-1} yr^{-1})
(Kelland *et al.*, 2020)	100	1250	basalt	2 -4
(Buckingham *et al.*, 2022)	100	125-250	basalt	0.01 ± 0.008 (10.2 ± 0.8 kg CO_2 ha^{-1} yr^{-1})
(Amann *et al.*, 2020)	220	43.5 1020	dunite	0.023-0.049* (2.3-4.9 t CO_2 km^{-2} yr^{-1})
(Renforth *et al.*, 2015)	127	125	olivine	1.86** (2 t olivine ha^{-1} yr^{-1})

1.7.3 Uncertainties and research needs

Accurately constraining the CDR due to EW is difficult due to the inability to accurately predict at least two primary factors: (i) the weathering rates of crushed rock across catchments characterised by distinct soil compositions and environmental parameters, and (ii), the subsequent fate of these weathered products once they are released from the rock.

1.7.3.1 Weathering rates

Due to the diverse environmental conditions, both globally and within the UK, EW weathering rates are expected to vary at catchment scale, causing discrepancies in CDR estimations. For instance, two recent studies provide contrasting estimates for the CDR potential of EW in the UK, primarily due to the uncertainty surrounding the influence of water availability on EW weathering rates. Buckingham *et al.*, (2022) conducted a core-based investigation on the impact

of natural UK hydrological conditions on the dissolution of 100 t ha^{-1} of 125 µm crushed basalt to typical lime rich, loamy soil from southeastern England. They exposed their soil cores to ambient UK temperatures and regional water flux. Their findings highlighted that the low water flux characteristic of southeastern UK areas significantly decreased dissolution rates. Consequently, they estimate that low water flux could limit CDR of EW in the UK to ~1.3 Mt CO_2 yr^{-1}. This estimation markedly contrasts with the higher estimate from a modelling-based UK study by Kantzas *et al.*, (2022) (6-30 Mt CO_2 yr^{-1}), who reported higher water fluxes for the same regions. Such a difference in CDR estimates highlights the necessity to fully understand how catchment scale variations in water availability- as well as other environmental drivers- might impact EW CDR locally and globally.

1.7.3.2 Fate of the weathered material

The assessment of the carbon dioxide removal resulting from EW also necessitates understanding the fate of the dissolved products. This involves being able to distinguish the fraction that re-precipitate as carbonates or other secondary minerals in soils or in rivers, and the portion that enters the ocean. This distinction is critical as the dissolved components transported to the ocean facilitate higher CO_2 removal (1.4-1.7 moles of CO_2 per mole of divalent cation- see discussion in Section 1.4), than those forming carbonates in the soil zone (1.0 mole per mole of divalent cation). Therefore, understanding the destination of the weathered products is crucial for accurate estimates of CDR, yet this factor remains unclear.

For instance, in their pot study investigating EW olivine dissolution, Amann *et al.*, (2020) observed significantly higher Mg^{2+} concentrations in the topsoil layers compared to the leachate. They proposed that the Mg^{2+} released from olivine dissolution was being retained within the soil, possibly through incorporation into secondary minerals or adsorption onto the surface of clay minerals. When cations resulting from enhanced weathering reactions form secondary minerals in soils, it can impact the total CDR by reducing alkalinity from soil porewaters. This result highlights the importance of understanding the fate of the released cations from EW weathering reactions.

Likewise, if EW products precipitate as secondary carbonates during river transport, the subsequent CO_2 re-release could decrease the overall efficiency of CDR from EW. The importance of this process to EW remains unclear.

As the dissolved products of EW enter rivers, they combine with the baseline flux of natural weathering DIC and can potentially alter the river chemistry. Whether a river can accommodate the additional EW products depends on the change in calcite saturation index (SI_{calc}) of the water in response to EW products, following Equation 1.18 (Zeebe and Wolf-Gladrow, 2001)

$$SI_{calc} = log(\frac{\gamma_{Ca} * \gamma_{CO_3}}{K_{sp}}) \quad (1.18)$$

Where K_{sp} is a temperature and pH dependent constant, and Ca and CO_3 are the activities of Ca and CO_3^{2-} respectively. When $SI_{calc} > 0$, the water is saturated with respect to calculate, and carbonates may precipitate. If rivers already transport a substantial baseline flux of DIC from natural weathering, they might be nearing or exceeding saturation. In such instances, they might lack the capacity to accommodate a significant amount of EW products.

Globally, using riverine natural SI_{calc} and geochemical data, it has been demonstrated that rivers could accommodate between 7-21.3 Gt CO_2 of EW derived DIC before carbonate precipitation would be significant (Zhang *et al.*, 2022). However, the capacity of UK rivers to accommodate EW- derived material depends on specific catchment parameters within the UK. These include the quantify of arable land in the catchment land (and the EW spreading rate adopted on this land), determining the potential flux of material to rivers, as well as the natural baseline flux of weathering derived DIC in the river. This thesis will explore these parameters in line with the research objectives outlined in the section below.

1.8 Thesis Research Objectives

This research aims to provide knowledge which could facilitate possible pursuit of EW as a CDR practice in the UK. To meet this aim, the following main research objectives were identified:

Research Objective One: *A first estimate of the annual quantity of carbon dioxide removal (CDR) due to natural weathering in the UK*

This was considered essential for comparing baseline weathering levels with those proposed by enhanced weathering. This objective was achieved through the following research goals:

1. Explore the spatial and temporal variation in chemistry at catchment scale by conducting a two-year sampling campaign of two major UK catchments (the Severn and the Thames)
2. Use the river chemical data gathered from sampling activities alongside historical datasets to quantify the flux of solutes originating from weathering processes in the UK.
3. Assess the potential significance of strong acids in reducing the amount of CDR attributed to weathering processes
4. Explore whether secondary carbonate precipitation, cation exchange and the alkalinity of seawater may impact the potential maximum values.
5. Determine the primary environmental drivers of weathering, and in doing so identify optimal zones for weathering across the UK.

Research Objective Two: *Explore the impact of EW applications on UK river calcite saturation*

This objective was considered important because, despite the potential to decrease the CDR potential of EW, at this studies onset, prior research had largely overlooked how EW might impact the calcite saturation of rivers, and the possibility of carbonate precipitation. This objective was achieved by:

1. Evaluating the potential alterations in the chemistry of UK rivers if solutes added to soils at typical application rates (10-50 t ha^{-1}) were to reach the river.
2. Establishing the threshold calcite saturation index required for carbonate precipitation using river water and carbonate precipitation experiments
3. Estimating the extent of carbonate precipitation likely across multiple UK catchments
4. Assessing the potential impact of silica saturation on restricting the transport of EW-derived products to rivers
5. Quantifying the reduction in CDR attributed to secondary precipitation in UK rivers
6. Determining the optimal locations for the adoption of EW in the UK

Chapter 2

2 Extended Methodology

2.1 Introduction to the methods utilized in this thesis

The main objective of this thesis was to quantify the atmospheric CO_2 drawdown due to both natural and enhanced weathering in the UK and investigate how this might vary across the UK. Additionally, it aimed to assess the processes responsible for lowering this flux, such as strong acid weathering or secondary carbonate precipitation in rivers. This Chapter outlines the methodologies used to address this aim and the broader research objectives stated in Chapter 1.

The aim of Chapter 3 is to assess natural weathering variations in two major UK catchments- The Severn and the Thames. For this aim, an extensive sampling campaign along the main stem and major tributaries was conducted over two years for the Severn, and one year for the Thames. The assessment involved on- site pH and temperature measurements, followed by the collection and analysis of alkalinity (Section 2.2.2), major and trace cations and anions using auto-titration, ICP-MS (inductively Coupled Plasma Mass Spectrometry, Section 2.2.4) and IC (Ion Chromatography, Section 2.2.3) methods respectively. Chapter 3 then employed the MEANDIR model (Mixing Elements AND Dissolved Isotopes in Rivers) (Section 2.2.4) to attribute the river chemistry from the sampling campaigns to distinct catchment sources, such as rock weathering, rainfall and human activity. The aim of Chapter 4 was then to quantify CDR across the UK. I do this by utilising MEANDIR alongside UK historic environmental datasets from the Environmental Agency (Section 2.4.2) to examine weathering fluxes across UK catchments and estimate the total annual CO_2 flux resulting from natural weathering processes in the UK.

The aim of Chapter 5 was to assess the response of UK rivers to the addition of crushed alkaline silicate rock to the arable cropland within the catchment. I performed some carbonate precipitation beaker experiments to assess the SI required for significant carbonate precipitation (Section 2.2.5). The results of the experiments were fed into the geochemical

model PHREEQC to predict the potential for riverine secondary carbonate precipitation of the products of EW (Section 2.3) and hence quantify the overall reduction in carbon dioxide removal (CDR) efficiency.

2.2 Geochemical analytical methods

2.2.1 Sample collection and preservation

Prior to the field campaigns, the sample bottles were prepared following standard cleaning procedures. Briefly, HPDE 60 ml bottles for major and trace cations were first rinsed in ultra-pure (18Ω (MQ)) water, and then left overnight in a 2% HNO_3 solution. The bottles were then rinsed again with MQ water and dried in a clean lab fume hood. Amber HDPE bottles for anion and alkalinity collection were rinsed with MQ water only and allowed to dry. These were then stored in ziplocked bags to prevent contamination.

Sampling sites (for Chapter 3) were chosen near flow monitoring stations where possible so that fluxes could be calculated from concentration and discharge data. Sites were also chosen in locations upstream of any major tributaries, to prevent any backflow impacting the chemical signature of the sample.

The pH and temperature of the river water was measured at the site. Samples were 'spot collected' from an accessible, but flowing region of the river. The sampling vessel was first rinsed in the site's river water three times before the river sample was collected. The river water was then filtered immediately to 0.2 μm for all cation, anion, and alkalinity samples, using PES membrane filters and syringes that were pre-rinsed in the site water. Sample bottles were filled to the brim to ensure no CO_2 degassing post collection. In a metal free laboratory, samples for cation analysis were acidified to 2% HNO_3 using concentrated nitric acid (70% HNO_3), within a week of return from the field. Samples were then stored in cold conditions (~4 °C) until analysis. Alkalinity analyses were performed within one week of returning to minimise chance of alteration due to secondary carbonate precipitation.

2.2.2 Alkalinity

Solution alkalinity was measured for 155 filtered river samples and 48 experimental samples in Chapters 3 and 5 respectively. Alkalinity was measured using a Metrohm Ti-Touch auto-titrator in the Oxford Department of Earth Sciences. Before use, the auto-titrator eco-vessel was rinsed three times with deionized water and dried using Kim-Wipes, and the associated pH probe was calibrated using pH 4, 7 and 10 calibration fluids. If the pH probe calibration was outside an acceptable range (~96%) then the fluids would be replaced, or the pH probe topped up with KCl.

For measurements, a 2-3 mL aliquot of sample solution was pipetted into the auto-titrator eco-vessel. The mass of this sample aliquot was measured to 5 significant figures and recorded in the interface of the auto-titrator. The temperature and initial pH of the solution was also recorded, and a magnetic stirrer was inserted into the sample. The auto-titrator then incrementally added 0.01N HCl titrant into the eco-vessel until the solution reached a pH of 2.9, at which alkalinity was obtained by finding the second equivalence point of titration.

To test the precision of the alkalinity measurements, a certified reference standard (CRS) solution of 10 mmol L^{-1} $CaCO_3$ was repeatedly tested. The percentage difference between the measured alkalinity and the actual alkalinity of the CRS averaged 0.19%. The replicated measurements are given in (Appendices, Table A.1). The CRS was also tested daily before commencing measurements, and then after every 10 samples, to ensure no loss in experimental precision. If the measured alkalinity of the CRS drifted outside the range considered acceptable for this study (± 0.1 mmol L^{-1}), corrective measures were taken. Drift in precision could often be corrected by checking for any errors in the titration setup, i.e.,

i) Ensuring that any variation in temperature was accurately input into the auto-titrator interface,
ii) Checking that the magnetic stirrer was free to mix the solution adequately,
iii) By re-calibrating pH probe and replacing calibration fluids if necessary,
iv) Or by replacing the standard or acid titrant.

2.2.3 Ion Chromatography

Concentrations of major anions (sulphate, nitrate, nitrite, phosphate, bromine, chloride, and fluoride) in solution were measured using Ion Chromatography (IC) in the Oxford School of Geography and the Environment. 155 river water samples and 4 experimental samples were measured for Chapters 3 and 5 respectively.

In the IC laboratory, the conductivity of each filtered sample was measured using a handheld conductivity meter. A small aliquot of each sample was then pipetted into a 10 mL sample vial and diluted with Milli-Q ultra-pure water to the required conductivity of between 50-100 ppm. An eluent solution was prepared using a certified reference solution of 1000 mg L^{-1} Na_2CO_3 and $NaHCO_3$. The reference solution was added to a PES container and diluted to 10 mg L^{-1} using Milli-Q water. The eluent was then placed in a sonic bath for 30 minutes to degas the solution and prevent pressure decreases during the run which may impact the IC machine function.

Five standard solutions were prepared to 1, 2, 5, 10 and 20 mg L^{-1} using individual 1000 mg L^{-1} certified reference solutions of SO_4^{2-}, PO_4^{3-}, NO_3^-, NO_2^-, Cl^-, $B^-$and F^-, and Milli-Q ultra-pure water. These solutions were run to generate a calibration curve that plots the peak areas of each of the standard ions against each of their known concentrations. This curve is used by the chromatography data software to quantify concentrations of ions within the sample solutions by comparing the ion's peak areas to those within the calibration curve (Campbell *et al.*, 2023). The results of the standard solution measurements were on average 1.46% (0.07-3.1%) from the expected values. To account for the initial conductivity dilutions, results of the analyses were then corrected by multiplying by the dilution factor to obtain final concentrations. Duplicate IC measurements were taken on one sample for each IC run to assess instrument precision. On average, there was a 2.2% (0.34-4%) difference between the duplicate measurements for each analysed anion. However, there was a notably high percentage difference (48%) in one duplicate measurement for fluorine (F), attributed to potential instrument error owing to its very low concentrations.

2.2.4 ICP-MS

The concentrations of dissolved major (Ca, Mg, Na, Si, K) and trace (Li, Sr, Mn, Fe, Al, Zn, Ni, Cu and Ba) cations in river and experimental waters were measured using a PerkinElmer NexION 350 Inductively Coupled Plasma Mass Spectrometer (ICP-MS) in the Oxford Earth Science Department. To create the calibration curves needed for quantifying elemental concentrations from detector signals, calibration standards were externally prepared from certified solutions (Merck Centipur ICP Standards). These standard solutions were diluted to reflect ion concentrations approximating river chemistry. Internal standards (Rh, Ir and In) were added to all the samples, blanks, and standards to correct for any drift of the machine.

A certified reference material for trace metals in river water (SLRS-6) was analysed to assess the accuracy of the ICP-MS measurements. Analytical uncertainty between the certified value and the results of the analysis averaged 3.5%, however the uncertainty varied for individual elements. The average uncertainty for major elements was 1.7% (Ca), 4.5% (Mg), 5.8% (Na), 3.7% (Si) and 7.7% (K). For trace elements, the average uncertainty was 5.2%.

2.2.5 Carbonate precipitation experiments

River water carbonate precipitation experiments were carried out to determine the saturation level required for carbonate precipitation in UK rivers (see Section 5.4, Chapter 5). In these experiments, additional alkalinity (Ca^{2+}, Mg^{2+}, Na^{+} and K^{+}) was added to natural river water from the River Severn and the River Thames, and the impacts on the geochemistry of the dissolved and suspended load was assessed. As the main objective of Chapter 5 was to consider the impact of EW applications on riverine chemistry, the added alkalinity aimed to represent the addition of basalt derived alkalinity.

Approximately 10 L of unfiltered river water was collected from an accessible but flowing area mid-way along the River Severn and the River Thames, at Hampton Loade and Wallingford respectively (Appendices, Figure D1). The pH and the temperature of the water were immediately tested when sampled. Aliquots of the river water were filtered to 0.2 μm to test the natural alkalinity (Section 2.2.2) and initial cation and anion concentrations (using ICP-MS and Ion Chromatography respectively, Section 2.2.4 and Section 2.2.3). The collected water

was then stored in cold conditions (~4 °C) for 1-2 weeks until the commencement of the experiments.

In the laboratory, separate concentrated solutions of alkalinity (Solutions A and B) were prepared in two clean 1L glass containers. The concentration of the solutions aimed to mimic the stoichiometry of Ca, Mg, K and Na in a basalt of average composition (given in Appendices for Chapter 5, Table D.3). In solution A, 10.2903 g of hydrated calcium chloride ($CaCl_2.2H_2O$) and 14.0565 g of hydrated magnesium chloride ($MgCl_2.6H_2O$) were dissolved into 500 mL Milli- Q water to achieve a Ca^{2+}: Mg^{2+} molar ratio of 1.01:1 (i.e., 140 mmol L^{-1} Ca^{2+} and 138.3 mmol L^{-1} Mg^{2+}). In solution B, 9.5395 g and 0.3779 g of powdered Na_2CO_3 and K_2CO_3 were dissolved into 500 mL of Milli-Q water to achieve a concentration of 180 mmol L^{-1} Na^+ and 5.47 mmol L^{-1} K^+. Excess Na^+, which drove the molar ratio of Na: K in Solution B to greater than that of basalt (4.02:1), was added to balance the negative charge caused by the excess Cl^- in solution A.

The collected unfiltered river water was then distributed into 5 × 500 ml conical beakers, which were placed on a magnetic multi-stir plate to represent flowing river conditions. The two concentrated solutions were added to the beakers to represent the addition of basalt derived alkalinity to river water under the two EW scenarios discussed in Chapter 5 (Scenario 1- the maximum riverine alkalinity increase caused from the complete dissolution of 10-50 t ha^{-1} of basalt applied to arable land in both catchments, Scenario 2- minimum alkalinity release from silica limitations to basalt dissolution). The volume of Solution A and B added to each beaker was calculated using Equation 2.1, i.e.-

$$C_f V_f = C_i V_i + C_A V_A + C_B V_B \quad (2.1)$$

where $C_i V_i$ is the concentration and volume of the initial river water before addition, $C_A V_A$ is the concentration and volume of solution A, $C_B V_B$ is the concentration and volume of solution B, and $C_\mathrm{f} V_\mathrm{f}$ is the final concentration and volume once the solutions were added. The calculated volumes are given in (Appendices: Table A.2 (Thames) and Table A.3 (Severn)

The water was then left on the multi-stir plate for 4 days (Severn) and 5 days (Thames), a duration which Worrall *et al.*, (2014) calculated as the mean residence time for water within the two rivers. During this period, alkalinity and pH were tested daily. At the end of the

experiment, a final sample was collected from each beaker and filtered for cation analysis, and the remaining 450 ml of water was filtered to collect any accumulated precipitate. The filtered sediments were oven dried at 40 °C, and then weighed on a microbalance to five significant figures. To account for the mass of the filter, this was initially weighed and subtracted from the combined mass of the filter paper and accumulated precipitate. Further, to account for the natural suspended sediment within the river, the mass of the suspended sediment collected on the filter of the control beaker (to which no alkalinity was added) was also subtracted from the mass of the other beakers.

To analyse the composition of the precipitate, the sediment was scraped from the filter and placed in a centrifuge tube to homogenise the sample. A 10 mg aliquot of the precipitate was retained from each centrifuge tube for X-ray diffraction (XRD) to determine bulk mineralogy (provided in Appendices for Chapter 5, Table D.6). The remaining sediment was then dissolved using concentrated nitric acid which was then diluted to 2% HNO3 with Milli -Q water. The diluted acidified sample was then filtered to remove any silicate material present, and then analysed with ICP-MS to determine the concentration of cations present in the solid precipitate.

2.3 PHREEQC

The geochemical model PHREEQC (version 3) (Parkhurst and Appelo, 2013) and database minteq.v4.dat, was used in all chapters to calculate the solution calcite saturation index ($SI_{Calcite}$), the carbonate speciation, predict the amount of secondary carbonates expected to precipitate at the calculated $SI_{Calcite}$, and assess the charge balance of the solution.

First, an assessment of the quality of the results obtained from alkalinity, ICP-MS and IC was made using the percentage error in charge balance obtained from inputting the concentrations derived from ICP-MS, alkalinity, and IC techniques into PHREEQC, i.e. Equation 2.2:

$$\%\ Error\ in\ charge\ balance = 100 * \frac{|cat-an|}{\frac{cat+an}{2}} \quad (2.2)$$

Where cat = total cation concentration (mmol L^{-1}), and an= total anion concentration (mmol L^{-1}). Any samples with a percentage error higher than 5% were re-analysed or discarded. Four of the initial IC anion measurements were re-analysed with the second round of water samples, as they recorded a charge balance percentage error in PHREEQC >5%. High error was first attributed to the IC (over ICP-MS or alkalinity) due to the higher potential in human error during sample preparation (i.e., pipetting errors during conductivity dilutions). Consequently, the results from the second batch of measurements led to percentage errors in charge balance of <5%.

The solution calcite saturation state is calculated in PHREEQC using Equation 2.3, which relates the activities of Ca^{2+} and CO_3^{2-} in solution to the equilibrium constant (Ksp) for calcite precipitation, i.e.-

$$SI_{Calcite} = log\left(\gamma Ca^{2+} * \gamma CO_3^{2-} / Ksp\right) \qquad (2.3)$$

The value of the equilibrium constant depends on temperature and ionic strength and is determined in PHREEQC from calculating the activities of ions in the input solution.

To predict the amount of possible carbonate precipitation in UK rivers due to the addition of crushed silicates to UK agricultural farmland (Chapter 5) in PHREEQC, the variable 'EQUILIBRIUM_PHASES' was used. Inputs into the EQUILIBRIUM_PHASES variable included: the phases assessed (calcite, Mg-carbonate, and magnesite), the expected saturation at which precipitation occurs ($SI_{Calcite} > 1$) and the initial amount of solid phase present in the solution (which is only of importance if assessing possible carbonate dissolution). Following the experimental results and assessment of natural river $SI_{Calcite}$ in Chapter 5, precipitation was only predicted once the solution reached a $SI_{Calcite} > 1$.

2.4 MEANDIR

Chapters 3 and 4 utilise a geochemical model called MEANDIR (Mixing Elements And Dissolved Isotopes in Rivers) to estimate the flux of dissolved ions from silicate and carbonate

sources in UK rivers. MEANDIR is an open- source MATLAB based code developed by Kemeny and Torres, (2021). It was designed to allocate dissolved solutes in rivers to their source endmembers via a Monte Carlo inversion technique, drawing from methods initially applied to river chemistry by Gaillardet *et al.*, (1999). This technique has been extensively utilised in various studies to examine natural silicate and carbonate weathering fluxes across local and global catchments (Gaillardet *et al.*, 1999; Moon *et al.*, 2014; Burke *et al.*, 2018; Bufe *et al.*, 2021). However, the outcomes of the inversion heavily rely on the parameter inputs, underscoring the importance of justifying each choice thoroughly. This section provides a brief overview of the model's underlying concepts, followed by an assessment of parameter choices influencing the inversion outcomes. Specific adaptions made for each chapter will be detailed in the respective chapters.

2.4.1 Introduction to the model

To partition major elements (X) into their source endmembers, MEANDIR uses mixing equations in the form of Equation 2.4 which relate normalised elemental concentrations in river water ($^{X}/_{Na_{river}}$) with the chemistry of each endmember ($^{X}/_{Na})_i$:

$$^{X}/_{Na_{river}} = \sum(^{X}/_{Na})_i * \propto Na_i \quad (2.4)$$

$$\propto Na_{silicate} + \propto Na_{carbonate} + \propto Na_{evaporite} + \propto Na_{rain} = 1 \quad (2.5)$$

X refers to the dissolved ions chosen to be included in the inversion. This study uses X = Ca^{2+}, Mg^{2+}, Cl^{-}, and Na^{+}. K^{+} is not included in the inversion due to the increased possibility of contamination from an anthropogenic endmember (i.e., K-rich fertilizer). However, K^{+} concentrations in all UK rivers examined throughout Chapters 3 and 4 are consistently an order of magnitude lower than Ca^{2+}, Mg^{2+}, and Na^{+}- typically constituting less than 3% of the total cation flux in all rivers (see Table 4.1, Chapter 4). Consequently, disregarding K^{+} is assumed to have minimal impact on the overall weathering derived atmospheric carbon dioxide removal (CDR) flux calculations performed in Chapters 3 and 4. X is normalised with respect to a

certain element (Equation 2.4), to account for variability in absolute concentrations due to dilution or evaporation. Sodium (Na^+) is commonly used as a normalising ion and here, Na^+ is used following the approach of Burke *et al.*, (2018).

i refers to the endmembers which have contributed to the river chemistry- typically silicate, carbonate, evaporite and rain, although other endmembers, such as anthropogenic sources, could be added. Because of the chemical complexity of the anthropogenic endmember, this endmember is dealt with separately by assessing the impact on each main element independently (mainly SO_4^{2-}, NO_3^- and Cl, see Chapter 3 and 4). Therefore, in this study, the endmembers considered are i =silicates, carbonates, evaporites and rain (discussed in detail in Section 2.4.3.2). $\propto Na_i$ is the proportion of riverine Na from each endmember i, the sum of which should Equal 1 (Equation 2.5).

Before running MEANDIR, the river chemistry (Section 2.4.2) and endmember chemistry (Section 2.4.3.2) are collated and input into excel spreadsheets. MEANDIR will then perform a Monte Carlo inversion simulation individually for each chemical data point in the river chemistry spreadsheet. The simulation iterates through the mixing equations (Equations 2.4 and 2.5) for a predetermined number of iterations set by the user (This study set this as 10,000). The endmember chemistry is not precisely known and is given as a range rather than discrete values (see Section 2.4.3.2 for the discussion on endmembers). Therefore, for each of the 10,000 runs of a simulation, values are randomly selected from this range and fed into the mixing equations. The user can choose whether the model selects an endmember value over a uniform or normal distribution, with the latter favouring selections closer to the mean (explained in Section 2.4.3.2). The mixing equations are then solved to find a series of fractions: $\propto X_i$, the fraction of each solute from endmember i.

A cost function is then employed to evaluate the outcomes of all 10,000 runs (Section 2.4.3.1), to find the best-fit result. This aims to identify the run that most accurately replicates the initial chemistry, and this determines the final output of the inversion. The best fit fractions $\propto_{X_i}$ are output into a folder for each datapoint at the end of the inversion.

These fractions are used in Chapter 3 and 4 to find the concentration of each solute from each endmember (Equation 2.6) and flow weighted flux of each solute (Equation 2.7). The silicate and carbonate fluxes are then employed in subsequent calculations to calculate the total amount of atmospheric CO_2 removed due to natural weathering (discussed in more detail in Chapters 3 and 4).

$$X_i\ (mol\ L^{-1}) = X_{river} * \propto_{X_i} \quad (2.6)$$

$$X_i\ (mol\ s^{-1}) = X_i * discharge\ X_i\ (mol\ s^{-1}) = X_i * discharge \quad (2.7)$$

After the Monte Carlo inversion has distributed the major cations between their source endmembers, a simple conservative mixing model within MEANDIR distributes a fraction of the riverine SO_4^{2-} to each of the endmembers ($SO_4^{2-}{}_i$):

$$SO_4^{2-}{}_i = \left(SO_4^{2-}/_{Na}\right)_i * \propto_{i(Na)} \Big/ \left(SO_4^{2-}/_{Na}\right)_{river} \quad (2.8)$$

$\left(SO_4^{2-}/_{Na}\right)_i$ is the molar ratio for each endmember i, $\propto_{i(Na)}$ is the proportion of Na from each endmember (calculated previously in the inversion) and $\left(SO_4^{2-}/_{Na}\right)_{river}$ is the molar ratio of the river water. Sulphate is dealt with separately post inversion due to the possibility of a portion of the SO_4^{2-}being derived from an endmember not included within the study. By not including alternate sources of SO_4^{2-} within the mixing model, an 'excess' of SO_4^{2-} ($X_{excess\ SO_4^{2-}}$) will remain which cannot be attributed to the endmembers (Equation 2.9):

$$X_{excess\ SO_4^{2-}} = X_{river\ SO_4^{2-}} - \sum\left[SO_4^{2-}{}_i\right]^n \quad (2.9)$$

$\sum\left[SO_4^{2-}{}_i\right]^n$ is the sum of contributions of sulphate from each endmember (i), and n is the number of endmembers (4). This remaining excess riverine SO_4^{2-} ($X_{excess\ SO_4^{2-}}$) will be a combination of SO_4^{2-} sourced from volcanic atmospheric deposition, biogenic emissions, and anthropogenic pollution. Additionally, SO_4^{2-} from the oxidative weathering of pyrite can be incorporated within $X_{excess\ SO_4^{2-}}$ by selecting a low silicate endmember $\left(SO_4^{2-}/_{Na}\right)_{silicate}$ value which represents that of silicate minerals not sourced from pyrite. This study uses $\left(SO_4^{2-}/_{Na}\right)_{silicate}$ = 0.019, from (Burke *et al.*, 2018). Chapters 3 and 4 will discuss the use of

$X_{excess\ SO_4^{2-}}$ to quantify how much weathering may be attributed to sulphuric acid derived from the oxidative weathering of sulphides.

2.4.2 Solute chemical data for UK rivers

Riverine chemical data was first collected and organised into an excel spreadsheet formatted specifically for MEANDIR. For Chapter 3, riverine chemistry was obtained from a combination of sampling completed as part of this study (i.e. Section 2.2.1) and historic data from the Environmental Agency providing a longer period of timeseries sampling of mainstem and tributaries of the Severn and Thames: the Harmonised Monitoring Scheme (HMS) dataset (DEFRA, 2013). For Chapter 4, historic data from the HMS dataset was collated for 52 UK catchments representing 39% of the total land area of the UK (further discussed in Chapter 4). Analytical error was also accounted for in the formatted spreadsheet. For the timeseries sampled dataset, the average uncertainty from the IC (Section 2.2.3) and ICP-MS (Section 2.2.4) measurements was used (1.5% and 3.5% respectively). Analytical uncertainty was not provided within the HMS dataset, and so a 5% error was apportioned to all historic measurements, which is typically within the range of usual uncertainty in IC and ICP-MS measurements.

2.4.3 Model Selections

Several parameters can influence the inversion results, necessitating thorough justifications for each selection made. Key factors affecting the inversion results include the selection of cost function (Section 2.4.3.1), and the endmember choice and distribution pattern (normal or uniform) of these endmembers (Section 2.4.3.2): particularly the treatment of the rain endmember (point i), and the choice of the silicate endmember (point ii). In this section, a brief explanation is provided for each choice, and the reason for each choice. Subsequently an analysis is conducted to assess how each of these choices impact the overall calculations for the silicate and carbonate derived CDR of a catchment- the aim of Chapters 3 and 4.

2.4.3.1 Cost function

Each inversion iteration produces fractions representing the contribution of individual endmembers to the overall riverine concentration of each element X (where X= Ca^{2+}, Mg^{2+}, Cl^{-} and Na^{+}). The objective is to ensure that the sum of these fractional contributions closely aligns to the initial riverine observations. The cost function is the equation which finds the best-fit iteration results that most closely match the initial river chemistry. It accomplishes this by assigning a 'cost' to each run. For each run, each variable X will be assigned their own individual cost. Two primary methods exist for assigning this cost: an 'absolute' cost function that distributes this cost equally amongst variables based on the absolute value difference between the results and the inversion, and a 'relative' cost function, in which the cost is distributed dependent on the proportional difference of each variable from the river observations.

A relative cost function becomes important when one or more variables exhibit notably lower riverine concentrations. Kemeny and Torres, (2021) show this by comparing how absolute and relative cost functions would assign the cost to the results from two hypothetical iterations (Run 1 and Run 2, Table 2.1). They show that an absolute cost function would assign the cost of each of these two runs equally, since both Run 1 and Run 2 are a value of 1 away from the observations. However, a relative cost function would assign a lower cost to Run 1, based on the lower overall proportional difference in the results (Table 2.1).

Table 2.1- (From Kemeny et al 2021). Given the river observation Ca/Na and K/Na and the results from two hypothetical runs (Run 1 and Run 2), Table 2.1 demonstrates the difference between how absolute and relative cost functions would assign cost.

	Ca/Na	K/Na
River observation	10	1
Run 1	11	1
Run 2	10	2
Absolute	Equal	
Relative run 1	10%	0%
Relative run 2	0%	100%

In this study, the variables used in the inversion are X= Ca^{2+}, Mg^{2+}, Na^{+} and Cl^{-}. While river chemistry exhibited variability, the typical order of abundance was $Ca^{2+} > Na^{+} \approx Cl^{-} > Mg^{2+}$. Mg/Na_{river} values were typically significantly lower than Ca/Na_{river}. To mitigate potentially erroneous results for Mg^{2+}, a relative cost function was used in this study. A sensitivity test was performed to assess the influence of this cost function choice on the inversion outcomes. Two inversions were performed using the same chemical dataset (The Severn historical HMS dataset, provided in the datasheets in the supporting information). For one of these inversions, an absolute cost function was used, while the other used a relative cost function. All other parameters were kept constant. The results of these inversion were subsequently used in CDR equations (discussed in detail in Chapters 3 and 4) to calculate the total annual CO_2 removed due to natural silicate and carbonate weathering for the Severn catchment. The calculated silicate and carbonate derived annual CDR was only 0.12% and 1.4% higher using the absolute cost function than when using the relative cost function (Table 2.2). Therefore, it is assumed that the use of cost function will not significantly influence the results here.

MEANDIR inversion results for this test are provided in the supporting datasheets in supporting information.

*Table 2.2- Shows the difference in the overall calculated CO_2 consumed due to natural silicate and carbonate weathering in the Severn catchment due to changing the cost function used in the MEANDIR inversion. The chemical dataset used for both runs was the historical dataset for the River Severn (provided in the supporting information). *Run 1 was run using a relative cost function, and is the default used in this study. Run 2 was run using an absolute cost function. All other parameters were kept constant. CDR was calculated using methods described in Chapters 3 and 4.*

	Silicate derived CDR (Mt CO_2 yr^{-1})	**Carbonate derived CDR (Mt CO_2 yr^{-1})**	**Combined CDR**
Relative cost function*	0.662	0.230	0.296
Absolute cost function	0.663	0.233	0.299
% difference	-0.12%	-1.34%	-1.12%

2.4.3.2 Defining the End-Member compositions

Predicting the number of endmembers influencing river chemistry, and assigning a chemical composition to these endmembers, can be challenging due to catchment complexity in bedrock

leading to chemical heterogeneity, and input from anthropogenic sources. Therefore, an estimated compositional range of each endmember is used rather than exact values. This study assumes that anthropogenic influences contribute mostly SO_4^{2+}, NO_3^-, PO_4^{3-}, Cl^- and Na^+, and once corrected for (See point (ii) for correcting for Cl^-, and Chapter 3 for correcting for SO_4^{2+} (Section 3.6.3), NO_3^-, (Section 3.6.4)), the main endmembers contributing to dissolved chemistry in the rivers within the study are: silicate, carbonate and evaporite rock weathering and rain sources. The endmember ranges used in this study are given in Table 2.3. For the carbonate and evaporite endmember, this study uses global ranges defined previously by Gaillardet *et al.*, (1999) and used in other river inversion studies i.e., Moon *et al.*, (2014). The rain endmember is used to correct the river chemistry prior to the inversion to distinguish between rain and evaporites (point (i) below). The silicate endmember is defined using local endmember geology (point (ii) below).

Table 2.3- End members used in the inversion calculations. Silicate endmembers were derived from UK silicate draining rivers (Figure 2.2). Carbonate and evaporate endmembers are global endmembers from Gaillardet et al., (1999) and Moon et al., (2014). The rain endmember represents the average composition of the 'cyclic' endmember- the average composition of rain, which is derived entirely from sea salts, taken from Moon et al., (2014). It is assumed that any other dissolved Ca^{2+}, Mg^{2+} and Na^+ present in rain other than this cyclic endmember will be derived from weathering.

	Silicate		**Carbonate**		**Rain**		**Evaporite**	
	Median	Stdev	Median	Stdev	Median	Stdev	Median	Stdev
Ca/Na	0.669	0.77	60	30	0.023	0.01	0.17	0.09
Mg/Na	0.325	0.27	30	15	0.11	0.01	0.02	0.01
$SO4/Na$	0.019	0.005	0.06	0.03	0.060	0.01	0.4	0.2
Cl/Na	0	0	0	0	1.15	0.1	1	0

(i) Correcting for rain inputs (Cl critical)

Although both rain and evaporites are included within the endmember list, the inversion simulation may not correctly apportion solutes between the two sources due to their similar Cl/Na values (Table 2.3) (Kemeny and Torres, 2021). Therefore, independently estimating the

proportion of riverine Cl^- from rain ($Cl_{critical}$) prior to the inversion can increase the ability of MEANDIR to interpret the river chemistry.

$Cl_{critical}$ (in µmol L^{-1}) can be calculated by multiplying the concentration of Cl^- in rain with the catchment's evapotranspiration factor, which can be captured by the ratio between total annual rainfall divided by discharge (Equation 2.8):

$$Cl_{critical} = Cl_{rain} * \frac{Annual\ rainfall}{Annual\ discharge} \quad (2.10)$$

To derive Cl_{rain}, UK precipitation chemistry was acquired from the Environmental Change Network Precipitation Chemistry dataset (ECN, 2015). In Chapter 3, the mean Cl^- concentration in rain (Cl_{rain}) was taken from ECN site measurements closest to the Severn and Thames catchments: Snowdon for the Severn, and Wytham, near Oxford, for the Thames (ECN, 2015). In Chapter 4, the rain chemistry in both datasets was collated and the mean Cl^- concentration was used for Cl_{rain} in catchment calculations for $Cl_{critical}$ ($Cl_{rain} = 116.5$ µmol L^{-1}). Average daily rainfall (mm) and flow rate ($m^3\ s^{-1}$) were taken from the National River Flow Archive (NRFA, 2023) for each catchment included in Chapters 3 and 4. This was converted to L yr^{-1} $catchment^{-1}$ (Table 2.4). The $Cl_{critical}$ value derived from these data sources was then used with the rain endmember (Table 2.3) in MEANDIR to derive the portion of other elements from rain.

Table 2.4- Rainfall data and catchment characteristics from the Severn and the Thames- used to equate the $Cl_{critical}$. Average discharge and annual precipitation were taken from the National River Flow Archive (NRFA, 2023). Chemical data was obtained from the Environmental Change Network (ECN, 2015). $Cl_{critical}$ values given in table are then used in the inversion for both the River Severn and Thames.

	Severn	**Thames**
Median Cl^- concentration in Rain	90 µmol L^{-1}	63 µmol L^{-1}
Annual discharge (median)	3.38×10^{12} L yr^{-1}	2.06×10^{12} L yr^{-1}
Annual Precipitation (median)	9.26×10^{12} L yr^{-1}	1.17×10^{12} L yr^{-1}
Evapotranspiration factor	2.74	5.66
$\boldsymbol{Cl_{critical}}$	242 µmol L^{-1}	358 µmol L^{-1}

The remaining Cl^- in the river ($Cl_{remaining} = Cl_{river} - Cl_{critical}$) is then assumed to originate from either evaporites or pollution. Sources of pollutive Cl^- to river water include sewage and wastewater inputs, road salts, and certain agricultural fertilizers (Berner and Berner, 1996). While evaporites and rain exhibit similar Cl/Na ratios (1 and 1.15 respectively), anthropogenic sources typically have much higher ratios (Moon *et al.*, 2014). This implies that if there was a significant input of anthropogenic Cl^- into rivers, the Cl/Na ratio would surpass ($Cl/Na > 1.15$).

The historical Cl/Na trend analysis of the Severn and the Thames catchments indicates that the majority of Cl/Na values cluster around or below the 1.15 value (Figure 2.3). However, infrequent spikes in Cl^- cause 6% (Severn) and 3% (Thames) of the data to exceed this value. To ensure that the anthropogenically sourced Cl^- does not impact the weathering fluxes calculated by the inversion, this study follows Moon *et al.*, (2014) and discards any data points (in both Chapters 3 and 4) with a $Cl/Na > 1.15$.

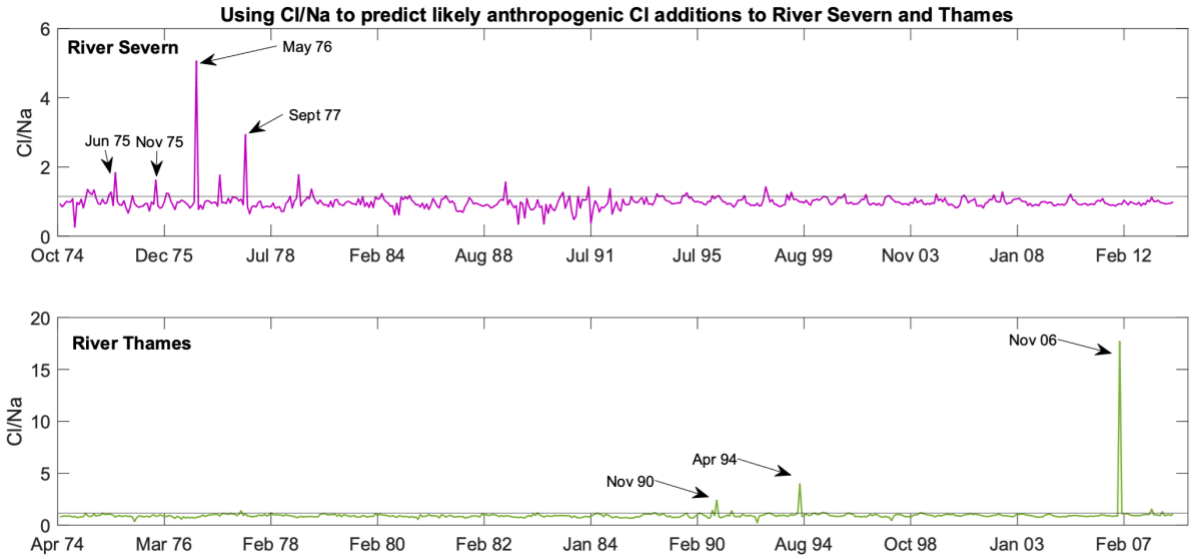

Figure 2.1- Variations in Cl/Na ratios of the River Severn and Thames to assess anthropogenic input of Cl^-.

The impact of using the $Cl_{critical}$ value in the inversion was tested by running two inversions on the historic data for the River Severn; one treating rain as a separate endmember in MEANDIR, and the other using the calculated $Cl_{critical}$ values, keeping all other parameters constant. The percentage difference in calculated carbon dioxide removal from silicates and carbonates differed by 7.7% and 2.0% respectively (and the combined impact differed by 3%), with $Cl_{critical}$ values resulting in the higher values (see datasheets in supporting information). Because $Cl_{critical}$ values are calculated using known river discharge, rain chemistry and rainfall data, it is assumed that these will lead to more accurate estimates for Cl_{rain}, and therefore this study chooses this method for correcting for the rain endmember.

(ii) Silicate endmember

The compositional range in the silicate endmember can vary based on the types of silicate rocks present in the catchment, (e.g., primary rocks of volcanic origin or secondary silicates). Consequently, utilising a global average (as in Gaillardet *et al.*, 1999) may not accurately represent UK lithologies. Moreover, silicate minerals typically undergo non- stoichiometric

weathering, resulting in discrepancies between river dissolved load chemistry and the actual bedrock lithology (Gaillardet *et al.*, 1999). In an attempt to encompass the diversity of UK silicate lithology and account for the non- stoichiometric weathering behaviour of silicate minerals, this study, following Gaillardet *et al.*, (1999), estimates the local silicate endmember by analysing the chemical loads of four small UK catchments exclusively draining silicates (River Fal, Fowey, Carnon and Wick). These catchments encompass a variety of silicate rock types (muds, sands and siltstones, felsic intrusions), making them representative of numerous UK rivers draining silicate materials.

To find the chemical range of the silicate endmember using these catchment data, the dissolved chemistry from these four catchments was first corrected for rain inputs and anthropogenic sources of chloride (Cl^-) as introduced above. Briefly, first a filtering of the dataset was employed to identify potential anthropogenic Cl^- inputs to the river chlorine concentration (Cl_{river}). Data with Cl/Na > 1.15 were discarded on the assumption that ratios higher than the evaporite or cyclic endmember indicate an additional anthropogenic source of Cl^-. Discarded datapoints did not exceed > 5%, which suggested that anthropogenic Cl^- input may be minimal. Based on geological maps of the catchment (BGS, 2023a), the absence of evaporites in the area was also assumed. Consequently, for the remaining datapoints not excluded due to high Cl^-, it was presumed that Cl_{river} was entirely sourced from rain.

River chemistry was then corrected for cyclic input (sea salts within rain), i.e., Equation 2.11:

$$X_{corrected} = X_{river} - Cl_{river} * X/Cl_{cyclic} \quad (2.11)$$

Where X = Ca^{2+}, Na^+, and Mg^{2+}, and the composition for X/Cl_{rain} given in Table 2.3. Once the cyclic input is removed, it is assumed that the remaining chemical composition of the river water is entirely sourced from silicate lithologies.

The range in Ca/Na and Mg/Na for the Rivers Fal, Fowey, Carnon and Wick were collated, and the average and standard deviation was selected as the silicate endmember for this study (Figure 2.2). The Values for Ca/Na, with a median of 0.67 mol/mol, were similar to those reported in Moon et al 2014 (which ranged between 0.1-1 mol/mol). The median Mg/Na value

was also similar than the globally assumed values of previous work ($^{Mg}/_{Na} =$ 0.25 ± 0.2, and $^{Mg}/_{Na} =$ 0.1-0.6. from Gaillardet *et al.*, (1999) and Moon *et al.*, (2014) respectively).

Although it is assumed that the local geology of these catchments is primarily silicate based, the potential existence of minor carbonate or evaporite inclusions within the lithology cannot be discounted. Although, regional geological maps do not suggest the presence of carbonate or evaporite lithologies in these catchments, even small outcrops of these rock types, known for their increased weathering compared to silicates (Lasaga, 1984) can impact river chemistry. However, the resemblance between the silicate endmember in this study and that in Moon *et al.*, (2014) suggests that the potential impact from these sources might be insignificant here.

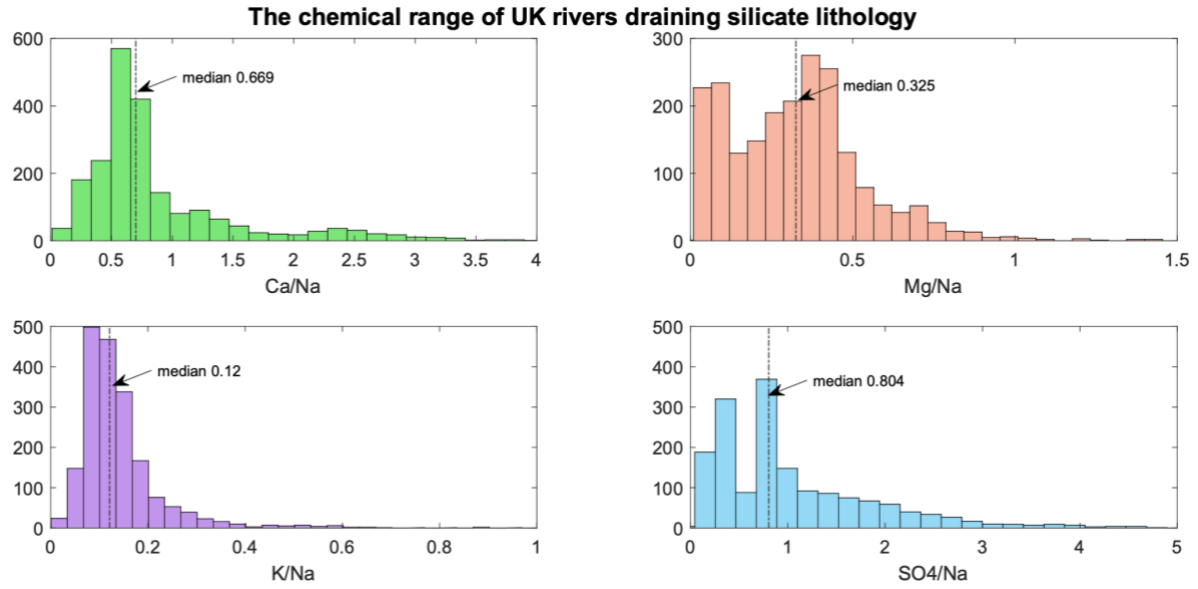

Figure 2.2- Using the chemistry of rivers that drain silicate lithologies to derive the silicate endmember. Histograms represent the chemical range of four UK catchments (Fal, Fowey, Carnon, Wick). The median and standard deviation were used in MEANDIR.

(iii) Distribution of the endmembers (normal vs uniform)

As introduced in Section 2.4.1, the inversion simulation iterates 10000 times, randomly selecting a specific endmember value from the given range for each run to apply in the mixing equations (Equations 2.4 and 2.5). The selection method depends, in part, by the distribution

of the endmembers, i.e. whether they follow a normal or uniform distribution. A normal distribution biases the Monte Carlo simulation towards values closer to the mean, while a uniform distribution equally considers all values within the range.

Because the silicate endmember was selected based on the mean and standard deviation of the river chemistry of the four rivers, a normal distribution was selected here, consistent with Gaillardet *et al.*, (1999). Conversely, Moon *et al.*, (2014) reported their endmembers as minimum and maximum values, around a uniform distribution.

(iv) Endmember Sensitivity Tests

Sensitivity tests were employed to test the impact of the endmember selection on the overall results. Repeated inversion simulations were executed within MEANDIR using the historical HMS Severn dataset. The initial simulation employed the local UK endmembers derived from the four silicate rivers (Table 2.3). Subsequent simulations used the global endmembers from Gaillardet *et al.*, (1999) and Moon *et al.*, (2014). The annual CDR from silicates and carbonates was then computed based on the results of these simulations (Table 2.6).

The sensitivity analysis confirmed that, not only is the selection of the silicate endmember important, but also the distribution chosen. Overall, there is only a 1-3 % difference between the calculated combined CDR (of silicates and carbonates), using the different endmembers- with the local UK endmembers resulting in slightly higher values (Table 2.5). However, there are larger differences between the calculated CDR from silicates.

The difference was the greatest between the results of using local UK endmembers and Gaillardet *et al.*, (1999) (Table 2.5). This is because the silicate endmember from Gaillardet *et al.*, (1999) had a lower mean and standard deviation for each chemical ratio than that used in this study. Because the silicate endmember of Gaillardet *et al.*, (1999) is derived from rivers draining granites and not a range of silicate lithologies, we suggest that using our range better encompass the variety of silicate lithologies in UK catchments.

The CDR calculated using the results from the sensitivity test utilising UK endmembers aligned more closely with the values calculated from Moon *et al.*, (2014). The local UK endmember resulted in a 2.5% higher combined CDR, while the silicate derived CDR was 26% higher, and the carbonate endmember was 3.4% lower (Table 2.5). However, the inversion using Moon *et*

al., (2014) endmembers was run with a uniform distribution, due to the absence of mean and standard deviation data, whereas the baseline inversion using UK endmembers utilised a normal distribution. This difference in distribution selection may have contributed to the observed difference between the two results. To account for this difference, an additional sensitivity test was conducted, this time employing local UK silicate endmember values with a uniform distributional range instead of a normal distribution. This adjustment lowered the silicate CDR (Table 2.5), indicating that at least half of the discrepancy between Moon *et al.*, (2014) and the local endmember CDR can be attributed to the distributional range rather than the endmember values themselves.

Despite a variation in results in the calculated silicate derived CDR, it is noteworthy that all model runs exhibit similar magnitudes of CO_2 removal. It is considered here that the utilisation of UK local endmembers with a normal distribution (Figure 2.2) would more accurately reflect UK lithology than the use of global endmembers. Therefore, despite uncertainty remaining, using UK endmembers still provides a reliable first estimate for CO_2 removal due to silicate weathering in the UK.

These sensitivity analyses highlight the significance of endmember selection when configuring the inversion model runs. To better constrain the UK silicate endmember, the following would be beneficial: (i) a comprehensive database of UK silicate bedrock geochemistry which illustrates the potential variability in values across the UK, and (ii) a predictive model assessing the impact of non- stoichiometric silicate weathering on river chemistry.

Table 2.5- Outcomes of sensitivity tests for using different endmembers.

Sensitivity run	**EM distribution**	**Sil $MtCO_2\ yr^{-1}$**	**Carb $MtCO_2\ yr^{-1}$**	**Combined $MtCO_2\ yr^{-1}$**
UK Local (Table 2.3)	Normal	0.066	0.23	0.295
Global (Gaillardet *et al.*, 1999)	Normal	0.045	0.24	0.288
Global (Moon *et al.*, 2014)	Uniform	0.051	0.24	0.288
UK Local (Table 2.3)	Uniform	0.057	0.23	0.292

2.4.4 Summary of other parameter choices

A summary of the parameter choices, and the reason behind the choices can be found in Table 2.6. Detailed information into the impact of each parameter on the inversion results from MEANDIR can also be found in Kemeny and Torres (2021).

Table 2.6- MEANDIR inversion parameter choices used in this study, and the justification for each choice

Parameter	Possible choices	Selection	Reason
Type of cost function	absolute or relative	relative	In relative cost, error is distributed fairly between each variable- absolute cost gives less error to high ratios
End member	Global (defined by previous studies) or local endmembers	Global (carbonate, evaporite), Local (silicate)	Silicate EM is highly variable in the UK
EM distribution	Uniform or normal	normal	Silicate EM is derived using median and standard deviation.
Variables used	15+ choices including isotope ratios	Ca^{2+}, Mg^{2+}, Na^{+}, Cl^{-}	Anthropogenic influence is higher on other elements, such as K^{+}, SO_4^{2-}, NO_3^{-}
Normalisation variable	Ca^{2+}, Na^{+}, sum cations	Na^{+}	To compare with Gaillardet *et al.*, (1999) and Burke *et al.*, (2018).
Error included (charge balance)	85-115% or 1% of misfit	85-115%	Recommended by Kemeny- 1% doesn't always come up with end chemistry which matches the observed

Dealing with rain endmember	Have as an endmember, or use Cl critical values	Cl critical	MEANDIR struggles to determine between rain and evaporite
End members with negative values (i.e. Carb precipitation	Yes or no	No	Secondary carbonates not significant (see chapter 3)

Chapter 3

3 The origin and fate of dissolved inorganic carbon in the Rivers Severn and Thames, UK

Abstract

In the current global effort to reduce carbon dioxide emissions and achieve net zero objectives, it is essential to better understand the inherent natural sources and sinks of atmospheric CO_2 which contribute to a nation's baseline levels. The dissolution of silicate and carbonate rocks contribute to these CO_2 exchanges and can be quantified by investigating the dissolved inorganic carbon and major solute fluxes in rivers. This research investigates the roles of catchment weathering and anthropogenic influences on the solute chemistry of two major UK catchments: the River Severn and the River Thames. The inversion model MEANDIR is applied, using geochemical data acquired through timeseries sampling of both the mainstem and major tributaries of each river between 2019-2021. In conjunction with datasets spanning three decades from the Environmental Agency, this investigation seeks to establish the temporal and spatial patterns of solute chemistry and silicate and carbonate weathering fluxes. Additionally, this study also explores the roles that secondary carbonate precipitation and strong acids play in reducing the overall quantity of atmospheric CO_2 removed by natural weathering.

Results reveal that during the summer months with reduced river flow, there is an increased proportion of cations derived from silicate weathering. Nevertheless, the geochemical composition of both the River Severn and the River Thames are predominately influenced by cations sourced from carbonate dissolution. Assuming no carbonate re-precipitation or involvement of strong acids in weathering, the maximum annual quantity of carbon dioxide removal (CDR) by natural weathering processes in the River Severn falls within the range of

0.24-0.37 Mt CO_2 yr^{-1}, with an average of 22% sourced from silicates. In the Thames, annual weathering-based CDR ranges from 0.19-0.26 Mt CO_2 yr^{-1}, with carbonate weathering contributing most of the flux (94%).

Sulphuric and nitric acids, derived from the dissolution of pyrite and the addition of agricultural fertilizer nitrates, will reduce the maximum value of CDR for both catchments. Using a conservative mixing model, a maximum percentage of 36% and 26% riverine sulphate is sourced from the oxidative weathering of pyrites in the Severn and Thames, respectively. Sulphuric acid weathering may lower the CO_2 drawdown potential by natural weathering by up to 35% and 22% in the Severn and Thames respectively. In contrast, while ~70% of river nitrate was originally derived from fertilizer in the River Severn and Thames, nitric acid weathering in soils only lowers the CDR by 2-3%.

Overall, having corrected for sulphuric and nitric acid dissolution, CDR from natural weathering in the Severn and the Thames catchments are assessed as 0.15-0.23 Mt CO_2 yr^{-1} and 0.14-0.20 Mt CO_2 respectively. Area normalised, this is equivalent to 152-232 CO_2 ha^{-1} yr^{-1} for the Severn and 140-232 kg CO_2 ha^{-1} $yr^{-1}$for the Thames; a comparable rate to the global average yields of larger catchments (~200 kg CO_2 ha^{-1} yr^{-1}, the combined average silicate and carbonate yields calculated from Moon *et al.*, (2014) and Zeng *et al.*, (2019) respectively). Given the typically low runoff and average temperatures observed in the UK, which usually lead to low weathering rates, these findings imply that additional drivers, potentially anthropogenic influences, or extended fluid residence times, may assume a more prominent role in maintaining weathering rates in these two catchments.

3.1 Introduction

Atmospheric carbon drawdown by the dissolution of silicate and carbonate rocks is of global relevance and has been assessed at global and regional scales, using a variety of geochemical tools which link riverine solute geochemistry to bedrock composition (Negrel *et al.*, 1993; Gaillardet *et al.*, 1999; Moon *et al.*, 2014; Bickle *et al.*, 2015; Chen *et al.*, 2022). Natural rock weathering releases solutes as cations (i.e. Ca^{2+}, Mg^{2+}, Na^{+}, K^{+}) into solution and can convert atmospheric CO_2 into its dissolved form (bicarbonate, HCO_3^{-}). This can transfer up to two moles of atmospheric CO_2 per mole of divalent cation released from silicates, and one mole of CO_2 per divalent cation released from carbonate, i.e. (Table 3.1, Equation 3.4 & 3.7). The cations and sequestered carbon will be removed from the site of weathering to rivers via runoff, or deeper flow paths. In this way, weathering contributes ions and dissolved inorganic carbon (DIC) to river water, which is eventually exported from the continents to the ocean. The CO_2 drawdown of carbonate and silicate weathering, however, can be reduced if other strong acids such as sulphuric acid (from sulphide mineral oxidation) and nitric acid (potentially released from nitrogen fertilisers) dissolve rock minerals in place of carbonic acid (Perrin *et al.*, 2008; Torres *et al.*, 2014; Relph *et al.*, 2021). Investigating variations in cation and DIC concentrations in rivers can identify the magnitude and style of weathering within a catchment and assess the net CO_2 drawdown (Gaillardet *et al.*, 1999; Moon *et al.*, 2014; Bickle *et al.*, 2015; Burke *et al.*, 2018).

In the UK context, there have been few assessments of silicate and carbonate weathering fluxes at national level, nor for individual catchments. There has been no quantification of how strong acids may reduce CO_2 drawdown by weathering, despite the likely presence of sulphide minerals in rocks (Spears, 1997) and widespread application of nitrogen-based fertilisers (Defra, 2022). Such baseline weathering estimates are needed to underpin climate mitigation scenarios such as enhanced silicate weathering (see Chapter 5, and Harrington *et al.*, (2023) and could be fed into existing models and CO_2 budgets created to predict enhanced carbon drawdown by these strategies (Renforth, 2012; Kantzas *et al.*, 2022). Previous studies have investigated overall DIC fluxes in UK rivers (Jarvie *et al.*, 2017; Tye *et al.*, 2022). These have revealed that variations in the export of river DIC vary with lithology across the UK and suggest an unequal contribution of carbonates over silicates to weathering fluxes (Jarvie *et al.*, 2017; Tye *et al.*, 2022). In a recent study by Tye *et al.*, (2022), results of regression modelling based on hydrochemistry data demonstrated that riverine DIC concentrations increase in catchments

dominated by carbonates, such as in the southeast of England which is underlain by a Jurassic-Cretaceous chalk.

Here, we address these knowledge gaps by quantifying the spatial and temporal patterns of natural silicate and carbonate weathering within two major UK catchments: the Severn and the Thames. Using water chemistry of the River Severn and the River Thames, derived from timeseries sampling of the rivers and from historic datasets, coupled with the mixing model MEANDIR (Kemeny and Torres, 2021) (see Chapter 2 for full description), the contributions of silicate and carbonate weathering to the overall flux of riverine cations exported to the estuary has been quantified. The results of the inversion are used to explore the temporal and spatial patterns of weathering and estimate the CO_2 removal due to these two weathering processes. These baseline estimates provide a useful comparison between natural CO_2 sequestration, and the predicted carbon dioxide removal (CDR) suggested for different negative emissions strategies, such as enhanced silicate weathering (Chapter 5).

3.1.1 Study catchments and strong acid sources

The Rivers Severn and Thames are two of the UK's largest river catchments. The River Thames has been extensively monitored historically for variations in suspended sediment fluxes (Neal *et al.*, 2006; Bussi *et al.*, 2017) and nutrient levels (Neal *et al.*, 1998, 2012), with nitrate concentration data from the lower Thames extending back to 1868 (Bowes *et al.*, 2018). The River Severn is more data lean, however the headwaters at Plynlimon have been intensively studied for decades, with assessments focusing on various hydrological and water quality parameters, including the effects of forestry on catchment hydrology and water quality (Whitehead *et al.*, 2004; Marc and Robinson, 2007), and investigating localised hydrological variations (Kirchner *et al.*, 2004).

Presently the only estimations for weathering rates within these two catchments is based on the Plynlimon catchment (Shand *et al.*, 2007). $^{87}Sr/^{86}Sr$ isotope ratios were utilised to estimate the Ca^{2+} and Sr^{2+} release rates from rock weathering. These findings indicated an approximate release rate for calcium of 8.5 kg Ca ha^{-1} yr^{-1} and strontium 57 Sr g ha^{-1} yr^{-1}. However, these measurements did not distinguish between carbonate and silicate sources and were limited to the upper headwaters of the Severn catchment. The assessment of natural weathering yields in the River Severn is particularly significant due to planned research in Plynlimon, which aims

to assess the feasibility of Enhanced Weathering (EW) as a CDR method. Similar field trials are scheduled for Rothamsted, an area in the UK characterised by a higher prevalence of carbonate lithology within the Thames catchment.

The net atmospheric CO_2 drawdown by silicate and carbonate weathering is lowered when the reagent involved is not carbonic acid (Table 3.1). The oxidation of sulphides (e.g., from pyrite present in sediments such as shales which are common in the UK; Spears *et al.*, 1999 and Spears, 2015) forms sulfuric acid (Equation 3.1) which, when dissolving carbonate leads to a net source of CO_2 into the atmosphere (Table 3.1, Equation 3.9) (Torres *et al.*, 2014). When dissolving silicates, sulfuric acid neither releases nor consumes carbon (Equation 3.6).

Oxidation of pyrite to form sulphuric acid:

$$4FeS_2 + 15O_2 + 14H_2O \rightarrow 4Fe(OH)_3 + 8H_2SO_4 \quad (3.1)$$

Growing evidence suggests that sulphuric acid may play a significant role in weathering and hence the carbon cycle, particularly in rapidly eroding terrains rich in shales (Torres *et al.*, 2016; Bufe *et al.*, 2021). At large spatial and temporal scales, it has been suggested that the amplified CO_2 drawdown during the Cenozoic uplift of the Himalayas due to increased erosion and silicate weathering was actually in part balanced by an increase in sulfuric acid induced carbonate weathering (Torres *et al.*, 2014). In contrast, relatively little is known about sulphide oxidation in catchments where anthropogenic activities have changed land use and potentially enhanced local erosion (Walling, 1999). In both the Severn and the Thames catchments, pyrite has been found within geological formations (i.e. The Upper and Middle Coal Measures Formations, Severn Catchment; Spears, 2015). Quantifying this involvement is important for calculation of the net CDR due to weathering.

Another important feature of weathering in anthropogenically-modified landscapes such as the UK is the potential for nitric acid, produced from the nitrification of ammonia (Equation 3.2) and ammonium-nitrate (Equation 3.3) fertilizers in soils, acting as the reagent during weathering and, on timescales of <3000 years, may also reduce the CDR of rock weathering (Semhi *et al.*, 2000; Perrin *et al.*, 2008; Barnes and Raymond, 2009; Gandois *et al.*, 2011). In the UK, approximately 118 kg ha^{-1} yr^{-1} of nitrogen rich fertilizer is applied to soils to replenish bioavailable N which is quickly depleted due to the annual harvesting of crops (Defra, 2022).

When the protons created in Equation 3.2 and 3.3 act as the acid source in carbonate weathering, CO_2 is released (Perrin *et al.*, 2008), while there is no impact on carbon for silicate weathering by nitric weathering (Barnes and Raymond, 2009), i.e. Equations 3.9-3.10.

Nitrification of ammonium and ammonium nitrate from fertilizers:

$$NH_4^+ + 2O_2 \rightarrow HNO_3 + 2H_2O + H^+ \quad (3.2)$$

$$NH_4NO_3 + 2O_2 \rightarrow 2HNO_3 + H_2O \quad (3.3)$$

3.2 Calculating the maximum and net carbon dioxide removal from natural weathering

This study quantifies atmospheric CO_2 removal through natural silicate and carbonate weathering in the Severn and Thames basins using river chemistry. Directly quantifying weathering derived CO_2 removal using dissolved inorganic carbon (DIC) concentrations in river water is challenging due to the contribution to DIC from carbonate rock itself during the weathering of carbonates (Equation 3.8). Consequently, this study uses cation chemistry as a tracer for atmospheric CO_2 released as carbonate alkalinity during natural weathering. However, multiple processes can introduce or remove cations in a river, not all of which result in atmospheric carbon dioxide removal (Table 3.1). Here, we first focus on key inorganic processes affecting river chemistry, including silicate, carbonate and evaporite rock weathering and cyclic inputs (i.e., sea salts in rain). Anthropogenic inputs via agriculture are discussed in Sections 3.6.3-3.6.4.

When weathering is driven by carbonic acid, silicate weathering can remove up to 2 moles of atmospheric CO_2 for each divalent cation released from the rock (and for every 2 moles of monovalent cations), while carbonate weathering will remove 1 mole (Equations 3.5 and 3.8). Evaporite weathering and cyclic inputs do not contribute atmospheric CO_2 to the dissolved load (Table 3.1).

Using river chemistry from the Severn and the Thames catchments (Section 3.4), the first key step involves separating the cations sourced from silicate and carbonate weathering from the total riverine load, using approaches outlined in (Section 3.5). Using these silicate and

carbonate derived cations, this section calculates the maximum CDR, if all weathering reactions proceeded via carbonic acid weathering.

After quantifying the riverine Ca^{2+}, Mg^{2+} and Na^{+} derived from silicate and carbonate weathering, it is important to differentiate the acids responsible for their release. This is because only dissolution by carbonic acid leads to CDR. Additionally, for carbonate weathering, weathering by sulphuric acid or nitric acid leads to CO_2 re-release (Equation 3.9-3.10, Table 3.1). Therefore, the next step is to disentangle the portion of cations originating from silicate and carbonate rocks that underwent weathering through sulphuric and nitric acids. The CDR calculated in Section 3.5 assumes all weathering is by carbonic acid and is therefore adjusted at the end of Section 3.6 to account for strong acid weathering.

Secondary processes, namely carbonate precipitation and cation exchange, may also impact the CDR calculations. Carbonate precipitation re-releases CO_2 and will therefore lower CDR (Equation 3.4). In Section 3.6.2, the potential for carbonate precipitation is assessed by examining the calcite saturation level of both rivers. For river samples exhibiting a saturation index which surpasses the threshold necessary for carbonate precipitation (discussed in more detail in Section 3.6.2), the quantity of precipitation required to restore the river to the threshold saturation index is calculated (using PHREEQC). This is used to modify the CDR calculated in Section 3.5.3.

$$Ca^{2+} + 2HCO_3^- \rightarrow \ CaCO_3 + CO_2 + H_2O \quad (3.4)$$

Finally, cations loosely bound to suspended sediment introduced into rivers can be released into the river, in exchange for dissolved cations in the water column. This exchange usually involves replacing water Ca^{2+} for Na^{+}. This can impact the river chemistry which is needed in the inversion calculations (Section 3.5). The possible impact that this process has on the inversion results is discussed in Section 3.6.1.

Table 3.1- Processes which add and remove cations and anions to the river water column.

Process		Chemical Equation	Equation	Cations transferred to river	Anions transferred to (and out of) river
Silicate weathering	carbonic acid	$CaSiO_3 + 2H_2CO_3 \rightarrow Ca^{2+} + 2HCO_3^- + SiO_2 + H_2O$	*(3.5)*	Ca^{2+}, Mg^{2+}, $2Na^+$	2 moles HCO_3^- (atmospheric)
	sulphuric acid	$CaSiO_3 + H_2SO_4 + H_2O \rightarrow Ca^{2+} + SO_4^{2-} + H_4SiO_4$	*(3.6)*	Ca^{2+}, Mg^{2+}, $2Na^+$	1 mole SO_4^{2-}
	nitric acid	$CaSiO_3 + 2HNO_3 + H_2O \rightarrow Ca^{2+} + 2NO_3^- + H_4SiO_4$	*(3.7)*	Ca^{2+}, Mg^{2+}, $2Na^+$	2 moles NO_3^-
Carbonate weathering	carbonic acid	$CaCO_3 + H_2CO_3 \rightarrow Ca^{2+} + 2HCO_3^-$	*(3.8)*	Ca^{2+}, Mg^{2+}	1 mole HCO_3^- (atmospheric) 1 mole HCO_3^- (carbonate)
	sulphuric acid	$CaCO_3 + H_2SO_4 \rightarrow CO_2 + H_2O + Ca^{2+} + SO_4^{2-}$	*(3.9)*	Ca^{2+}, Mg^{2+}	1 mole SO_4^{2-} ***-1 mole CO_2 released***

	nitric acid	$CaCO_3 + 2HNO_3 + 2O_2 \rightarrow Ca^{2+} + 2NO_3^- + H_2O + CO_2$	*(3.10)*	Ca^{2+}, Mg^{2+}	2 moles NO_3^- ***-1 mole CO_2 released***
Evaporite Weathering (i.e. Gypsum , Halite)		$CaSO_4 * 2H_2O \rightarrow Ca^{2+} + SO_4^{2-} + 2H_2O$ $NaCl * H_2O \rightarrow Na^+ + Cl^- + H_2O$	*(3.11)* *(3.12)*	Na^+ >> Mg^{2+} > Ca^{2+}	Cl^-, SO_4^{2-}
Cyclic inputs		n.a.		Na^+ >> Mg^{2+} > Ca^{2+}	Cl^- >> SO_4^{2-} >> HCO3-
Secondary carbonate precipitation		$Ca^{2+} + 2HCO_3^- \rightarrow CaCO_3 + CO_2 + H_2O$	*(3.13)*	***-1 mole Ca2+ (carbonate)***	***-1 mole C (carbonate)*** ***-1 mole CO_2 re-released***
Cation exchange		$Na^+_{exhange} \leftrightarrow Ca^{2+}_{solution}$		+ Na^+ ***-Ca^{2+}***	***n.a. (*But may impact CDR calcs- see text)***

3.3 Catchment Characteristics for the Severn and Thames Basins

3.3.1 Geology and topography of the basins

3.3.1.1 The River Severn

The Severn Basin is 0.9895 Mha (from Haw Bridge, NRFA) and is located across the Wales and England boundary. The origin of the River Severn lies in Plynlimon, Wales, a forest plantation largely made up of Sitka Spruce within the Welsh Cambrian mountains, emerging at approximately 700m above sea level (Neal *et al.*, 2011). Within the Upper Severn Plynlimon catchment, long term (20-40 years) research investigates the hydrological impacts of felling and replanting of forest (Whitehead *et al.*, 2004; Marc and Robinson, 2007; Neal *et al.*, 2011). The bedrock surrounding the Plynlimon catchment consists of Ordovician-Silurian muds, silts, sands (Rhayader, Bryn-Glas, Cwmere, Glaslyn formations- Figure 3.1c).

Leaving Plynlimon, the River Severn flows through Wales, crosses the Welsh-England Border near Shrewsbury, and passes through Worcester, Tewkesbury, and Gloucester before discharging into the Bristol Channel. Joining the main stem of the River Severn are the main tributaries- the River Avon (joining the Severn at Tewkesbury), the River Teme (joining at Worcester), the River Tern (joining near Atcham, south-east of Shrewsbury) and the River Vyrnwy (joining at Crew Green, Wales). The River Severn is the longest river in the UK (272 km) (Worrall *et al.*, 2014).

The bedrock gets progressively younger towards the mouth of the river (Figure 3.1c). Carboniferous-Permian mud, silt, and sand formations dominate the lithology near Shrewsbury (with small zones of Ediacaran conglomerate, i.e. Bayston Oakwood formation), Triassic mud formations (i.e. Sidmouth and Branscombe formations) by Upton on Severn, and Triassic-Jurassic muds by Gloucester (i.e. Lias group and Charmouth muds). Carbonate lithology is absent in the older formations of upper Severn catchment, but carbonate content increases in younger formations, particularly between Worcester and Gloucester (i.e.- Sidmouth formation, Rugby Limestone member).

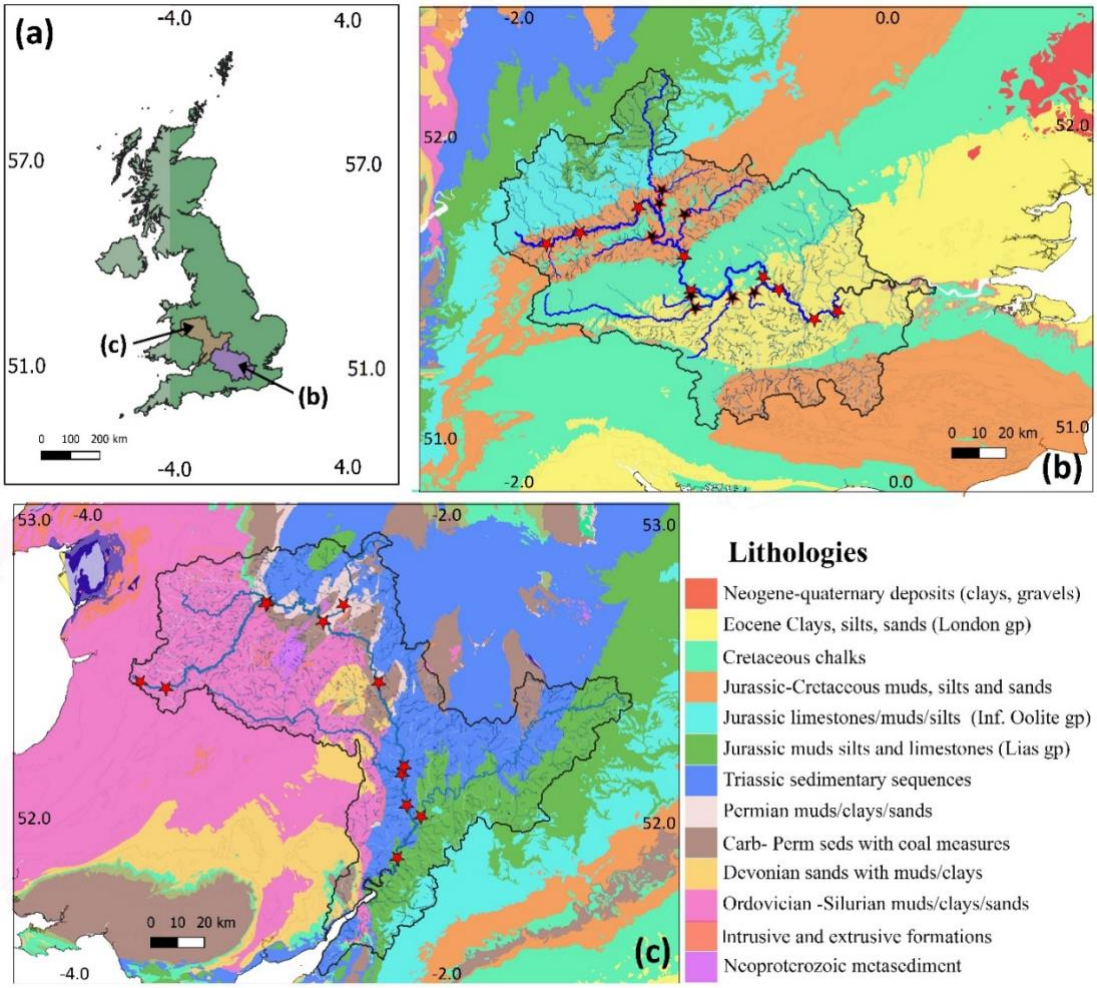

Figure 3.1- Catchment geology of the River Severn (c) and River Thames (b) catchments. (a) is the insert map to show location of catchments in the UK. Main river is coloured darker and bolder to differentiate between main river and tributaries. Sampling locations are highlighted by red stars for main body and tributaries. Geological map was simplified from the British Geological Survey 625k Geological map (BGS, 2023a). *Catchment boundaries were collated from NRFA who derived these using the Centre of Ecology and Hydrology's Hydrological Digital Terrain Model (IHDTM)* (Morris and Flavin, 1990; NRFA, 2023).

3.3.1.2 The River Thames

The Thames basin area is 0.9948 Mha (at Teddington Lock, NRFA), although alternative sources use different boundaries and therefore assign contrasting areas (i.e. CEH- 1.093 Mha; Environmental Agency- 1.6 Mha). This study uses NRFA values to be consistent with the approach used for the River Severn. The source of the River Thames lies about 3 miles from Cirencester in the Cotswolds, at a group of springs near Coates (Figure 3.1b). The bedrock at the source is dominated by Jurassic limestones.

From the initial spring, the Thames runs through Cricklade, then through several major UK urban regions- Oxford, Wallingford, Pangbourne, Reading, Maidenhead, Windsor, before entering the tidal reaches of the Thames estuary, in London. From source to the tidal reach,

located at Teddington Lock, London, the Thames runs for 239 km (Worrall *et al.*, 2014). Several main tributaries flow into the River Thames, including those sampled in this study- the River Cherwell, Thame, Ock, Pang, Kennet, Loddon, Ray and the Cut.

The bedrock varies from sedimentary silicates to limestones and chalks. The Cricklade to Oxford portion of the Thames runs over Jurassic clays (i.e. Oxford, Kimmeridge and Ampthill formations). From Wallingford to Reading, Cretaceous chalks dominates the lithology (i.e. Seaford, Lewes Nodular, Zig Zag and West Melbury Marly Chalk). After Reading and until the tidal reach at Teddington Lock, the geology returns to silicate rich (i.e. the London Clay and Lambeth Group formations). Of the main tributaries, the River Pang and Kennet run almost exclusively over the permeable chalk aquifer, while the river Thame, Cherwell, and Loddon run over impermeable clays. The remaining tributaries run over a mixture of clay and chalk lithologies.

3.3.2 Hydrology and Land Use

Flow rate varies significantly in both the Severn and the Thames (Appendices, Figure B.1), with the average flow rates of 111 $m^3 s^{-1}$ (Severn) and 65.5 $m^3 s^{-1}$ (Thames) for the period on record at the National River Flow Archive (1971-2021 Severn and 1883-2021 Thames). This has a seasonal pattern and for the time span of the historic dataset and timeseries sampling (1974-2021), higher flow rates are typically observed in the winter in both catchments (Figure 3.2).

Land use in the Severn catchment is split into arable (29.8%), grassland (47.6%), urban (7.6%) and woodland (12%). Land use in the Thames catchment is split into arable (35.6%), grassland (32%), urban (14%) and woodland (16%). The arable land is distributed relatively evenly within the catchments, with a slight increase in arable land content from Crewgreen in the Severn (Figure 3.3a), and a slightly higher proportion of arable land near the source of the Thames (Figure 3.3b).

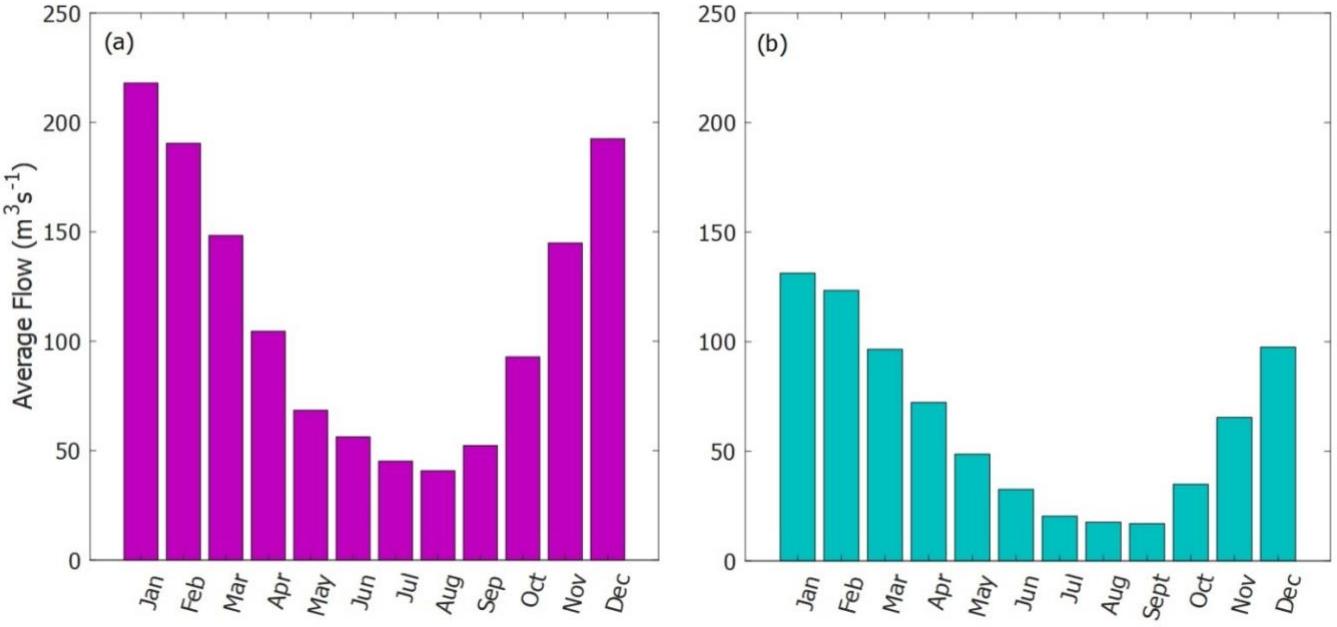

Figure 3.2-Average flow rate per month for the period between the start of the historic chemical measurements (1974) and the end of the timeseries sampling period (2021) for the Severn catchment (a), and the Thames (b). Flow rate data was obtained from the NRFA (NRFA, 2023).

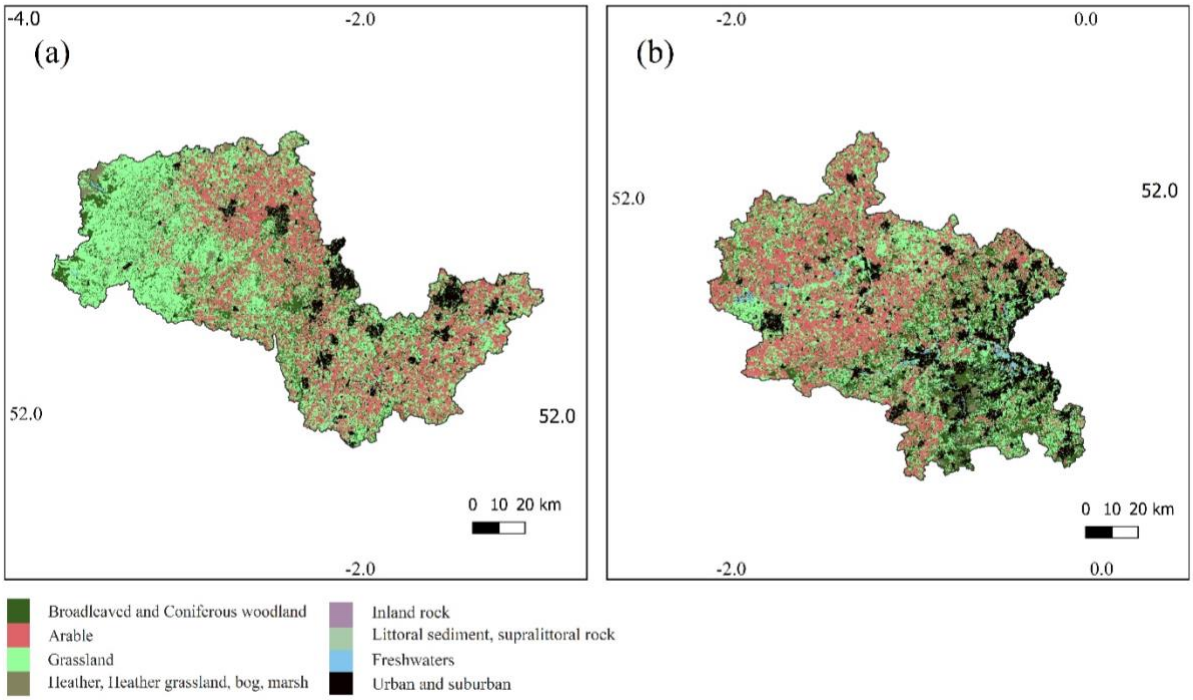

Figure 3.3- land use variations in the Severn (a) and Thames (B). Catchment boundaries taken from the National River Flow Archive (NRFA, 2023)*, and catchment land use data from the Centre of Ecology and Hydrology Land Cover Map 2021* (Marston *et al.*, 2022).

3.4 Chemistry of the Severn and Thames waters

3.4.1 Sampling methods

River water samples were collected over a two-year period between Dec 2019- Dec 2021 for the River Severn, and over the period Apr 21-Dec 21 for the Thames. Locations for sampling along the mainstem were chosen due to their proximity to either a flow monitoring station or a major tributary (Figure 3.1). Four tributaries were also sampled from the Severn catchment: Rivers Avon, Teme, Tern and Vyrnwy, along with 8 from the Thames: Ray, Cherwell, Thame, Ock, Pang, Kennet, Loddon, and The Cut (Figure 3.1).

From each sampling location, water was collected from an accessible, but flowing region, using a bucket rinsed 3 times with river water prior to sampling. River water was filtered on site using 0.2 µm PES membrane filters and stored in acid-washed polyethylene bottles for cation analysis, and in amber (MQ water rinsed but not acid washed) polyethylene bottles for anion analysis. A larger sample was collected for possible later isotope work, as well as river particulates which were collected in large 20L bags and filtered in the evening to collect particulates >0.8 µm. The pH and the temperature were taken at site.

For alkalinity measurements, river water was filtered and amber bottles filled to the brim to ensure that CO_2 would not escape in the period between collection and measurement (typically within 1 week) and stored in the departmental cold room (~4 °C). Total alkalinity was tested with a Metrohm Autotitrator, using methods and precision testing described in Chapter 2, methodology. Major and trace cations were measured using Inductively Coupled Plasma Mass Spectoscopy (ICP-MS) in the Oxford Earth Science department, and anions were measured using Ion Chromatography in the Oxford School of Geography and Environment department. Chemical data for the two catchments obtained from the above analyses have been collated and provided in the datasheets within the Supporting Information.

The Geochemistry of the River Severn and Thames time series was compared to Historic datasets from the Environmental Agency: the Harmonised Monitoring Scheme (HMS), which span from the 1970s-2013, and the Water Quality Archive, spanning 2000-2020 (DEFRA, 2013, 2022d). Samples from the HMS dataset were collected from locations on the mainstem closest to the mouth of the river: Teddington Lock and Haw Bridge for the Thames and Severn respectively (Figure 3.1a, b). The time series was collected to provide recent information on

the spatial variability in geochemistry along the rivers, while the HMS dataset provides information on the historic trends of ion fluxes and the variations in weathering.

3.4.2 DIC and cation chemistry

The concentration of dissolved inorganic carbon (DIC) in µmol CO_2 L^{-1} was calculated for each sample using carbonate speciation equations within PHREEQC (Version 3; Parkhurst and Appelo, (2013), database- Minteq) and the measured alkalinity, pH and temperature of the water (Table 3.3). At the closest chemical monitoring point to the ocean, the average historic concentration of DIC for both rivers are similar (Table 3.2). However, converting to a flow weighted flux (µmol s^{-1}) and upscaling to year, shows that the River Severn transports the most annual DIC (0.34 Mt CO_2 yr^{-1}). Of all the UK catchments (> 100 individual catchments; NRFA, 2023), the Severn and the Thames catchments are the second and third largest exporters of DIC from continent to ocean respectively. Only the Trent catchment exports more annually (0.369 Mt CO_2 yr^{-1}, see Chapter 4, Table 3.2).

The DIC flux determined from the samples collected at Kingston upon Thames during the sampling period aligned with the historical dataset (Table 3.2). Conversely, there was a notable difference between the historic Severn DIC and the average calculated from the collected samples at Maisemore. This variance may be attributed to sampling conducted during three periods of exceptionally large discharge (Dec 19, Mar 20, and Dec 20).

The distinct river chemistry of the Severn and Thames implies potential differences in the source of this DIC (Table 3.3). The Thames has elevated alkalinity, pH and Ca^{2+} concentrations and decreased molar ratios Mg/Ca, Na/Ca, K/Ca, and Li/Ca compared to the Severn, indicating a greater influence of carbonate lithologies to the dissolved load of the Thames (Figure 3.4).

Table 3.2- Average dissolved inorganic carbon fluxes in the River Severn and Thames. The average historic values (Severn: 1974-1992, Thames: 1976-2003) compared to those within this study (Severn: Dec 2019- Nov 2021, Thames: Apr 2021- Nov 2021). Maisemore and Kingston upon Thames are the closest sampling points to the tidal reach.

DIC	Severn (Historic)	Severn (Maisemore)	Thames (Historic)	Thames (Kingston)
Concentration (mmol CO_2 L^{-1})	2.6	2.7	2.7	3.7
Flux (mol CO_2 s^{-1})	246	397	205	240
Annual flux (Mt CO_2 yr^{-1})	0.34	0.55	0.29	0.33
Average yield (kg CO_2 ha^{-1} yr^{-1})	346	558	287	336

Table 3.3- Average Historic Chemical Data for the River Severn and the Thames from the Harmonised Monitoring Scheme (DEFRA, 2013). *Severn data is taken from Haw Bridge, Thames data is from Kingston on Thames. DIC and SI calcite for each chemical sample were calculated using PHREEQC (version 3* Parkhurst and Appelo, 2013*) and the average is given here.*

	Temp (°C)	Flow ($m^3 s^{-1}$)	pH	Alk (mEq L^{-1})	Ca^{2+} (mmol L^{-1})	Mg^{2+} (mmol L^{-1})	Na+ (mmol L^{-1})	K^+ (mmol L^{-1})	SO_4^{2-} (mmol L^{-1})	NO_3^- (mmol L^{-1})	Cl^- (mmol L^{-1})	DIC (mmol L^{-1} as CO_2)	SI calcite
Severn	11.2	100.5	7.9	2.58	1.71	0.61	1.68	0.14	0.93	0.1	1.53	2.62	0.21
Thames	11.64	64.9	8.0	3.79	2.43	0.22	1.59	0.19	0.68	0.12	1.44	2.68	0.44

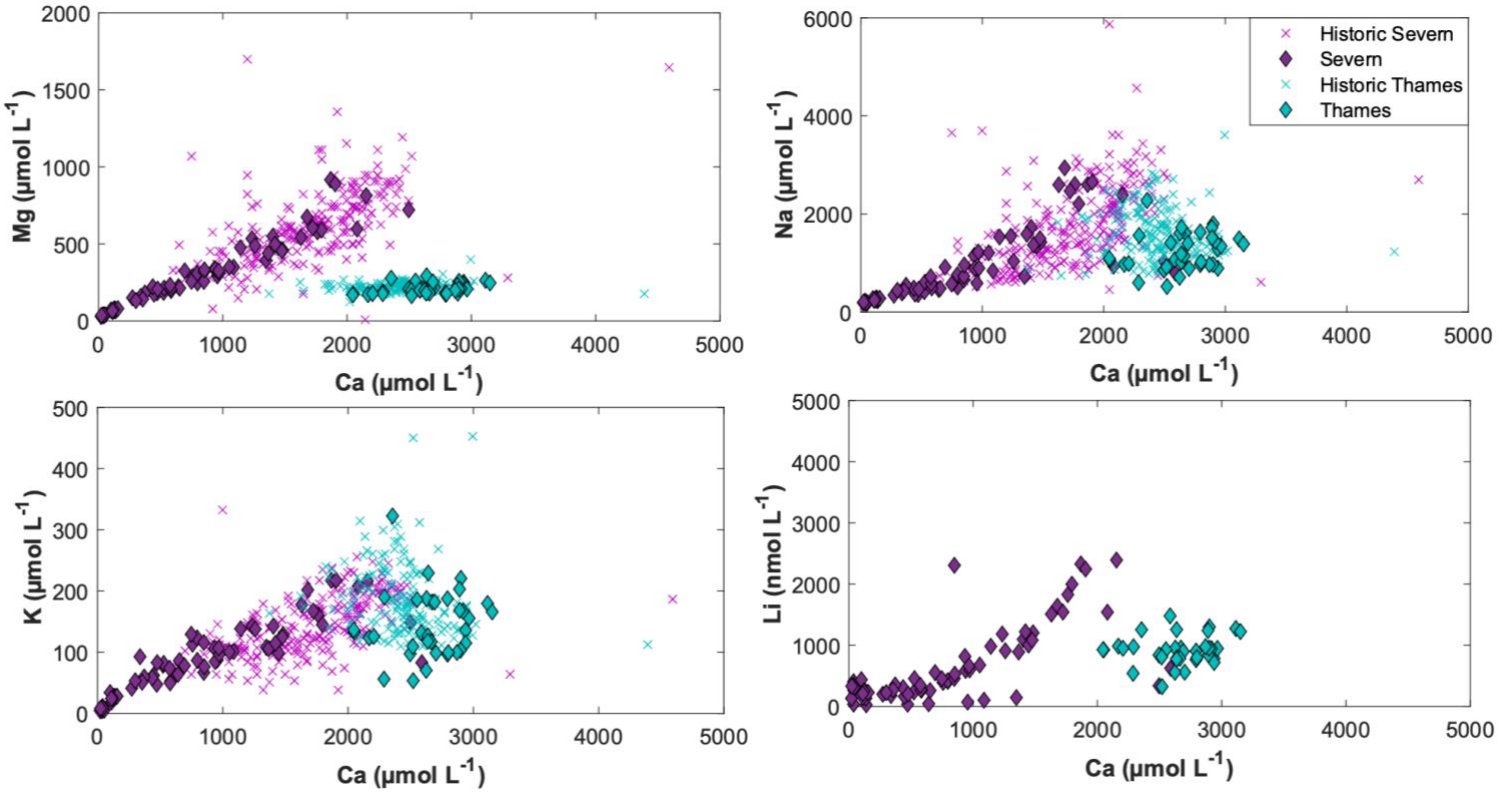

Figure 3.4- Geochemical differences between dominating cations in the River Severn and the Thames. Crosses denote historic data (Appendix A5- Severn, Appendix A6- Thames). Diamonds represent the concentrations from field sampling sites (Appendix A7). Note that y- axis is different for each plot, and that Li concentrations are in nmol L^{-1}

3.4.2.1 Temporal variations in chemistry

Dissolved Inorganic Carbon (DIC) concentration and flux in the River Severn and Thames demonstrate short-term fluctuations throughout the historical sampling period, including high flow events (Appendices, Figure B.2). Separating the historic data into winter (Oct- Mar) and summer months (Apr- Sept) indicates that the DIC flux is on average 2 times (Severn) and 3 times (Thames) higher in the winter than in the summer (Table 3.4). The overall trend in DIC suggests that the transported DIC magnitude by both rivers has not undergone significant changes over the sampling period. Both catchments also have a slightly higher average ratio of $Ca/(Na + K)$ in winter months than summer months (Appendices, Figure B.3), suggesting a possible increase in carbonate derived ions in winter. This trend is evident for the Severn during the sampling period studied, however it is less pronounced in the Thames (Figure 3.5).

Table 3.4-Seasonal variations in DIC flux and concentrations. Values given in table are averages taken from historic dataset. DIC calculated using PHREEQC, as discussed in text.

	Thames		**Severn**	
DIC	Concentration (mmol CO_2 L^{-1})	Flux (mol CO_2 s^{-1})	Concentration (mmol CO_2 L^{-1})	Flux (mol CO_2 s^{-1})
Winter	2.9	298	2.3	320
Summer	2.5	96	3.0	155

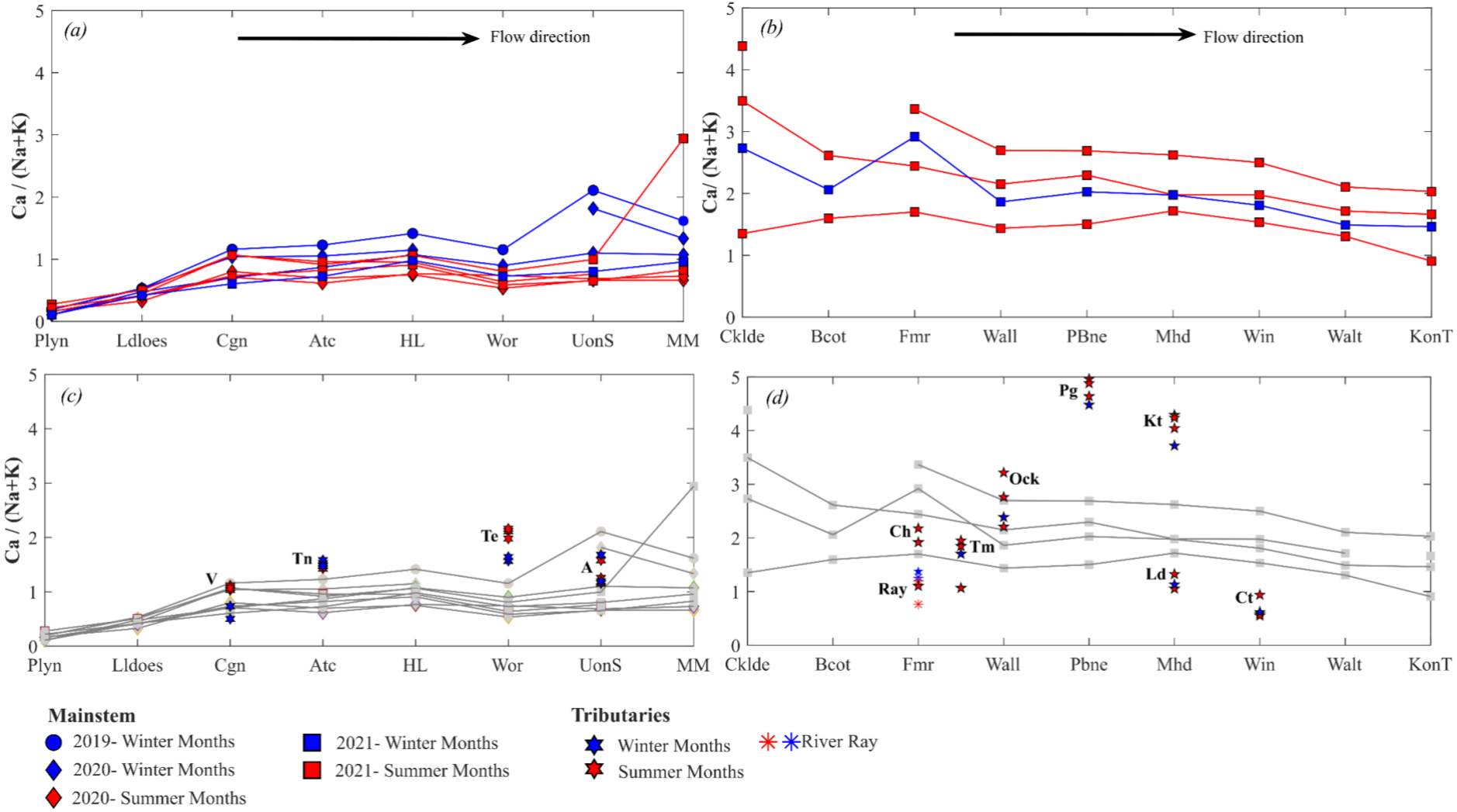

Figure 3.5- Ca/(Na+K) molar ratio variations in (a) the River Severn mainstem, (b) River Thames mainstem, (c) the main tributaries of the River Severn (V= Vyrnwy, Tn= Tern, Te= Teme, A= Avon), and (d) the main tributaries of the Thames (Ch= Cherwell, Tm= Thame, Pg= Pand, Kt= Kennet, Ld= Loddon, Ct= The Cut). Symbols represent measurements taken at the sampled locations on x-axis. And separated into year by symbol type and colour for season. In (a) Plyn= Plynlimon, Ldloes =Llanidloes, Cgn= Crewgreen, Atc= Atcham, Hl= Hampton Loade, Wor= Worcester, UonS= Upton on Severn, Mme= Maisemore. Flow direction is from left to rightIn b) Cklde= Cricklade, Bcot= Buscot, Fmr= Farmoor, Wall=Wallingford, Pbne= Pangbourne, Mhd= Maidenhead, Win= Windsor, Walk= Walton and KonT= Kingston on Thames. Flow direction is left to right

3.4.2.2 Spatial variations in chemistry

Increasing $Ca/(Na + K)$ ratios downstream in the River Severn indicates an increased proportion of total cations from carbonates, while decreasing ratios in Thames suggests the opposite (Figure 3.5 a,b). This is consistent with the regional geology in both catchments (Figure 3.1 b, c), and suggests that lithology may impart a significant signal on catchment chemistry. However, it could also reflect some degree of carbonate precipitation within the river as the dissolved products move downstream. Alternatively, it could also be explained in part by a mixing of tributaries with different chemical compositions (Figure 3.5c and 3.5d).

3.5 Inverting the chemistry to assess silicate and carbonate weathering

Silicate and carbonate weathering within the Severn and Thames catchments was then assessed using the geochemical inversion model MEANDIR. A detailed description of MEANDIR and the methodology used is provided in Chapter 2. To provide a brief overview here, MEANDIR is a set of MATLAB scripts developed by Kemeny and Torres, (2021) which distributes riverine major chemistry between endmember sources using mixing equations such as in Equation 3.14:

$$X/Na_{river} = \sum(X/Na)_i * \propto Na_i \qquad (3.14)$$

$$100 = \propto Na_{sil} + \propto Na_{carb} + \propto Na_{evap} + \propto Na_{rain} \qquad (3.15)$$

Here, X= Ca^{2+}, Mg^{2+}, Na^{+}, Cl^{-} and SO_4^{2-}. $\propto Na_i$ is the proportion of Na from endmember i, where $i =$ silicate, carbonate, evaporite and rain, and the sum of which should equal 100% (Equation 3.15). X/Na_{river} is the chemical composition of the river water and $(X/Na)_i$ is the composition of the endmember (i). As the exact chemical composition of each endmember is unknown, a range in values is commonly used Negrel *et al.*, (1993), Gaillardet *et al.*, (1999), Moon *et al.*, (2014), Burke *et al.*, (2018).

River chemical datasets and endmember chemistry are read into MEANDIR, and then, for each individual river sample, a Monte Carlo simulation will iteratively cycle through the endmember ranges 10,000 times. During each iteration, a randomly selected value within the range is then employed in the mixing equations. Post inversion, MEANDIR will generate a result table for each dataset which presents a series of fractions (f_i^X); the best-fit fraction of the total river concentration of element X from endmember i. An example of the results generated from the inversion is provided in Table 3.6. These fractions are then converted to concentrations by Equation 3.16.

$$X_i = f_i^X * X_{river} \qquad \textit{Equation 3.16}$$

The endmembers used are provided in Table 3.5. This study uses the global endmember ranges for carbonate and evaporite following Gaillardet *et al.*, (1999) Moon *et al.*, (2014). The chemical range of the silicate endmember can vary significantly dependent on mineralogy. To account for local UK silicate compositions, the silicate endmember is constrained using monolithic UK rivers which drain silicates (Chapter 2). To investigate the uncertainty associated with the selection of the silicate endmember, Chapter 2 conducted a comparative analysis of inverting historical data from the River Severn using the global endmember ranges from Moon *et al.*, (2014), and Gaillardet *et al.*, (1999), in comparison to the endmembers employed in this study. This sensitivity test confirmed that the choice of endmember can impact the results of the inversion, underscoring the necessity of careful consideration in their selection. The globally defined alternative endmember composition by Gaillardet *et al.*, (1999) is derived from rivers draining granitic terrains, and therefore exhibits a more constrained range. Consequently, it is suggested here that the broader range in this study better accommodates the heterogenous nature silicates rocks in the UK.

Table 3.5- (From Chapter 2) Endmember compositions used throughout the study. Rain endmember is determined from the average composition of sea-salts and was taken from Gaillardet et al., (1999), SO_4/Na from Moon et al., (2014). Carbonate and evaporite endmembers from Gaillardet et al., (1999).

	Silicate		**Carbonate**		**Rain**		**Evaporite**	
	Median	Stdev	Median	stdev	median	Stdev	median	Stdev
$Ca/_{Na}$	0.669	0.77	60	30	0.023	0.01	0.17	0.09
$Mg/_{Na}$	0.325	0.27	30	15	0.11	0.01	0.02	0.01
$SO4/_{Na}$	0.019	0.005	0.06	0.03	0.060	0.01	0.4	0.2
$Cl/_{Na}$	0	0	0	0	1.15	0.1	1	0

An average global cyclic (sea- salt) chemistry was also used in this study to define the rain endmember (Table 3.5) (Gaillardet *et al.*, 1999; Burke *et al.*, 2018). The treatment of this rain endmember differed to the others. First, samples which have a $Cl/_{Na_{river}}$ > 1.15 are assumed to be influenced by anthropogenic Cl^-: given that $Cl/_{Na_{evap}}$ and $Cl/_{Na_{cyclic}}$ < 1.15 (Table 3.5), and therefore these samples were excluded from the study. For the remaining samples, the maximum portion of Cl_{river} from rain sources (termed $Cl_{critical}$) is calculated given the average concentration of Cl^- in rain (Cl_{rain}), the catchment annual rainfall and discharge data (Equation 3.17).

$$Cl_{critical} = Cl_{rain} * Catchment\ annual\ rainfall/_{Annual\ riverine\ discharge} \quad (3.17)$$

Average annual rainfall (mm yr^{-1}) and annual discharge (L yr^{-1}) for the Severn and Thames catchments was calculated using data from NRFA monitoring stations Haw Bridge and Kingston upon Thames respectively (Accessed at NRFA, 2023). The average concentration of Cl^- in rain (Cl_{rain}) was found from precipitation chemical data from Snowdon (Severn) and Wytham (Thames) (ECN, 2015). The Severn and Thames River chemistry is then corrected using the average $Cl_{critical}$ values calculated (242 and 358 µmol L^{-1} respectively) within the MATLAB scripts, prior to inversion.

There are several methods of assessing the rain endmember in MEANDIR. Chapter 2 tested the legitimacy of using $Cl_{critical}$ to correct for the rain endmember by inverting the historic Severn chemical dataset using an alternative approach: treating rain as a separate endmember. These two inversion results were then used to calculate the annual CDR from weathering in the Severn catchment. Using a $Cl_{critical}$ value led to slightly higher values (percentage difference between the two methods: 7% silicates and 2% carbonates). Due to concerns raised by (Kemeny and Torres 2021) regarding the accurate attribution of solutes when rain is treated as an endmember, this study opts for the use of the $Cl_{critical}$ method to correct for rain.

The raw results from the inversion calculations are provided in the datasheets within the supporting information.

3.5.1 Results from the Inversion (sources of solutes)

Results from the inversion show that the average percentage of major cations Ca^{2+}, Mg^{2+} and Na^{+} sourced from natural rock weathering ($f_{weathering(sil+carb)}$) in the Severn and the Thames is 57% and 62% respectively. In both rivers, the primary source of Ca^{2+} and Mg^{2+} is carbonate weathering (Figure 3.6), while the average portion of total cations derived from silicates is approximately 11% (ranging between 0.5-16% for the Severn, and 1.5-11% for the Thames).

66% and 73% of Na^{+} is sourced from evaporites in the Thames and Severn respectively, in line with previous global estimates by Berner and Berner, (1996). (Berner and Berner, 1996). suggested that, due to the fast dissolution kinetics of evaporites, even minor evaporitic outcrops can contribute substantial Na^{+} (and Cl^{-}) to riverine systems. Collectively, f_{evap} accounts for 29.8% and 36.7% of the major cations in the River Thames and Severn respectively. f_{rain} only contributes on average 8.7% (Thames) and 6.5% (Severn).

For a summary of the ranges in $f_{sil,}$ $f_{carb,}$ $f_{rain,}$ and f_{evap} derived from inversion results for both rivers, see (Appendices, Table B.1).

3.5.2 Temporal variation in the weathering source of cations

Results from the inversion were collated into month of sampling to determine the monthly average (f_{sil} and f_{carb}). This illustrates clear seasonal trends in the proportion of cations from

silicate and carbonate sources (Figure 3.7). In both catchments, the average proportion of cations from silicates increases in summer months, while the opposite is true for carbonates. This seasonal trend is more pronounced in the River Thames than the River Severn (Figure 3.7). The trend can also be observed in multiple places along the River Severn throughout the sampling period (2019-2021); although is more pronounced during 2020 than 2021 (Figure 3.8).

This seasonal variation in the source of solutes is expected following previous studies which find an increase in carbonate derived ions during periods of high flow (Tipper *et al.,* 2006) and at lower temperatures (Gaillardet *et al.,* 2019). The kinetics of carbonate dissolution are faster than silicate weathering (Plummer, L.N., Wigley T.M.L, and Parkhurst, D.L (1978); Palandri and Kharaka 2004), which means that during interactions with fast surficial water during high flow events, carbonate weathering reactions are likely to proceed while silicate reactions may be too sluggish to respond. Conversely, in the lower-flow summer months, the input of silicate ions may increase as the rivers may receive a higher proportion of their flow from groundwater sources. Groundwater, having prolonged contact with the underlying bedrock, enables slower silicate dissolution reactions to proceed and a greater potential for enhanced accumulation of silicate ions in the water. Moreover, these seasonal variations align with the temperature-dependent nature of silicate and carbonate weathering reactions, with silicate weathering increasing with higher temperatures (Lasaga, 2018) and carbonate weathering increasing with colder temperatures (Gaillardet *et al.,* 2019) (See discussion in Chapter 1).

Table 3.6- Example table of a selection of the results from the MEANDIR inversion of River Severn Historic Data (for Ca^{2+} only). Full results also include fractions for riverine Mg^{2+} and Na^{+}, and 237 individual samples for the Severn, and 168 for the Thames. The full results can be found in datasheets within supporting information.

Date	Median f_{Sil}^{Ca}	25% f_{Sil}^{Ca}	75% f_{Sil}^{Ca}	Median f_{carb}^{Ca}	25% f_{carb}^{Ca}	75% f_{carb}^{Ca}	Median f_{evap}^{Ca}	25% f_{evap}^{Ca}	75% f_{evap}^{Ca}	Median f_{cyclic}^{Ca}	25% f_{cyclic}^{Ca}	75% f_{cyclic}^{Ca}	…
17/10/1992	0.221	0.102	0.387	0.618	0.454	0.743	0.149	0.096	0.197	0.005	0.003	0.007	…
22/05/1992	0.249	0.121	0.406	0.596	0.434	0.725	0.157	0.105	0.214	0.003	0.002	0.004	…
18/06/1992	0.321	0.165	0.497	0.539	0.353	0.691	0.132	0.090	0.173	0.003	0.002	0.004	…
13/08/1992	1.66E-4	9.05E-7	0.044	0.836	0.737	0.919	0.129	0.087	0.173	0.004	0.003	0.005	…
20/08/1992	0.059	0.014	0.139	0.813	0.709	0.902	0.115	0.077	0.161	0.004	0.003	0.005	…
17/09/1992	0.083	0.029	0.173	0.800	0.687	0.886	0.106	0.072	0.148	0.005	0.004	0.006	…
27/10/1992	0.062	0.014	0.165	0.797	0.684	0.880	0.108	0.069	0.145	0.003	0.002	0.004	…

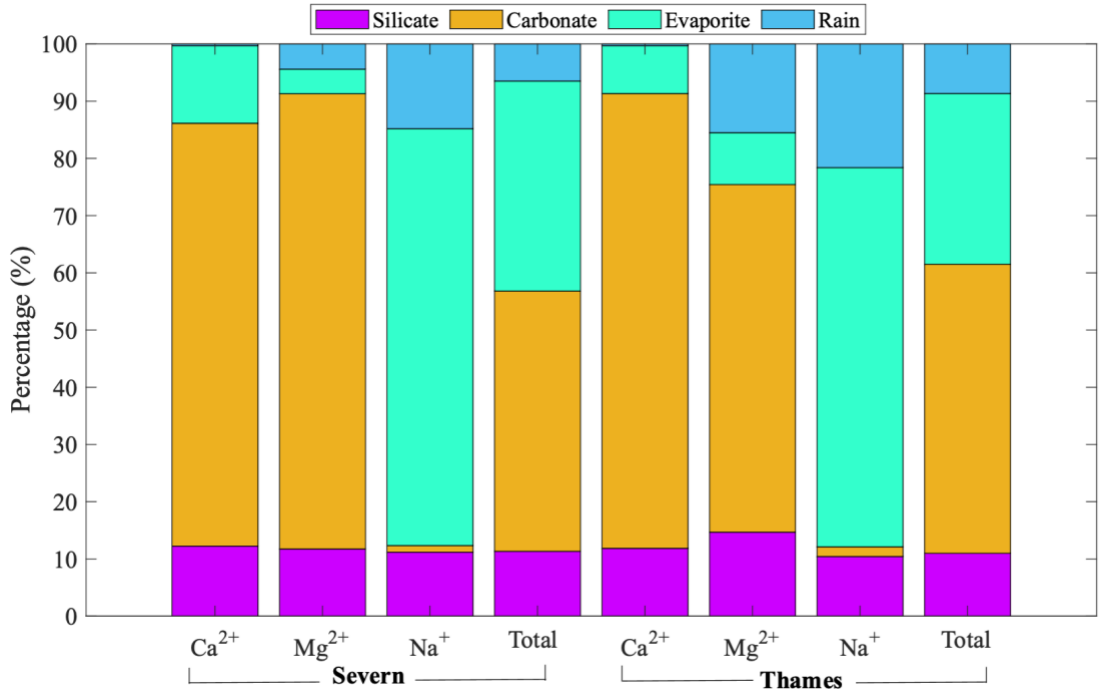

Figure 3.6- Results from the inversion. Average percentage of each cation from each source endmember (silicate, carbonate, evaporite and rain) in the Severn and Thames catchments. Total= the total percentage flux of major cations from each endmember. Values were normalised to 100% where they did not equal 100%

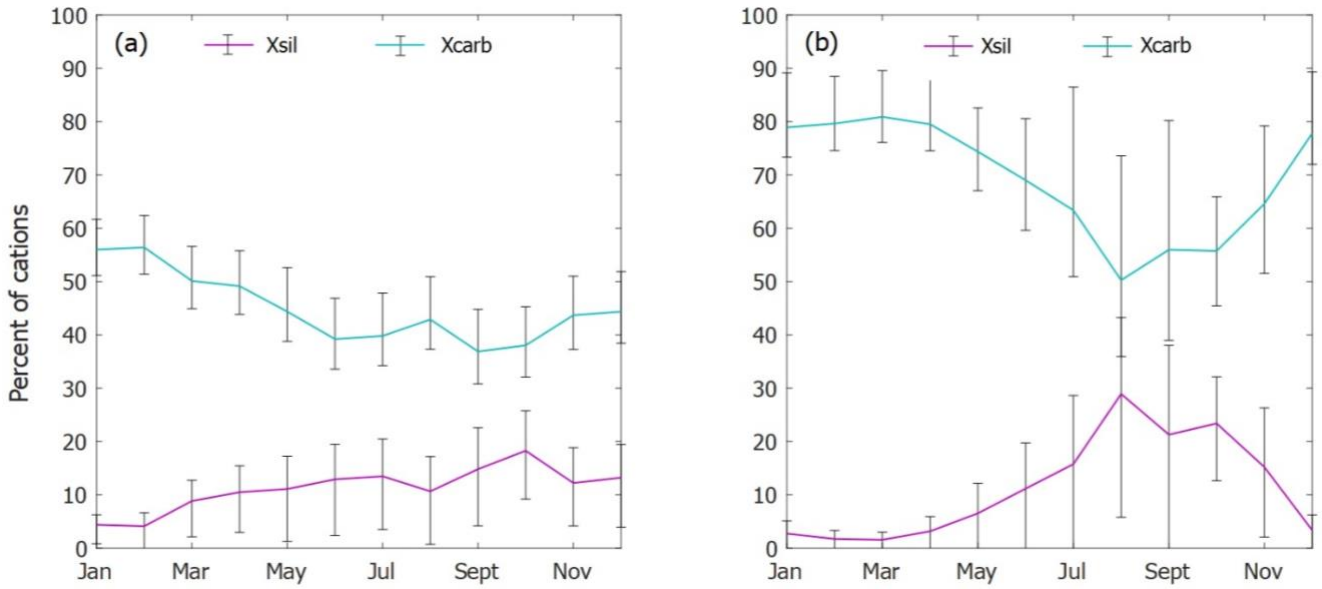

Figure 3.7- Monthly average of the fraction of cations (Ca^{2+}, Mg^{2+}, Na^{+}) sources from silicates and carbonates (Xsil and Xcarb) for the River Severn and Thames (from HMS data).

The long- term trend in the magnitude of the weathering flux was also assessed for both rivers. Concentrations of cations from silicate and carbonate weathering (X_{sil} and X_{carb}) were converted to flux (Q_{X_i}, mol s^{-1}) using Equation 3.18, as well as the average daily flow rate, provided with the chemical data in the supporting information datasheets.

$$Q_{X_i} = X_i * d \quad (3.18)$$

Where d= discharge in L s^{-1} and Q_{X_i} is the flux of element X from endmember i.

Like DIC, the total flux of major cations from silicates ($Q_{sil}, i.e. Q_{Sil_{ca}} + Q_{Sil_{Mg}} + Q_{Sil_{Na}}$) and carbonates ($Q_{carb}$) varies substantially over short-term annual cycles, however longer-term trends suggest that the overall weathering flux in both rivers has remained stable throughout the sampling period (Appendices, Figure B.5).

3.5.3 The annual Carbon Dioxide Removal in the Thames and Severn catchments

Using the annual flux estimates above, the maximum amount of CO_2 consumed by weathering processes was calculated assuming that i) carbonic acid is the weathering agent, ii) all ions remain dissolved in the water column, iii) carbonate weathering removes 1 mole of CO_2 per mole of Ca^{2+} and Mg^{2+}, and iv) silicate weathering removes between 1.4-1.7 mole of CO_2 per mole of Ca^{2+} and Mg^{2+} (and per 2 moles of Na^{+}), depending on the molar ratio of CO_3^{2-} to HCO_3^{-} in the ocean (see Section 5.5 of Chapter 5 for extended discussion). To account for the range in uncertainty in the value of CO_2 removed per mole of silicate, the maximum sequestered CO_2 was calculated using both 1.4 and 1.7.

The total annual carbon dioxide removed by rock weathering (silicates and carbonates) in the Severn and Thames catchments is 0.24-0.37 Mt CO_2 yr^{-1} and 0.19-0.22 Mt CO_2 yr^{-1}. Of this, approximately 22% and 6% is sourced from silicates (Table 3.7, with ranges relating to uncertainty in the MEANDIR inversion results).

Table 3.7 Maximum potential CDR due to natural weathering in the Severn and the Thames catchments (for w= 1.7). Given in annual flux (Mt CO_2 yr^{-1}) and yield (kg CO_2 ha^{-1} yr^{-1}). The latter of these is useful when comparing weathering rates between catchments of different sizes.

	Severn			**Thames**		
	Silicates	**Carbonates**	**Combined**	**Silicates**	**Carbonates**	**Combined**
Max CDR (Mt CO_2 yr^{-1})	0.065	0.232	0.297	0.014	0.207	0.22
Range	0.04-0.11	0.20 0.26	0.24-0.37	0.0028-0.043	0.19-0.22	0.19-0.26
Yield (Kg CO_2 ha^{-1} yr^{-1})	66	234	300	14	208	222
Range	36-110	204-260	240-371	3-43	187-221	190-265

It is important to recognise that on geological timescales, only the silicate component will contribute to a long-term reduction in atmospheric carbon, and when carbonate is eventually formed in the ocean, the net CO_2 removed by silicate weathering will reduce by approximately half that calculated here. Nevertheless, the products of weathering, including those from carbonate weathering, can persist in the dissolved load of the oceanic water column for up to 10,000 years (Renforth and Henderson, 2017). Therefore, these maximum values may be important over the timescales required to address anthropogenically induced climate change.

3.6 Riverine processes which may reduce the maximum CDR

Apart from strong acid weathering (Section 3.6.3 and Section 3.6.4), several processes may alter the calculated flux of ions from silicate (Q_{sil}) and carbonate (Q_{carb}) weathering and therefore the resultant maximum drawdown of CO_2- including cation exchange and precipitation of secondary minerals in the soil or river. Here we consider the potential impact of these processes.

3.6.1 Cation Exchange

Cations bonded weakly onto riverine suspended sediment can be exchanged with cations in the dissolved load, leading to shifts in the chemical signature of river water (Cerling *et al.*, 1989; Lupker *et al.*, 2016; Tipper *et al.*, 2020). Previous research indicates that, prior to entering the river environment, the exchange pool of suspended sediment is often dominated by Na^+. This is especially true for sediment which initially originated from a marine setting. In contrast, the riverine dissolved load is typically characterised by a higher concentration of dissolved Ca^{2+}. This chemical distinction between suspended sediment and the dissolved load results in ion exchange, whereby the Na^+ is removed from the sediment into solution and replaced by riverine Ca^{2+} to establish equilibrium. This exchange is governed by charge, whereby two monovalent Na^+ ions will be exchanged for one divalent Ca^{2+}.

Consequently, river water can become enriched in Na^+ and depleted in Ca^{2+} due to cation exchange occurring during riverine sediment transport. As MEANDIR uses the river chemistry and the chemical signatures of endmembers to predict the proportion of cations from silicate

and carbonate weathering, this chemical change to the dissolved load has the potential to impact the results of the inversion. The silicate endmember ($^{Ca}/_{Na_{sil}}$) is much lower than the carbonate endmember ($^{Ca}/_{Na_{Carb}}$), (Table 3.5), and therefore excess Na^+ in solution may cause MEANDIR to overestimate the silicate component and underestimate the carbonate component. If so, this may alter the overall CDR due to weathering. The process of cation exchange may have resulted in an overestimation of the global CDR attributed to silicate weathering of between 12-28% (Tipper *et al.*, 2020).

The impact of cation exchange on the results discussed in 4.2 depends on- i) the flux of suspended sediment compared with the dissolved load, ii) the cation exchange capacity (CEC) of the sediment, which is mineralogy dependent and typically expressed in (mEq $100g^{-1}$) (Tipper *et al.*, 2020), and iii) the sediment's depositional environment, which will control the chemical composition of the initial sediment exchange pool. Both the Severn and Thames catchments have bedrock of marine origin, raising the possibility that cation exchange may have altered the chemistry in both rivers. Given the lack of data for the CEC (or the composition) of suspended sediment in both basins, it is difficult to estimate the exact contribution of cation exchange to the dissolved load. Instead, the potential maximum overestimation due to cation exchange is calculated here which should provide a conservative assessment of the impact of this process.

Suspended sediment information for each measured historic datapoint was firstly collated (Given in datasheets within supporting information). The average quantity of suspended sediment in the Severn and Thames is 38 and 17 mg L^{-1} respectively, which is on the lower end of the average suspended sediment load transported by global rivers (0-10 g L^{-1}) (Tipper *et al.*, 2020). The maximum quantity of Na^+ that can be bound to the exchange sites of this sediment can then be equated by Equation 3.19, i.e.-

$$Na_{exchange} = CEC * S \quad (3.19)$$

Where S= the quantity of suspended sediment (g L^{-1}), and CEC is the cation exchange capacity (mEq $100g^{-1}$). The range in CEC of global suspended sediment is given by Tipper *et al.*, (2020) as <1-40 mEq $100g^{-1}$. To calculate the maximum cation exchange, this study uses the upper endmember CEC value of 40 mEq $100g^{-1}$.

Under the assumption that (i) the whole exchange load is initially composed of Na^+, and (ii) all this Na^+ from Equation 3.3.16 enters the dissolved load, results suggest that, on average, ~0.015 mEq L^{-1} (Severn) and ~0.007 mEq L^{-1} (Thames) of the riverine Na^+ was from the exchange pool of suspended sediment, and therefore the charged equivalent amount of Ca^{2+} would have been lost from the dissolved load. For the River Thames, this would lead to the initial Na_{river} being on average 0.6% lower and Ca_{river} being 0.2% higher. In the River Severn, the initial Na_{river} would be 1.4% lower and the initial Ca_{river} 0.54% higher.

Subsequently, an assessment was made regarding the potential impact of this on the inversion results and, consequently, on the maximum CO_2 consumed due to silicate and carbonate weathering. To do this, the inversion was re-run using the river concentrations corrected for cation exchange (see datasheets in supporting information), and the same methodology as described in (Section 3.5) to calculate the annual CO_2 consumed by silicate and carbonate weathering. These calculations demonstrate that adjusting river chemistry for cation exchange would result in a negligible alteration in the combined (silicate and carbonate) CDR- less than 1% for both catchments (Table 3.8). When differentiating between the silicate and carbonate weathering, results show that the silicate CDR may be most influenced by this correction- potentially reducing by up to 7% in both catchments (Table 3.8). However, this is a maximum adjustment for CEC which assumes that (i) all initial cations in the exchangeable load of the suspended sediment were originally Na^+ and (ii) that the cation exchange capacity of all suspended sediment in both rivers is high. Consequently, for these UK catchments, this study concludes that cation exchange does not constitute a significant source of uncertainty in CDR calculations.

Table 3.8- Potential Impact of cation exchange on the CDR for the Severn and the Thames

	Combined Max Mt CO_2 yr^{-1}	**Combined CEC Mt CO_2 yr^{-1}**	**Sil Max**	**Sil CEC**	**Carb Max**	**Carb CEC**
Severn	0.2974	0.2969	0.065	0.0604	0.232	0.236
Thames	0.2204	0.220	0.014	0.013	0.2066	0.2073

.

3.6.2 Riverine Secondary Carbonate Precipitation

If the cations liberated from weathering reactions are removed from river water to form secondary carbonates, CO_2 is re-released (Equation 3.4). Consequently, secondary carbonate precipitation has the potential to lower the overall CDR of weathering. A recent finding revealed that the incorporation of EW products into secondary carbonates during transport via river systems has the potential to reduce the CDR Potential of EW in the United Kingdom by as much as 27% (Chapter 5, and Harrington *et al.*, 2023). Here, a brief assessment is made of the likelihood of carbonate precipitation during the transport of natural weathering products in these two large UK catchments.

(i) Chemical ratios

Variations in riverine Na/Ca and $1000 * Sr/Ca$ (Figure 3.8) can be used to infer carbonate precipitation. Increases in these ratios have historically been used to suggest the scavenging of dissolved Ca^{2+} into carbonates (Bickle *et al.*, 2015; Bufe *et al.*, 2021; Erlanger *et al.*, 2021), and compositions deviating above the silicate and carbonate mixing line (A- B) in Figure 3.8 may signify a degree of carbonate precipitation (Bufe *et al.*, 2021). Despite being regularly oversaturated with respect to calcite (Figure 3.9), all datapoints for the Severn and Thames mainstem lie below this mixing line, suggesting that carbonate precipitation may not be significant in these specific rivers. The four points above the line in Figure 3.8 are the from River Avon samples, suggesting carbonate precipitation may impact the chemistry within this river.

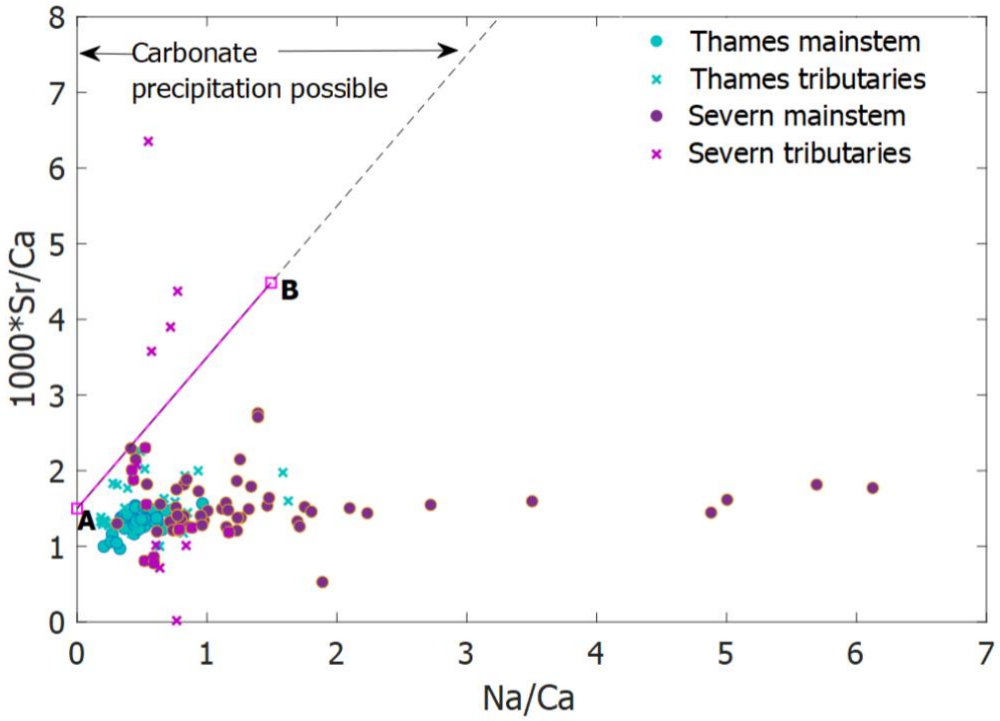

Figure 3.8- Relationship between Sr/Ca and Na/Ca in the River Thames and Severn and their main tributaries. Line A-B indicates the line of best fit through a global carbonate endmember (A) and silicate endmember (B). Values for the global endmembers are taken from Bufe *et al.*, (2021). *In the mentioned study, they use a carbonate 1000* Sr/Ca of 1-1.5. This study assigns the value of carbonate 1000*Sr/Ca at 1.5. The four points lying above the A-B endmember line are all the River Avon, which had consistently high Sr/Ca, despite flowing over carbonate rich lithologies.*

(ii) Carbonate chemistry

The calcite saturation index ($SI_{calcite}$) of river water can be used to predict the likelihood of secondary carbonate precipitation. $SI_{calcite}$ is defined by Equation 3.20 (eg, Zeebe & Wolf-Gladrow, 2001):

$$SI_{Calcite} = log\left(\gamma Ca^{2+} * \gamma CO_3^{2-} \Big/ Ksp\right) \quad (3.20)$$

Where γCa^{2+} and γCO_3^{2-} are the activities of Ca^{2+} and CO_3^{2-} respectively, and Ksp is the equilibrium constant, which is dependent on salinity and temperature (Mucci, 1983). In an ideal solution, when $SI_{Calcite} > 0$, the solution is saturated or oversaturated with respect to calcite and secondary carbonate formation is expected. In practice, the presence of inhibiting ions in solution (i.e. PO_4^{3-}, Mg^{2+}, SO_4^{2-}) can suppress precipitation reactions (Katz *et al.*, (1993), Lin. Y. and Singer, P. (2005), Nielsen *et al.*, (2016)), meaning that the actual threshold SI for precipitation ($SI_{threshold}$) is often higher than this. The specific value for $SI_{threshold}$ is unclear.

However, in a recent study that assessed carbonate precipitation in river water at various $SI_{Calcite}$, it was suggested that significant precipitation may not occur until $SI_{threshold} \geq 1$ (Harrington, Hilton and Henderson (2023), see Chapter 5). Therefore, here it is expected that precipitation will not substantially impact the CDR calculations unless the riverine SI is driven above this $SI_{threshold}$ value.

$SI_{calcite}$ is calculated using the measured alkalinity, pH and Ca^{2+} concentration of each sample in the historic and timeseries dataset, within PHREEQC (Version 3, database- Minteq.v4). Calculations of the $SI_{calcite}$ for the samples within the historic dataset reveal that $SI_{calcite}$ exceeds the threshold ($SI_{threshold} \geq 1$) in 14 and 19 datapoints for the Thames and Severn respectively (9% and 10% of the total data, Appendices, Figure B.6). All samples which surpass the threshold value were collected within summer months during low flow (Apr- Sept), suggesting that significant precipitation is unlikely.

Nevertheless, in instances where samples exceeded the $SI_{threshold} \geq 1$, it might be that some carbonate will precipitate between the historic sampling locations (Kingston upon Thames and Haw Bridge) and the estuary to return the water to $SI_{threshold} = 1$. To explore the potential significance of this precipitation in reducing CDR in the catchment, saturation index equations (Equation 3.18) were utilized in PHREEQC to predict the quantity of precipitation needed to restore the water to $SI_{Calcite} = 1$ (see datasheets within the supporting information)

For the small percentage of data where $SI_{Calcite} > 1$, the quantity of carbonate precipitation predicted was compared to the total flux of ions from weathering for the same date. For these samples, carbonate precipitation was only 0.1-16% that of the total weathering flux in the Thames, and 0.1-12% of the Severn. Notably, of this range, only 5 samples displayed more than 1% of precipitation. Given that these samples represent less 1% of dataset collected for both rivers, it is likely that carbonate precipitation will not greatly impact the CDR of natural weathering in either catchment. The impact of carbonate precipitation on the calculated CDR (Section 3.5.3) is therefore ignored.

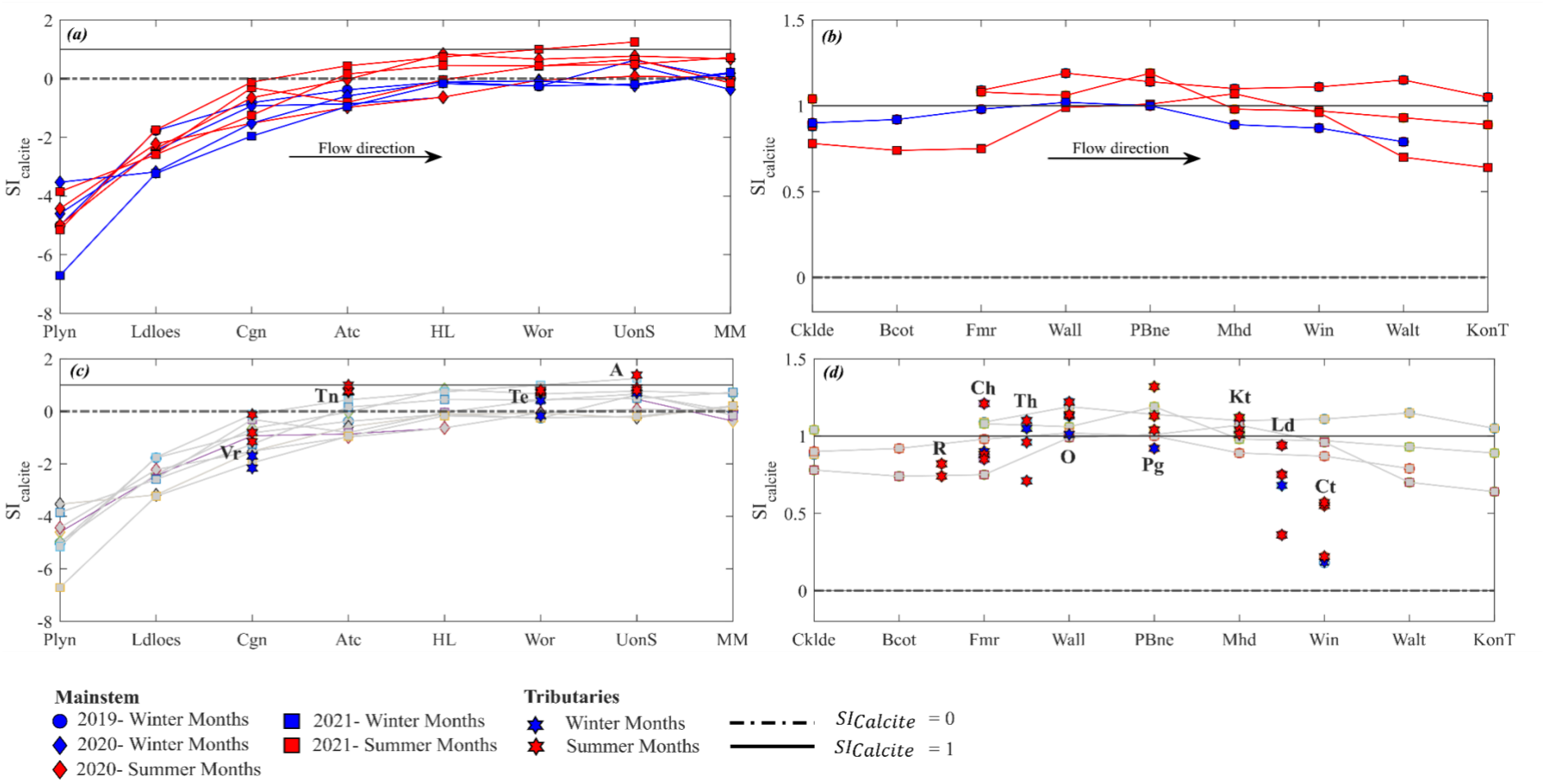

Figure 3.9- Saturation Index variations along stream in (a) Severn and (b) Thames. (c) and (d) show the saturation indexes of the main tributaries to enter (c) the Severn and (d) the Thames. Dashed lines indicate the saturation of secondary carbonates under ideal conditions, while full black horizontal line at SI=1 shows the threshold index used in Chapter 5 to account for suppression of precipitation due to inhibitant ions in solution. Sampling periods are categorised into summer months (Apr- Sept) and winter months (Oct- Mar) to show any seasonal variation in saturation index. Tributaries in (c) A= Avon, Te= Teme, Tn= Tern, Vr= Vyrnwy. Tributaries in (d) R= Ray, Ch= Cherwell, Th= Thame, O= Ock, Pg= Pang, Kt= Kennet, Ld= Loddon, Ct= The Cut. Sampling Locations in (a) Plyn=Plynlimon, Ldloes= Llanidloes, Cgn= Crew Green, Atc= Atcham, HL= Hampton Loade, Wor= Worcester, UonS= Upton on Severn, MM= Maisemore. Sampling locations in (b) Cklde= Cricklade, Bcot= Bscot, Fmr= Farmoor, Wall= Wallingford, PBne= Pangbourne, Mhd= Maidenhead, Win= Windsor, Walt= Walton, KonT= Kingston upon Thames

3.6.3 Sulphuric acid weathering from sulphides

The extent of weathering induced by sulphuric acid, and hence reduction to natural CDR, can be evaluated by examining the concentration and flux of sulphate in river systems. Important sources of riverine sulphate include geological formations within the watershed, such as evaporites and sulphides. Additionally, anthropogenic activities, such as agriculture and urban waste disposal, as well as natural emissions from volcanic and biogenic sources, are known to contribute to the sulphate load of global rivers (Meybeck, 2003; Kemeny *et al.*, 2021). Isolating the portion of sulphate from sulphides is needed to correctly quantify the contribution of sulphuric acid to weathering reactions.

3.6.3.1 Sulphate concentrations in the Severn and the Thames

The average sulphate (SO_4^{2-}) concentration (µmol L^{-1}) and flux (mol s^{-1}) are both greater in the Severn than the Thames (Table 3.9). The SO_4^{2-} concentrations in both rivers exhibit short term annual variations, which are more pronounced in the Severn (Appendices, Figure B.7). In the River Severn, these variations follow a distinct seasonal pattern, with higher concentrations observed during summer months (Apr- Sept, see Table 3.9). However, the SO_4^{2-} flux is significantly higher in both rivers during winter months (Oct- Mar) because of the higher river flow.

Overall, there is a significant decline in sulphate concentration in the Thames from the year 2000 (Appendices, Figure B.7). This decline aligns with the broader trend of decreasing riverine SO_4^{2-} concentrations across the UK from 1988-2008, attributed to the reduction in sulphur dioxide emissions resulting from the combustion of fossil fuels (Environmental Agency, 2019). The mean concentration of SO_4^{2-}at Kingston on Thames during the sampling period (530 µmol L^{-1}) also reflects this decrease. Conversely, riverine sulphate has remained relatively stable in the Severn over the sampling period.

Table 3.9- Average concentration and flux of riverine sulphate in the River Severn and Thames taken from the historic datasets. Overall (yearly average) compared to average in winter months (Oct- Mar) and summer months (Apr- Sept), show that the flux of sulphate is significantly higher in winter for both rivers.

	Concentration			**Flux**		
	Overall (µmol L^{-1})	**Winter (µmol L^{-1})**	**Summer (µmol L^{-1})**	**Overall (mol s^{-1})**	**Winter (mol s^{-1})**	**Summer (mol s^{-1})**
Severn	994	829	1092	82	105	52
Thames	683	696	668	41	58	20

From these riverine sulphate trends, the following observations can be made:

(i) A portion of the historical riverine sulphate in the Thames may have been derived from anthropogenic fossil fuel emissions. Conversely, fossil fuel emissions may not have exerted a substantial influence on the chemical composition of the River Severn.

(ii) The Thames has more arable land than the Severn (Figure 3.3a, b), and therefore if agricultural fertilizer was an important source of sulphate to the rivers, SO_4^{2-} concentrations might be expected to be higher in the Thames. However, this expectation is not met (Table 3.9), suggesting that an alternative source of sulphate may dominate riverine sulphate concentrations.

This significant sulphate source may be from sulphides, given that outcrops of the Pennine Coal Measures Formation, known to contain pyrites minerals (Spears *et al.*, 1999), are found between Shrewsbury and Worcester (for the River Severn Figure 3.1c). Nevertheless, the influence of evaporites cannot be ignored. The inversion results (Figure 3.6, Section 3.5) suggest that evaporites contribute an average of 30% and 37% of the dissolved cations in the Thames and Severn respectively. Consequently, the subsequent analysis follows methods used in (Burke et al 2018) to remove the evaporite- derived sulphate component to better constrain the fraction of riverine SO_4^{2-} sulphate from sulphides ($SO_4^{2-}{}_{sulphide}$).

3.6.3.2 Excess sulphate ($X_{excess\,SO_4^{2-}}$)

The method for removing the evaporite and non-silicate component of riverine sulphate from riverine SO_4^{2-} sulphate has been discussed elsewhere (Chapters 2 and 4). To briefly summarise here, after apportioning major cations (Ca^{2+}, Mg^{2+}, Na^{+}) between source endmembers using the Monte Carlo inversion technique (Chapter 2, and Section 3.5), a simple conservative mixing model within MEANDIR allocates a portion of the riverine SO_4^{2-} to each of the endmembers ($SO_4^{2-}{}_i$), where i = silicate, carbonate, evaporite and rain, e.g., Equation 3.21 (Kemeny and Torres, 2021):

$$SO_4^{2-}{}_i = \left(SO_4^{2-}/_{Na}\right)_i \propto_{i(Na)} \Big/ \left(SO_4^{2-}/_{Na}\right)_{river} \quad (3.21)$$

$\left(SO_4^{2-}/_{Na}\right)_i$ is the molar ratio for each endmember i, $\propto_{i(Na)}$ is the proportion of Na^+ from each endmember (calculated previously in the inversion) and $\left(SO_4^{2-}/_{Na}\right)_{river}$ is the molar ratio of the river water. Molar ratios for each endmember can be found in (Table 3.5). The value for the silicate endmember is purposefully low, $\left(SO_4^{2-}/_{Na}\right)_{silicate}$ = 0.019, to represent any SO_4^{2-} within silicates that is not sourced from pyrite minerals (Burke *et al.*, 2018). By not including pyrite, as well as alternate sources of SO_4^{2-} within the mixing model, an 'excess' of SO_4^{2-} ($X_{excess\ SO_4^{2-}}$) will remain which cannot be attributed to the endmembers (Equation 3.22):

$$X_{excess\ SO_4^{2-}} = X_{river\ SO_4^{2-}} - \sum\left[SO_4^{2-}{}_i\right]^n \quad (3.22)$$

$\sum\left[SO_4^{2-}{}_i\right]^n$ is the sum of contributions of sulphate from each endmember (i), and n is the number of endmembers (4). This remaining excess riverine SO_4^{2-} ($X_{excess\ SO_4^{2-}}$) will be a combination of SO_4^{2-} sourced from volcanic atmospheric deposition, biogenic emissions, anthropogenic pollution, and the oxidative weathering of pyrite. Results of the mixing equations are provided as concentrations ($X_{excess\ SO_4^{2-}}$ µmol L^{-1}) and as fractions ($f_{excess\ SO_4^{2-}}$) in the output data (see datasheets in supporting information).

Results reveal that the average $f_{excess\ SO_4^{2-}}$ is higher for the Severn than the Thames (Table 3.10). On average, 46% (Severn) and 36% (Thames) of the riverine sulphate can be attributed to $X_{excess\ SO_4^{2-}}$. These averages are both lower than the global average reported by Burke et al 2018 (65%), although there was a large variation in $X_{excess\ SO_4^{2-}}$ across the rivers within their study (0- 97%) (Burke *et al.*, 2018). There are significant short-term variations in these trends. $f_{excess\ SO_4^{2-}}$ is only slightly higher in the summer than the winter (Table 3.10), however when concentrations are converted into a flow weighted flux (mol s^{-1}), both rivers export substantially more $X_{excess\ SO_4^{2-}}$ in winter months (Table 3.10, Figure 3.10). The overall annual flux of $X_{excess\ SO_4^{2-}}$ is an order of magnitude higher in the Severn than the Thames (Figure 3.10).

Table 3.10- Average fraction of riverine sulphate from excess sources in the River Severn and Thames. Overall is the overall average over the historic sampling period. Average taken for all data sampled in summer months (Apr-Sept) and winter months (Oct-Dec) to assess for possible seasonal trends.

		Severn	**Thames**
$f_{excess\ SO_4^{2-}}$	Overall	0.46	0.36
	Winter months	0.42	0.28
	Summer months	0.50	0.39
$X_{excess\ SO_4^{2-}}$ (µmol L^{-1})	Overall	436	242
	Winter months	453	282
	Summer months	431	195
$X_{excess\ SO_4^{2-}}$ **flux** (mol s^{-1})	Overall flux	43	19
	Winter months	82	29
	Summer months	31	7.5

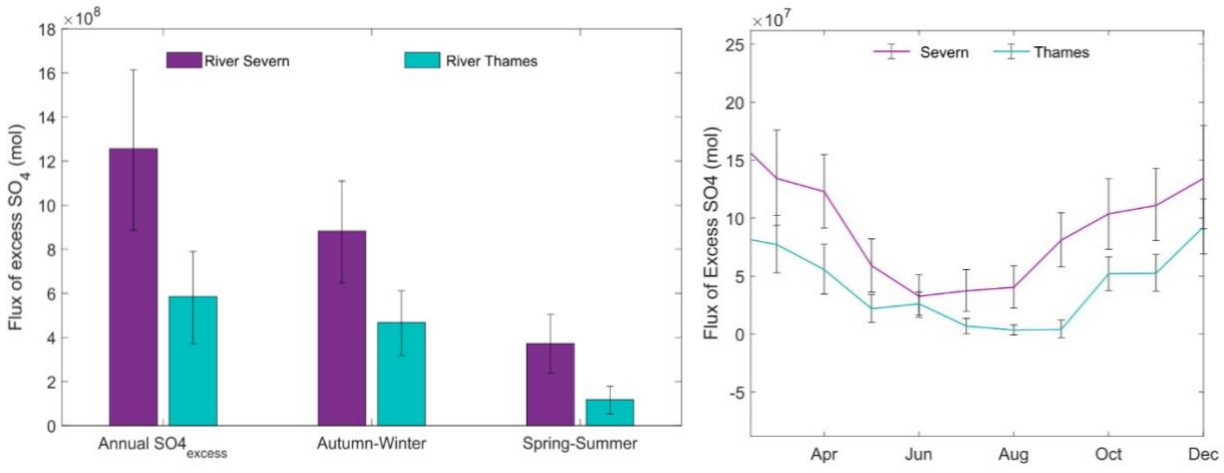

Figure 3.10-Flux of excess riverine sulphate ($X_{excess\ SO_4^{2-}}$) which has not been sourced from the four end member sources (carbonate, evaporite, rain, and silicates (not including sulphides)). Results collated from the historic dataset. Comparing seasonal trends in the River Severn and the Thames (a), along with the monthly flux of $X_{excess\ SO_4^{2-}}$, calculated by upscaling from monthly averages. Error bars represent the range using 25-75 percentile results of $X_{excess\ SO_4^{2-}}$.

There is an overall decrease in the fraction of sulphate from excess sources towards the estuary in the Thames. For the Severn, the fraction of excess sulphate decreases until Worcester, then

increases to the estuary (Figure 3.11). The seasonal trend in fraction of excess sulphate is less clear in the samples collected during this study (Figure 3.11).

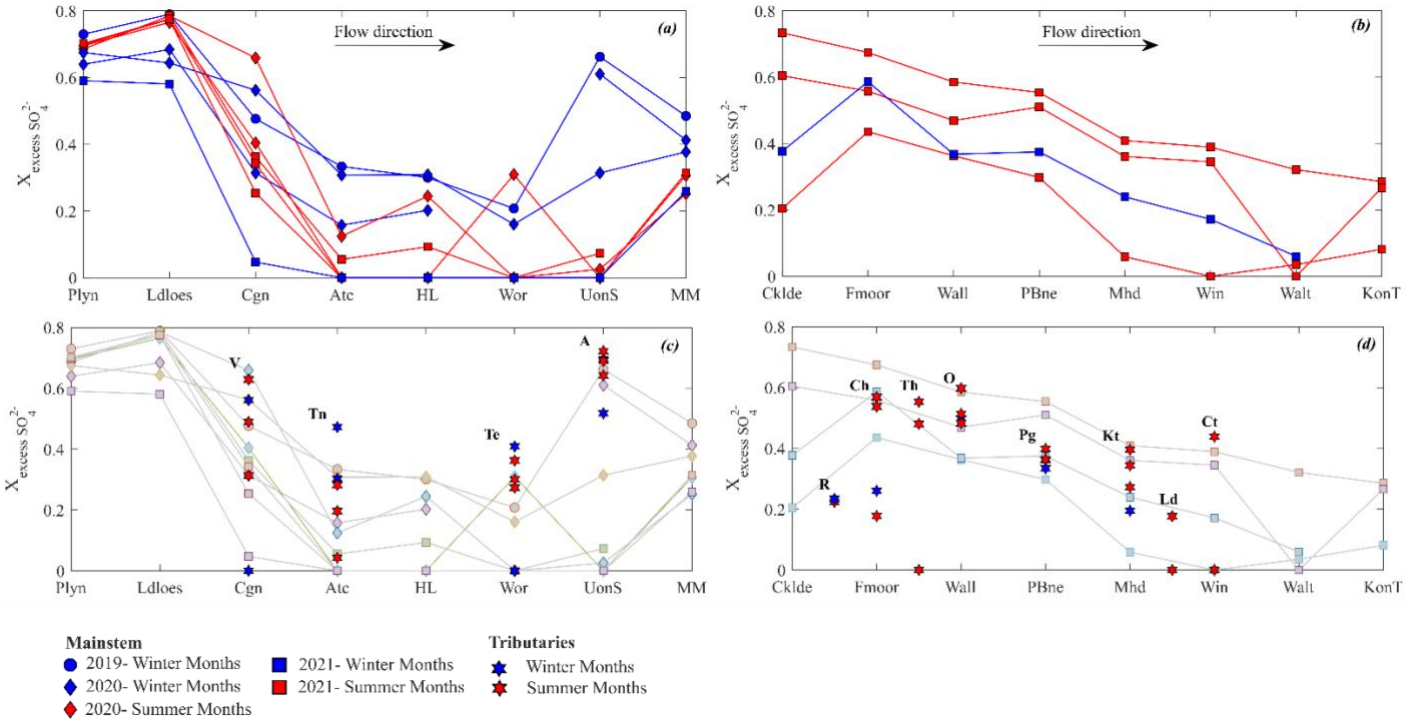

Figure 3.11- The variation in excess SO_4^{2-} along the mainstem of the river (a) Severn and (b) Thames, as well as the Severn's tributaries (c) and Thames tributaries (d). Sampling periods are defined into summer months (Apr-Sept) and winter months (Oct- Mar), and year of sampling. Severn sampling localities: Plyn= Plynlimon, Ldloes= Llanidloes, Cgn= Crewgreeen, Atc= Atcham, HL= Hampton Loade, Wor= Worcester, UonS= Upton on Severn, MM= Maisemore. Thames sampling localities: Cklde= Cricklade, Fmoor= Farmoor, Wall= Wallingford, PBne= Pangbourne, Mhd= Maidenhead, Win= Windsor, Walt= Walton, KonT= Kingston upon Thames. Severn tributaries: V= Vyrnwy, Tn= Tern, Te= Teme, A= Avon. Thames tributaries: R= Ray, Ch= Cherwell, Th= Thame, O= Ock, Pg= Pangboune, Kt= Kennet, Ld= Loddon, Ct= Cut.

Some observations can be made from these results:

(i) The decrease in $f_{excess\ SO_4^{2-}}$ from the mouth to estuary in the Thames may be related to a change in fertilizer derived input, given a similar decrease in arable land % from source of the river to estuary (Figure 3.3). Equally however, this could also be driven by a change in lithology at Pangbourne from silicate to carbonate chalks (Figure 3.1b).

(ii) It is unclear what causes the large spatial variation in $X_{excess\ SO_4^{2-}}$ across the Severn catchment (Fig 3.11). The variation does not follow changes in arable land (Figure 3.3). If $X_{excess\ SO_4^{2-}}$ is primarily sourced from lithology, it might be that the increase in carbonate content within bedrock from source to estuary decreases the flux of sulphide sourced sulphate to the river. However, this does not

satisfactorily explain the significant increase from Upton on Severn to Maisemore (Figure 3.12).

(iii) The increased flux of $X_{excess\ SO_4^{2-}}$ in winter months aligns with the increased contribution of carbonate derived ions to the river (Figure 3.7). If $X_{excess\ SO_4^{2-}}$ is mostly derived from sulphides, then this could indicate that sulphide weathering may have a greater potential to impact the CDR of carbonates than silicates. This observation matches the current understanding of the ideal conditions for sulphide weathering (Calmels, 2007; Burke *et al.*, 2018). Water transported during winter months has a greater potential to be oxic, due to higher flow rates which often follow shorter and shallower flow paths (i.e. via direct runoff). Under these conditions, sulphides have a greater potential for oxidation, and may react at similar rates as carbonate minerals (Calmels, 2007). In contrast, in summer months of low flow, waters may become anoxic (if, for example, a greater proportion of water is sourced from groundwater), and therefore carry less potential to oxidise sulphides.

To evaluate the potential impact of $X_{excess\ SO_4^{2-}}$ on reducing the CDR of weathering in both catchments, the absolute value of $X_{excess\ SO_4^{2-}}$ is initially adjusted for volcanic and biogenic emissions. In alignment with the approach outlined in Burke *et al.*, (2018), this study applies reductions of 7% and 3% respectively, which correspond to the globally averaged proportion of riverine sulphate attributed to these natural processes, as discussed in Meybeck, (1983). The $SO_4^{2-}{}_{river}$ has therefore been corrected for evaporites, non-sulphide silicates, volcanic and biogenic emissions. the remaining $SO_4^{2-}{}_{river}$ will be derived from sulphides and from anthropogenic activity, namely fertilizer input. Due to the challenging nature of distinguishing between these two sources, it is first assumed that all remaining sulphate is derived from sulphides.

During rock weathering, one mole of sulphuric acid will liberate one mole of Ca^{2+} and Mg^{2+} and two Na^{+}, as well as release one mole of SO_4^{2-} (Equations 3.6 and 3.9). Therefore, every mole of riverine SO_4^{2-} attributed to sulphides $\left(SO_4^{2-}{}_{sulphides}\right)$ can be paired with one mole of Ca^{2+} and Mg^{2+} and 2 moles of Na^{+} from silicate and carbonate weathering. $SO_4^{2-}{}_{sulphide}$ is split between silicate and carbonate weathering in the ratio that they weather in the catchment (i.e.,

as detailed in Chapter 4). The percentage of weathering driven by sulphuric acid is then given by Equation 3.23:

$$(\%\ H_2SO_4)_i = \frac{SO_4^{2-}{}_{sulphides_i}}{total\ acid\ (umol\ L^{-1})_i} * 100 \quad (3.23)$$

Where $SO_4^{2-}{}_{sulphides_i}$ is the portion of $SO_4^{2-}{}_{sulphides}$ allocated to endmember (i) where i = silicate or carbonate, and $total\ acid\ (umol\ L^{-1})_i$ is the total acid needed to liberate all the cations from endmember i (where the total ionic charge of acid must balance the total cationic charge from weathering). This can then be used to reduce the CDR of silicate and carbonate weathering by Equations 3.24 and 3.25 respectively:

$$Net\ CDR_{sil}\ (mol\ s^{-1}) = Max\ CDR_{sil} * (100 - (\%\ H_2SO_4)_{sil}) \quad (3.24)$$

$$Net\ CDR_{carb}\ (mol\ s^{-1}) = \underbrace{Max\ CDR_{carb} * (100\% - \%\ H_2SO_4)}_{Reduced\ drawdown} + \underbrace{Max\ CDR_{carb} * \%\ H_2SO_4}_{Re\text{-}released\ CO_2} \quad (3.25)$$

Equation 3.25 accounts for the extra CO_2 re-released to the atmosphere (Table 3.1, Equation 3.9).

Table 3.11- The maximum estimated CO_2 consumption due to silicate and carbonate weathering in the Severn and the Thames, compared to the possible reduction in efficiency due to sulphuric acid weathering.

	Severn			Thames		
	Silicates	**Carbonates**	**Combined**	**Silicates**	**Carbonates**	**Combined**
Max CDR (Mt CO_2 yr^{-1})	0.065	0.232	0.297	0.014	0.207	0.22
Sulphide reduced CDR (Mt CO_2 yr^{-1})	0.054	0.14	0.194	0.012	0.16	0.17
range	0.03-0.091	0.12-0.16	0.16-0.24	0.003-0.039	0.14-0.17	0.15-0.21
% reduction	16.7%	39.6%	34.6%	10.2%	22.3%	21.5%

These calculations reveal the CDR attributed to natural weathering processes in the Severn catchment may be reduced by up to 35%, when influenced by sulphuric acid weathering (Table 3.11). The reduction is greatest for the carbonate component in the catchment. The Thames catchment experiences a comparatively smaller reduction in CDR, with a maximum decrease of 22%. Once again, the carbonate component demonstrates the highest potential for reduction (Table 3.11).

Incorporating pollutive SO_4^{2-} into calculations could improve the accuracy of the CDR reduction estimations given here (Table 3.11). It is likely that UK rivers receive some SO_4^{2-} from anthropogenic sources. A significant amount of fertilizer SO_3^- is added to grass and crops in the UK, with an average application rate of 5 and 30 kg ha^{-1} yr^{-1} respectively in 2021 (Defra, 2022). UK riverine SO_4^{2-} concentrations typically increase in catchments dominated by agriculture or urban zones (Neal *et al.*, 2012). The Severn and the Thames have average SO_4^{2-} concentrations which match those typically observed in agricultural rivers, as discussed in Neal 2012. Furthermore, as mentioned in Section 3.6.3, UK riverine $SO_4^{2-}$was shown to decrease in the early 2000's due to reductions in SO_2 emissions from fossil fuels.

Whilst high SO_4^{2-} concentrations can suggest anthropogenic influence and must be accounted for, available evidence implies that lithological influences may be more important in these catchments, i.e.-

(i) The use of sulphate fertilizer has increased significantly since the 1900's, however this is not reflected in the river SO_4^{2-} concentrations in either catchment (Appendix, Figure B.7).

(ii) As mentioned, both sulphate concentrations and $X_{excess\ SO_4^{2-}}$ are greater in the River Severn than the Thames, despite the latter having more arable land.

(iii) In a recent study (Chapter 4), it was observed that in UK catchments with extensive arable land, the $X_{excess\ SO_4^{2-}}$ was highly correlated with nitrate concentrations. $f_{excess\ SO_4^{2-}}$ was observed to be greater than average in these catchments. It was assumed that for these catchments, fertilizer is a significant source of $SO_4^{2-}{}_{river}$. There is no correlation between $X_{excess\ SO_4^{2-}}$ and nitrate in the Severn or the Thames catchments, suggesting that arable land may not be a significant source of sulphate in river water in these specific UK catchments.

Future work needs to focus on developing a method that can constrain the contribution of pollution to $SO_4^{2-}{}_{river}$. This will allow us to place further constraints on the total quantity of atmospheric CO_2 removed from natural weathering reactions.

3.6.4 Nitric Acid

Replacing carbonic acid with nitric acid can lead to a decrease in the overall CDR potential of weathering within a catchment (Table 3.1, Equations 3.7 (silicate) and 3.10 (carbonate)). An important source of nitric acid in the weathering environment is from N- rich fertilizers. Fertiliser application can supply significant nitrogen to soils: in 2021 for example, approximately 130 kg N ha^{-1} yr^{-1} and 51 kg N ha^{-1} yr^{-1} was spread on arable land and grassland respectively in the UK (Defra, 2022). A significant fraction of this nitrogen is not directly engaged in weathering reactions but is instead either extracted from the soil through plant uptake, washed or degassed from the field, or is re-released to the atmosphere as N_2 during denitrification (Oh and Raymond, 2006). The residual nitrogen may undergo nitrification which forms protons which can then be utilized in weathering reactions (Equation 3.26).

$$NH_4^+ + 2O_2 \rightarrow NO_3^- + H_2O + 2H^+ \text{ (3.26)}$$

Despite this initial decrease in potential CDR attributed to nitric acid induced weathering reactions (Equations 3.7 and 3.10), this reduction may be reversed dependent on the fate of the nitrate (NO_3^-) generated. Key fates of NO_3^- include:

(i) Retention within the soil for plant uptake.

(ii) Denitrification during river transport and re-release to the atmosphere as N_2. About 70% of nitrate introduced to the river will undergo denitrification (Gruber and Galloway, 2008)

(iii) Transport to the ocean with the cations sourced from weathering, i.e., the nitric acid weathering route.

When NO_3^- is lost from freshwater, through plant uptake or from denitrification, another anion must be introduced to maintain charge equilibrium in solution. This balance is typically achieved by the generation of bicarbonate (HCO_3^-) from atmospheric CO_2. Consequently, for scenarios (i) and (ii), the overall reduction to CDR is assumed to be negligible given the substitution of NO_3^- for HCO_3^- in the water column. Moreover, the oceanic residence time of nitrate (~3000) is on average much shorter than the residence time of the weathering- derived cations (e.g., calcium has a residence time of ~1 million years; Tipper *et al.*, 2010). As a result, it is expected that the CDR reduction, even via point (iii), will undergo reversal on timescales greater than 3000 years.

Nonetheless, on the durations necessary to address anthropogenic greenhouse gas emissions, the resultant decrease to calculated CDR via nitric acid weathering may be significant. Given that 29.8% and 35.6% of land in the Severn and the Thames catchment is attributed to arable land, and 47.6% and 32% to grassland, nitric acid weathering may still be a significant contributor to reductions in CDR.

Here, it is assumed that the (geologically) short-term reduction in CDR via nitric acid weathering reaction may be traced by assessing the fertilizer derived portion of riverine nitrate at the closest chemical monitoring station to the estuary for each river (See datasheets in supporting information).

i) Nitrate concentrations and $^{NO_3^-}/_{Cl}$ ratios

In the UK, the majority of riverine nitrate (70%) is attributed to agriculture, with sewage a second important contributor (25-30%) (Environmental Agency, 2019). The average nitrate concentration remains relatively stable across the seasons, exhibiting similar means during both summer and winter months (Table 3.12). When accounting for discharge, both rivers export slightly more nitrate in the winter months (Oct- Mar, Table 3.12).

Table 3.12- Seasonal variation in nitrate concentrations and flux. Data split into summer months (Apr- Sept) and winter months (Oct- Mar).

	Severn		**Thames**	
	Concentration (µmol L^{-1})	Flux (mol s^{-1})	Concentration (µmol L^{-1})	Flux (mol s^{-1})
Overall	91	9.8	116	7.2
Summer	90	5.0	105	3.2
Winter	91.5	13.5	125	10.5

River $^{NO_3^-}/_{Cl}$ ratios can be utilized to predict the origin of riverine NO_3^-: untreated effluents from manure and sewage typically exhibit low $^{NO_3^-}/_{Cl}$ ratios, whereas nitrate rich fertilizers have high $^{NO_3^-}/_{Cl}$ ratios (Xu *et al.*, 2021). Historic $^{NO_3^-}/_{Cl}$ indicates a seasonal variation in pollutive sources for both rivers (Figure 3.12), with a higher input of nitrates originating from fertilizer during the winter months. This may be attributed to increased runoff in late autumn and early winter (Marsh *et al.*, 2015), which facilitates the re-mobilization of excess fertilizer nitrate in soils, and increased transport of NO_3^- to rivers.

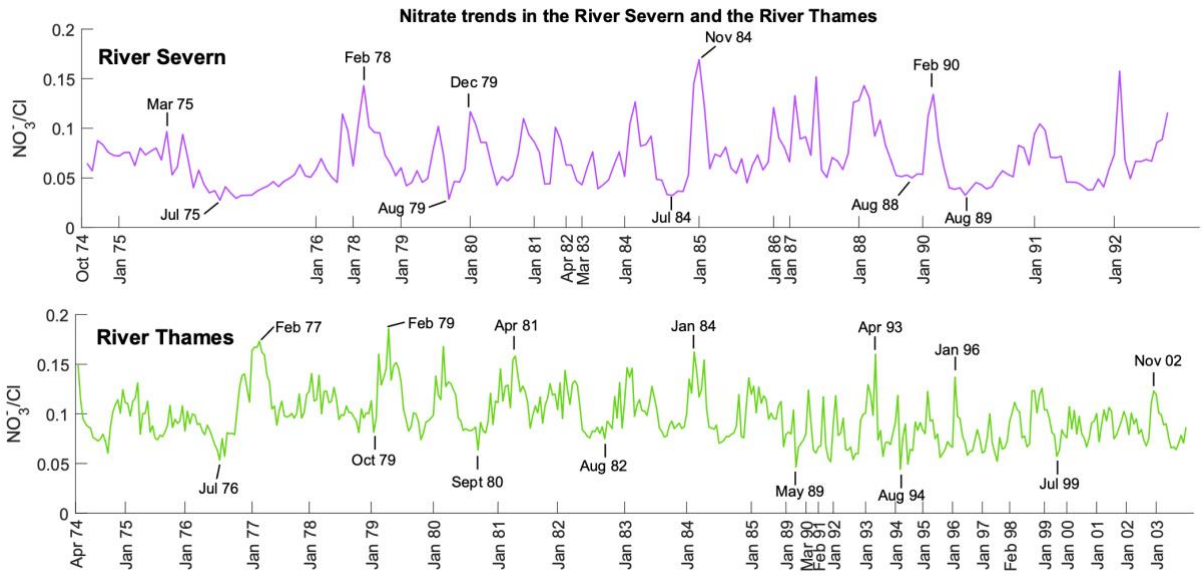

Figure 3.12- Historic NO_3^-/Cl in rivers Severn and the Thames. For both rivers, the historical annual quantity of samples collected was variable, with some years having extensive records while others had fewer. The x-axis of the graphs therefore represents individual sampling dates organised chronologically (See datasheets in supporting information). Random data points were highlighted in both plots to illustrate seasonal variations.

The River Thames has a slightly higher mean historic $^{NO_3^-}/_{Cl}$, suggesting a greater overall input of fertilizer derived NO_3^- than the River Severn, which is supported by the increased arable land content throughout the catchment (Figure 3.3a, b). In the river Thames, $^{NO_3^-}/_{Cl}$ decreases slightly downstream (Appendices, Figure B.9b), which may be due to a higher distribution of arable land towards the headwaters (Figure 3.3b). In contrast, the River Severn has an increasing $^{NO_3^-}/_{Cl}$ along stream (Appendices, Figure B.9a), which is probably due to an increase in the area utilized for arable land from Crewgreen (Figure 3.3a).

Neal *et al.*, (2006) demonstrated that $^{NO_3^-}/_{B}$ ratios can be employed in a similar manner to predict the source of nitrate in rivers. Low ratios are indicative of sewage point source input, while high ratios are associated with elevated fertilizer input (Neal *et al.*, 2006) utilized this relationship to quantify the proportion of nitrate in solution originating from fertilizer or animal waste, i.e. Equation 3.27:

$$\%NO_{3\,diffuse}^- = 100 * {([NO_3^-] - (R * C * [B]))}/{[NO_3^-]} \quad (3.27)$$

Where R is the ratio of nitrate to boron in waste effluent (0.104 mg NO_3^- ug B^{-1}), and C is the factor to correct for alternative sources of B (C= 0.6) (Neal *et al.*, 2006). Using this calculation, the average percentage of riverine nitrate from agriculture is 75% (66-87%) for the Severn, and 79% (71-89%) for the Thames. These values align with the Environmental Agency's prediction that on average 70% of nitrate in English rivers is sourced from fertilizer (Environmental Agency, 2021).

(ii) Impact of nitric acid on CDR

Here, given that both the calculations (using Equation 3.27) and the Environmental Agency result in similar estimates for the percentage of riverine nitrate sourced from fertiliser and animal waste, this study defines by $\%[NO_3^-]_{agriculture}\ as\ 70\%$ of riverine NO_3^-. Given the stoichiometry of Equations 3.7 and 3.10, every 2 moles of $[NO_3^-]_{agriculture}$ may be associated with 1 mole of Ca/ Mg, and 2 moles of Na. CO_2 reduction via nitric acid weathering was then calculated with the same principles as for sulphuric acid (discussed in Section 3.6.3) i.e. that i) nitric acid will likely dissolve silicate and carbonate rocks in the same ratio in which they are being weathered in each catchment, that ii) nitric acid weathering results in no drawdown of atmospheric CO_2 due to silicate weathering (Equation 3.7), and (iii) releases CO_2 due to carbonate weathering (Equation 3.10).

Table 3.13- Potential impact of nitric acid on the CDR budget of natural weathering in the Severn and the Thames. In (Mt $CO_2\ yr^{-1}$)

	Severn			**Thames**		
	Combined	Silicate	Carbonate	Combined	Silicate	Carbonate
Max	0.297	0.065	0.23	0.207	0.0137	0.21
Reduced	0.288	0.064	0.22	0.213	0.0135	0.20

Calculations suggest that nitric acid weathering may lower the CDR of weathering in the Severn by 3.0% (1.9-2.9%) and in the Thames catchment by 3.1% (2.1-6.6%), which implies that nitric acid will not significantly impact the CDR of UK weathering.

3.6.5 Overall reduction to CDR via riverine processes and comparison to other UK and global basins

In summary, this study shows that the total decrease in the calculated CDR, after correcting for processes that might be involved in altering riverine cation loads apart from carbonic-acid weathering (strong acid weathering, cation exchange and carbonate precipitation), may be up to 38% and 25% respectively. Most of the correction is caused by sulphuric acid weathering, while other processes lead to much smaller corrections to the CDR calculations (Table 3.14).

Table 3.14- Maximum potential CDR due to natural weathering in the Severn and the Thames catchments, assuming that all weathering derived cations are balanced in the river by HCO_3^-. Given in annual flux (Mt CO_2 yr^{-1}) and yield (kg CO_2 ha^{-1} yr^{-1}). Compared to the reduced CDR due to correcting for the river cations derived from sulphide and nitric weathering, as well as for carbonate precipitation and cation exchange.

	Severn			**Thames**		
	Combined	Silicate	Carbonate	Combined	Silicate	Carbonate
Maximum CDR (Mt CO_2 yr^{-1})	0.297	0.065	0.232	0.22	0.014	0.21
Maximum CDR yield (kg CO_2 ha^{-1} yr^{-1})	300	66	234	222	14	208
- **Sulphides**	34.6%	16.7%	39.6%	21.5%	10.2%	22.3%
- **Nitric acid**	3.0%	1.7%	3.4%	3.1%	2.0%	3.2%
- **Cation exchange**	0.17%	7.1%	-1.7%	0.18	7.1%	-0.33
- **Carbonate precipitation**	n.a	n.a	n.a	n.a	n.a	n.a
Overall CDR Mt CO_2 yr^{-1}	0.185	0.0484	0.136	0.165	0.0112	0.157
Overall CDR yield (kg CO_2 ha^{-1} yr^{-1})	182	49	137	166	11	158
Overall yield range (kg CO_2 ha^{-1} yr^{-1})	152- 232	27- 82	120- 153	140- 201	2- 35	140- 170

3.7 Conclusions

This study aimed to provide a first assessment of the potential CO_2 sequestration due to natural silicate and carbonate weathering in two major UK catchments: the River Severn and the River Thames. Chemistry from a two-year time series sampling campaign was compared with a historic dataset from the Environmental Agency to evaluate potential spatial and temporal variations in the sources of ions to each river.

Although the catchments had clear distinctions in chemistry attributed to differences in lithology, model results suggest that the flux of cations in both rivers is dominated by carbonate weathering. Initially assuming that carbonic acid is the only weathering agent, and all weathering products remain dissolved in the water, this research predicts that the maximum annual atmospheric CO_2 removed due to weathering will range between 0.24-0.37 and 0.19-0.26 Mt CO_2 yr^{-1} for the Severn and the Thames respectively. Silicate weathering is expected to contribute to approximately 22% (Severn) and 6% (Thames) of this total drawdown estimate.

These values of CDR must be corrected for processes that might be involved in altering riverine cation loads apart from carbonic-acid weathering. Of these, sulphuric acid weathering is the largest correction and reduces calculated CDR fluxes by up to 35% (River Severn) and 22% (River Thames). Nitric acid weathering may also reduce calculated CDR fluxes by 2-3%. Overall, once corrected for sulphuric and nitric acid weathering, the range in the CDR calculated from natural weathering in the Severn and the Thames catchments is 0.15-0.23 and 0.14-0.20 Mt CO_2 yr^{-1} respectively.

The silicate and carbonate CO_2 yields of these two UK catchments closely resemble the global average calculated from other major larger basins. This observation is unexpected, as optimal weathering conditions, typically associated with sub-equatorial regions featuring higher temperatures and runoff, are not characteristic of the UK. This suggests that factors such as lithology, agricultural practices, and extended water residence times, may play a significant role in raising weathering rates in the Severn and the Thames basins.

The results expressed here can be employed in future modelling to provide baselines from which to compare the effect of enhanced weathering in UK catchments (Chapter 5).

Chapter 4

4 Atmospheric carbon dioxide removal due to chemical weathering processes in the UK

Abstract

The chemical weathering of both silicate and carbonate rocks via carbonic acid provides a natural sink for atmospheric carbon dioxide and has regulated global climate over geological timescales. Although the magnitude of CO_2 removal via natural weathering been estimated at a global scale, it is not well constrained for the United Kingdom. Quantifying this sink would enhance our current understanding of the UK's carbon cycle and benefit future climate projection models. Using river chemistry and a geochemical inversion model (MEANDIR), this study first identifies the proportion of solutes from silicate and carbonate sources within UK rivers, before providing a first estimate of the annual CO_2 consumed by natural weathering.

Results of the inversion suggest that the fraction of solutes sourced from silicates ranges between 0-46% (median 7%) across the rivers in the study, whilst for carbonates, this range is between 9-82% (median 49%). The remainder of major solutes are derived from evaporite weathering (1-48%, median 24%) and cyclic sources (2-76%, median 11%).

The maximum annual quantity of carbon dioxide removed through combined silicate and carbonate weathering is 2.54 Mt CO_2 yr^{-1} for the catchments within the study (which represent 40% of total UK area). Of this, approximately 21% is sourced from silicate weathering. Extrapolating to the area of the whole UK landmass results in an annual natural weathering CDR of 6.3 Mt CO_2 yr^{-1}. These estimates assume that reactions are proceeding via carbonic acid weathering. However, if sulphuric acid replaces carbonic acid as the reagent, the CDR reported here may be significantly reduced. Geochemical mixing equations suggest that this reduction could be up to 17% and 29% for silicate and carbonate weathering respectively. A conservative estimate which takes into consideration the potential for sulphuric acid weathering

suggests that the net combined CDR is 1.8 Mt CO_2 yr^{-1} for the catchments within the study and 4.6 Mt CO_2 yr^{-1} for the whole UK.

The values reported here lie on the lower end of current estimates for the potential CDR via the application of Enhanced Rock Weathering in the UK. This suggests that for EW to provide the scale of CDR previously proposed for the UK, it will have to at least replicate, but likely exceed, natural weathering fluxes. This will have implications for riverine chemistry which will need to be considered prior to the widespread application of ERW in the UK.

4.1 Introduction

The natural sources and sinks of carbon dioxide set the context in which anthropogenic changes in the carbon cycle are set, and human emissions measured. One such sink is the weathering of silicate and carbonate rocks which consumes atmospheric CO_2 (via Equations 4.1 and 4.2) (Berner *et al.*, 1983; Gaillardet *et al.*, 1999). These fluxes can vary spatially (White and Blum, 1995; West *et al.*, 2005; Moon *et al.*, 2014) and temporally (Raymo and Ruddiman, 1992; Tipper *et al.*, 2006), and the environmental drivers of weathering may respond to ongoing future climate and land use change (Regnier *et al.*, 2013; Raymond and Hamilton, 2018; Zeng *et al.*, 2019; Hilton and West, 2020). Identifying the potential variability of these weathering fluxes is crucial to accurately assess the natural carbon cycle. In addition, proposals to enhance mineral weathering (See Chapter 5 and Renforth, 2012; Hartmann *et al.*, 2013; Beerling *et al.*, 2020; Kantzas *et al.*, 2022) benefit from knowledge of the baseline, natural weathering reactions, as these govern the natural water chemistry and potential for streams and rivers to carry excess solution and carbon species (i.e. Knapp and Tipper, 2022; Zhang *et al.*, 2022; Harrington, Hilton and Henderson, 2023).

$$Mg_2SiO_4 + 4H_2CO_3 \rightarrow 2Mg^{2+} + 4HCO_3^- + H_4SiO_{4(aq)} \quad (4.1)$$

$$CaCO_3 + H_2CO_3 \rightarrow Ca^{2+} + 2HCO_3^- \quad (4.2)$$

Silicate and carbonate weathering both contribute atmospheric CO_2 as dissolved inorganic carbon (DIC) to rivers. However, whilst the DIC from silicate weathering is entirely sourced from the atmosphere (Equation 4.1), the DIC from carbonates partially originates from the rock itself (Equation 4.2). Therefore, the total atmospheric carbon dioxide removed (CDR) due to natural weathering is not equal to the total flux of DIC in rivers. Additionally, due to the eventual re-precipitation of carbonates in the ocean (via Equation 4.3), carbonate weathering does not lead to the long-term removal of CO_2. Therefore, correctly apportioning the DIC between the two endmember sources is critical when studying the role chemical weathering plays in the natural long-term carbon cycle.

$$Ca^{2+} + 2HCO_3^- \rightarrow CaCO_3 + CO_2 + H_2O \quad (4.3)$$

Silicate and carbonate contributions to DIC are determined from attributing riverine dissolved chemistry to different source endmembers of a known composition or compositional range (Gaillardet *et al.*, 1999; Tipper *et al.*, 2006; Moon *et al.*, 2014) (i.e., Chapter 1). Previous global assessments have demonstrated that natural annual carbon dioxide removal (CDR) due to silicate weathering may range between 330-510 Mt CO_2 yr^{-1} (Gaillardet *et al.*, 1999; Moon *et al.*, 2014), and for carbonates, between 730-2570 Mt CO_2 yr^{-1} (Gaillardet *et al.*, 1999; Zeng *et al.*, 2019). This CO_2 consumption is not evenly distributed globally, due to spatial variations in environmental drivers which are known to influence weathering reactions, such as geological heterogeneity and mineral composition; variability in permeability and aquifer content (Maher, 2011), water availability (Buckingham *et al.*, 2022; Brantley *et al.*, 2023) and the residence time of this water within the catchment (Maher, 2011; Maher and Chamberlain, 2014); amount of erosion supplying fresh minerals (Maher and Chamberlain, 2014); temperature; presence of sulphide minerals (Torres *et al.*, 2014; Burke *et al.*, 2018; Hilton and West, 2020; Bufe *et al.*, 2021); and arable land (Perrin *et al.*, 2008; Barnes and Raymond, 2009; Raymond and Hamilton, 2018) (See Chapter One for full discussion on these drivers of weathering). As such, the silicate weathering CDR yield of 43 global catchments spans two orders of magnitude (1.18-450 kg CO_2 ha^{-1}) (Moon *et al.*, 2014). Due to the sensitivity of carbonate weathering to climate and increased runoff, CDR yield in tropical equatorial regions is significantly higher than in arctic zones: 1700 and 2 kg CO_2 ha^{-1} respectively (Zeng *et al.*, 2019). The UK is typical of many nations, with large spatial variability in these catchment parameters. As such, CDR weathering yields may also be significantly heterogenous across the UK.

The UK's annual riverine DIC flux, and the variation observed between catchments, has been established by two key studies. Jarvie *et al.*, (2017) utilised an extensive geochemical dataset of river chemistry within a carbonate speciation model (THINCARB) to derive DIC flux estimates across all major UK catchments. The study found that average DIC concentrations increased from northwest to southeast, and attribute this to increases in carbonate content within the underlying lithology. Recently, to estimate DIC fluxes and investigate potential environmental drivers of this flux, Tye *et al.*, (2022) performed an extensive year-long sampling campaign across 43 UK catchments, representing 36% of the UK landmass. They report the annual DIC flux to be 647 kt C as DIC yr^{-1} (2.4 Mt CO_2 yr^{-1}) across the catchments within their study. They also conclude that variability in DIC concentrations is primarily

controlled by lithology, whilst total annual yields (kg CO_2 ha^{-1} yr^{-1}) are also influenced by water availability.

These two studies add to our understanding of the DIC flux and variation in UK rivers, however the magnitude of CO_2 removed from the atmosphere nationally via the natural chemical weathering of silicate and carbonate minerals is yet to be quantified. This study will therefore expand on the contributions of Jarvie *et al.*, (2017) and Tye *et al.*, (2022) by quantifying silicate and carbonate weathering rates across the UK, using river geochemical data from catchments representing a broad range in weathering environments. The aims of this work are to (i) provide a value for the annual flux of CO_2 removed due to weathering processes in the UK, and (ii) quantify the spatial and temporal variability of these fluxes across catchments.

An understudied process is the role of strong acids in weathering. Rather than dissolution by carbonic acid, which acts as a sink, these strong acids can lead to CO_2 release (for carbonate dissolution, via Equations 4.4 and 4.6):

Sulphuric acid

- $CaCO_3 + H_2SO_4 \rightarrow CO_2 + H_2O + Ca^{2+} + SO_4^{2-}$ *(4.4)*
- $CaSiO_3 + H_2SO_4 + H_2O \rightarrow Ca^{2+} + H_4SiO_4 + SO_4^{2-}$ *(4.5)*

Nitric acid

- $CaCO_3 + 2HNO_3 + 2O_2 \rightarrow Ca^{2+} + 2NO_3^- + H_2O + CO_2$ *(4.6)*
- $CaSiO_3 + 2HNO_3 + H_2O \rightarrow 2NO_3^- + Ca^{2+} + H_4SiO_4$ *(4.7)*

Sulphuric acid forms from the oxidative weathering of sulphide minerals, common in UK bedrock. However, the distribution of sulphide- rich lithologies is not uniform (Figure 4.2) and consequently, it is expected that the underlying geology of a catchment will dictate the extent of CDR reduction by sulphuric acid. This reduction may be significant: a focused study of the Severn and the Thames catchments found that sulphuric acid weathering may reduce the annual combined CDR (i.e. silicates + carbonates) by 22-44% and 11-22% respectively (Chapter 3). A significant source of nitric acid to the weathering zone is fertilizer nitrate. In the Severn and Thames catchments, nitric acid only decreased the total CDR of weathering by 1-3% (Chapter 3). However, there may be potential for greater reduction in catchments which have a high

percentage of arable land and carbonate lithologies (i.e. the Wensum, Nene, Great Ouse, see Appendices Table C1 for % arable land).

Through the evaluation of the UK's baseline weathering CDR fluxes, the objective of this investigation has been to inform future modelling studies and contribute to the current understanding of the United Kingdom's natural carbon cycling processes.

4.2 Summary of the approach

The main objective of this study was to assess the natural CDR from weathering in the UK and distinguish the proportion from silicate and carbonate weathering. The following summarizes the approach used to quantify CDR:

i) The chemistry of 52 rivers was collated, representing variable UK weathering conditions (Section 4.3.1).
ii) The average DIC concentration (in µmol CO_2 L^{-1}) was calculated using the natural alkalinity and pH of each river in carbonate speciation equations (Section 4.4).
iii) The atmospheric portion of DIC (i.e., CDR) was then quantified by assessing the portion of river alkalinity from silicate and carbonates. Under the assumption that: (i) conservative alkalinity is dominated by three main cations (Ca^{2+}, Mg^{2+}, Na^{+}- see discussion in Section 4.5.2), and (ii) only four endmembers influence their concentrations (silicate, carbonate, evaporite and cyclic sources- see Chapter 2 for discussion about anthropogenic influences), inversion mixing equations were then used to distribute Ca^{2+}, Mg^{2+}, Na^{+} between each end- member source. These results are given as fractions (Section 4.5).
iv) Fractions were converted to cation fluxes using river discharge. As the cyclic and evaporite endmembers do not influence CO_2 drawdown, catchment CDR was calculated from the fluxes derived from silicate and carbonate weathering. Results were collated and upscaled to account for the whole UK land mass. The maximum CDR is compared to the total DIC (Mt CO_2 yr^{-1}) to quantify the proportion of DIC from the carbonate rock itself. (Section 4.6).

v) Post inversion, riverine SO_4^{-2} concentrations were then used in simple conservative mixing models to predict the total SO_4^{-2} from sulphides. This value is then used to correct for strong-acid dissolution and predict the net CDR (Section 4.7).

4.3 UK catchment characteristics

Fifty-two separate UK river catchments were chosen to be included in the study (Figure 4.1) and are assumed to capture the range in weathering styles within in the UK due to variations in geology (Section 4.3.2, Figure 4.2a), topography (Section 4.3.2, Figure 4.2b), land use (Section 4.3.4, Figure 4.3), climate, and water availability (Section 4.3.3). The total catchment area of the studied catchments is 9.45 Mha, accounting for 40% of the total land within the UK (23.35 Mha; Marston *et al.*, 2022). Variations in catchment parameters are also provided in (Appendices, Table C1)

4.3.1 River chemistry

UK geochemical data was taken from an extensive dataset from the Harmonised Monitoring Scheme (HMS), Environmental Agency (DEFRA, 2013), spanning between 1970-2013. Rivers from this dataset could only be included within the study if the complete suite of geochemical data needed for the inversion and subsequent calculations was available (i.e., Ca^{2+}, Mg^{2+}, Na^{+}, Cl^{-}, SO_4^{2-}, NO_3^{-}, pH, alkalinity, flow rate, temperature). Therefore, for each river, the data was first sorted to exclude any sampling dates without this complete set (provided in datasheets within supporting information). Where data was available, the 20 rivers with the highest flow rate were included (Marsh *et al.*, 2015). Rivers with high amounts of arable land were also included to compare the natural weathering fluxes with the potential increased fluxes calculated in Chapter 5 due to the application of silicate material to the arable land. Only rivers with at least 40 separate measurements (median number of measurements included in the inversion for each river was 160) were chosen to be included within the study to try to capture the potential seasonal variability in flow and chemistry of each river. Moon *et al.*, (2014) found that the annual silicate weathering rates of global rivers with 40 datapoints was calculated within 40% uncertainty of those with extensive measurements. However, an exception was made for the

Rivers Ouse and Hull (which had only 14 and 21 datapoints with the complete set of geochemical information needed in the inversion respectively) as they are major UK catchments with high arable land content (and therefore potential sites to be used for the application of enhanced silicate weathering, i.e. see Chapter 5. There is a need for caution when considering the results of these two catchments.

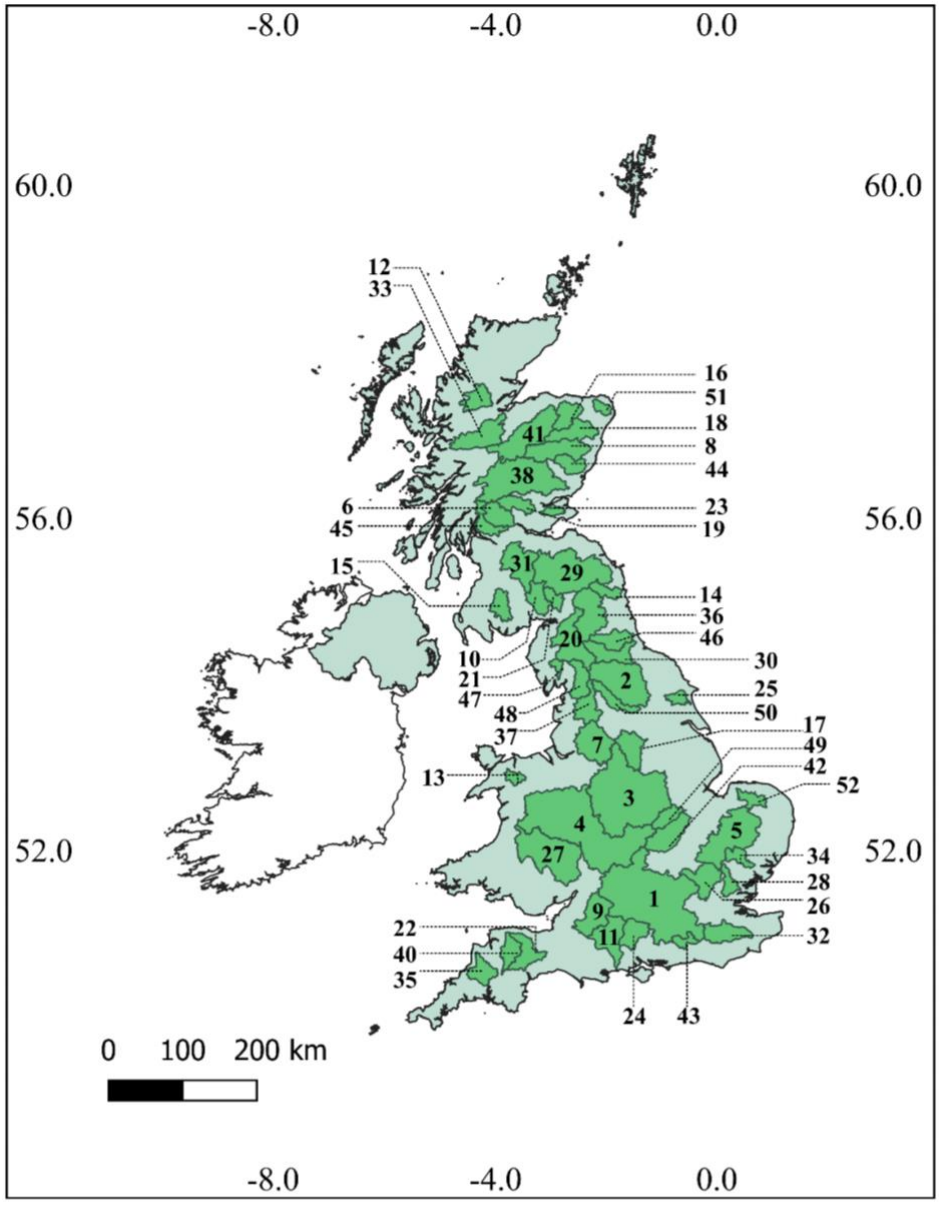

1. Thames
2. Ouse
3. Trent
4. Severn
5. Ely Ouse
6. Forth
7. Mersey
8. Dee, Ab'shire
9. Avon, Bristol
10. Annan
11. Avon, H'shire
12. Conon
13. Conwy
14. Coquet
15. Dee, Glenlochar
16. Deveron
17. Don, Ouse
18. Don, Ab'shire
19. Earn
20. Eden, B'mont
21. Esk
22. Exe
23. Eden, F o' Tay
25. Hull
24. Test
26. Lee, London
27. Wye
28. Chelmer
29. Tweed
30. Tees
31. Clyde
32. Medway
33. Ness
34. Stour
35. Tamar
36. Tyne
37. Ribble
38. Tay
39. Nith
40. Taw
41. Spey
42. Nene
43. Arun
44. Nth Esk
45. Leven, R
46. Wear
47. Leven, H
48. Lune
49. Welland
50. Wharfe
51. Ugie
52. Wensum

Figure 4.1-UK Catchments included in this study. Catchment boundaries were supplied from the National River Flow Archive, by the Centre of Ecology and Hydrology's Integrated Hydrological Digital Terrian Model (IHDTM) (Morris and Flavin, 1990; NRFA, 2023). *For specific catchment details see Table 4.4.1 (for area, flow, land use variables and chemistry), and for data used in model see datasheets with supporting information*

Table 4.1- Average chemical composition of the UK rivers within the study. Data collated from the Harmonised Monitoring Scheme dataset (DEFRA, 2013)

Catchment	Average Discharge (m^3s^{-1})	Average suspended sediment (mg L^{-1})	NRFA catchment area (GHa)	Alkalinity (μEqL^{-1})	Ca^{2+} ($\mu molL^{-1}$)	Mg^{2+} ($\mu molL^{-1}$)	Na^{+} ($\mu molL^{-1}$)	K^{+} ($\mu molL^{-1}$)	Cl^{-} ($\mu molL^{-1}$)	SO_4^{2-} ($\mu molL^{-1}$)	NO_3^{-} ($\mu molL^{-1}$)
Conon	50.3	1.7	0.096	99.6	41.2	39.3	228.9	10.2	282.5	24.6	1.7
Conwy	19.2	4.1	0.034	157.5	115.0	31.9	255.5	20.9	341.1	52.4	6.2
Ness	90.8	1.6	0.184	166.8	75.8	40.0	193.7	0.0	258.7	20.9	3.6
Dee (Aberdeenshire)	47.3	3.1	0.184	374.6	176.5	71.0	300.2	26.1	336.1	60.9	12.9
Spey	65.7	6.5	0.115	403.6	164.1	66.1	289.1	24.9	314.0	38.7	5.2
Deveron	16.9	8.2	0.095	436.1	412.3	217.1	612.9	63.8	681.2	114.6	47.0
Tay	172.5	4.4	0.459	441.4	206.4	65.7	206.0	19.0	202.3	38.4	9.6
Forth	46.3	9.2	0.104	553.3	230.0	97.0	306.9	32.2	301.6	83.9	8.0
Ugie	5.0	8.7	0.033	697.2	453.6	256.8	1033.5	85.9	1159.9	191.1	81.6
Tamar	22.9	23.5	0.092	725.4	433.7	198.2	553.5	80.7	641.8	161.5	43.2
Don (Aberdeenshire)	21.1	10.5	0.127	851.9	431.8	220.0	714.4	60.2	739.0	127.3	48.0
Annan	31.0	9.8	0.093	1040.5	512.0	201.5	355.8	37.0	366.5	128.7	23.1
Exe	25.4	14.4	0.119	1259.3	664.9	247.2	613.1	80.6	625.7	193.7	57.6
Tyne	45.3	11.7	0.218	1384.8	801.2	272.5	443.5	49.1	507.5	361.6	13.9
Esk	18.0	9.0	0.050	1417.2	615.3	233.3	325.6	20.1	311.7	79.9	8.8
Tweed	81.8	9.0	0.439	1477.8	627.8	339.3	376.4	34.8	455.7	205.8	27.1
Clyde	48.6	14.3	0.190	1671.3	802.4	424.3	1443.7	104.7	1387.1	398.5	32.2
Tees	20.8	12.5	0.126	1796.6	1036.3	467.7	1030.0	84.4	879.6	643.6	61.1
Eden (Beaumont)	54.6	13.9	0.229	1938.7	992.2	297.3	641.2	63.2	710.0	264.1	34.7
Coquet	8.7	11.6	0.057	2006.5	857.1	438.2	696.9	57.2	557.4	364.2	18.4
Welland	4.1	18.4	0.072	2018.4	3311.6	468.8	1581.5	168.9	1612.3	1607.4	118.6

Wye	73.5	23.7	0.401	2055.7	1016.6	304.3	448.7	58.6	461.7	165.8	40.4
Test	11.2	14.4	0.104	2074.8	2357.2	86.7	435.8	38.4	503.2	173.2	77.8
Medway	11.2	19.7	0.126	2196.9	1655.7	276.0	1356.6	151.1	1268.4	676.1	97.0
Severn	111.6	40.8	0.990	2542.0	1719.8	619.7	1690.1	145.9	1579.2	930.4	95.5
Ouse	52.1	17.0	0.332	2588.4	1508.0	446.9	667.0	76.1	749.3	513.8	55.3
Ribble	34.5	19.4	0.115	2765.1	1461.4	168.7	1299.7	87.6	714.0	271.6	137.7
Trent	90.7	25.9	0.823	3259.6	2568.6	997.9	3473.0	274.8	3050.5	1822.8	143.6
Wear	15.0	23.5	0.101	3416.1	1504.8	1004.2	3066.3	209.5	1785.1	1561.4	52.1
Avon (Hampshire)	20.1	9.2	0.171	3740.8	2326.1	98.3	529.8	57.1	599.4	254.7	79.3
Thames	65.5	19.4	0.995	3799.0	2482.2	221.3	1411.9	171.2	1256.1	682.9	117.7
Hull	5.3	7.2	0.038	3815.2	2099.4	179.6	553.5	7.0	595.8	226.5	75.6
Nene	9.3	18.7	0.163	4014.3	3292.3	440.5	2242.6	256.1	2063.0	1708.9	139.4
Lee	5.6	20.2	0.136	4094.3	2884.0	452.2	3199.7	347.8	3032.3	1088.6	197.7
Chelmer	1.9	15.9	0.053	4196.4	3211.1	485.9	1957.0	208.6	2071.9	1696.9	46.8
Avon (Bristol)	20.4	21.0	0.161	4557.9	2806.2	273.3	1259.5	0.2	1172.1	590.1	118.9
Ely Ouse	15.5	13.3	0.343	4699.1	3694.4	391.1	1763.6	201.8	1760.8	1463.4	136.6
Stour	2.9	14.8	0.058	4945.4	3401.5	358.6	1909.7	178.5	1906.7	1034.5	126.3
Wensum	4.1	8.2	0.057	4957.2	3232.3	187.1	960.1	110.1	1333.4	637.9	112.1
Arun (Sussex)	5.6	25.0	0.038	1580.3	960.3	237.6	1413.8	176.7	1080.2	523.6	89.5
Taw	18.2	15.7	0.083	723.7	373.7	200.6	563.8	68.6	557.7	123.4	44.8
Lune	36.9	7.1	0.098	1465.3	842.0	149.7	362.6	47.9	392.0	241.8	15.0
Dee (Glenlochar)	41.6	3.0	0.081	133.9	82.8	53.4	209.4	14.4	224.2	43.5	4.3
Leven (Renton)	45.7	3.6	0.078	279.7	120.8	53.1	229.6	17.0	250.4	31.4	0.0
Leven (Haverwaite)	14.2	4.1	0.025	347.8	199.5	51.3	287.5	18.8	285.4	112.4	8.2
Don (Ouse)	16.5	27.1	0.126	3236.6	1467.0	916.6	3716.0	244.6	2776.0	1519.5	121.3
Wharfe (Ouse)	17.7	4.8	0.073	137.4	113.6	52.4	275.5	16.9	242.0	72.6	7.4

North Esk	19.6	8.5	0.073	773.9	334.6	120.3	334.1	27.4	312.3	81.1	31.4
Earn	29.6	5.7	0.078	662.5	321.5	101.6	234.8	21.3	219.3	50.3	20.9
Mersey	36.7	20.2	0.203	1696.4	1109.8	344.0	2716.0	190.0	2142.8	817.2	72.3

4.3.2 Geology and topography

The heterogeneity in bedrock and topography across the UK is likely to influence the chemistry across the catchments within the study. The highlands of NW Scotland are silicate rich and dominated by Precambrian and Cambrian metasediments (Lewisian Gneiss) and meta-igneous intrusions. From the northwest to southeast, lithology gets progressively younger, (Figure 4.2a) and the proportion of carbonate lithology increases. Within the midlands and Wales, carboniferous clays and limestones are also associated with coal measures which are known to have pyrite inclusions (Spears *et al.,* 1999).

High permeability within bedrock can indicate increased weathering within a catchment (Worthington *et al.,* 2016) due to increased fluid residence times (Maher, 2010) and therefore an increased flux of weathering sourced solutes to the river. The percentage of high permeability bedrock also increases moving from north to south across the UK. The National River Flow Archive classifies over 70% of the bedrock in the Ely Ouse, Avon and Stour (Hampshire), Test, Wensum and Hull catchments as highly permeable (these catchments have high proportions of carbonate lithologies). In contrast, 17 catchments in the study have zero bedrock classified as highly permeable (Appendices, Table C.1).

Topography in the UK is typically elevated in the northwest of Scotland, North England, and Wales (Figure 4.2b), however only 8 catchments within the studied regions have maximum elevations > 1000 m, and the highest point is ~1300 m (above sea level). Lowland areas are found in the southeast of England, and for 13 catchments the maximum elevation does not exceed 300 m (Appendices, Table C.1).

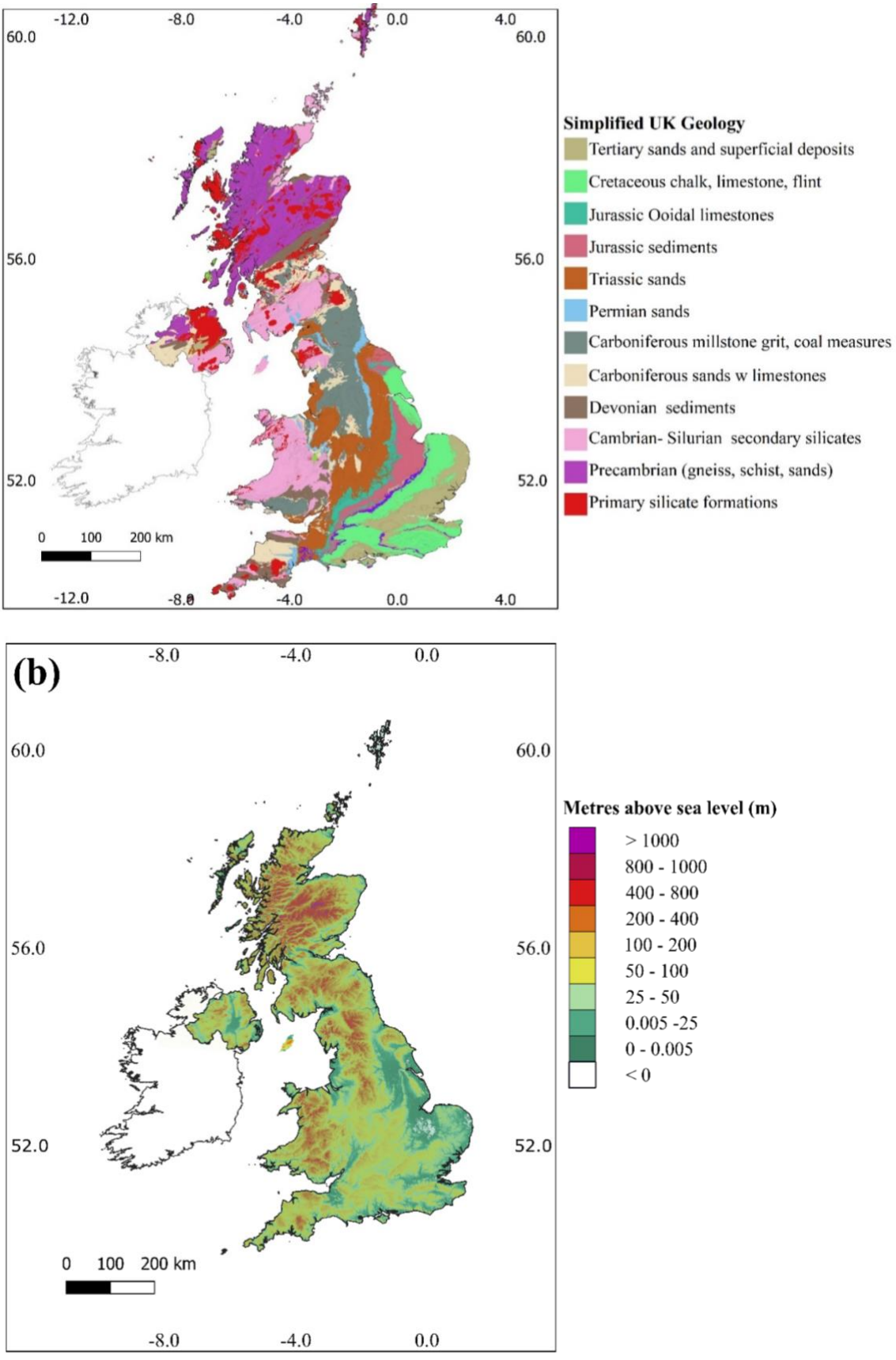

Figure 4.2 (a) UK geology (simplified from the British Geological Survey) (BGS, 2023a), *(b) Topography (LIDAR Composite 10m DTM)* (DEFRA, 2022b)

4.3.3 Hydrology

(i) Rain, evapotranspiration, soil moisture

Chemical weathering rates can be increased by increased water availability and fluid residence time (Maher, 2010, 2011), and hydrological conditions vary significantly across the UK (Kay *et al.*, 2013; Buckingham *et al.*, 2022). The average annual UK rainfall is 1175 mm (30- year average, MET office), however this varies across the country due to a rainfall gradient which increases from the southeast to northwest (Kay *et al.*, 2013). As such, Scotland and Wales have a much higher average annual rainfall than England (1600, 1450 and 875 mm yr^{-1} respectively, i.e. NRFA, 2023). In contrast, the potential evaporation (PE) within northern catchments is much lower than the southeast.

The variation in rainfall and evapotranspiration impacts the amount of moisture found within catchment soils. The average proportion of time that soils within a catchment are defined as 'wet' (PropWET, i.e. see Appendices, Table C.1; NRFA, 2023) also increases from South to North (The National River Flow Archive define this by the time that soil moisture deficits are less than 6 mm), with catchments in the South East of England having PropWet < 0.3, while Scottish catchments typically have indexes between 0.5-0.8 (Appendices, Table C.1).

(ii) River discharge, BFI and aquifer content

There is a dense network of rivers and streams within the UK. The average riverine discharge varies across the catchments within the study by two orders of magnitude (Table 4.1). Within individual catchments, seasonal variation tends towards a winter maximum flow for most rivers in the UK. The seasonal variation is related to temperature, which increases the potential evaporation of catchments to a maximum during the summer months (April- September). Evaporation increases lead to summer declines in flow rates, the impacts of which is most noted in lowland south-eastern areas.

Groundwater is recharged by approximately 7 billion m^3 yr^{-1} of water annually (Bloomfield *et al.*, 2013), which accounts for 4.2% of the total riverine discharge to the ocean (Marsh *et al.*, 2015). The main aquifers (the Chalk, the Permo-Triassic sands, the Jurassic limestones and

Lower Greensands) appear in the younger geology of the UK (Figure 4.1) and are distributed primarily in the southeast of England and Wales. Scotland has no major aquifers.

The baseflow index (BFI) of catchments, the measure of the proportion of river flow derived from stored sources (i.e. aquifers) varies within the catchments studied, from <0.4 in northern catchments, up to 0.9 in the southeast of England (Appendices, Table C.1).

4.3.4 Land Use

UK land is extensively used for agricultural purposes (Figure 4.3). The total area utilized for arable croplands and grasslands was approximately 17.0 Mha in 2021 (4.9 and 12.2 Mha respectively) (Marston *et al.*, 2022). Croplands are heavily distributed around the lowland southeastern areas, with 90% of all arable land located within 36 catchments (see Chapter 5, Figure 4.1a). Total agricultural land use has been remained between 17 and 18 Mha for the last two decades (2000-2021) (DEFRA, 2022a). The land use values reported here differ slightly to those used in recent DEFRA publications for the same period (i.e. EFRA), due to a slight distinction in the categorization of grassland types. Nevertheless, the overall combined land area for grassland and arable land is comparable for both data sources.

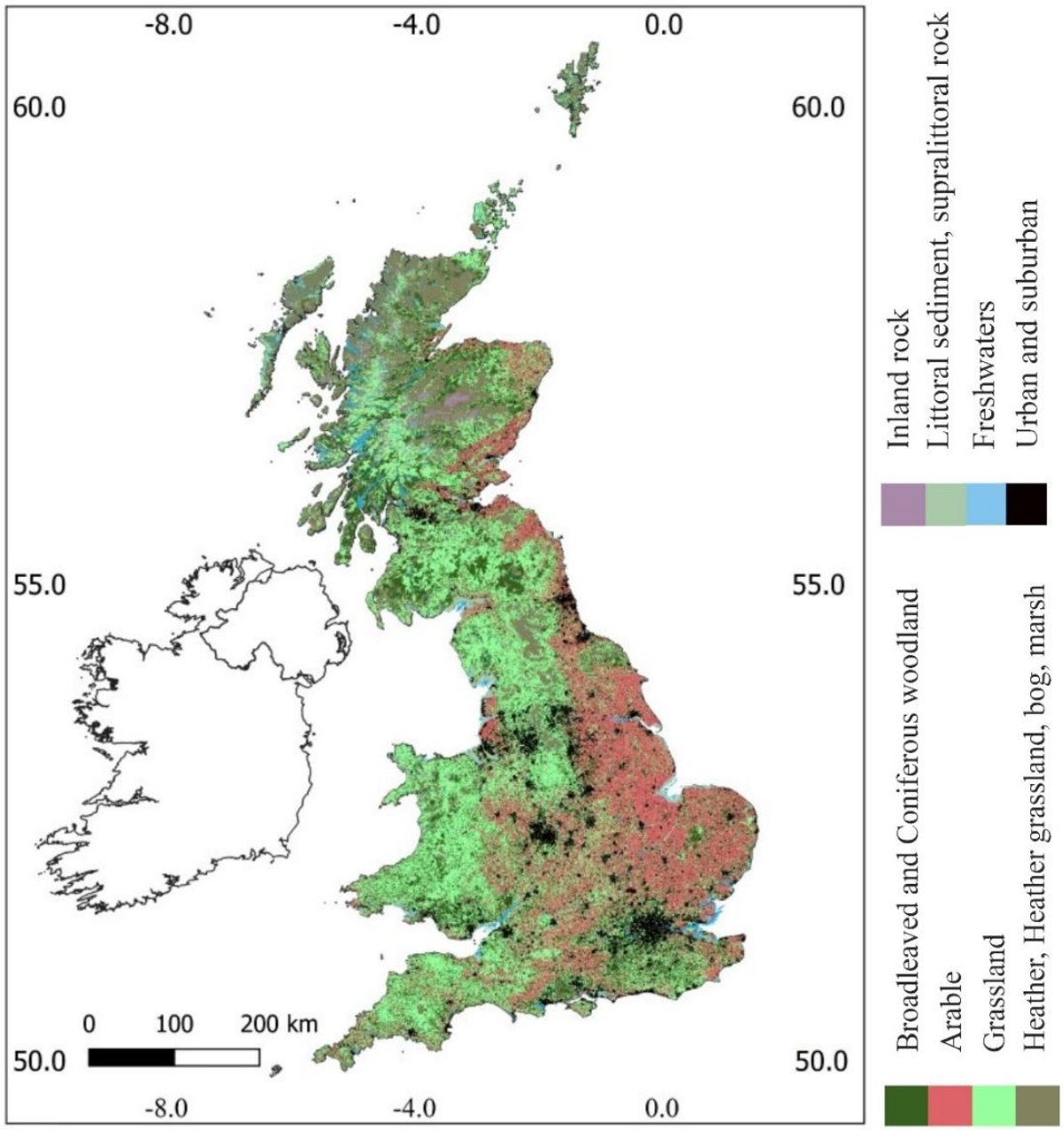

Figure 4.3- Land use variations within the UK. QGIS shapefile is the Land Cover Map 2021 (Marston *et al.*, 2022), *from the Centre of Ecology and Hydrology)*

4.4 Dissolved Inorganic Carbon (DIC) in UK rivers

Given the average alkalinity and pH of each river (Table 4.1), the average total dissolved inorganic carbon (DIC) concentration (in µmol CO_2 L^{-1}) was calculated for each catchment using carbonate speciation equations in PHREEQC (version 3) (Parkhurst and Appelo, 2013) and a temperature of 10°C, the approximate annual average temperature of UK rivers (Jonkers and Sharkey, 2016; Worrall *et al.*, 2022) (Figure 4.4a). Concentrations were then converted to a flow weighted annual flux (mol CO_2 yr^{-1}), and flow weighted annual yields (Figure 4.4b, kg CO_2 ha^{-1} yr^{-1}). Combined, this indicates that ≈3.4 Mt CO_2 yr^{-1} of DIC is annually transported by the catchments within our study, or 8.4 Mt CO_2 yr^{-1} when upscaling to account for the whole UK land area (23.35 Mha; Marston *et al.*, 2022). Six of the catchments (Tweed, Ouse, Wye, Thames, Severn and Trent) transport 45% of this flux (Table 4.2).

Table 4.2- Top ten UK rivers in terms of DIC flux (in Mt CO_2 yr^{-1}). Compared to the total of the 52 catchments within this study, as well as accounting for the whole UK land mass.

Catchment	Mt CO_2 yr^{-1}
Trent	0.369
Severn	0.354
Thames	0.300
Wye	0.186
Ouse	0.169
Tweed	0.150
Eden Beaumont	0.132
Ribble	0.117
AvonBristol	0.114
Tay	0.106
Total catchments	*3.4*
Scaling to UK landmass	*8.4*

The total UK DIC flux reported in this study is slightly higher than given in Tye et al 2022. They report a DIC flux of 647 kt C DIC yr^{-1} for 2017 (or 2.37 Mt CO_2 yr^{-1}) for the catchments that they studied, which represented 36% of the total land area in the UK. Extrapolating their reported value by UK land mass results in a value of 6.6 Mt CO_2 yr^{-1}. The difference between

DIC concentrations in this study and Tye et al 2022 is likely related to variations in the sampling period; (Bell et al 2021) suggests that the UK DIC flux is annually variable and ranges between 2000 and 3000 kT C (7.3-11.0 Mt CO_2 yr^{-1}).

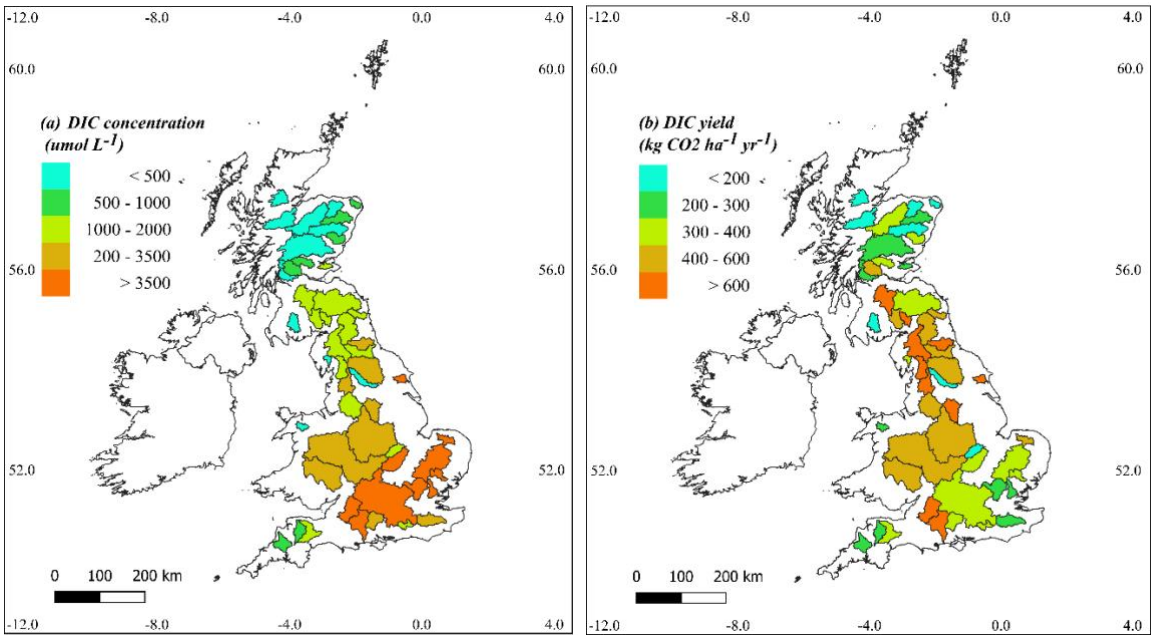

Figure 4.4- DIC concentrations (as CO_2, in µmol L^{-1}) (a) and DIC yields per hectare (kg CO_2 ha^{-1} yr^{-1}) (b) across the catchments within the study area.

Observing the variation in DIC concentrations (µmol L^{-1}) across the UK suggests that much of this DIC may be sourced from the weathering of carbonate lithologies, a link which was also made previously by Jarvie *et al.*, (2017) and Tye *et al.*, (2022). There is a significant increase in DIC from the northwest of Scotland to the southeast of England (Figure 4.4a, ranging 200-5100 µmol L^{-1}), corresponding with the increase in carbonate lithological units, (Figure 4.2). This link is also supported by a broad correlation between Ca^{2+} and DIC concentrations and the average DIC yield per hectare (Figure 4.5a, b).

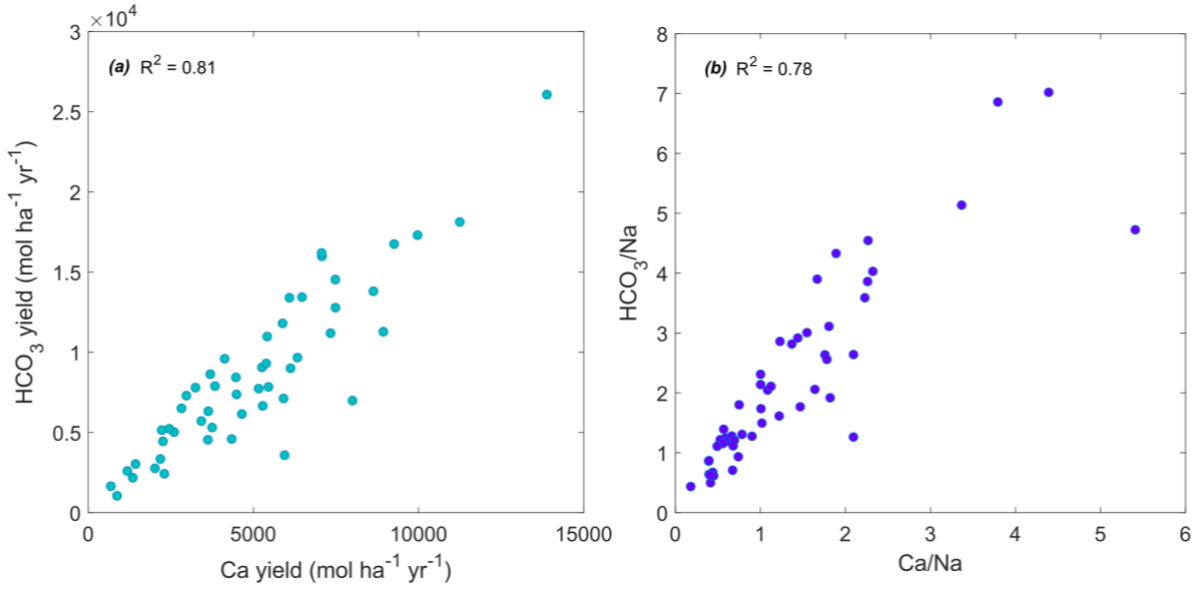

Figure 4.5- Comparing the annual yield of Ca^{2+} and HCO_3^- (a) and the ratio of Ca/Na and HCO3/Na (b) of UK rivers. Both can be used to infer the increased contribution of carbonates. Each datapoint represents an individual river within the study and was calculated using average concentrations (Table 4.4.1).

An increased riverine $^{Ca}/_{Na}$ and $^{HCO3}/_{Na}$ can also be used to infer an increased contribution from carbonates, given the large variation in the end-member chemical ratios of silicate and carbonate lithologies (Table 4.1) (Gaillardet *et al.*, 1999). There is a large range in $^{Ca}/_{Na}$ and $^{HCO3}/_{Na}$ within the UK rivers (Figure 4.5b). Values typically increase from the northwest to southeast, with the lowest in River Conon ($^{Ca}/_{Na} = 0.2$) and the highest in the River Test, Hampshire ($^{Ca}/_{Na} = 5.4$).

The variation in DIC concentrations and chemical ratios initially suggest that (i) lithology plays a dominant role in determining the chemistry of UK rivers, (ii) carbonate weathering dominates the DIC load, and (iii) southeastern catchments may be the most productive exporters of DIC to the ocean. However, the NW-SE trend in DIC concentration (Figure 4.4a) also mirrors the NW-SE hydrological gradients discussed in (Section 4.3.3), and when converting from concentration into flux weighted yields, it is catchments within the middle of the UK (Wales, Midlands) which are the most productive annual exporters of DIC (Figure 4.4b). This suggests that high riverine DIC concentrations do not necessarily imply high export of DIC in UK rivers, and that this export is not only influenced by lithology, but by other catchment parameters, such as hydrology, topography, and land use (discussed further in Chapter 6).

4.5 Inverting chemistry to assess the sources of solutes

4.5.1 MEANDIR inversion

Selected river chemistry was inverted using the geochemical model MEANDIR. Chapter 2 (Section 2.4) provides a detailed summary of the model set up and parameter choices used, and Chapter 3 introduces the use of MEANDIR to apportion major cations to endmember sources in two UK rivers: the Severn and Thames. In summary, MEANDIR is a set of MATLAB scripts developed by Kemeny and Torres, (2021) which distributes major solutes (X) to their end-member sources (i) using mixing equations such as in Equation 4.8:

$$ {}^{X}/_{Na_{river}} = \sum({}^{X}/_{Na})_i * \propto Na_i \qquad (4.8) $$

$\propto Na_i$ is the proportion of Na^+ in endmember i, where i = silicate, carbonate, evaporite and rain. ${}^{X}/_{Na_{river}}$ is the chemical composition of the river water. The number of solutes used in the study should ideally be equal to or greater than the number of endmembers ($X \leq i$). If there are more endmembers than solutes ($X > i$), then multiple combinations of the endmembers may be able to predict the river chemistry, particularly when two or more of the end member chemical ranges overlap (Kemeny and Torres, 2021). This study uses X = Ca^{2+}, Mg^{2+}, Na^+, and Cl^-; the latter of which is used to define the rain portion (see relevant section below). The assumption here is that Ca^{2+}, Mg^{2+} and Na^+ are the main contributors to riverine alkalinity. This is likely a valid assumption for the UK rivers in this study: these three elements average 96.5% (± 1.3%) of the total concentration of the four major cations (Ca^{2+}, Mg^{2+}, Na^+, and K^+, see Table 4.1). The concentrations of other trace cations (i.e., Fe^{3+}/ Fe^{2+}, Mn^{2+}, Zn^{2+}) are two orders of magnitude lower than major ions, and therefore will not influence flux calculations substantially. While there is no data for (Al^{3+}, Sr^{2+} and Ba^{2+}), these elements are also unlikely to contribute significantly to flux calculations: Al^{3+}, Sr^{2+} and Ba^{2+} contributed on average 0.03 (± 0.04), 0.09 (± 0.01) %, and 0.01 (± 0.01) % to the cation concentrations of the samples collected from Severn and the Thames rivers during the Dec 2019-Nov 2021 sampling campaign (i.e. Chapter 3).

Within this chapter, the same compositional ranges were used to define the silicate, carbonate, cyclic and evaporite endmembers (Table 4.3) as in Chapter 3. It is not possible using the methods reported here to distinguish between the portion of Ca_{river} from lime and Ca_{carb}, and therefore it is important to note that the concentration of calcium in waters from carbonate sources (Ca_{carb}) may also include Ca_{lime}. The potential for lime to be a significant source to riverine Ca^{2+} will be discussed further in Chapter 5.

Table 4.3- Endmember compositions used throughout the study. Ca/Na, Mg/Na and Cl/Na are used in the main inversion, whilst SO₄/Na is used in post-inversion mixing equations to derive $X_{SO4excess}$. Values for carbonates are derived from Gaillardet et al., (1999). Silicates are derived from UK small sub-catchments draining silicates (described in Chapter 2). The evaporite endmember was taken from (Moon et al 2014).

	Silicate		**Carbonate**		**Cyclic**		**Evaporite**	
	Median	Stdev	Median	Stdev	median	Stdev	median	Stdev
Ca/Na	0.669	0.77	60	30	0.023	0.01	0.17	0.09
Mg/Na	0.325	0.27	30	15	0.11	0.01	0.02	0.01
$SO4/Na$	0.019	0.005	0.06	0.03	0.060	0.01	0.4	0.2
Cl/Na	0	0	0	0	1.15	0.1	1	0

The potential average proportion of riverine Cl^- from rain was determined for each river by deriving the 'critical' value of Cl^- ($Cl_{critical}$), as introduced in Chapter 2, and using Equation 4.9, i.e.-

$$Cl_{critical} = Cl_{rain} * {Annual\ rainfall}/{Annual\ discharge} \quad (4.9)$$

Average rainfall (mm day^{-1}) and flow rate ($m^3\ s^{-1}$) for each catchment was obtained from the National River Flow Archive and converted to annual rainfall and discharge (L yr^{-1} $catchment^{-1}$). Precipitation chemistry for the UK was obtained from the Environmental Change Network (ECN, 2015). Because precipitation chemistry was collected from sites not directly linked to the catchments, the data from these sources was collated and the average UK rain Cl^- concentration was used for Cl_{rain} (116.5 µmol L^{-1}).

$Cl_{critical}$ values for each river varied between 130-2600 µmol L^{-1}, with an average of 290 µmol L^{-1} (See datasheets in supporting information). For any data with a $Cl_{river} > Cl_{critical}$, the

remaining Cl^- is assumed to be sourced from either evaporites or anthropogenic sources. As discussed in Chapter 3, to minimise the impact of anthropogenic Cl^-, any datapoints with a $Cl/Na_{river} > 1.2$ were excluded from the study. Therefore, the remaining Cl^- is assumed to be entirely sourced from evaporites, i.e. Equation 4.10:

$$Cl_{evaporite} = Cl_{river} - Cl_{critical} \quad (4.10)$$

Other parameter choices needed for the inversion model and further discussion is provided within the text of Chapter 2. Input files (datasheets in supporting information) were inverted within MEANDIR using the Oxford University Advanced Research Computing Facility (ARC).

For every sample within a catchment's dataset, the MEANDIR inversion uses the river chemistry and endmember compositional range to predict f_x^i: the fraction of the total riverine concentration of element X derived from endmember i (where X= Ca^{2+}, Mg^{2+} and Na^+, and $i =$ silicate, carbonate, evaporite and rain). These fractions were then used to calculate X_i, the concentration of ion X from each endmember (i) (µmol L^{-1}) Equation 4.11:

$$X_i = f_X^i * X_{river} \quad (4.11)$$

Where X_{river} is the total concentration of element X in the river. SO_4^{2-}concentrations are not used in the inversion calculations, however $\left(\frac{SO_4^{2-}}{Na}\right)_i$ are used in conservative mixing equations after the Monte Carlo simulations to calculate $X_{SO_4^{2-}\,excess}$, the 'excess' portion of SO_4^{2-} not derived the four end members (discussed in detail within Section 4.7.2).

Calculations were performed for each field measurement within a catchment's dataset. Results from the inversion (the median, 25 and 75 percentile fractions of Ca^{2+}, Mg^{2+} and Na^+ from each endmember source (f_X^i) and the fraction of riverine SO_4^{2-} which is excess), were then collated into output files (datasheets in supporting information) for each river.

4.5.2 Sources of solutes

The inversion results suggest that the total fraction of dissolved cations derived from combined silicate and carbonate rock weathering in UK rivers ($f_{total}^{weathering}$, i. e. $f_{Ca}^{sil+carb} + f_{Mg}^{sil+carb} + f_{Na}^{sil+carb}$) averages 60%; ranging from 23% (River Conon, Scotland) to 84% (River Test, Hampshire). These overall contributions by silicate and carbonate weathering reactions align with the global values given in Gaillardet *et al.*, (1999). Of the total, the average percentage of solutes sourced from silicates is 7% (0.3%-46%), and 49% from carbonates (9% -82%) (Figure 4.6).

The remaining dissolved ion load derives from, in part, evaporite weathering and cyclic (rain) sources. Rivers draining Scotland, with high discharges and relatively low cation concentrations (Table 4.1), typically have higher percentages of solutes sourced from rain (i.e. Figure 4.6). The high dissolution kinetics of evaporitic rocks means that even the presence of small outcrops within a catchment can influence catchment chemistry by contributing a substantial amount of Na^+ to rivers (Berner and Berner, 1996). For example, the British Geological Survey reports thick halite units within the Mercia mudstone formation, (BGS, 2023d) which outcrops throughout the midlands, particularly in Trent and Don (Ouse) catchments. This outcrop could potentially be the source of the high evaporite component in these catchments (i.e. Figure 4.6).

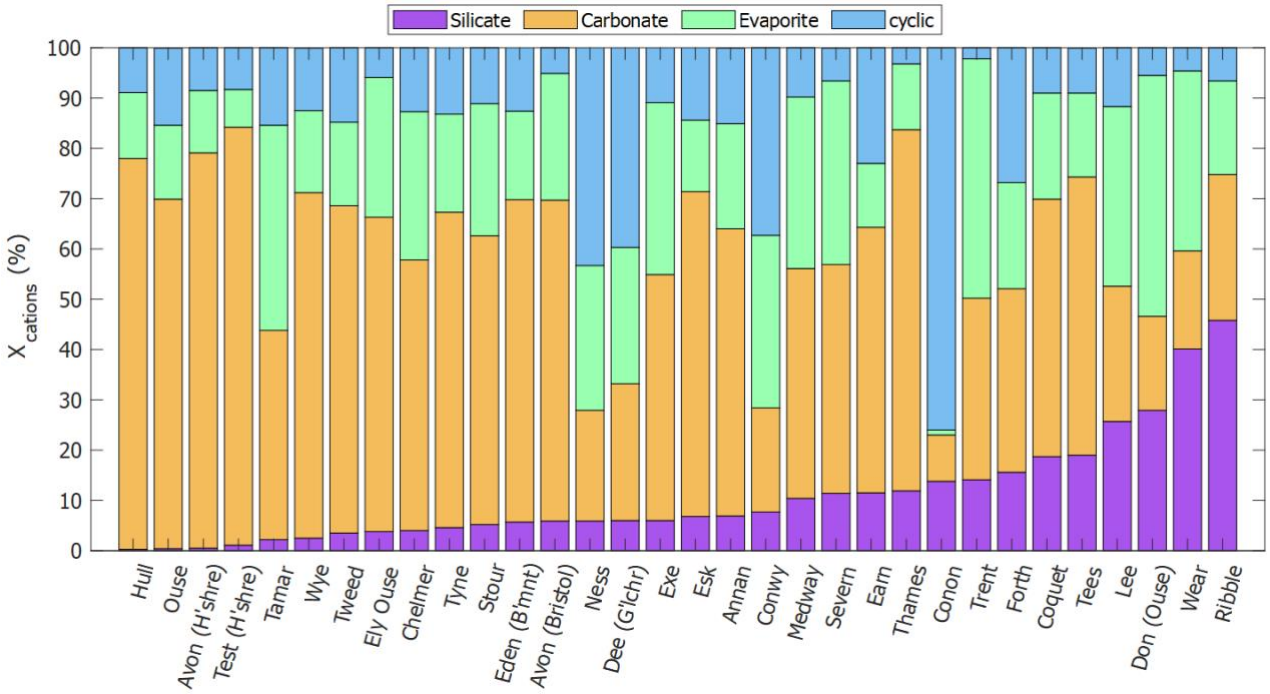

Figure 4.6- Results of the inversion showing the fraction of total major cations (Ca^{2+}, Mg^{2+}, and Na^{+}) from each source endmember I (where i = silicate, carbonate, evaporite and rain) in UK rivers, following (Gaillardet et al., 1999). Rivers are ranked in ascending order of silicate %. H'shre = Hampshire, B'mnt= Beaumont, G'lcr = Glenlochar

4.6 Annual CDR from natural weathering in the UK (Maximum)

4.6.1 Calculating weathering fluxes and CO_2 removed

The concentration of each major cation (X) from silicate and carbonate rock weathering was then converted into a flow weighted average flux (Q), using the daily average flow rates given in input files (supporting information) i.e., Equation 4.12:

$$Q_i^X = X_i * d / 10^6 \ (mol\ s^{-1}) \quad (4.12)$$

Where i = silicates and carbonates. Cations derived from evaporitic and cyclic sources do not contribute to carbon drawdown and are not important to the following CDR calculations (see below).

The flux of each cation (X) from silicates (Q_X^{sil}) and carbonates (Q_X^{carb}) was then used to calculate the maximum quantity of CO_2 consumed (in mol s^{-1}) under the same assumptions given in Chapter 3, i.e., that-

i) All cations remain dissolved in the water column and are transported directly to the ocean.
ii) Bicarbonate is the only weathering agent involved in the reactions (the impact of SO_4^{2-} to these calculations is considered in Section 4.7.2)
iii) Carbonate weathering removes 1 mole of CO_2 per mole of Ca^{2+} and Mg^{2+}
iv) Silicate weathering removes between 1.4-1.7 moles of CO_2 per mole of Ca^{2+} and $Mg^{2+}$and per 2 moles of Na^+ (see discussion in Chapters 3 and 5 for information on the range in 1.4-1.7. Briefly, the total amount of atmospheric CO_2 removed per mole of divalent cation depends on ratio of HCO_3^- to CO_3^{-2} in the ocean, which depends on the temperature, salinity and pCO_2 of the oceanic water column (Renforth and Henderson, 2017))

$$CO_{2_{sil}}(mol\ s^{-1}) = (Q_{Ca}^{sil} + Q_{Mg}^{sil} + Q_{Na}^{sil}/2) * w \quad (4.13)$$

$$CO_{2_{carb}}(mol\ s^{-1}) = (Q_{Ca}^{sil} + Q_{Mg}^{sil}) \quad (4.14)$$

Where w is the molar amount of CO_2 consumed for every mole of divalent silicate ion dissolved. As w could be between 1.4-1.7, we calculate using both values and express the results of both to highlight the possible uncertainty in the choice of w.

$CO_{2_{sil}}$ and $CO_{2_{carb}}$ therefore, represent the maximum quantity of CO_2 removed by cationic weathering fluxes at the time the measurement was taken (in mol s^{-1}). To predict the annual CO_2 consumed by weathering processes in each catchment, the $CO_{2_{sil}}$ and $CO_{2_{carb}}$ calculated for each datapoint was sorted by month sampled, and the average $f_{sil}, f_{carb}, CO_{2_{sil}}, CO_{2_{carb}}$ (mol s^{-1}) taken and converted to (mol $month^{-1}$). This was done to assess for any seasonal

variation, and to remove any potential bias from variations in flow rates (i.e., from storm events). The maximum annual CO_2 consumed by weathering was calculated by collating the monthly averages and converting to Mt CO_2 yr^{-1}. The annual maximum CO_2 removed due to weathering therefore represents an average value over the period of sampling for each river within the study.

MATLAB source codes used to calculate results, MEANDIR result files and calculated results are given in the supporting information files.

4.6.2 Maximum CDR for UK

These calculations suggest that the maximum total combined quantity of atmospheric CO_2 consumed due to silicate weathering for the catchments within the study is 0.54 (0.22-0.95) $MtCO_2\ yr^{-1}$, assuming a rate of CO_2 drawdown of 1.7 moles of CO_2 for every divalent cation (and every two moles of Na^+) present in solution (Table 4.4). Under the simple assumption that these 52 catchments capture the range in weathering conditions in the UK (i.e., from differences in geology, topography, temperature, land use and water flux, discussed in section 2), upscaling these values to account for the whole UK landmass (23.35 Mha) (Marston *et al.*, 2022) leads to a national maximum silicate CO_2 consumption rate of 1.3 Mt CO_2 yr^{-1}. In comparison, the maximum quantity of CO_2 consumed due to carbonate weathering for the catchments combined is 2.0 Mt CO_2 yr^{-1}. Upscaling this in the same way to account for the whole UK landmass increases this value to 5.0 Mt CO_2 yr^{-1} (Table 4.4).

Table 4.4- Maximum consumed CO_2 due to silicate and carbonate weathering in the catchments studied, and upscaled to include the whole UK landmass. Implied C flux from carbonates= DIC flux- CDR total

	DIC flux Mt CO_2 yr^{-1} (this study)	**CDR silicates Mt CO_2 yr^{-1} (w=1.7)**	**CDR carbonates Mt CO_2 yr^{-1}**	**CDR total Mt CO_2 yr^{-1}**	**Implied C flux from carbonates Mt CO_2 yr^{-1}**
Studied rivers	3.4	0.54 (0.22-0.95)	2.0 (1.7-2.2)	2.54 (1.99-3.15)	0.86
UK total	8.5	1.3 (0.7-2.4)	5.0 (4.4-5.7)	6.3 (5.1-8.1)	1.9

To effectively compare catchments of different sizes, the annual CO_2 flux sequestered during weathering for each catchment was converted to yield (kg CO_2 ha^{-1} yr^{-1}). The average carbonate weathering yield in UK catchments was significantly higher than silicate yield: 197 and 60 kg CO_2 ha^{-1} yr^{-1} respectively.

The CO_2 yield due to carbonate weathering increased from north to south (Figure 4.7b). High CO_2 yields were typically observed in catchments with increased carbonate lithologies, i.e. those that drain the chalk aquifers (i.e., Thames, Hull, Stour, Avon (Hampshire), Test), or the Jurassic Ooidal limestone (i.e., Severn, Avon (Bristol), Trent) (Figure 4.2, 4.7b). High carbonate yields were also seen in catchments within the north of England and the south of Scotland (Clyde, Tees, Esk, Eden), likely due to the presence of localised limestone outcrops. Carbonate rich lithology that may have contributed to the high yields within these catchments include the Clackmannan group, part of the limestone coal formation (Vincent *et al.*, 2010) (Clyde, Eden), the Edlington, Seaham and Roxby formations (Tees) (Tucker, 1991), and the Yoresdale group (Esk) (BGS, 2023c). Positive correlations were also observed between the carbonate CO_2 yield and the percentage of arable land (Figure 4.9a), as well as the increased permeability of the bedrock (Figure 4.8a). In contrast, CO_2 yield from carbonates decreased with increased runoff (Figure 4.9c) and elevation (Figure 4.8b).

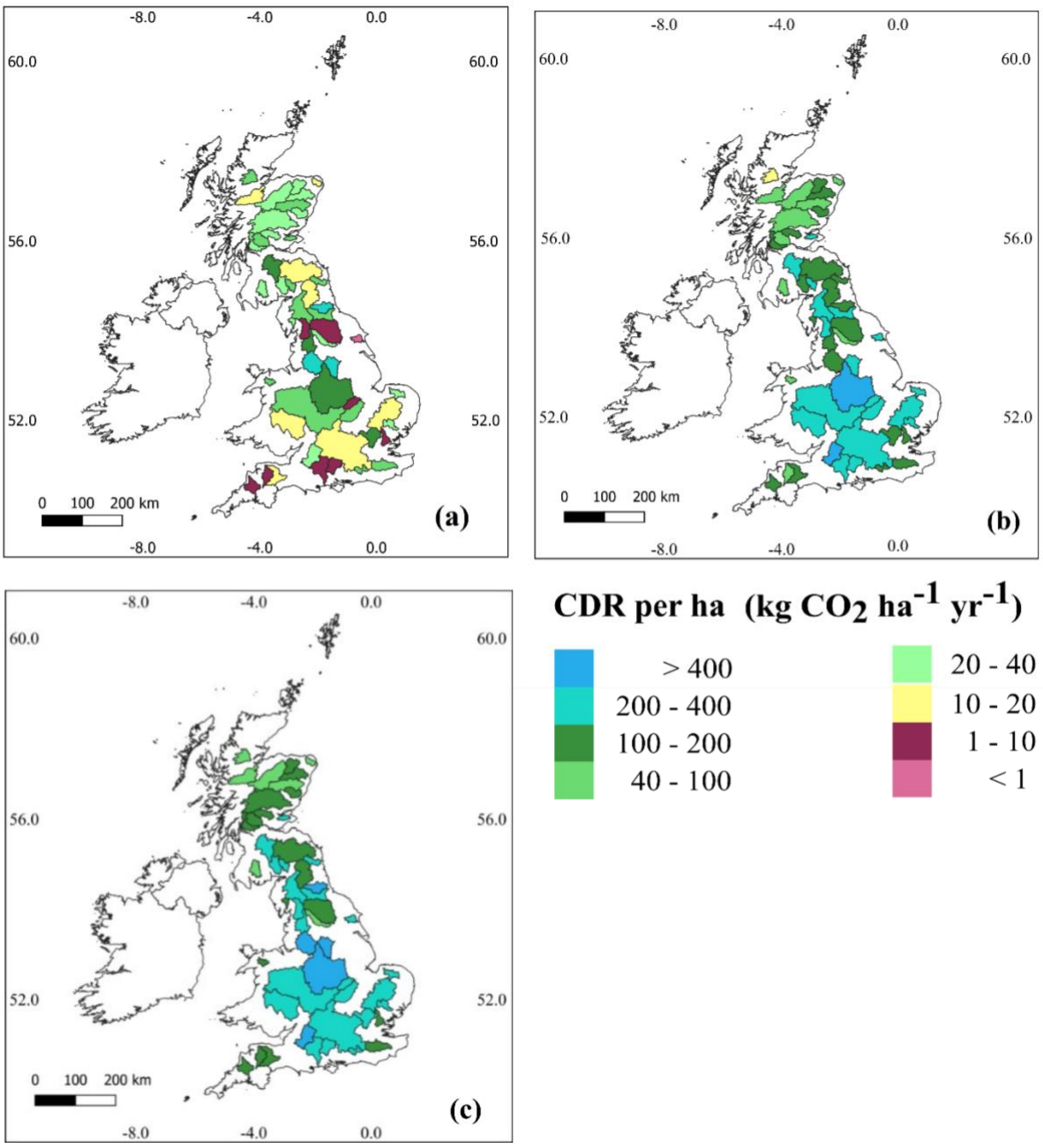

Figure 4.7- The potential maximum quantity of CDR due to natural (a) silicate and (b) carbonate weathering in the UK catchments within the study. (c) is the total combined CDR for natural weathering. Given in CO_2 yield (kg CO_2 ha^{-1} yr^{-1}). Yields are calculated from the median fraction of ions from silicate and carbonate sources as predicted by the inversion results (supporting information).

The CO_2 yield due to silicate weathering varied significantly across the UK (Figure 4.7a). There are typically higher CO_2 yields from silicate weathering in silicate rich, Scottish catchments, and lower yields are seen in catchments which drain the chalk (Figure 4.7b). However, there is no clear relationship between bedrock geology and silicate yield (i.e., Figure 4.2, Figure 4.7a). Similarly, there are no notable trends between silicate yield and runoff (Figure 4.9f), elevation (Figure 4.8d), permeability (Figure 4.8c), percentage of arable land

(Figure 4.9d) or grassland (Figure 4.9e), suggesting that there is no single dominant driver for silicate weathering in the UK, and that weathering is driven by a range of factors.

A deeper discussion on the environmental controls on silicate and carbonate weathering, as well as a comparison between UK yields and other global catchments, will be a focus of Chapter 6.

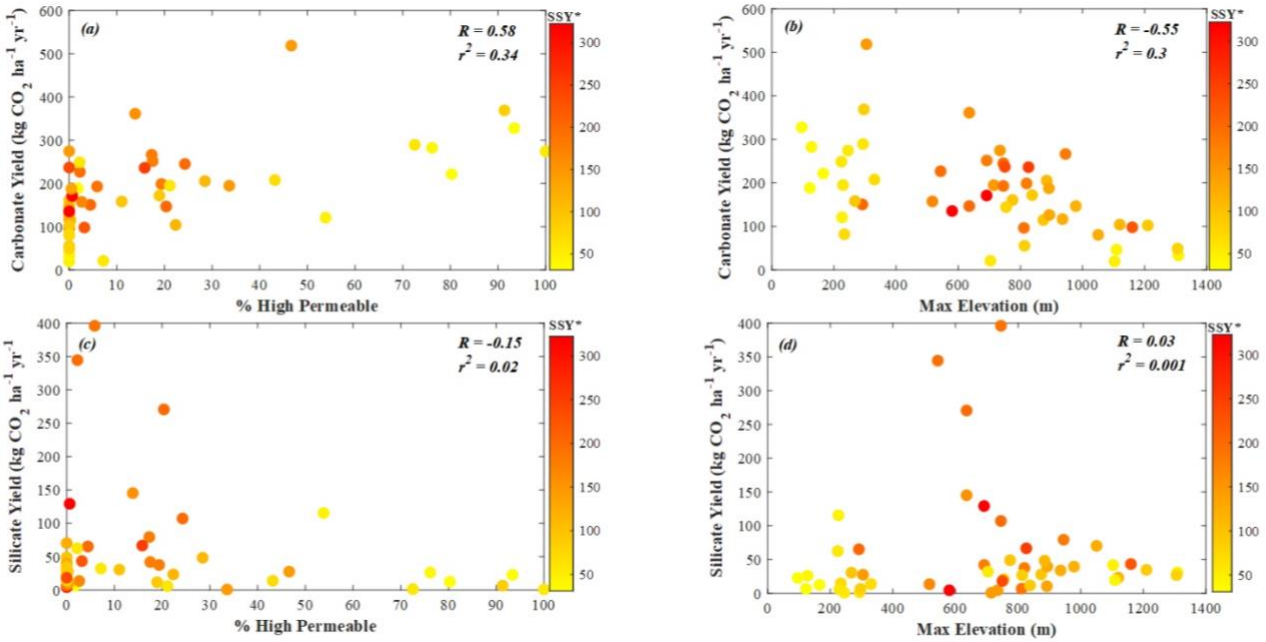

Figure 4.8- A medium positive correlation can be between carbonate yield and (a) the percentage of high permeable lithology within the catchment, while a medium negative correlation can be seen between carbonate yield and (b) the maximum elevation. In contrast, no correlation can be seen between silicate yield and (c) permeable lithology, and (d) the maximum elevation.

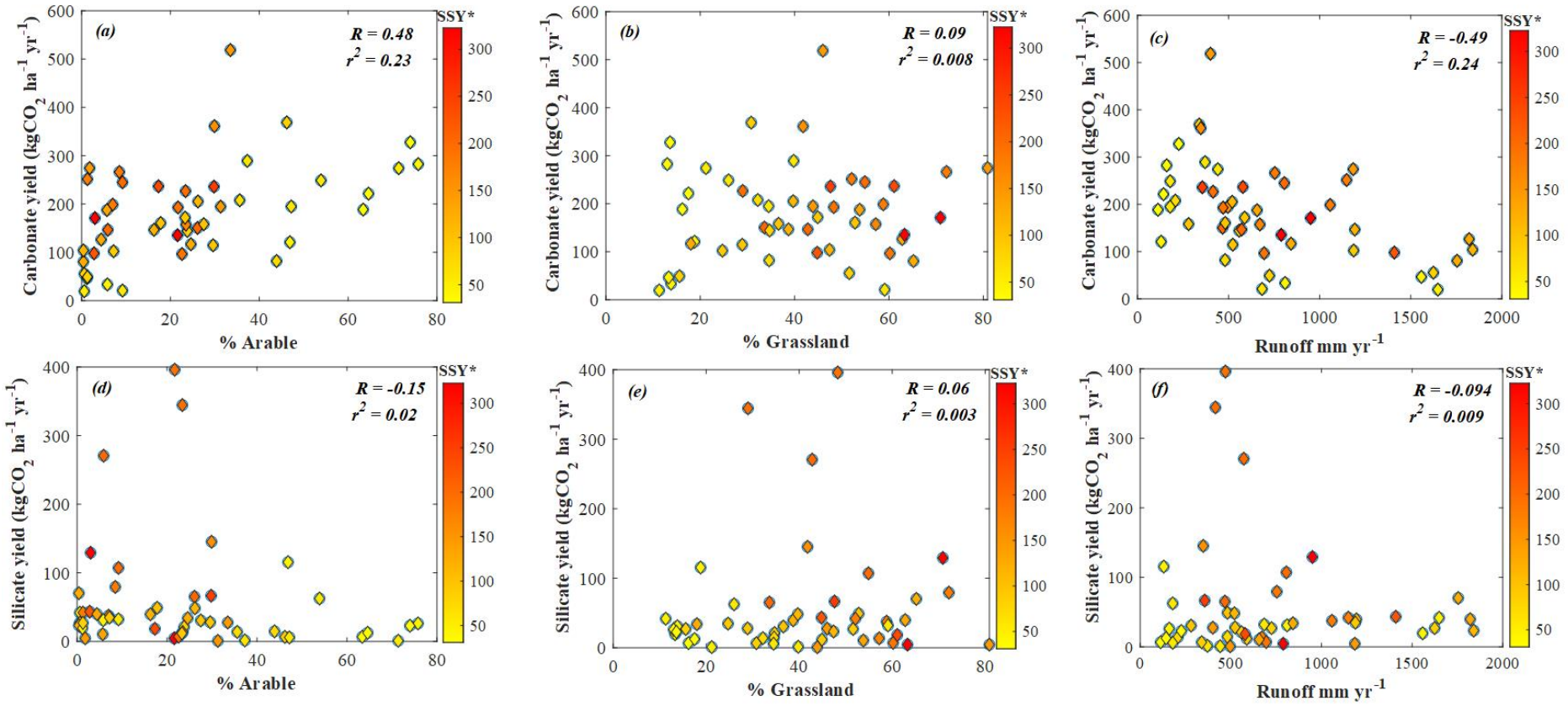

Figure 4.9- Correlations between catchment parameters and weathering yields. First three plots show medium correlations between carbonate yield ($kgCO_2\ ha^{-1}\ yr^{-1}$) and (a) Percentage arable land, (b) percentage grassland and (c) Catchment runoff ($mm\ yr^{-1}$). Last three show no correlation in silicate yield vs (d) percentage arable land, (e) percentage grassland and (f) Runoff ($mm\ yr^{-1}$).

4.7 Factors that may make the maximum CDR value an over-estimate

4.7.1 Variations in how the sequestered CO_2 speciates in solution (w value)

In natural waters, divalent cations could either be charge balanced in solution by two moles of HCO_3^-, or one mole of CO_3^{2-} (assuming that they are balanced by carbonate and not by other anions such as SO_4^{-2} or NO_3^-. For discussion of these ions, see Sections 4.7.2 and Section 4.7.3. respectively). The exact molar quantity of atmospheric CO_2 consumed per mole of divalent cation weathered (*w*) therefore depends on the pH and alkalinity of the water, as these parameters control how the sequestered CO_2 speciates. In pure water HCO_3^- is the dominate ion, and therefore 2 moles of CO_2 are removed per divalent cation (*w* =2). In the ocean, to which the river water eventually flow, the pH and alkalinity lead to a ratio of carbonate and bicarbonate such that the w value is in the range 1.4-1.7 (depending on temperature; Renforth and Henderson, 2017).

The maximum values reported in Section 4.6.2 use a *w*= 1.7: the maximum endmember of the oceanic range given above. Using the lower endmember value for *w* (*w*= 1.4), drops the total CO_2 consumed due to silicate weathering to 1.1 (0.5-1.9) Mt CO_2 yr^{-1} when upscaling to account for the total UK landmass (a 17.6 % reduction).

4.7.2 Sulphuric acid mediated weathering

When sulphuric acid (H_2SO_4) replaces carbonic acid (H_2CO_3) as the reagent in silicate and carbonate weathering reactions, the overall CDR is reduced (Burke *et al.*, 2018; Hilton and West, 2020). As sulphate ions (SO_4^{2-}) are released from sulphuric acid weathering (via Equations 4.4 and 4.5), variations in riverine SO_4^2 can be used to estimate the extent of sulphuric acid weathering within a catchment. However, there are multiple potential sources of SO_4^{2-} to rivers: sulphides, evaporites, non- sulphide silicates, volcanic deposition, biogenic emissions, and agricultural fertilizers. The goal of this section is to extract the sulphide portion

of riverine SO_4^{2-} and use this to quantify the reduction in calculated maximum values for CDR caused by the presence of some sulphide weathering (Net CDR_{sil} and Net CDR_{carb}).

4.7.2.1 Variations in riverine SO_4^{2-}

Sulphate concentrations (µmol L^{-1}) increase significantly from the northwest to the southeast. Rivers within Scottish catchments have SO_4^2 concentrations typically below < 200 µmol L^{-1}, while south-eastern catchments have concentrations of up to 2000 µmol L^{-1} (i.e., Table 4.1). There are at least 4 possible explanations for this NW-SE increasing trend:

i. Higher water availability in the northern catchments (due to increased rainfall caused by the NW-SE rain gradient discussed in Section 3.3); typically leading to dilution in Scottish catchments, and higher evapotranspiration and lower flows concentrating sulphate within south-eastern catchments (Kay *et al.*, 2013)
ii. An increased contribution from sulphides from Carboniferous coal deposits and late- Triassic/Jurassic sediments (i.e., Figure 4.2a)
iii. Increased presence of evaporite deposits, particularly where late Triassic- early Jurassic sediments outcrop (Howard *et al.*, 2008; Newell, 2018)
iv. An increased contribution from sulphate derived from agricultural fertilizers, as arable land content increases towards the southeast (Figure 4.3)

Sulphate concentrations (µmol L^{-1}) are converted into annual flux-weighted yields (mol ha^{-1} yr^{-1}) to investigate the impact of water availability, i.e., point (i). This reveals that although southeastern catchments have higher sulphate concentrations, it is the Midlands catchments which have the highest overall sulphate yields per hectare (Figure 4.10a). These high yields could equally result from an increased contribution of sulphides or evaporites: given the presence of both Carboniferous coal deposits and evaporitic deposits (i.e. the Mercia Mudstones) (Newell, 2018) in the region. To disentangle (and remove) the evaporite contribution to better predict the amount of sulphate from sulphides, this study follows the methodology of Burke *et al.*, (2018) to calculate $X_{excess\ SO_4^{2-}}$, the proportion of riverine sulphate which is not derived from evaporites and non-sulphide silicates.

4.7.2.2 Predicting the proportion of riverine sulphate from sulphides

The methodology for calculating $X_{excess\ SO_4^{2-}}$ has been introduced previously in Chapter 3. Briefly, once the Monte Carlo simulation within MEANDIR has best fit the major cations (Ca^{2+}, Mg^{2+}, Na^{+}) to their sources, a conservative mixing equation will then attribute a portion of riverine SO_4^{-2} to each endmember, given the endmember's SO_4^{2-}/Na ratio (Table 4.3). Any SO_4^{-2} unaccounted for by the four endmembers is the excess sulphate ($X_{excess\ SO_4^{2-}}$), i.e., Equation 4.15-

$$X_{excess\ SO_4^{2-}} = X_{river\ SO_4^{2-}} - \sum[SO_4^{2-}{}_i]^n \quad (4.15)$$

Where $\sum[SO_4^{2-}{}_i]^n$ is the sum of contributions of sulphate from each endmember (i), and n is the number of endmembers (i.e., 4). This remaining excess riverine SO_4^{2-} ($X_{excess\ SO_4^{2-}}$) will be a combination of SO_4^{2-} sourced from volcanic atmospheric deposition, biogenic emissions, anthropogenic pollution, and the oxidative weathering of pyrite.

Results derived from the conservative mixing equations in MEANDIR suggest that the fraction of $X_{excess\ SO_4^{2-}}$ relative to the total riverine SO_4^{2-}, varies considerably amongst UK catchments- from 0% in some Scottish catchments, to up to 92% in the River Nene catchment, a range similar to that of global rivers derived in Burke *et al.*, (2018). Like sulphate concentrations, $X_{excess\ SO_4^{2-}}$ (µmol L^{-1}) in UK rivers increases in a NW-SE direction (Figure 4.10b), however, converting to a flux weighted yield suggests that it is again the midlands catchments which transport the most annual $X_{excess\ SO_4^{2-}}$ per hectare (in mol ha^{-1} yr^{-1}).

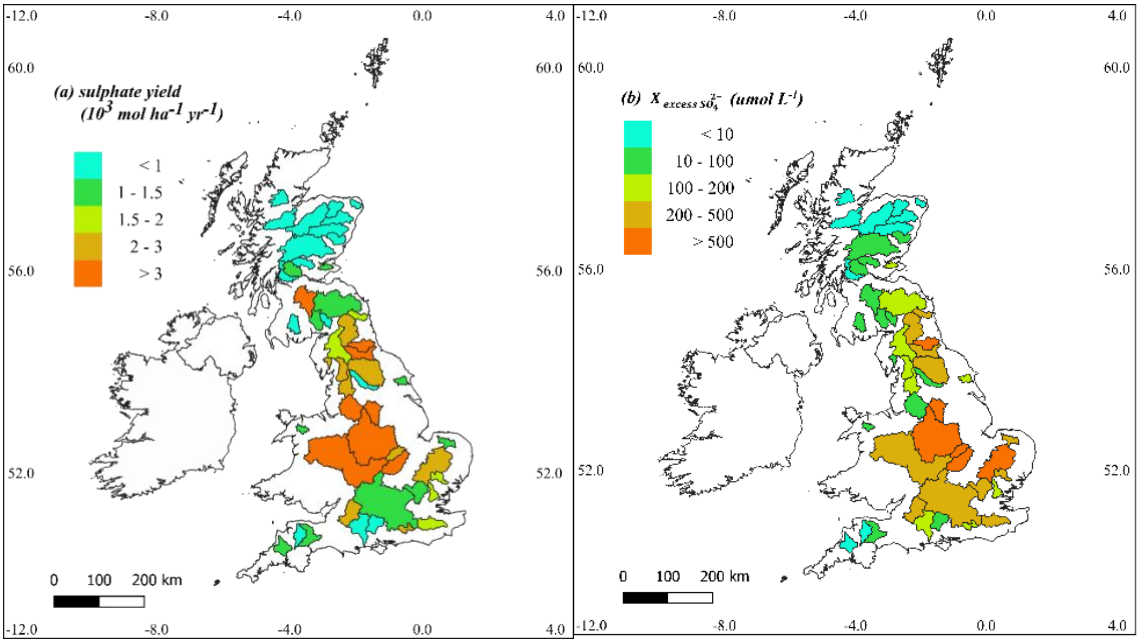

Figure 4.10- Presents the contrast in (a) sulphate yields (mol ha^{-1} yr^{-1}) and (b) the amount of total sulphate from excess (µmol L^{-1}) for the catchments in the study.

$X_{excess\ SO_4^{2-}}$ is corrected for volcanic atmospheric deposition and biogenic emissions, given that these sources account for an average of 7% and 3% of global river sulphate concentrations, respectively (Meybeck, 2003). The remaining riverine SO_4^{2-} ($SO_4^{2-}{}_{corrected}$ = River SO_4^{2-}-SO_4^{2-} (evaporite + non-sulphide silicate + volcanic + biogenic)) will be from a mixture of two sources: sulphides and agricultural fertilizer. It is difficult to accurately disentangle these two sources without extra data (for instance, through $\delta^{34}S$ water measurements) (Relph *et al.*, 2021). This study therefore first quantifies the maximum reduction to CDR, under the assumption that the remaining $SO_4^{2-}{}_{corrected}$ is completely derived from sulphide oxidation ($SO_4^{2-}{}_{sulphide}$). A discussion about the impact of fertilizer SO_4^{2-} to these calculations will then follow in 7.2.6.

4.7.2.3 Apportioning $SO_4^{2-}{}_{sulphide}$ between silicate and carbonates

There is a greater potential for reduction in the CDR by sulphuric acid weathering of carbonates than silicates, due to the additional re-release of CO_2 (Equation 4.4). It is therefore important to correctly apportion the $SO_4^{2-}{}_{sulphide}$ between the carbonate and silicate endmembers.

If we assume that H_2SO_4 weathers the two end members equally and reduces catchment max CDR_{sil} and CDR_{carb} by the same amount, then the CDR reduction of one endmember will be

overestimated. This is because of the difference between the silicate and carbonate weathering yields within a given catchment (Figure 4.9). For instance, in the Severn catchment, the median flux of carbonate ions (101 mol s^{-1}) is 5.5 times more than the median flux of silicate ions (16 mol s^{-1}, Table 4.5). Equally apportioning the $SO_4^{2-}{}_{sulphide}$ (43 mol s^{-1}) would totally deplete the silicate component and imply that all silicates in the Severn catchment are weathered by sulphuric acid. This study shows that sulphuric acid makes up less than half of the total acid involved in the reactions (Table 4.5). Therefore, to account for this and variations in weathering rates, $SO_4^{2-}{}_{sulphide}$ is split in the ratio of weathering in each catchment.

Table 4.5- Comparing the total cation flux from silicate and carbonate weathering of four different catchments within the study. The median value for each variable is given in each column.

	Total cations from carbonates ($\sum X_{carb}$ in mol s^{-1})	**Total cations from silicates ($\sum X_{sil}$ in mol s^{-1})**	$carb/_{sil}$	$SO_4^{2-}{}_{sulphide}$ **(mol s^{-1})**
Thames	75.0	6.1	11.5	14.3
Severn	101.0	16.0	5.5	43.9
Wear	7.3	19.1	0.31	12.5
Stour	5.7	0.2	24.1	1.2

For each sample in a river's dataset, the sum of the major cations from carbonates (X_{carb}) is divided by the sum of the major cations from silicates (X_{sil}) to find $carb/_{sil}$, the ratio of cations from carbonates to silicates (Equation 4.16).

$$carb/_{sil} = \sum X_{carb} \,/ \sum X_{sil} \quad (4.16)$$

$SO_4^{2-}{}_{sulphide}$ was apportioned to each endmember according to the $carb/_{sil}$ calculated for each datapoint within each river's dataset.

4.7.2.4 Net CDR

The reduction in CDR due to sulphuric acid weathering of silicates and carbonates ($Net\ CDR_{sil}$ and $Net\ CDR_{carb}$) can then be equated by Equations 4.17 and 4.18, i.e.-

$$Net\ CDR_{sil}\ (mol\ s^{-1}) = Max\ CDR_{sil} * (100 - \%\ H_2SO_4)\ \textit{(4.17)}$$

$$Net\ CDR_{carb}\ (mol\ s^{-1}) = \underbrace{Max\ CDR_{carb} * (100\% - \%\ H_2SO_4)}_{\textit{Reduced drawdown}} + \underbrace{Max\ CDR_{carb} * \%\ H_2SO_4}_{\textit{Re-released } CO_2}\ )$$

(4.18)

The results suggest that the impact of sulphuric acid weathering on the quantity of CO_2 consumed due to silicate and carbonate weathering is highly variable across catchments (Figure 4.11a, b). Scottish catchments, with very low $X_{excess\ SO_4^{2-}}$, see very small reductions to natural weathering CDR (Figure 4.11). In contrast, catchments in the middle of the UK are most prone to significant reductions. Large catchments such as the Severn, Trent and Ouse, experience 17, 24, 35% reductions in CO_2 consumed by silicate weathering, and 40, 46 and 32% reductions in CO_2 consumed by carbonate weathering (datasheets in supporting information). Combined, CO_2 consumed by silicate weathering in the 52 UK catchments studied (Figure 4.1) is reduced by a maximum of 17% (11-25%), lowering annual CO_2 consumed from 0.54 Mt CO_2 yr^{-1} to 0.43 (0.39-0.46) Mt CO_2 yr^{-1}. In comparison, the potential maximum quantity of CO_2 consumed by carbonate weathering is reduced by 29% (21-40%); from 2.0 Mt CO_2 yr^{-1} to 1.38 (1.16-1.53) Mt CO_2 yr^{-1}.

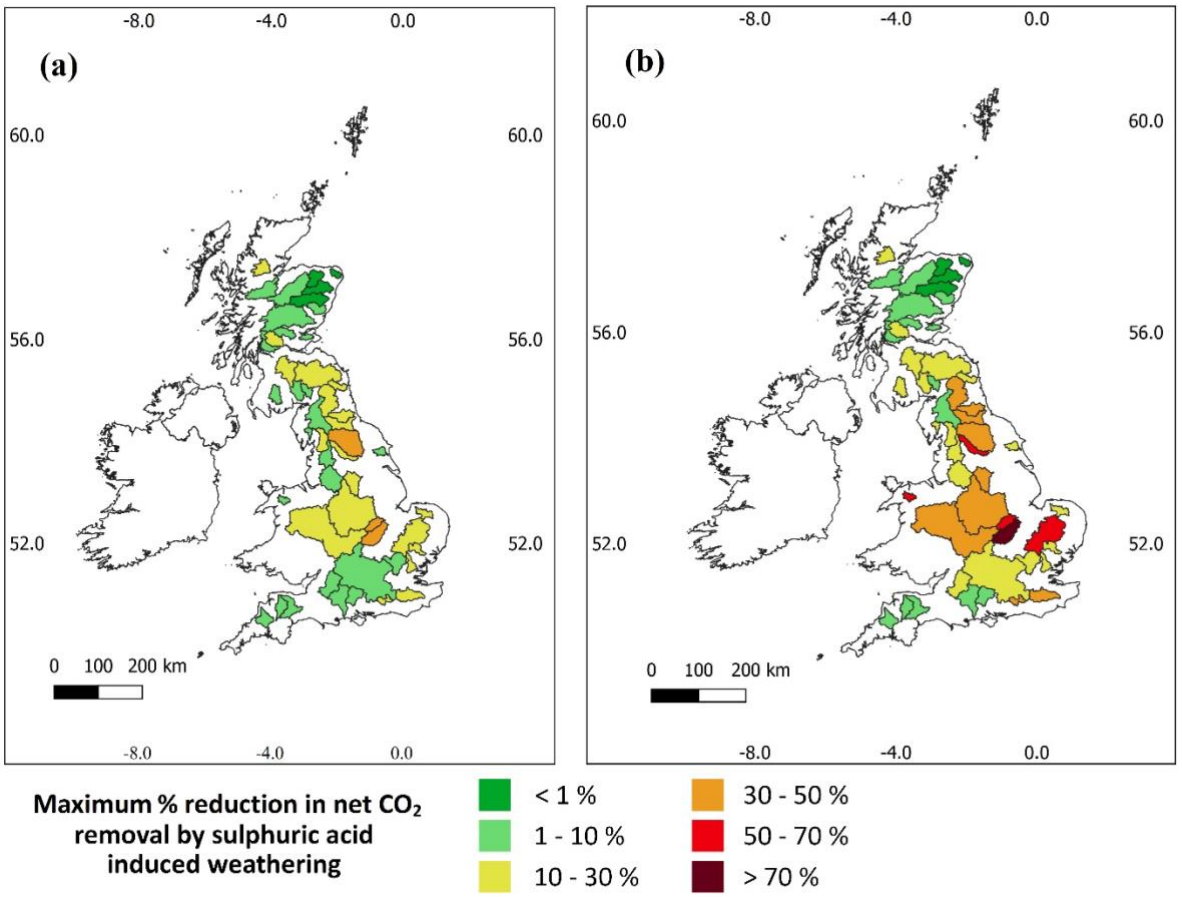

Figure 4.11- The potential maximum reduction to the net quantity of CO_2 consumed due to sulphide produced sulphuric acid weathering of (a) silicates and (b) carbonates in the catchments studied. In percentage reduction from the maximum total CO_2 removed per catchment (given in Mt CO_2 yr^{-1} per catchment).

4.7.2.5 *The problem of f*ertilizer contribution to $X_{SO4excess}$

Previous calculations have ignored the contribution of agricultural fertilizers to $X_{SO4excess}$. However, it is important to consider the influence of agriculture to improve the estimates previously set out in Section 4.7.2.4. As 70% of riverine nitrate is sourced from fertilizer (DEFRA, 2015), this study uses nitrate as a proxy for agricultural influence. Catchments with a low proportion of arable land have no correlation between $X_{SO4excess}$ and NO_3^- (Figure 4.12, columns 1 and 3). However, catchments with a high percentage of arable land have a strong positive correlation (Figure 4.12, column 2), suggesting a greater influence of agriculture on $X_{SO4excess}$.

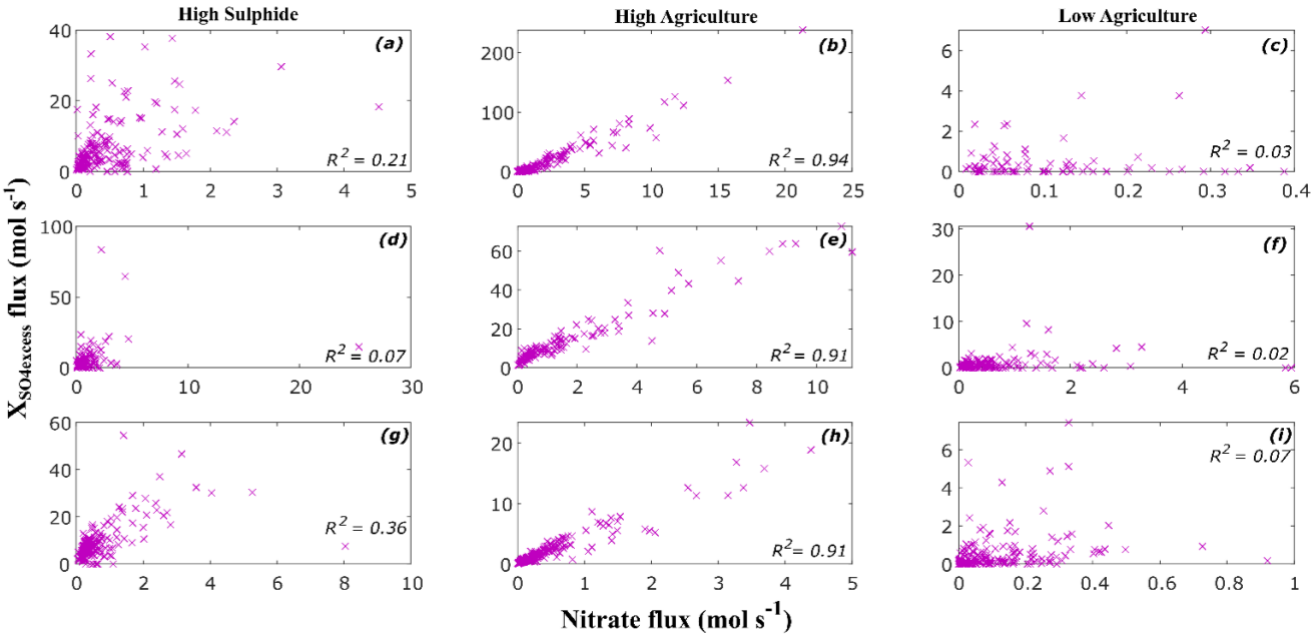

Figure 4.12- Riverine nitrate flow weighted flux versus the flux of sulphate from excess sources (mol s^{-1}), showing that for catchments with high agriculture, excess sulphate and nitrate are very highly correlated. Column one in the figure are catchments with high expected sulphide weathering due to presence of Mesozoic shales within catchment lithology- (a) Tyne, (d) Tees, (g) Wear); column two are catchments with a high percentage of arable land (High Agriculture- (b) Ely Ouse, (e) Nene, (h) Chelmer); column 3 are a subset of catchments which have very little agriculture and minimal expected sulphide weathering (Low Agriculture- (c) Conon, (f) Annan, (i) Leven H.

The top ten catchments with the most arable land (> 46% arable) have an average fraction of excess sulphate ($f_{X_{SO4excess}}$) higher than the remaining catchments ($f_{X_{SO4excess}} = 0.57$ and $f_{X_{SO4excess}} = 0.31$ respectively). Some of the difference between these two values may be due to the additional flux of agricultural fertilizer. The lower value $f_{X_{SO4excess}} = 0.31$ is similar to the fraction of sulphate from sulphides reported by Burke et al 2018 ($f_{sulphides} = 0.28$) suggesting that this could be used to define the upper limit to the fraction of sulphate from sulphides.

However, using $f_{X_{SO4excess}} = 0.31$ is potentially misleading as there are numerous examples of low arable catchment with high $f_{X_{SO4excess}}$. For example, the Ely Ouse and Tyne catchments have 65% and 5% of arable land respectively, yet very similar $f_{X_{SO4excess}}$ (0.63 and 0.68 respectively, i.e. Figure 4.3). For the Tyne catchment, which is located within a high sulphide region, using a $f_{X_{SO4excess}} = 0.31$ will likely underestimate the proportion of sulphate from sulphides. Therefore, whilst riverine nitrate concentrations may be useful for predicting which catchments have sourced significant $X_{SO4excess}$ from fertilizers, this method cannot be used here to define an upper limit for $f_{sulphides}$. Instead, future work will be needed to enable the

disentanglement of agricultural and sulphide derived sulphate (such as through $\delta^{34}S$ water measurements in rivers with highly arable catchments), taking a catchment specific approach.

4.7.3 Nitric acid weathering from fertilizers

As introduced in Section 4.1, the replacement of carbonic acid for fertilizer derived nitric acid in weathering reactions reduces the CO_2 removed due to weathering (through Equations 4.6-4.7). The extent of CDR reduction may depend on catchment locality, given the heterogeneous distribution of arable land throughout the UK (Figure 4.3). To investigate this and calculate the potential CDR reduction, the same assumptions given in Chapter 3 are used:

(i) Riverine NO_3^- concentrations can be used to infer nitric acid weathering, given that approximately 70% of riverine nitrate is typically sourced from agricultural fertiliser (Environmental Agency, 2021).

(ii) $NO_3^-{}_{agricultural}$ will be apportioned to riverine cations derived from silicate and carbonate weathering in the same ratio that they were weathered on the catchment (i.e., the carbonate to silicate weathering ratio, $carb/_{sil}$, see Section 4.7.2.3)

(iii) Given the stoichiometry of weathering reactions (Equation 4.6-4.7), 2 moles of $NO_3^-{}_{agricultural}$ are responsible for the release of 1 mole of Ca^{2+} and Mg^{2+} and ½ mole of Na^+.

In total, calculations suggest that nitric acid weathering reduces the CDR of silicate weathering by a very small amount (2%), from 0.54 to 0.53 Mt CO_2 yr^{-1}, and carbonate weathering by 3%, from 2 to 1.9 Mt CO_2 yr^{-1}. Most of this reduction takes place in a few major catchments (Appendices, Figure C.2). The UK is heavily modified by agriculture, which should indicate that nitric acid weathering will significantly reduce catchment CDR yields. However, this reduction is minimal. If other heavily modified catchments behave in a similar manner, then these results suggest that globally, nitric acid weathering may not be a significant source of CO_2 to the atmosphere.

4.8 Overall Carbon Dioxide Removal due to Natural Weathering in the UK

Table 4.6 summarises the various calculations made within Sections 4.5- 4.7. Notably, it highlights the potential for sulphide weathering to reduce the maximum estimates presented in Section 4.5.

Table 4.6- Maximum potential CDR due to natural weathering in the UK catchments, and upscaled to account for UK landmass. Given in annual flux (Mt CO_2 yr^{-1}). Compared to the reduced CDR due to sulphide weathering, nitrate weathering, carbonate precipitation and cation exchange.

	Studied Catchments			***Total UK***		
	Combined	*Silicate*	*Carbonate*	*Combined*	*Silicate*	*Carbonate*
Maximum CDR (Mt CO_2 yr^{-1})	2.54	0.54	2.0	6.3	1.3	5.0
Maximum CDR range (Mt CO_2 yr^{-1})	1.99-3.15	0.27-0.95	1.7-2.2	5.1-8.1	0.7-2.4	4.4-5.7
- **Sulphides**	-29%	-17%	-32%	-29%	-17%	-32%
- **Nitric acid**	-3%	-2%	-3%	-3%	-2%	-3%
Overall Reduced Mt CO_2 yr^{-1}	**1.76**	**0.42**	**1.34**	**4.3**	**1.0**	**3.4**
Maximum CDR range (Mt CO_2 yr^{-1})	**1.5-1.9**	**0.4-0.5**	**1.1-1.5**	**3.7- 4.7**	**0.9-1.1**	**2.9- 3.8**
- seawater alkalinity (w= 1.4)	-17.6%	-17.6%	-17.6%	-17.6%	-17.6%	-17.6%
Overall CDR Mt CO_2 yr^{-1}	1.45	0.35	1.1	3.6	0.9	2.7
Overall CDR range Mt CO_2 yr^{-1}	1.2-1.6	0.3-0.4	0.9-1.2	3.1-3.9	0.8-0.9	2.3- 3.0

4.8.1 Implications for carbon dioxide removal (CDR) utilizing Enhanced Weathering in the UK

To achieve the climate targets set by the United Kingdom to reach net zero by 2050 (Lezaun *et al.*, 2021), various strategies will need to be implemented to both drastically reduce emissions and remove carbon from the atmosphere. Enhanced Weathering (EW), the subject of Chapter 5, is a strategy aimed to enhance natural weathering processes and drawdown excess atmospheric CO_2 by adding crushed silicates to arable cropland. Current estimates for the potential for CDR by the application of EW to UK crops suggest sequestration from as much as 6-30 Mt CO_2 yr^{-1} (Kantzas *et al.*, 2022), to as little as 0.13 (± 0.1) Mt CO_2 yr^{-1} (Buckingham *et al.*, 2022).

It is useful to compare these estimates with the CDR due to natural weathering in the UK predicted here. The combined maximum CDR of natural silicate and carbonate weathering (CDR_{Max} = 6.3 Mt CO_2 yr^{-1}) in the UK lies on the lower end of the range predicted by Kantzas *et al.*, (2022). This suggests that EW would have to effectively double the natural weathering rates in the UK to reach the lower estimates of Kantzas *et al.*, (2022). Given the small particle size of applied silicates and acidic cropland this may be achievable (Beerling *et al.*, 2018), but further work is needed to investigate the possibility and potential impacts of doubling or an even greater increase to natural weathering rates on soil and groundwater chemistry, as well as the health of river ecosystems.

4.9 Conclusions

This study presents the first assessment of the annual amount of CO_2 consumed due to natural weathering processes in the UK. The analysis presented here demonstrates that on average, 7% of the major cations within UK rivers are sourced from silicate rock weathering, and 49% are sourced from carbonates. The annual CDR due to natural weathering in the 52 catchments studied here is 2.5 Mt CO_2 yr^{-1}, assuming an ideal scenario whereby no re-release of CO_2 occurs during transport, and all reactions proceed via carbonic acid weathering (Equations 4.1 and

4.2). This scales to 6.3 Mt CO_2 yr^{-1} when considering the whole area of the UK, of which 1.3 Mt CO_2 yr^{-1} is from silicates, and 5.0 Mt CO_2 yr^{-1} is from carbonates.

Strong acids (sulphuric and nitric) will reduce the true value of CDR from the maximum calculated CDR. Nitric acid does not, however significantly impact weathering CDR, reducing the overall CO_2 consumed by only 2% for silicates and 3% for carbonates. The potential reduction in the CO_2 consumption due to sulphuric acid is variable across catchments, with the maximum reduction in CO_2 yield occurring within midlands catchments- linked with shale and carboniferous coal deposits. The presence of sulphides could make the true CDR as much as 17% (silicates) and 29% (carbonates) lower than the calculated maximum CDR.

By quantifying the natural fluxes of silicate and carbonate weathering, this work expands the current understanding of the UK's carbon cycle. Constraining these baseline natural fluxes is critical to inform climate modelling and delimit the potential of various suggested land-based CDR strategies.

Chapter 5

5 Riverine Response, and Limitation to, Enhanced Weathering for Negative Emissions in the UK

Abstract

Enhanced silicate weathering, the application of crushed calcium and magnesium-rich rocks to arable cropland, has been proposed as a potential negative emissions technology for the drawdown of atmospheric CO_2. Previous estimates have suggested that enhanced silicate weathering (EW) has the potential to remove significant quantities of CO_2, as much as 6-30 Mt CO_2 yr^{-1} for the UK. However, if secondary carbonates are precipitated during the riverine transport of the products of EW, a portion of this CO_2 will be re-released, lowering the net carbon dioxide removal (CDR) potential of the mitigation strategy. Here, we assess the fluvial response to EW in the UK by calculating the expected riverine carbonate precipitation due to the dissolution of 10 to 50 t ha^{-1} yr^{-1} of silicate rock on available arable cropland in major UK catchments.

Increases in calcite saturation due to the export of soluble cations sourced from EW from soil to rivers are simulated to cross thresholds for spontaneous carbonate precipitation in several major UK river catchments (e.g. the Great Ouse, Thames). Catchments most susceptible to potential secondary carbonate precipitation are those with a high ratio of cropland to water discharge. On average, carbonate precipitation for major UK catchments is expected to make EW 16% (10 t ha^{-1}), 21% (20 t ha^{-1}) or 27% (50 t ha^{-1}) less effective at removing CO_2 than that predicted in the absence of such precipitation. Furthermore, when placing strict silica limitations on weathering reactions within soils, the CDR potential of EW is reduced considerably, to 0.23 Mt CO_2 yr^{-1}.

Although reducing the CDR potential of EW, we suggest that under rapid weathering conditions, carbonate precipitation in UK rivers will prevent pH increases over the safe level

for freshwater ecosystems (pH >9). Together, the simulations suggest that ambient hydrological conditions may make certain UK agricultural areas less effective for CDR by EW and call for methods to quantify secondary carbonate precipitation in response to EW treatments and to further investigate the role of silica saturation in suppressing weathering reactions.

5.1 Introduction

Humanity will need to employ various strategies over the coming century to halt increasing global temperatures and prevent catastrophic impacts of climate change (IPCC, 2018). One strategy will be to sequester CO_2 from the atmosphere using several proposed negative emissions technologies developed over the last two decades (Royal Society, 2018). Enhanced silicate weathering (EW) has been suggested as a valuable method for atmospheric carbon dioxide removal (CDR) and relies on applying crushed calcium- and magnesium-rich silicate rocks to arable cropland (Hartmann et al., 2013; Beerling et al., 2018, 2020).

Enhanced weathering aims to speed up the natural process of rock dissolution, normally of silicates. An example is the dissolution of forsterite (Equation 5.1) which removes up to two moles of carbon dioxide from the atmosphere for every one mole of Mg^{2+} released from the mineral:

Forsterite: $$Mg_2SiO_4 + 4CO_2 + 4H_2O \rightarrow 2Mg^{2+} + 4HCO_3^- + H_4SiO_{4(aq)} \quad (5.1)$$

Estimates suggest that globally upscaling EW, by applying between 10-30 tonnes of silicate rock (e.g., basalt) per hectare onto 900 Mha of equatorial cropland, has the potential to sequester 1.8-14.7 Gt CO_2 cumulatively by 2100. Early assessments of EW for the UK, e.g. Renforth, (2012) and Royal Society, (2018), involving spreading between 10-20 t ha^{-1} of silicate over half of the country's agricultural land suggested sequestration of 12-21 $MtCO_2$ per year (2.4-4.2% of the UK's annual emissions). A recent more sophisticated model of EW for the UK suggests sequestration potential of 6-30 $MtCO_2$ per year by 2050 from repeated additions to agricultural soils (Kantzas *et al.*, 2022). These estimates suggest the potential for EW to contribute to the UK's legally binding 2050 net zero emissions target.

The CDR potential of EW is, however, reduced by at least six processes that have been recognized by a number of previous studies (Köhler et al., 2010; Fuhr et al., 2021; Klemme et al., 2022; Knapp & Tipper, 2022):

i. Precipitation of secondary carbonates in the soil (i.e. pedogenic carbonates)
ii. Silica saturation of soil waters limiting dissolution rates according to rainfall water supply

iii. Precipitation of secondary silicates (e.g. clays) in the soil, which alleviates silica saturation, but also removes some cations released from the primary silicate dissolution.

iv. Precipitation of secondary carbonates in rivers as products are carried from soil to ocean.

v. Estuarine mixing, during which the high alkalinity of seawater decreases the ratio of carbon for a given increase in alkalinity.

vi. Organic (or inorganic) carbonate precipitation in seawater.

In this riverine study, we focus on an aspect that has not been well quantified: assessing the potential for reduced effectiveness of EW due to carbonate precipitation in rivers (point iv). We also consider the role of silica saturation and clay mineral precipitation (points ii and iii), given the importance of riverine discharge in transporting products, including Si, away from the soil.

When a mole of divalent cation (Ca^{2+} and Mg^{2+}) is released from primary minerals into freshwater with a close to neutral pH, the excess positive charge is mostly balanced by HCO_3^- (e.g., Equation 5.1) resulting in the uptake of two moles of atmospheric CO_2 into the water. However, if mineral saturation levels in the water result in the precipitation of secondary carbonate, one mole of this CO_2 is re-released to the atmosphere (Equation 5.2), lowering the net drawdown efficiency of EW:

Secondary Carbonate Precipitation: $Ca^{2+} + 2HCO_3^- \rightarrow CaCO_3 + CO_2 + H_2O$ *(5.2)*

Secondary carbonate minerals can form in soil, during riverine transport, or in the oceans. Previous studies have reported the link between secondary carbonates and the reduced drawdown efficiency of EW (Renforth, 2019; Kantzas et al., 2022), and it has gained recognition as an important variable, which two recent studies highlight. Kantzas *et al.*, (2022) reduced the overall CDR potential by 10-15% to account for ocean outgassing and (oceanic) carbonate precipitation in their model-based CDR calculations for EW in the UK. They also suggest that the alkalinity generated by EW increases the quantity of $CaCO_3$ precipitation in soils over time. Knapp and Tipper, (2022) consider the global impact of carbonate precipitation during riverine transport of the products of enhanced carbonate weathering (e.g. via liming of

agricultural land). Their study suggests that the dissolved products may be transported to the ocean if global rivers can maintain disequilibrium with respect to calcite (upholding a calcite saturation index of 1), however two thirds of the sequestered CO_2 via any enhanced carbonate weathering will be re-released due to secondary carbonate precipitation under equilibrium conditions (precipitation occurring at a saturation index= 0).

Additionally, to determine whether riverine transport of the products of EW would be a limiting factor, a conceptual model-based study by Zhang *et al.*, (2022) took baseline carbonate chemistry from US and global rivers and iteratively added ions from stoichiometric rock weathering until the water reached a specified saturation required for carbonate precipitation (as the exact value for this is unknown, they tested Ω= 5-25). They found that over baseline levels, global rivers could transport an extra 7-21.3 Gt CO_2 yr^{-1} of EW derived CO_2 before significant carbonate precipitation would lower the overall efficiency of EW.

Here, we build on their contributions by taking a catchment specific approach to question what the traditional spreading scenarios (10-50 t ha^{-1} yr^{-1}) will do to the carbonate chemistry of individual UK catchments. We suggest that because of the uneven distribution of UK arable land, there is a potential for large variations in the flux of EW derived ions to rivers. This heterogeneity may mean that, for catchments with low arable land, the potential CO_2 transport capacity as suggested by Zhang *et al.*, (2022) will not be met, whilst catchments with high arable land may cross thresholds for precipitation and cause reductions in the overall CDR efficiency of EW.

The flux of ions to the river will be controlled by the complexities of the soil environment. Environmental conditions in the soil- such as temperature (Pogge von Strandmann *et al.*, 2022), pH, availability of water (Buckingham *et al.*, 2022) and the extent of biological activity (Vicca *et al.*, 2022), will determine the weathering rates of the applied silicate and dissolution may be suppressed when conditions for weathering are not ideal (Brantley *et al.*, 2023). Once the applied silicate dissolves, soil processes, such as secondary mineral formation (secondary clays and pedogenic carbonates), cation exchange on soil mineral surfaces, equilibrium reactions in soil porewaters (Köhler *et al.*, 2010), and plant uptake of cations (Kelland *et al.*, 2020) may reduce the quantity of ions to leave the soil and enter the river. In contrast to the riverine environment, the impact of soil processes on the kinetics of weathering has been the subject of many studies, and therefore it is not the focus here. However, we do consider one area of the

soil environment which may significantly influence the flux of ions to rivers: the release of silicic acid during dissolution.

The release of silicic acid during weathering reactions may limit the CDR achievable by EW. During weathering, silicate minerals may dissolve completely, releasing cations and silicic acid into surrounding waters (e.g. Equation 5.1). Alternatively, they may preferentially release base cations into solution whilst retaining silica and some cations in secondary minerals, for example, the alteration of anorthite to kaolinite (Equation 5.3):

Anorthite dissolution:

$$CaAl_2Si_2O_8 + 2CO_2 + 3H_2O \rightarrow Ca^{2+} + 2HCO_3^- + Al_2Si_2O_5(OH)_4 \quad (5.3)$$

When weathering reactions release Si into porewaters, the saturation concentration of silica may be reached, which will inhibit weathering reactions until the porewater is recharged, or secondary silicate minerals precipitate (Köhler *et al.*, 2010). Silica saturation, therefore, has the potential to slow enhanced weathering reactions and lower the CDR potential of EW. To assess this limitation, Köhler *et al.*, (2010) modelled the outcomes of applying 1.58×10^4 Mt of olivine (~27 t ha^{-1}) onto the Amazon catchment and showed that silica saturation would reduce the carbon sequestration potential from 16 to 1.8 Gt CO_2 yr^{-1}. The difference between these two values demonstrates the importance of understanding the role of silicic acid release and secondary mineral formation during enhanced weathering.

In this study, we address these two limitations to EW by combining observed river water geochemistry for major UK basins, with geochemical modelling and carbonate precipitation beaker experiments. Across 36 UK river catchments, we calculate how the application of EW to arable land will modify river alkalinity, pH, calcite saturation and thus the quantity of secondary carbonate formation. Along with investigating the possible decrease in CDR potential due to fluvial carbonate precipitation and silica saturation, this study also explores whether the shift in catchment chemistry caused by EW will be within boundaries acceptable for aquatic life.

5.2 Predicting the impact of carbonate precipitation and silica saturation on EW CO_2 sequestration

We calculate the potential reduction in EW efficiency due to carbonate and silica saturation, from a theoretical maximum, due to the application of 10, 20 and 50 t ha^{-1} of a compositionally average basalt (Appendices Table D3) onto half of the arable land within major UK catchments (these values enable ready comparison with Renforth, 2012). Basalt was used as the applied silicate, as it is likely to be the rock of choice for large-scale adoption of EW.

Catchment data is used to calculate the total amount of basalt applied per catchment. A total of ~5 mega hectares (Mha) of land is used for arable agriculture in the UK (Royal Society, 2018), separated into ~90 catchments. Here we focus on 36 catchments which encompass 91% of this arable land (Figure 5.1b). These are a subset of UK catchments with the highest percentage of arable land; it is considered that the remaining omitted catchments would contribute less to the total CDR of EW in the UK as they have minimal land available for the application of crushed silicates. Each catchment's total area (A) was determined using the computer program qGIS and catchment boundaries from the Centre of Ecology and Hydrology (CEH, 2014), while the percentage of land that is arable (A_{arable} -Figure 5.2) is obtained from the National River Flow Archive (NRFA, 2023) (Figure 5.1B, Appendices- Table D1).

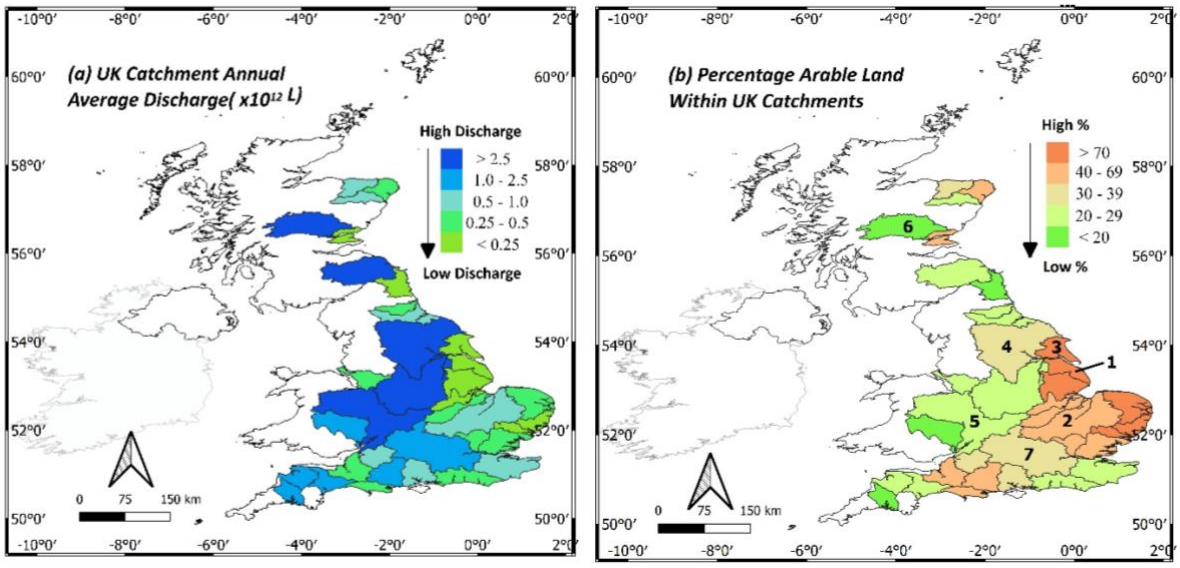

Figure 5.1 (a) Average annual discharge per catchment studied (10^{12} L yr^{-1}). (b) Percentage of arable land within each catchment. >90% of all UK arable land is housed within the 36 catchments shaded in figures (a) and (b). Numbered catchments in (b) will be compared in detail within the results and discussion, chosen due to their differences in arable land%, discharge and bedrock lithology. (1= Ancholme, 2= Great Ouse, 3= Hull, 4= Ouse, 5= Severn, 6= Tay, 7= Thames)

We consider two possible scenarios of alkalinity release to the river, depending on the extent of EW silicate mineral dissolution (see Section 5.3). These scenarios aim to explore the range in alkalinity release possible due to EW and reflect the uncertainty regarding the extent of a key inhibiting factor to dissolution: the degree that Si is released into porewaters. For each of these scenarios, we took the following steps to derive a reduced CO_2 sequestration budget:

i. Calculate the resulting riverine major ion chemistry and conservative alkalinity by combining baseline values with that released from EW in each catchment (Section 5.3).
ii. Predict how the riverine pH is impacted by this increased alkalinity (Section 5.6).
iii. Derive a threshold calcite saturation index at which rivers are expected to precipitate carbonate (Section 5.4).
iv. Using the calculated ion chemistry, alkalinity, pH, the threshold saturation index for precipitation, and the geochemical model PHREEQC (version 3) (Parkhurst and Appelo, 2013), predict the change in calcite saturation index for each UK river and the amount of carbonate precipitation (Section 5.5).
v. Use the percentage of ions which precipitate to calculate the reduced CO_2 sequestration due to carbonate precipitation and/or silica saturation (Section 5.5 and 5.7, respectively)

River geochemical data needed for step 1 was compiled from two UK Environmental Agency datasets (DEFRA, 2013, 2022d) to determine the natural background flux of ions in each river (F_B, Figure 5.2 and Appendices- Table D2) and annual runoff information was obtained from the NRFA (R; Figure 5.1a; Appendices- Table D1).

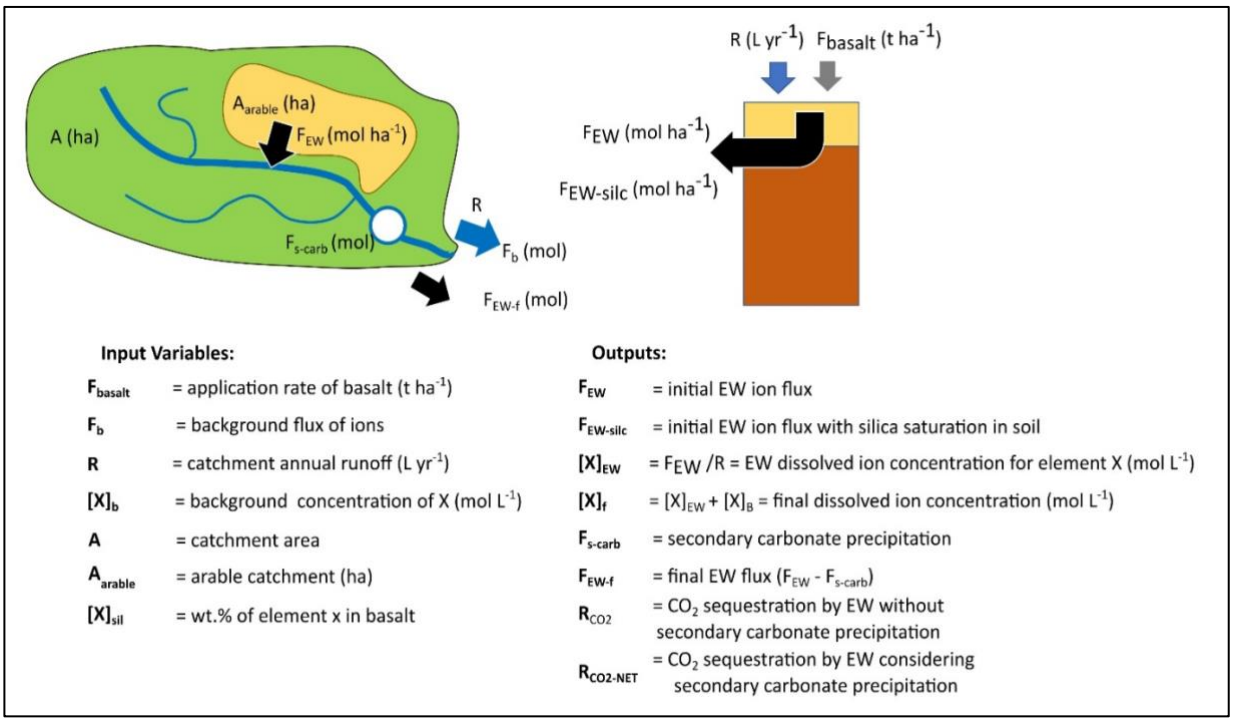

Figure 5.2- A summary of the variables and terms used in the study. Input variables are obtained from natural catchment data, as discussed in the main text. Outputs are the variables derived in this study: F_{EW} and $F_{EW-silc}$ are terms describing the flux of ions released from the applied basalt, which will be dependent on limitations by silica saturation ($F_{EW-silc}$) or carbonate saturation (F_{EW}) as discussed in Section 5.3. R_{CO2} is the maximum CO_2 drawdown expected from EW, and $R_{CO2-net}$ is the CO_2 drawdown once carbonate precipitation and silicic acid saturation are considered (Section 5.7).

For simplicity, we have neglected the flux of ions to groundwater sources. According to research from UK Research and Innovation (UKRI), the annual recharge to UK aquifers is 7 billion m^3 yr^{-1} (7x 10^{12} L yr^{-1}) (Bloomfield et al., 2013). Comparing this value to the UK annual riverine discharge to the ocean (1.59x 10^{14} L yr^{-1}, calculated from the National River Flow Archive (NRFA) (Marsh et al., 2015), the average flux to groundwater is approximately 4.2% of the total UK water discharge. Therefore, we assume that the dissolved ion flux to groundwater will not significantly impact our calculations here.

5.3 Scenarios for alkalinity release from applied basalt to fluvial systems

The alkalinity released to rivers due to EW will depend on the basalt dissolution rate once applied to the field. Dissolution is limited by three main factors: (1) the supply of rock to the catchment, (2) kinetic factors limiting weathering, such as temperature, pH, presence of microbes, flux of water onto the catchment, and amount of available acid, and (3) equilibrium reactions in the soil porewaters. For the first factor, we consider three spreading scenarios: 10, 20 and 50 t ha^{-1}. For the second, we assume that the kinetic limitations have been minimised by increasing the reactive surface area by crushing the rock to ~10 μm (Hangx and Spiers, 2009) and applying the crushed basalt onto agricultural soils with low pH and high microbial activity that promote fast dissolution reactions (Renforth 2012, Beerling et al., 2018). In this section, we then consider the third factor: the impact of equilibrium reactions between the dissolving basalt and the accumulation of silicic acid products.

The fate of Si during basalt dissolution is unclear. Either dissolved silica will accumulate in porewaters which will eventually reach saturation, preventing further dissolution of the applied rock (Köhler *et al.*, 2010). Alternatively, Si may be removed into Si bearing secondary minerals fast enough to prevent pore waters from reaching silica saturation (Schuiling *et al.*, 2011). We model two end-member scenarios that capture this range of potential response to silicic acid saturation on the alkalinity released from basalt: F_{EW}, the maximum EW derived flux of ions to the river with no imposed limitation by silica saturation or kinetics (i.e. assuming all cations are released from complete basalt dissolution); and $F_{EW-silc}$, the flux caused by stringent silica saturation limitations in which water flux constrains the release of cations.

5.3.1 Scenario one: The maximum alkalinity released to rivers due to EW (F_{EW})

The central assumption in this scenario is that that basalt dissolution is not affected by silica saturation in soil pore waters. This may be due to (i) Si concentrations reducing through plant uptake (Cornelis *et al.*, 2010) and/or incorporation into secondary Si bearing minerals which

do not contain the four major mobile cations (Mg^{2+}, K^{+}, Ca^{2+}, Na^{+}), or (ii) by major cations being released from the rock faster than silica (Peters *et al.*, 2004; Renforth *et al.*, 2015). In both situations, major ions leave the site of weathering before silica saturation in soil porewaters is attained. In this scenario, we assume that the supply of rock to the cropland is the only limitation to basalt weathering (10-50 t ha^{-1}), and therefore, once the system reaches steady state, that all applied basalt dissolves within one year of application. Further, we assume that mobile cations $Ca^{2+}, Mg^{2+}, Na^{+}, K^{+}$ supplied in one annual addition are released over an annual timescale from the soil; that is, all cations in applied basalt are released as alkalinity into the catchment river (or rivers).

Other assumptions made when deriving F_{EW} for this scenario:

i. Al^{3+} and Fe^{3+} from basalt dissolution are retained in soils (Al^{3+}; (Renforth *et al.*, 2015; Shao *et al.*, 2016), Fe^{3+}; (Renforth *et al.*, 2015))
ii. PO_4^{3-} (which makes up ~0.35 wt.% of common basalts Henderson & Henderson, 2009) will remain in the soil profile absorbed onto secondary clays (Kantzas *et al.*, 2022), or will be taken up by arable crops (Beerling *et al.*, 2018).
iii. Other anions (e.g Cl^{-}, NO_3^{-}, SO_4^{2-}) are not significant in basalt composition (Appendices, Table D.3), and therefore remain at baseline values in rivers.

The ions contributing to the flux of EW alkalinity to the river (F_{EW}) for this scenario are the major cations (Ca^{2+}, Mg^{2+}, Na^{+} and K^{+}). Using catchment characteristics and the composition of basalt, the increased concentration of these ions ($[X]_f$ − Figure 5.2) is calculated from their baseline concentration values $[X]_B$ (where X= Ca^{2+}, Mg^{2+}, K^{+}, Na^{+}) in each of the 36 catchments (supplementary information). The increased alkalinity from EW was then calculated by considering the charge balance in the river:

$$Conservative\ alkalinity\ (mEq/L) = \sum concentration\ of\ conservative\ cations\ (Ca^{2+}, Mg^{2+}, Na^{+}, K^{+}) - \sum concentration\ of\ conservative\ anions\ (Cl^{-}, NO_3^{-}, SO_4^{2-}, PO_4^{3-}) \quad (5.4)$$

The increase in cation flux to the water column is assumed to be balanced by an increase in carbonate species (HCO_3^{-} and CO_3^{2-}). The alkalinity calculated for this scenario (F_{EW}) represents the maximum increase in each catchment due to EW. This scenario is

therefore useful in constraining the maximum extent of secondary carbonate precipitation in UK rivers due to EW. However, we highlight that this is a theoretical maximum, and that while we assume that kinetic limitations could be minimised by a sufficiently small grain size and low pH conditions, some studies suggest that the dissolution of 10 μm basalt may take more than 10 years (Kelemen *et al.*, 2020). Unfavourable weathering conditions, i.e. low water supply (Buckingham *et al.*, 2022), may also slow the kinetics of weathering. Slow dissolution will of course lower the rate of alkalinity flux to the river calculated here.

5.3.2 Scenario two: The reduced EW alkalinity released to rivers due to limitations by silica saturation ($F_{EW-silc}$)

This scenario assumes that dissolution of minerals supplied by EW is limited by a saturation of Si in porewaters and provides a conservative estimate of EW effectiveness. In this scenario:

i. 100% of the weathered Si is released into porewater solution
ii. Silica saturation is reached when silicic acid concentration in soil porewater reaches 1.4 mmol L^{-1}, based on silica solubility equations (Henley, 1983; Van Cappellen and Qiu, 1997) (equations given in appendices for Chapter 5, and at 10 °C and at pH= 6)
iii. The amount of alkalinity transported from a catchment to a river is limited by the annual catchment runoff, which controls the recharge rate of porewaters (Köhler *et al.*, 2010)
iv. Once saturation is reached, all remaining basalt is left undissolved on the catchment
v. Fe remains in the soil profile as Fe-oxides, or, in instances where Fe reaches the river, would mostly form iron hydroxides (at pH 7-8, the average pH of rivers), which are relatively insoluble (Neubauer *et al.*, 2013)
vi. Si and Al are included in $F_{EW-silc}$ and, on entering the river system, are speciated according to the natural baseline riverine pH. Speciation was predicted using PHREEQC (version 3) (Parkhurst and Appelo, 2013) and was included in alkalinity equations.

Therefore, the major ions which contribute to the alkalinity flux in this scenario ($F_{EW-silc}$) are the major cations (Ca^{2+}, Mg^{2+}, Na^{+}, K^{+}), with an addition of Si and Al. The alkalinity flux $F_{EW-silc}$ derived from this scenario is useful in constraining the reduced flux under stringent silica limitations.

5.4 Determining the saturation state required for carbonate precipitation ($SI_{threshold}$)

Rivers may hold more EW alkalinity products in the dissolved load if they become supersaturated with respect to calcite (Knapp and Tipper, 2022). Predicting the quantity of secondary carbonate precipitation due to EW-derived alkalinity (F_{s-carb}) requires selection of a threshold saturation index at which rivers will precipitate carbonate ($SI_{threshold}$).

$SI_{Calcite}$ is defined by Equation 5.5, (Zeebe and Wolf-Gladrow, 2001):

$$SI_{Calcite} = log\left(\gamma Ca^{2+} * \gamma CO_3^{2-} \Big/ Ksp\right) \quad (5.5)$$

Where $\gamma Ca^{2+} * \gamma CO_3^{2-}$ are the activities of Ca^{2+} and CO_3^{2-} respectively, and Ksp is the equilibrium constant, which is dependent on salinity and temperature and is defined by Mucci, (1983). In an ideal solution, when $SI_{Calcite} \geq 0$, it is saturated with respect to calcite, and secondary carbonate precipitation is expected Zeebe and Wolf-Gladrow, (2001). In natural rivers, the $SI_{threshold}$ is often higher than $SI_{Calcite} = 0$, due to the inhibition of secondary mineral growth by the presence of specific ions in solution, such as Mg^{2+}, SO_4^{2-}, iron, phosphates, and organic molecules (Katz *et al.*, 1993; Nielsen *et al.*, 2016).

We estimate a $SI_{threshold}$ by considering the $SI_{Calcite}$ of natural rivers (Section 5.4.1). To test the chosen $SI_{threshold}$ predicts accurate quantities of precipitation; simple beaker experiments were performed with UK river waters to compare with modelled precipitation values (Section 5.4.2).

5.4.1 $SI_{Calcite}$ of global rivers

The global natural riverine distribution of $SI_{Calcite}$ in rivers can be examined using the global database GLORICH (Hartmann *et al.*, 2019). This analysis suggests that ~39% of rivers are saturated or oversaturated with respect to calcium carbonate ($SI_{Calcite}$>0) and 95% of the data have $SI_{Calcite} < 1$ (Figure 5.5). All the UK rivers studied here also have median natural

saturation indexes below 1 (ranging between -2.11 and +0.86). Based on the scarcity of natural rivers with an $SI_{threshold} > 1$, a threshold saturation index of 1.0 was used in this study.

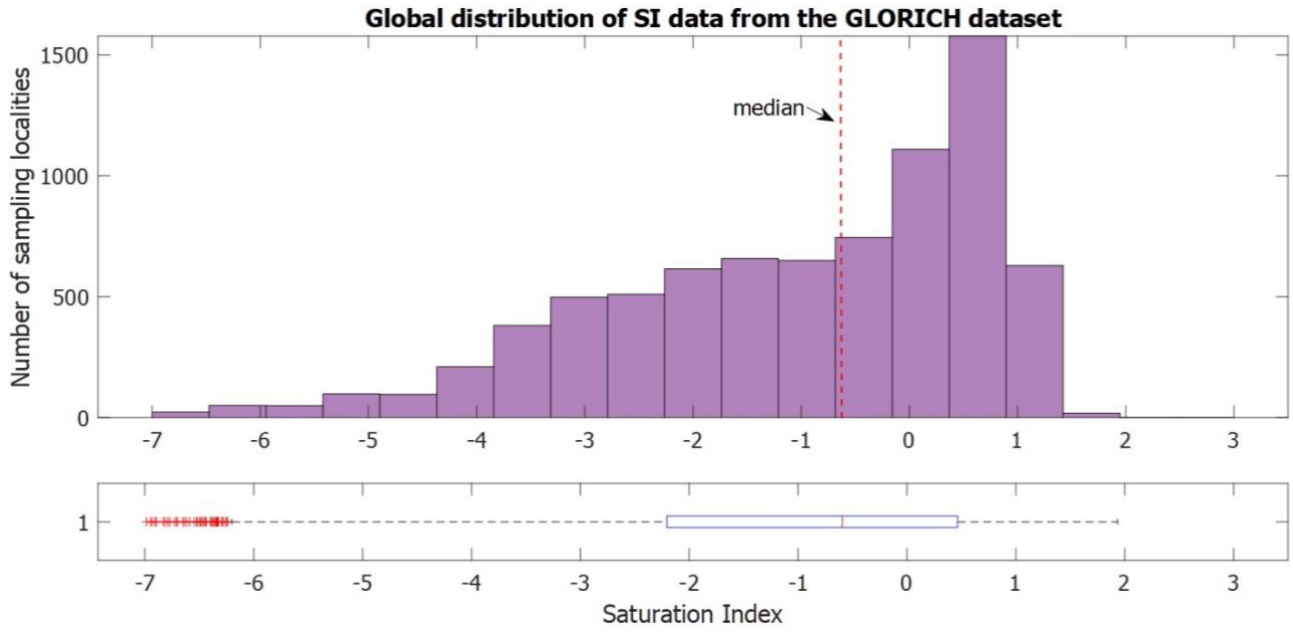

Figure 5.3- Global river saturation index data obtained from the GLORICH database. Bottom plot represents the interquartile range of the global river calcite saturation indexes (median = -0.59, 25 percentile= -2.21, 75 percentile = 0.47) Database from Hartmann et al., (2019).

To confirm that carbonates will precipitate in rivers at this threshold value, we then explored locations where secondary carbonates form in rivers. Carbonate deposits are found along the Slovenian karstic River Krka (Zavadlav *et al.*, 2017) in regions where $SI_{Calcite} = 0.8 - 1$, but not in locations were $SI_{Calcite} = 0.4$. In the Yalong river and tributaries (Chen *et al.*, 2022), 80-90% of dissolved Ca^{2+} is removed due to precipitation in rivers with a $SI_{Calcite} \sim 1$. In saturated rivers ($SI_{Calcite}$= 0.2-1.1) draining the Apennine Mountains (Italy), the fraction of Ca^{2+} removed due to precipitation increases from 0.1 to 0.8 with increased $SI_{Calcite}$ (Erlanger *et al.*, 2021). We also note that, independently to our analysis, a $SI_{Calcite} = 1.0$ was used in the study by Knapp and Tipper, (2022) as the theoretical upper limit that rivers could reach prior to carbonate precipitation. Therefore, we expect that carbonate precipitation will occur in rivers with $SI_{Calcite} \geq 1.0$, and that using this as a baseline value in PHREEQC will provide conservative estimates for secondary precipitation in the UK rivers studied here.

5.4.2 River water carbonate precipitation experiments to assess precipitation

River water carbonate precipitation experiments were carried out to provide an additional constraint on the saturation level required for carbonate precipitation in UK rivers and to test the selection of $SI_{threshold} = 1$. Unfiltered water from the River Thames and Severn was collected from accessible but flowing regions of both rivers (Appendices, Figure D.1). The water was distributed into 500ml beakers and alkalinity added which represented the two scenarios (F_{EW} and $F_{EW-silc}$) for application rates 10, 20 and 50 t ha^{-1}. Changes to pH, alkalinity, the end dissolved chemistry, and the quantity and composition of the precipitate were measured to calculate the resultant $SI_{Calcite}$ and quantity of precipitation. The carbonate precipitation experiments were run for 4 days (Thames) and 5 days (Severn) to reflect the average time water will remain in each river (Worrall *et al.*, 2014). A more detailed description of the experimental methodology is provided in the Appendices for Chapter 5.

Changes to the dissolved load over the course of the experiments suggest considerable carbonate precipitation. Dissolved Ca^{2+} reduced in the beaker water column by 68.3% (10 t ha^{-1}), 94.7% (20 t ha^{-1}) and 99% (50 t ha^{-1}) in the Severn experiments, and by 92.2% (10 t ha^{-1}), 99.2% (20 t ha^{-1}) and 99.3 % (50 t ha^{-1}) for the Thames, which has a naturally more saturated composition (Appendices, Table D.7). In the beakers representing 20 and 50 t ha^{-1}, the final concentration of Ca^{2+} was lower than in the control beaker. This implies carbonate precipitation in these beakers scavenged some of the natural Ca^{2+} as well as the added Ca^{2+}. Concentrations of Mg^{2+}, Na^{+} and K^{+} remain elevated in the beakers for the duration of the experiment, indicating limited removal through secondary precipitation.

The starting $SI_{Calcite}$ of each beaker was determined using PHREEQC. To confirm the validity of using $SI_{threshold} = 1$, for any given initial $SI_{Calcite}$, the amount of precipitation in the beakers was compared to the amount predicted in PHREEQC using $SI_{threshold} = 1$ and $SI_{threshold} = 0$ and the predicted calculated riverine chemical changes due to 10-50 t ha^{-1} application rates (Section 5.5). Using $SI_{threshold} = 0$ tends to over-predict the quantity of carbonate, while $SI_{threshold} = 1$ aligns closer to the observed data (Figure 5.4). Experiments confirm that using $SI_{threshold} = 1$ in PHREEQC will predict values of carbonate precipitation which may align closer to actual river values than those using $SI_{Calcite}$ =0.

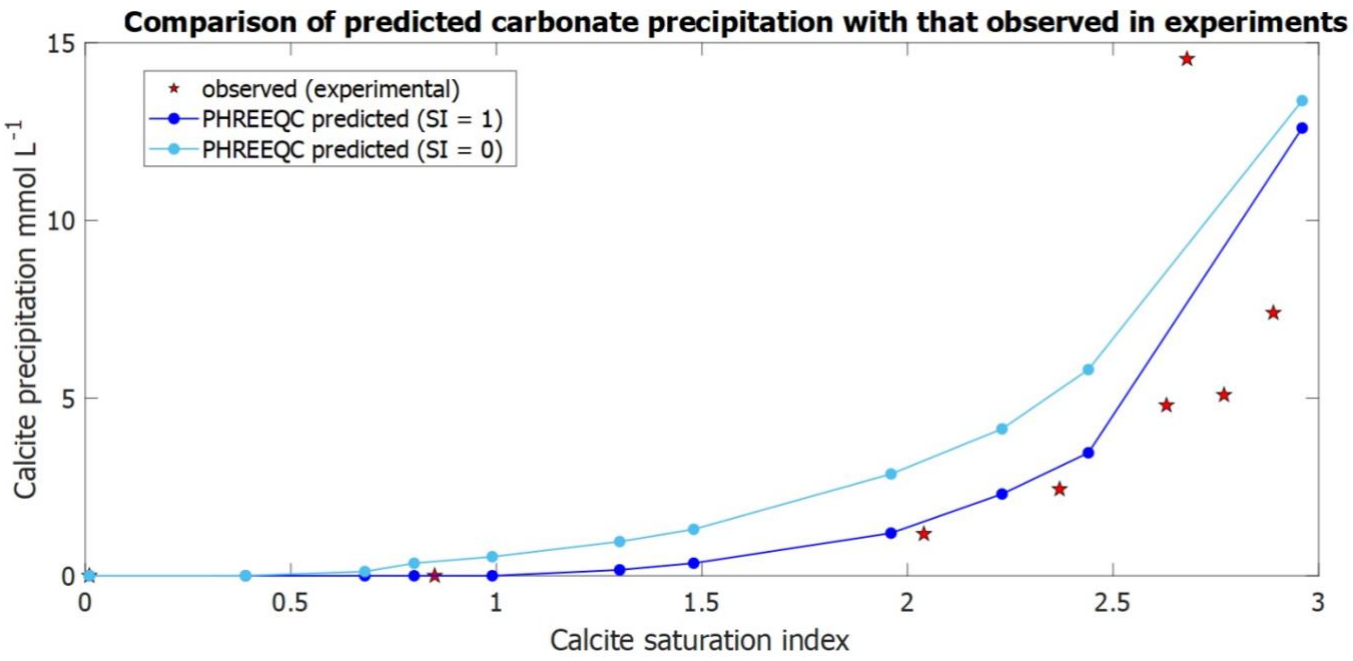

Figure 5.4- Experimental confirmation that a threshold saturation index of 1.0 is realistic for carbonate precipitation in UK rivers. The figure compares the predicted amount of carbonate precipitation for a given saturation index, with those of the river water carbonate precipitation experiments of this study

The experiments were also useful to constrain the kinetics of secondary carbonate precipitation. Significant precipitation occurred within the timeframe of the experiment, suggesting that, if UK rivers are pushed over the $SI_{threshold}$ by EW, secondary carbonate precipitation will occur during river transport; before the products reach the ocean.

5.5 The impact of Scenario 1 (maximum alkalinity release) on UK river chemistry and the potential for CO_2 removal

Under Scenario 1, where all basalt-derived alkalinity is released into rivers, the alkalinity flux resulting from application rates 10, 20 and 50 t ha^{-1} (F_{EW}) would lead to significant increases in riverine alkalinity and therefore to carbonate precipitation (Figure 5.5 and 5.8). For the 36 catchments in this study, and in the absence of carbonate precipitation, F_{EW} would increase the river alkalinity to a maximum of 9.4 mmol/ L^{-1}, 15.4 mmol L^{-1} and 35.6 mmol L^{-1} for 10, 20 and 50 t ha^{-1}, respectively. This is significantly higher than the natural value observed in UK rivers (median = 1.9 mmol L^{-1}). The extent of this increase is catchment specific and primarily

reflects the ratio of arable land content to water flux; the Hull and the Great Ouse catchments, for example, would see large increases in alkalinity due to their extensive arable land (71% and 65% respectively) and relatively low discharge (Figure 5.5).

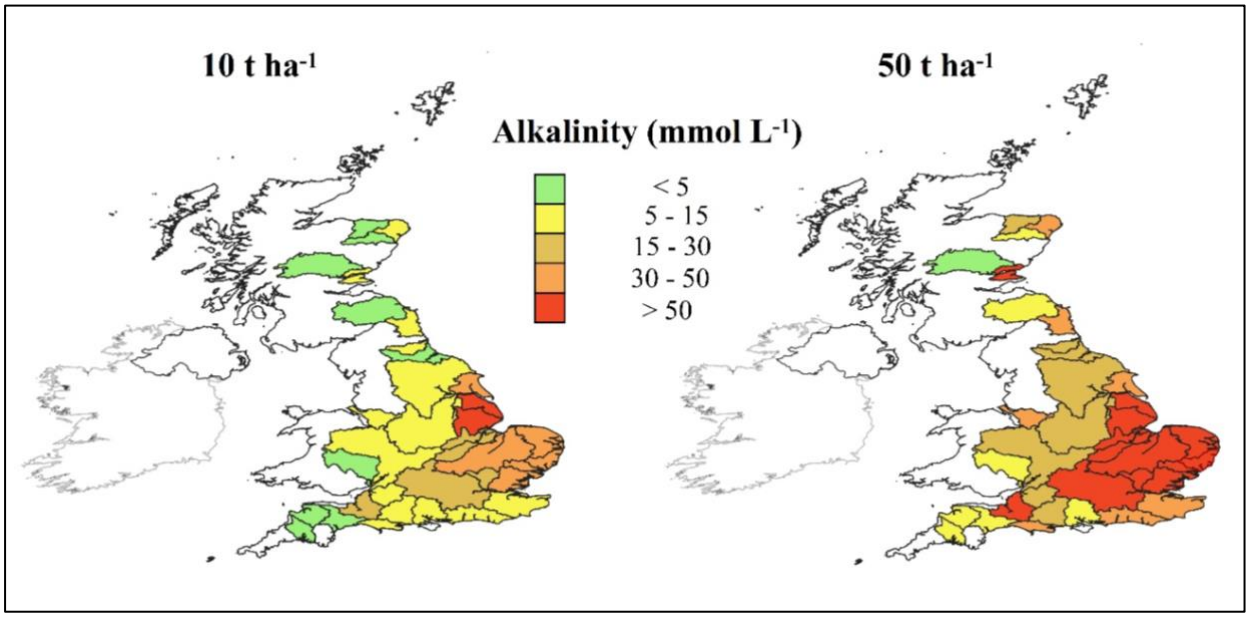

Figure 5.5- Derived EW initial alkalinity changes in UK catchments due to spreading scenarios 10 and 50 t ha^{-1} under scenario 1 in the absence of secondary carbonate precipitation and kinetic limitations. For comparison, the median natural alkalinity is 1.9 mmol L^{-1}. Alkalinity increase is calculated under the assumption that 10 and 50 t of basalt is applied to half of the available arable land in the catchment and that all the mobile cations Ca^{2+}, Mg^{2+}, Na^{+} and K^{+} within the basalt reach the river. River water flux used is the average discharge in each catchment (L yr^{-1}).

In the absence of carbonate precipitation, the $SI_{Calcite}$ in many UK rivers will be pushed over the threshold needed for carbonate precipitation ($SI_{threshold} = 1$). The rivers studied here have natural calcite saturation indexes ranging between -2.11 and 0.86 (median= 0.125). Due to EW scenario 1, the median $SI_{Calcite}$ without carbonate precipitation increases to 1.75 (10 t ha^{-1}), 2.18 (20 t ha^{-1}) and 2.83 (50 t ha^{-1}), driving 26, 31 and 35 rivers over the $SI_{threshold}$.

To compare our results with Zhang *et al.*, (2022), we estimate the basalt application rate needed to achieve the CO_2 transport potential for global rivers as suggested in their study (i.e. 10 -12 Gt CO_2 for a $SI_{threshold} = 1$). For a basalt of average composition (Appendices, Table D.3), a maximum of 0.295 tonnes of CO_2 is removed for every tonne of basalt dissolved (i.e. see discussion, re: Equation 5.7 below). 10-12 Gt CO_2 therefore corresponds to approximately 33.9-40.7 Gt basalt, which, if spread evenly over all global cropland (1.67 G Ha^{-1}, FAO), would equate to application rates of 24–29 t ha^{-1} yr^{-1}. In other words, Zhang *et al.*, (2022) show that rivers could hold the dissolved products of the complete dissolution of basalt applied at

approximately 24-29 t ha^{-1} yr^{-1} before the threshold saturation index for precipitation is achieved.

However, we suggest that these limits would only be achieved in practise if the world's arable land was spread in such a manner that EW derived ions evenly distributed themselves into global rivers. The distribution of arable land in the UK is uneven, and therefore our results suggest that, for spreading scenarios of 10-50 t ha^{-1}, the impact on UK rivers $SI_{Calcite}$ is highly dependent on the quantity of arable land in the catchment (Figure 5.1b. Figure 5.6).

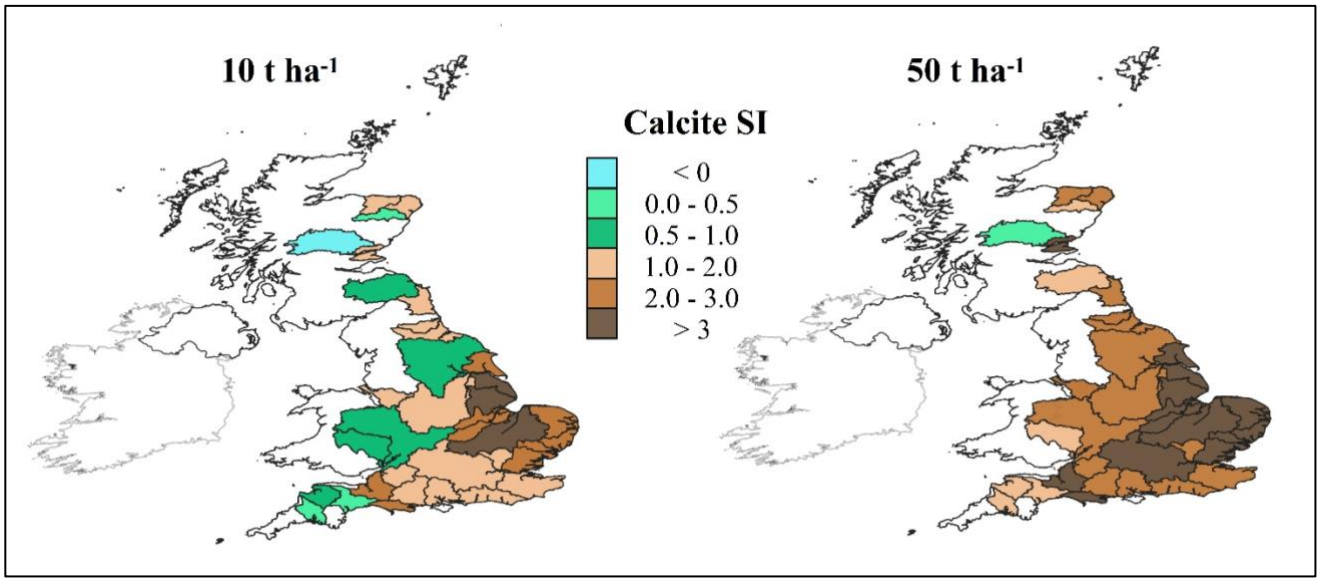

Figure 5.6- Catchment calcite saturation indexes for the 10 t ha^{-1} and the 50 t ha^{-1} application rates under scenario 1 in the absence of calcite precipitation. Saturation Index values were obtained using PHREEQC, and the alkalinity and chemistry were calculated using assumptions discussed in (section 3). Brown colours on this figure represent catchments in which riverine carbonate precipitation is expected (i.e. SI >1).

As scenario 1 would drive many UK rivers into disequilibrium with respect to calcite, PHREEQC predictions suggest that carbonate precipitation (F_{s-carb}) will occur to maintain river $SI_{Calcite} \leq 1$. We compared the quantity of Ca^{2+} (and Mg^{2+}) lost to carbonate precipitation predicted by PHREEQC with the initial EW derived alkalinity flux to the river (Figure 5.5); the median amount of alkalinity lost to F_{s-carb} in the 36 catchments studied was 6.2%, 10.4% and 31% for the 10, 20 and 50 t ha^{-1} application rates respectively. Most of the reduction in alkalinity was from Ca^{2+}, which decreased in the dissolved load by an average of 18%, 38% and 82% for the 10, 20 and 50 t ha^{-1} application rates (Appendices, Figure D.13); however, some catchments also lost smaller amounts of Mg^{2+} to Mg-rich carbonates.

The quantity of CO_2 consumed due to the complete dissolution of one tonne of basalt (R_{CO_2}) will be lowered by secondary carbonate precipitation (i.e., Equations 5.1-5.2). This reduction can be quantified by combining Equations 5.6-5.8. E_{pot} calculates the CO_2 consumed (in tonnes) by the percentage of EW derived alkalinity which remains dissolved until reaching the ocean, while C_{pot} calculates the quantity of CO_2 consumed due to alkalinity lost by the formation of riverine secondary carbonates, after Renforth, (2012) and 2019):

$$R_{CO_2} = E_{pot} + C_{pot} \quad (5.6)$$

$$E_{pot} = {}^{M_{CO_2}}/_{100} * \left({}^{\%CaO}/_{M_{CaO}} + {}^{\%MgO}/_{M_{MgO}} + {}^{\%Na_2O}/_{M_{Na_2O}} + {}^{\%K_2O}/_{M_{K_2O}} \right) * w_1 \quad (5.7)$$

$$C_{pot} = {}^{M_{CO_2}}/_{100} * \left({}^{\%CaO}/_{M_{CaO}} + {}^{\%MgO}/_{M_{MgO}} \right) * w_2 \quad (5.8)$$

M_{CaO}, M_{MgO}, M_{CO_2}, $\mathrm{M_{Na_2O}}$ *and* $\mathrm{M_{K_2O}}$ are the molar mass of CaO, MgO, CO_2, Na_2O, and K_2O respectively. w refers to the molar amount of CO_2 that will be removed from the atmosphere for every mole of oxide dissolved from the rock. In Equation 5.7, the term w_1 is a correction to account for the carbon speciation in solution. It is 2 in pure water and decreases with increasing alkalinity to values as low as 1.4-1.7 in the ocean (Renforth & Henderson, 2017). On the basis that river waters flow to the sea, and to allow comparison with a previous study[5] we use $w = 1.7$ in this study. However, to highlight how the choice of w would impact our results, we also calculate E_{pot} using w = 1.4. Additional future research to better constrain the w factor would be valuable for future CDR budgets.

The w value is impacted by the precipitation of carbonates: for calculation of C_{pot}, we used w_2 = 1.0 which is reduced from 1.7 due to the re-release of CO_2 during riverine precipitation (e.g., Equation 5.2). The presence of CO_3^{2-} in solution will lower this value to <1, but we assume here that in fresh water, carbonate speciation is dominated by HCO_3^- and therefore this reduction is assumed to be minimal.

The calculated R_{CO_2} may also be reduced by the presence of SO_3 in the rock, which may lead to the release of CO_2 by the formation of acids, as discussed in Renforth, (2019), but here we assume a minimal contribution of SO_3 given typical basalt compositions (Appendices, Table D.3), and on assumption basalt is most likely to be used for enhanced weathering.

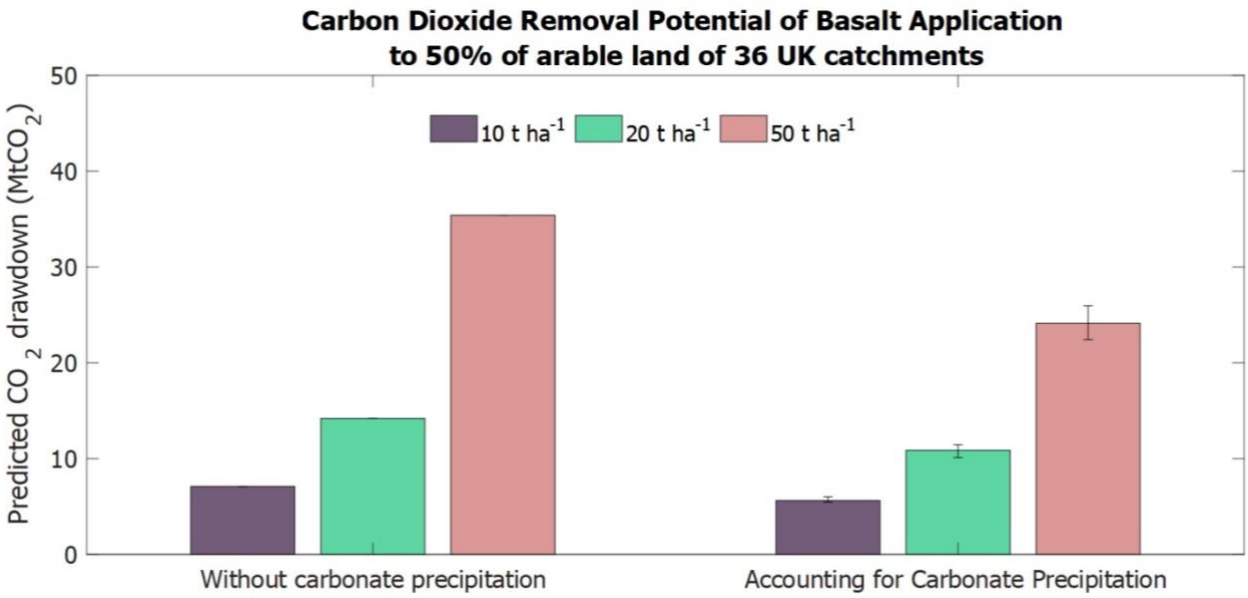

Figure 5.7-Total CO_2 drawdown due to EW. (a) Without carbonate precipitation= the total quantity of CO_2 which could be sequestered due to the application of basalt onto 50% of the arable land of 36 UK catchments. (b) The revised quantity which includes secondary carbonate precipitation in the calculations. Both (a) and (b) are without secondary limitations on weathering by silicic acid saturation.

The total annual CO_2 sequestration potential from EW for the 36 catchments was reduced due to carbonate precipitation (Figure 5.7). The maximum sequestered CO_2 due to the application of 10, 20 and 50 t ha^{-1} of basalt (R_{CO2}) across all 36 catchments is 8.3, 16.7 and 41.7 Mt CO_2 respectively. However, with carbonate precipitation this reduces to 7.0 (+0.2, -0.4), 13 (+0.5, -0.9), and 30 (+1.2, -2.2) Mt CO_2 for 10, 20 and t ha^{-1} respectively (Figure 5.7). Using $w_1 = 1.4$ in Equation 5.7 (instead of $w_1 = 1.7$) , reduces these results to 6, 11 and 27 Mt CO_2 for 10, 20 and 50 t ha^{-1} respectively.

Secondary carbonate precipitation during river transport of EW products is therefore expected to re-release 16% (+5%, -2%), 21% (+5%, -3%), and 27% (+5%, -3%) of the sequestered CO_2 from EW dissolution rates of 10, 20, and 50 t ha^{-1} yr^{-1} respectively. This calculated reduction in CDR due to carbonate precipitation (Figure 5.7) assumes that the rivers in this study can

maintain a supersaturation of $SI_{Calcite} = 1$. If UK rivers were to precipitate carbonates at a lower saturation index, (i.e. $SI_{Calcite} = 0 - 1$), then the result would be larger reductions to the EW CDR than that calculated here.

The CDR values expressed here represent conditions whereby rapid weathering occurs with little to no kinetic limitations. In the real soil conditions of the UK, some kinetic suppression of weathering would likely occur, the degree to which is currently debated. In Kantzas *et al.*, (2022) kinetic limitations were included in their model-based study of EW in the UK, which suggested that the CDR potential of EW would reach 6-30 $MtCO_2$ yr^{-1}, after 30 years of repeated 40 t ha^{-1} applications of 10-100 µm basalt particles. However, a significantly lower estimate (1.3 $MtCO_2$ yr^{-1}) was also derived from the results of a recent UK core study by Buckingham *et al.*, (2022). A one-off 100 t ha^{-1} application of 125-250 µm basalt was mixed into the topsoil of a soil core from the southeast of England, and the subsequent slow basalt dissolution rates during the experimental period was attributed primarily to low water flux. The results of these two studies, and the subsequent discussion raised by Buckingham *et al.*, (2023) and West *et al.*, (2023), highlights the importance of an accurate assessment of water flux when calculating/modelling EW dissolution rates and when upscaling CDR to regional or global levels.

The energy costs involved with mining, grinding, transportation and application will lower the net values for CO_2 sequestration predicted here. Moosdorf *et al.*, (2012) suggest a 10 -30% reduction in efficiency- primarily due to variations in energy needed to grind to different particle sizes (19.2%). Grinding to coarser sizes (greater than 10 µm) would lessen the energy requirements exponentially and reduce potential negative human respiratory impacts of fine dust, however this may come at a cost to CO_2 sequestration. The CO_2 release due to these processes may also be lowered by a switch to low carbon energy sources, i.e. solar, hydroelectric.

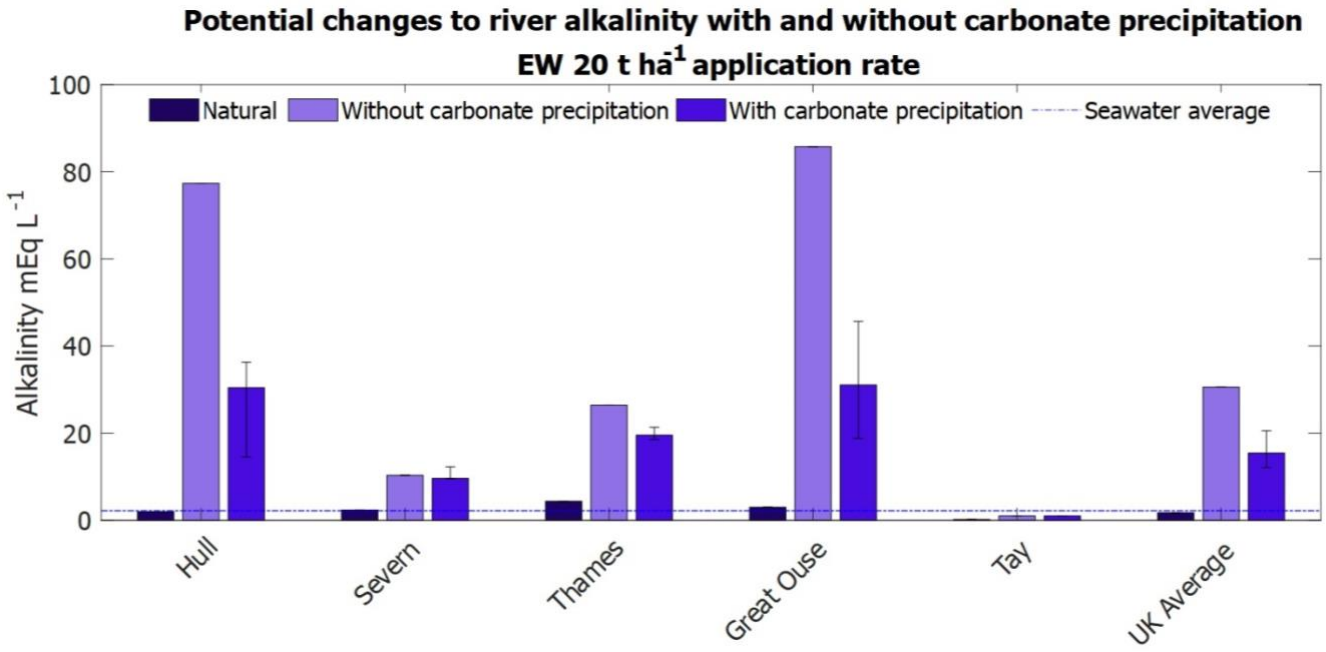

Figure 5.8- Maximum alkalinity increase in 5 example UK rivers, with and without secondary carbonate precipitation, due to the dissolution of 20 t ha^{-1} over half of the available land in the catchment. Values represent scenario 1 whereby all cations released reach the rivers. Alkalinity is compared to present-day average natural seawater levels (dashed line). Error bars represent the predicted amounts of carbonate precipitation, depending on the initial pCO_2 (see Section 5.6).

5.6 Impact on riverine pH

An increase in EW derived alkalinity to rivers will cause shifts in pH. We calculate this increase in riverine pH with and without carbonate precipitation. To do so we use conservative alkalinity, modified by addition of EW alkalinity, and the median natural riverine pCO_2 in the carbonate system equations (Zeebe and Wolf-Gladrow, 2001). Because the natural concentration of river pCO_2 varies by up to 2 orders of magnitude during the year (e.g. Appendices, table D.4), lower and upper pCO_2 bounds (5 and 95 percentile respectively) for each river were also used to provide an uncertainty range.

In the absence of carbonate precipitation, the addition of EW products from the complete dissolution of the applied silicate to rivers would result in large increases in pH (Figure 5.9a). However, if carbonate precipitation removes excess alkalinity as expected, in most rivers pH will remain close to natural levels (Figure 5.9b). These results indicate that secondary carbonate formation in rivers would be essential to buffer the potential pH increase caused by EW alkalinity addition and maintain riverine conditions suitable for freshwater ecosystems.

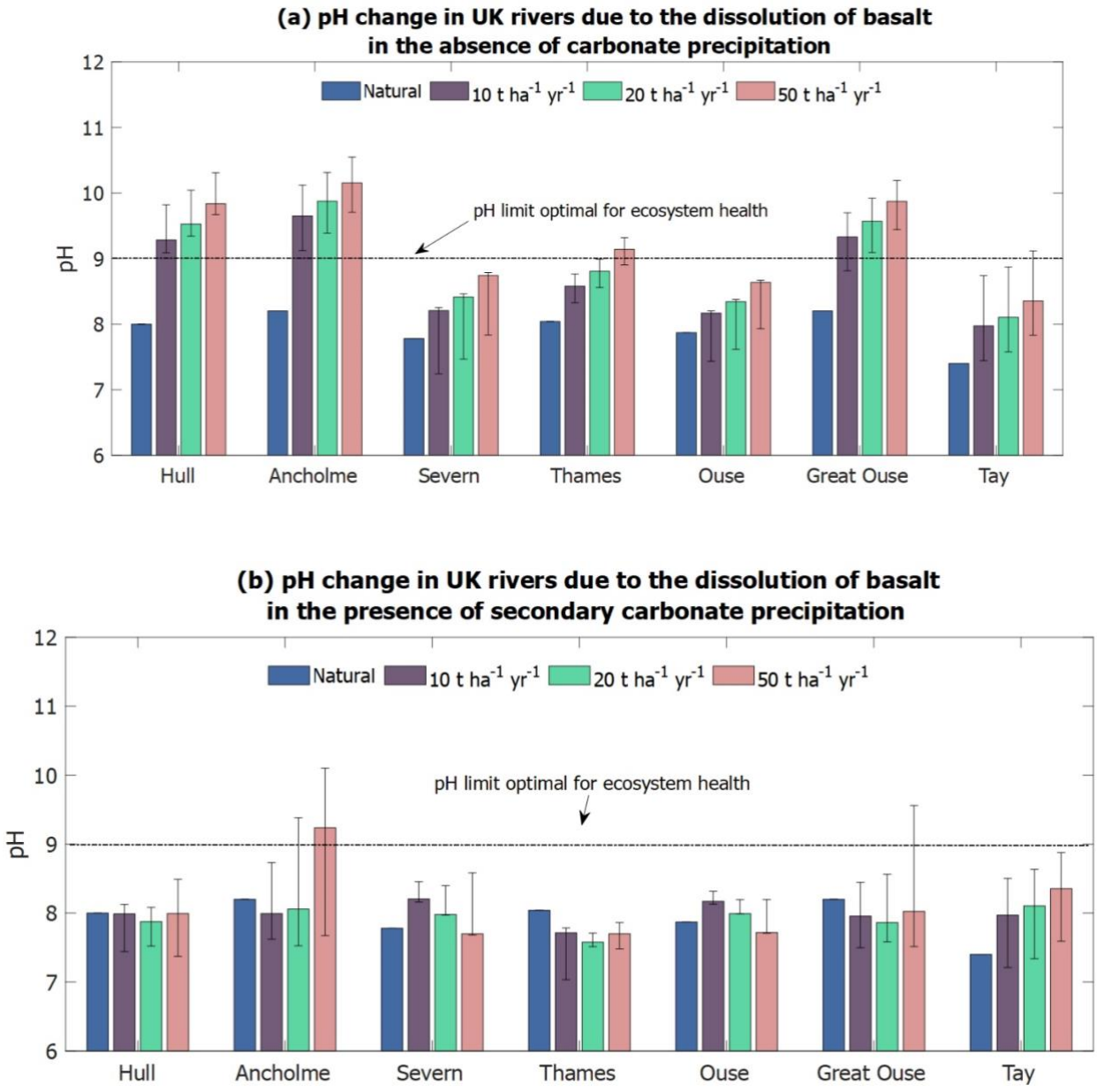

Figure 5.9- Modelled pH change in 7 UK catchments as a function of basalt dissolution rate (10-50 t $ha^{-1}yr^{-1}$). (a) prior to carbonate precipitation, (b) post precipitation. Maximum is compared with the minimum $Si_{limitation}$. Error bars are associated with the natural range in pCO_2, upper bound = 95 percentile, lower bound= 5 percentile. Ecosystem pH limit line (pH >9) based on values reported by the US Environmental Protection Agency (USEPA, 2022).

5.7 The impact of Scenario 2 (limitations caused by silica saturation) on UK river chemistry and EW CDR

The experiments and calculations in the previous sections have assumed that all major cations (Ca^{2+}, Mg^{2+}, Na^{+} and K^{+}) are fully released to rivers during EW basalt dissolution, without any limitation due to silica saturation (Scenario 1). In Scenario 2, where silica limitations are placed on weathering reactions, our calculations suggest that the release of cations ($F_{EW-silc}$) will be significantly reduced: leading to an increase in median river alkalinity only approximately double the natural median (from 1.9 to 3.6 mmol L^{-1}).

The lower degree of alkalinity released to rivers in scenario 2 prevents the degree of carbonate disequilibrium seen in Scenario 1 (Section 5.5). Nineteen rivers will remain under the $SI_{threshold}$ for carbonate precipitation, and the remaining rivers are driven between $SI_{Calcite} = 1.0 - 1.5$. Secondary carbonate precipitation presents only a marginal limitation to the riverine transport of EW products under scenario 2, removing between 0-7% of alkalinity from all rivers studied.

Under silica saturation, limited release of alkalinity to rivers, combined with the small secondary carbonate formation, reduces the CDR removal of EW in the 36 catchments to 0.23 $MtCO_2\ yr^{-1}$. This large reduction in CDR due to silicic limitations may, in part, explain why there are some differences between CDR calculated from modelling studies and lab/field research.

We reviewed previous research to investigate the likelihood of silica saturation imposing such strict limitations suggested by the results of scenario 2. Results from Peters *et al.*, (2004), Renforth *et al.*, (2015) and Montserrat *et al.*, (2017) suggest that during silicate weathering Si is either- removed from solution via secondary Si bearing mineral formation, enriched within surface altered layers which have already preferentially released cations, or released into solution at a slower rate than cations. If Si is removed from solution faster than it accumulates, saturation may not be reached in porewaters. However, to get around the limitation of silica saturation, Si will need to remain in the soil in some form: either absorbed, within a cation impoverished surface layer in the added silicate or in a secondary mineral. This would drive significant change in soil properties, which would be compounded by the application of further silicates in future years and must be considered before the pursuit and upscaling of EW.

Some silica will likely be removed from the soil through plant uptake. Of the main crops known to accumulate Si, wheat, rice and sugarcane have the potential to remove the most bioavailable silica: up to 113, 470 and 700 kg ha^{-1} yr^{-1} respectively (Keeping, 2017; Schaller *et al.*, 2021). Annual harvesting removes the silica from the system along with the plant, depleting the soils of Si. It has therefore been suggested that the addition of silicate minerals for enhanced weathering could provide a secondary benefit for arable crops by replenishing this lost silica (Kelland *et al.*, 2020; Manning, 2022). Plants could help alleviate some of the silica saturation developed from EW dissolution reactions however, given the maximum values of Si uptake (between 0.113-0.7 t ha^{-1}, species dependent) and the typical application rates discussed in literature, significant quantities of Si would likely remain in the soil profile, either undissolved, or as silicic acid.

Preliminary evidence from natural weathering terrains suggests that twice as much Si is typically retained in soils as is transported to rivers during silicate weathering. This evidence is derived from the difference between $Ca^{*}/_{Si_{river}}$ (where * = corrected for other sources of dissolved Ca^{2+}, such as carbonates and rain) and the bedrock $Ca/_{Si_{basalt}}$ in basaltic regions of Reunion Islands (Louvat and Allègre, 1997; Fretzdorff and Haase, 2002) the Deccan Traps (Dessert *et al.*, 2001; Das *et al.*, 2005), and Iceland (Georg *et al.*, 2007). The rivers in all three regions are approximately twice as enriched in Ca^{2+} than in Si, compared to the primary silicate rock (Figure 5.10). Based on the riverine Ca^{2+} enrichment under these weathering conditions, two times as much alkalinity is expected to be released during basalt weathering than that with stringent silica limitations. If conditions within the UK lead to similar weathering processes, then this would mean that the CDR potential calculated for realistic silica limitation would be approximately doubled (0.46 Mt CO_2 yr^{-1}), but still suggests that silica saturation imparts a considerable limitation on EW.

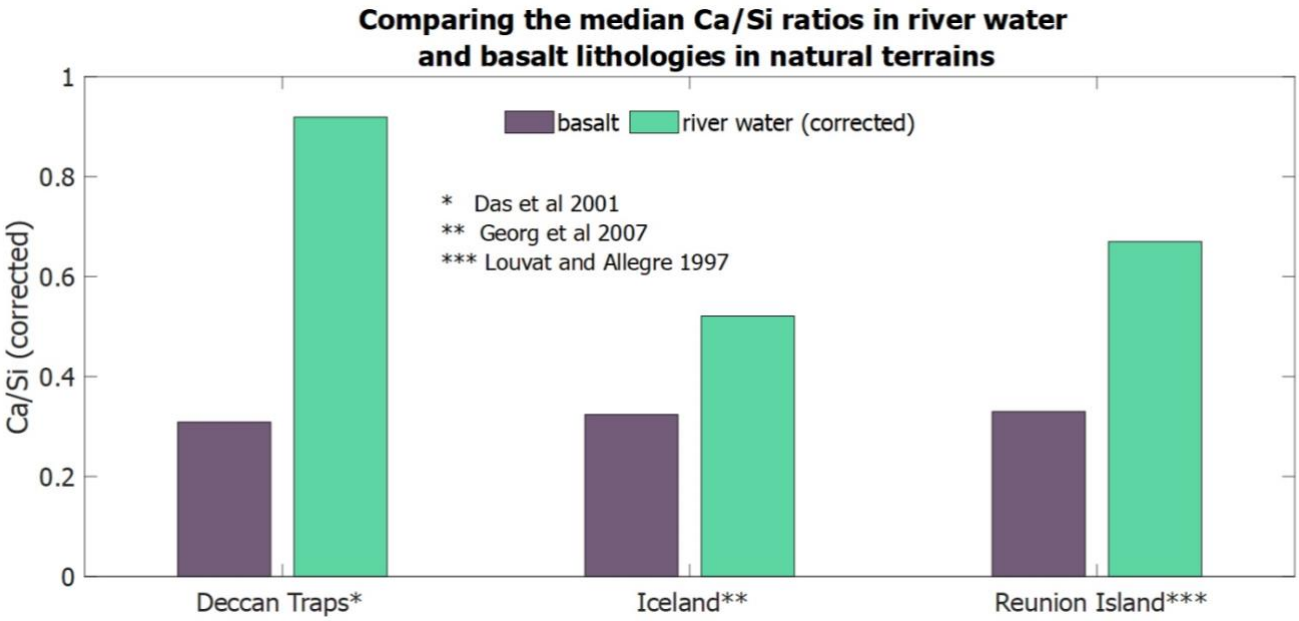

Figure 5.10- Ca/Si ratio of basalt vs Ca/Si of the river water that flowed over it. Basalt composition from Reunion Island was taken from Fretzdorff and Haase, (2002), other basalt compositions came from Das et al., (2005) (Deccan Traps) and Georg et al., (2007) (Iceland). The concentration of Ca^{2+} was corrected for other sources of Ca^{2+} (carbonate, cyclic, evaporites), so that the Ca/Si corrected represented the Ca/Si in the water which came from basalt.

5.8 Conclusions

This study presents an assessment of the limits on UK enhanced weathering due to the riverine transport of the chemical products. Calculations and experiments indicate that the complete dissolution of finely powdered basalt onto UK arable cropland will lead to significant shifts in river chemistry, resulting in substantial secondary carbonate precipitation. In the absence of silica saturation, riverine carbonate precipitation will reduce the CDR potential of EW by 16%, 21%, and 27% for application of 10, 20 and 50 t ha^{-1} respectively.

Under rapid weathering conditions where all the applied basalt is dissolved, riverine secondary carbonate precipitation will be necessary to negate ecosystem damage from significantly higher pH values in river waters. In a theoretical upper limit whereby all dissolved rock reaches the river and without carbonate precipitation, many UK rivers would pH reach pH > 9. However, the secondary carbonate which is expected to precipitate will buffer much of this pH increase and bring most of the rivers studied here back to environmentally safe pH levels.

Silica saturation may place an additional limitation on EW. Placing strict silica saturation limitations on basalt dissolution significantly lowers the annual CDR potential of upscaling

EW in the UK to a minimum of ~0.23 Mt CO_2 yr^{-1}, with consideration of the degree of silica saturation observed in other settings suggesting slight relaxation of this constraint and up to ≈0.5 Mt CO_2 yr^{-1}. In either case, Si saturation would lead to accumulation of Si-bearing minerals in soils and resulting shifts in soil properties which would need to be considered prior to the large-scale application of EW.

Chapter 6

6 General Discussion on Natural and Enhanced Weathering in the UK

6.1 Introduction

The objective of this Chapter is to build on the findings from Chapters 3 to 5 to assess (i) how UK weathering compares with other global catchments, (ii) the main drivers of weathering in the UK, (iii) prospective areas for future research to refine the conclusions presented in this thesis and (iv) the implications of the findings of this thesis for the adoption of enhanced weathering practices in the UK.

This thesis presented an assessment of the United Kingdom's suitability for adoption of enhanced weathering practices for carbon dioxide removal. At the outset of this research, the following key areas were identified as being important to determine:

1. The baseline flux of carbon dioxide removed (CDR) due to natural weathering in the UK.
2. The variation in CDR via natural weathering across different UK catchments.
3. The potential consequences on river chemistry when the dissolved byproducts of enhanced weathering are introduced into UK rivers, including the possibility of secondary carbonate precipitation and subsequent CO_2 re-release.
4. The potential impact of carbonate precipitation on the CDR estimates of enhanced weathering in the UK.

The results of this work have revealed significant variability in existing weathering yields across the UK, with silicate yields ranging from 0.8-395 kg CO_2 ha^{-1} yr^{-1}, and carbonate yields ranging from 19-518 kg CO_2 ha^{-1} yr^{-1} (Chapter 4). This variability suggests that certain environmental conditions (such as water availability, erosion, or permeability) or anthropogenic factors (such as land use), may be stimulating UK weathering reactions and increasing natural CDR. Consequently, certain UK regions may be more suitable for the

application of basalt for enhanced CDR purposes than others. These findings raise important questions about the primary drivers of weathering in the UK, optimal locations for the adoption of EW practises, and the overall suitability for the UK for EW in comparison to other global settings.

To implement EW requires identifying regions with favourable weathering conditions, but it is also essential to assess the river chemistry in these areas. What are the natural calcite saturation indices ($SI_{calcite}$) of the rivers in these catchments? Do they already transport significant quantities of weathering products, given the optimal weathering conditions within the catchment? Chapter 5 demonstrated that in southeastern catchments, where baseline $SI_{calcite}$ are high and arable land is abundant, there may be a greater potential for carbonate precipitation if EW were to be implemented. Conversely, rivers in northern regions, with high flow rates and lower initial $SI_{calcite}$, may be better suited to retain the products of EW. Consequently, the suitability of a catchment for the adoption of EW hinges on finding the right balance between ideal weathering locations (Chapter 3-4) and the river's capacity to retain the dissolved materials of EW (Chapter 5).

6.2 How does UK weathering compare to other global catchments?

Results of this thesis reveal that the annual CO_2 consumed by silicate and carbonate weathering in the UK may be as high as 1.3 and 5.1 Mt CO_2 yr^{-1} respectively (Table 6.1). This corresponds to approximately 0.3-0.4% and 0.2-0.7% of the total estimated global flux from silicates and carbonates respectively (Table 6.1) (Zeng *et al.*, 2019; Hilton and West, 2020).

Table 6.1- Comparison between the CO_2 consumed due to silicate and carbonate weathering in the UK, and the global estimates for silicate weathering from Hilton and West (2020), carbonate weathering (Zeng et al., 2019), Silicate CO_2 yields from Moon et al., (2014) and carbonate CO_2 yields from Zeng et al., (2019). Estimates were reported in Mt C yr^{-1} but converted to Mt CO_2 yr^{-1} for easier comparison with results here.

	UK (this study)	**Global (previous estimates)**
Silicate CO_2 consumption (Mt CO_2 yr^{-1})	1.3	330-510 (Hilton and West, 2020)
Carbonate CO_2 consumption (Mt CO_2 yr^{-1})	5.0	730-2600 (Zeng *et al.*, 2019)
Silicate CO_2 yield (kg CO_2 ha^{-1} yr^{-1})	60 (0.58 -400)	45 (Moon *et al.*, 2014) (1-189)
Carbonate CO_2 yield (kg CO_2 ha^{-1} yr^{-1})	197 (19-769)	150 (Zeng *et al.*, 2019) (55-1550)

In assessing the efficacy of weathering for carbon dioxide removal in the UK relative to other global catchments, to account for variable catchment sizes it is more informative to compare weathering CO_2 yields per unit area (in kg CO_2 ha^{-1} yr^{-1}). The weathering yields calculated in this thesis (Chapter 4 and given in Table 6.1) are compared to silicate yields from global catchments (Moon *et al.*, 2014), and carbonate yields from Zeng *et al.*, (2019). To allow comparison with (Moon *et al.*, 2014), their annual silicate weathering CO_2 consumption rates from 32 global catchments (in 10^9 mol yr^{-1}) were converted into yields (kg CO_2 ha^{-1} yr^{-1}), using published basin areas. It is worth noting that the UK yields are from a relatively small geographical area compared to these global basins. For instance, the median basin size in Moon *et al.*, (2014) was 40 Mha, while the combined basin area of all the 52 catchments here is 9.4 Mha.

Both the mean silicate and carbonate weathering yields in the UK, although variable, are slightly higher than the global catchment averages (Table 6.1). Notably, the average UK silicate yield exceeds that of numerous global rivers (Figure 6.1). It is unclear what is causing this. Catchments with elevated silicate yields (i.e., those positioned above the UK in Figure 6.1), are distributed across various latitudes, and exhibit a range of average temperatures. Moon *et*

al., (2014) observe a negative correlation between runoff and the proportion of solutes from silicates (i.e. X_{sil}) in the global catchments. They proposed that this relationship is linked to extended fluid residence time within catchments of reduced flow rates, which favours slower silicate reactions. However, a similar correlation does not exist between runoff and silicate yield. This suggests that although water availability must exert some influence on silicate weathering, other factors must play a significant role in controlling the range in yields observed in Figure 6.1; and the UK's place within this range.

For carbonate yields, we compare our research to that of Zeng *et al.*, (2019). They suggest that the average global CO_2 yield due to carbonate weathering is ~150 kg CO_2 ha^{-1} yr^{-1}, but this varies substantially with catchment location/latitude; Arctic regions have substantially lower yields than equatorial zones (2 and 1712 kg CO_2 ha^{-1} yr^{-1} respectively), which they attribute mostly to increased rainfall/runoff. They place the UK in the 180-370 kg CO_2 ha^{-1} yr^{-1} zone, which our average falls in line with, although some individual catchments are a little higher than this (Figure 6.2b).

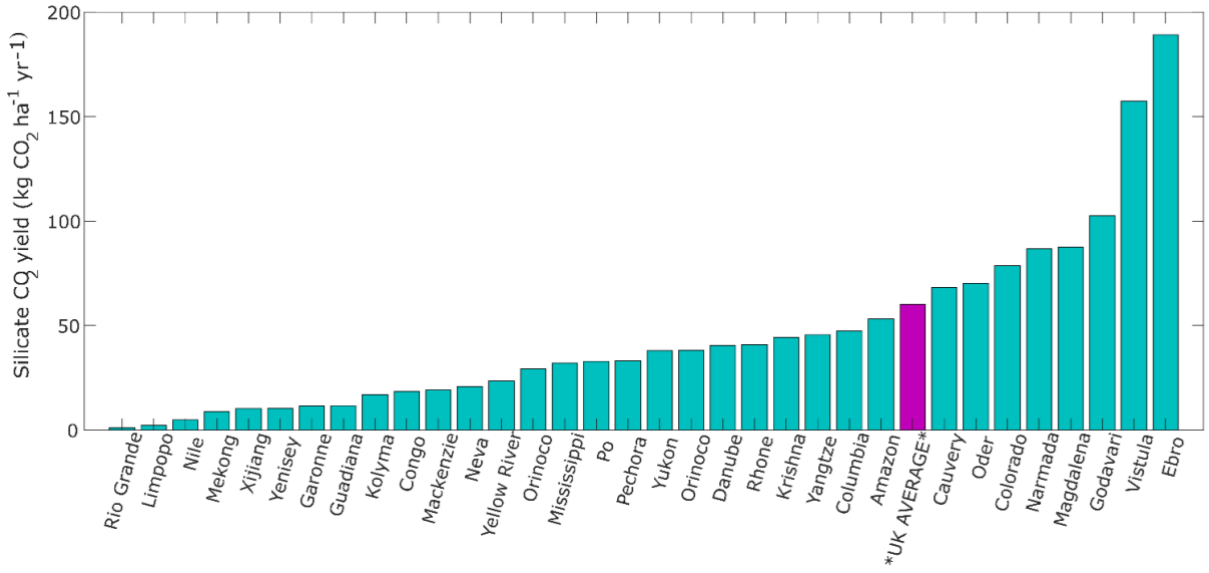

Figure 6.1– Comparing the average silicate yield in the UK (kg CO_2 ha^{-1} yr^{-1}) with averages from global catchments calculated from Moon et al (2014).

The fact that UK's mean weathering yields exceed global averages is an unexpected result. It challenges the conventional view that the UK's environmental conditions, with low temperatures, moderate runoff, and low erosion rates, are suboptimal for weathering. This

observation provides an initial indication that, in the context of weathering rates, the UK might be a suitable region for the effective deployment of EW for CDR.

6.3 What drives high weathering rates in the UK?

While the UK's elevated weathering derived CO_2 yields suggest its potential suitability for implementing EW practises, not all locations across the UK may be equally suited. Identifying the primary factors driving the accelerated dissolution rates in optimal weathering zones (Figure 6.2) can inform future site selection for enhanced weathering: both within the UK, and globally. The primary aim of this section therefore is to discern the main environmental or anthropogenic factor or factors contributing to the variation in weathering derived CDR observed across the UK (Figure 6.2).

As previously introduced in Chapter 1, numerous parameters have been shown to enhance weathering rates, such as temperature (Palandri and Kharaka, 2004; Gaillardet *et al.*, 2019), water availability (Buckingham *et al.*, 2022; Brantley *et al.*, 2023) and the duration that this water is in contact with the bedrock (Maher, 2011; Maher and Chamberlain, 2014), erosion (Maher and Chamberlain, 2014), vegetation and biogenic processes (Vicca *et al.*, 2022), availability strong acids (Torres *et al.*, 2014; Burke *et al.*, 2018; Hilton and West, 2020; Bufe *et al.*, 2021), and anthropogenic activity, particularly in agriculturally related land use (Perrin *et al.*, 2008; Barnes and Raymond, 2009; Raymond and Hamilton, 2018).

While all these variables have the potential to influence weathering, this section focuses on those that exhibit significant variations across the UK, suggesting their greater contribution to the observed variations in the weathering derived CO_2 yields (Figure 6.2). Specifically, given their high variability, this section focuses on water flow and availability, permeability, erosion, and the impacts of anthropogenic land use. In contrast, the average mean temperature across the UK only differs by ~1.4 °C (the average temperature in England in 2023 was 10.9 °C, while the average temperature in Scotland was 8.5 °C; (MET, 2023)). Consequently, although the role of temperature in driving seasonal changes in weathering is discussed (Section 6.3.1 (i)), it's impact on the spatial variation observed in Figure 6.2 is largely ignored here. Given the

larger spatial variability exhibited by the other parameters, it is presumed that they contribute more to the observed variation than temperature.

To evaluate the potential impact of these parameters on weathering yields, I employ statistical correlations between each variable and the CO_2 yields resulting from silicate and carbonate weathering. The primary limitation to this approach is the co-variation of many variables at national level across the UK (See Section 6.3.1). Therefore, in the following sections, I also take a catchment specific approach to attempt to determine the relative contribution of individual parameters.

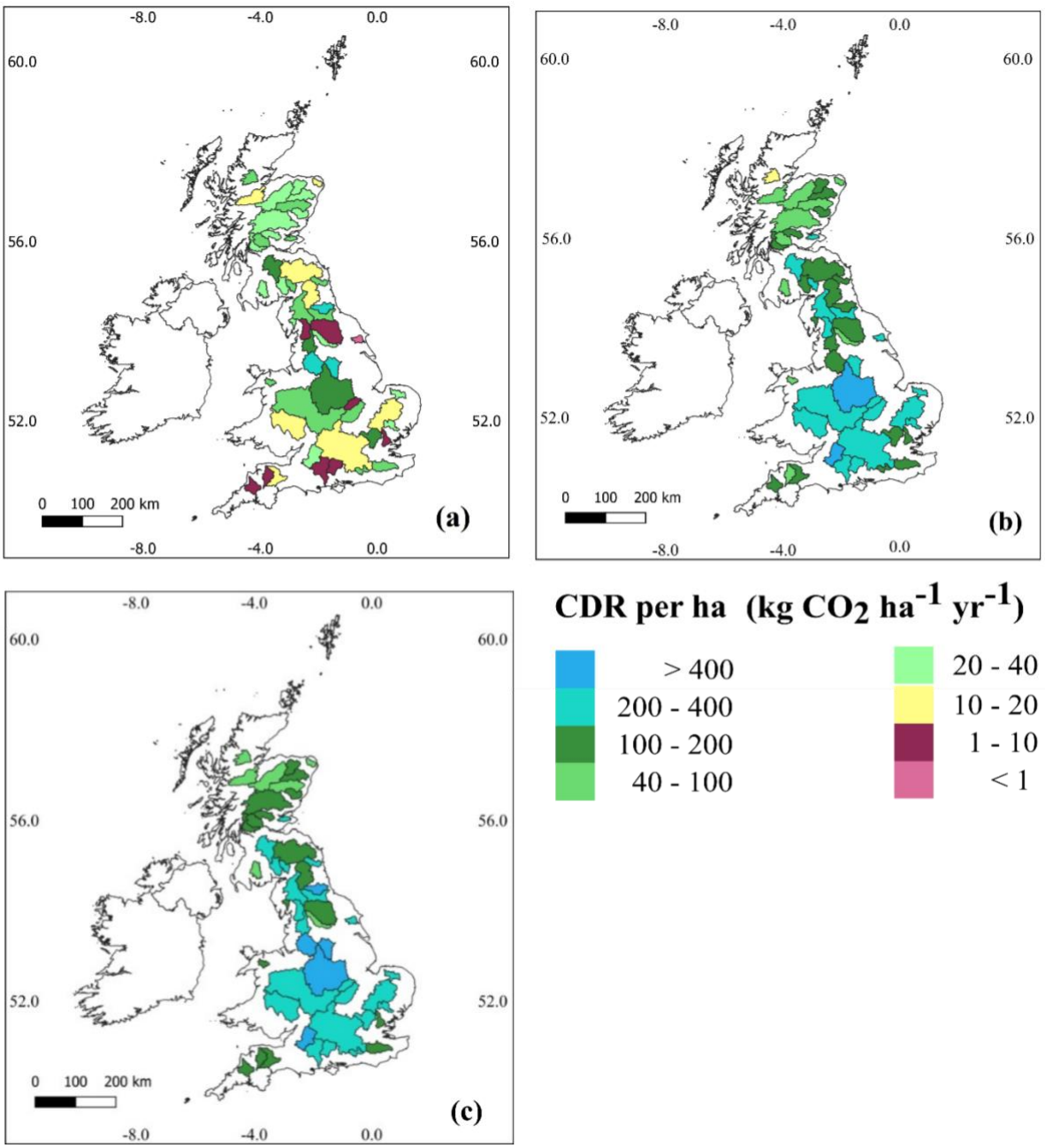

Figure 6.2 (From Chapter 4)- The potential maximum quantity of CDR due to natural (a) silicate and (b) carbonate weathering in the UK catchments within the study. (c) is the total combined CDR for natural weathering. Given in CO_2 yield (kg CO_2 ha^{-1} yr^{-1}). Yields are calculated from the median fraction of ions from silicate and carbonate sources as predicted by the inversion results (data within datasheets in supporting information).

6.3.1 UK nationwide relationships between drivers and weathering

Statistical analysis did not reveal any relationship between environmental parameters and silicate weathering yields (Figures 6.3-6.4) at national scale, although there were initial indications of lithology imparting some control over yield when comparing sites of high yields (Figure 6.2) with UK geology (See Chapter 4, Figure 4.2). This aligns with previous global

findings, which suggest that determining the main control over silicate weathering rates can be challenging because yields can be governed by multiple catchment parameters simultaneously (West *et al.*, 2005). Conversely, initial analysis revealed clear relationships between carbonate yield and various climatic, geomorphic and land use characteristics of the catchment areas (i.e., percentage arable land, runoff, elevation, permeability, Figures 6.3-6.4) at national scale. However, these patterns co-vary with the NW- SE pattern in lithology seen across the UK (Chapter 4, Figure 4.2). Consequently, it is challenging to isolate the key environmental drivers of carbonate weathering rates, because the presence (or absence) of carbonate lithologies is likely to be a primary factor driving variations in carbonate yield. Due to the difficulty in assessing drivers at national scale, the following sub-sections will therefore evaluate each environmental parameter independently and subsequently attempt to determine their relative importance on the variation in silicate and carbonate yield as presented in Figure 6.2.

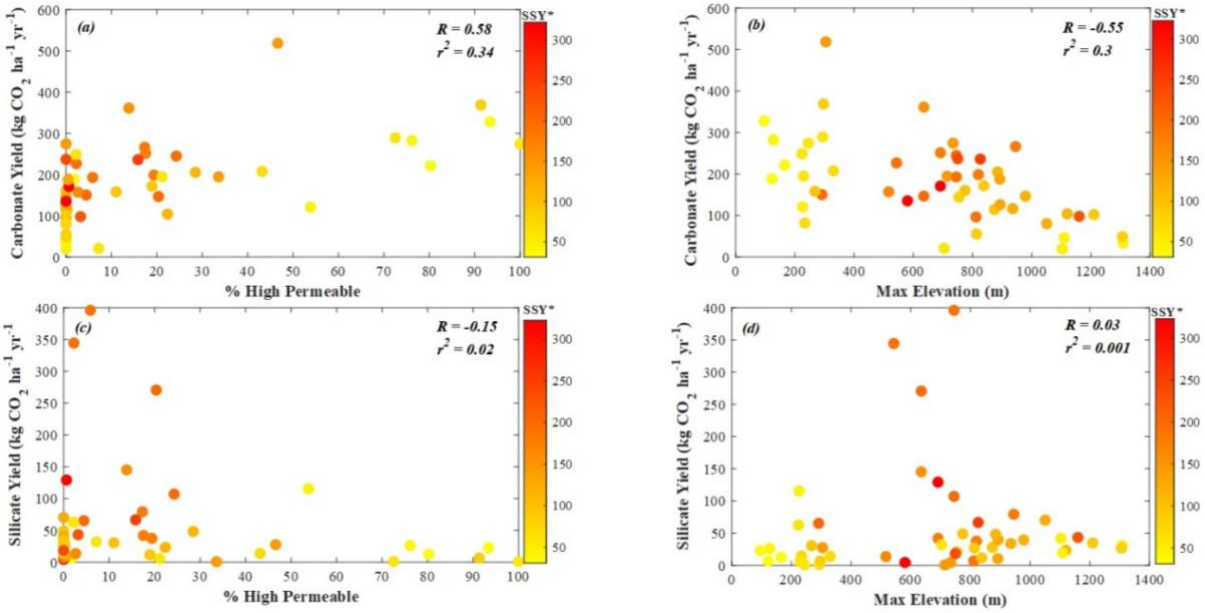

Figure 6.3 (From Chapter 4)- A medium positive correlation can be between carbonate yield and (a) the percentage of high permeable lithology within the catchment, while a medium negative correlation can be seen between carbonate yield and (b) the maximum elevation. In contrast, no correlation can be seen between silicate yield and (c) permeable lithology, and (d) the maximum elevation.

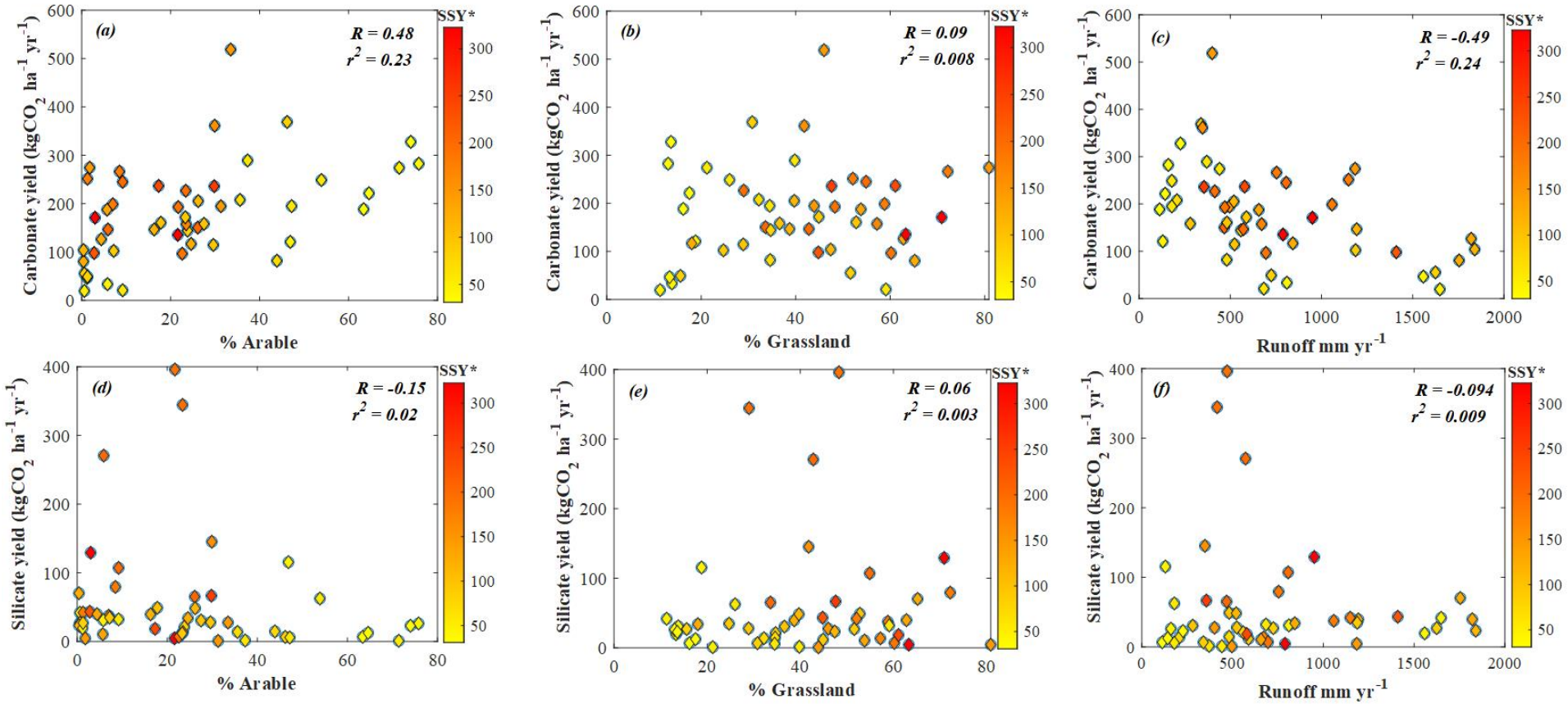

Figure 6.4 (From Chapter 4)- Correlations between catchment parameters and weathering yields. First three plots show medium correlations between carbonate yield ($kgCO_2$ ha^{-1} yr^{-1}) and (a) Percentage arable land, (b) percentage grassland and (c) Catchment runoff (mm yr^{-1}). Last three show no correlation in silicate yield vs (d) percentage arable land, (e) percentage grassland and (f) Runoff (mm yr^{-1}).

6.3.2 Natural variables that may influence UK weathering

6.3.2.1 Runoff/ water availability

Increased runoff is generally anticipated to drive increased carbonate weathering fluxes (Zeng *et al.*, 2019) by supplying solvent for reactions and allowing waters to remain far from carbonate saturation. As such, the observed negative relationship between carbonate weathering yields and runoff is unexpected (Figure 6.4c). However, as runoff typically decreases towards the southeast- and towards catchments with higher carbonate lithologies- there is a potential that the dominant lithological control on carbonate weathering discussed above is obscuring the impact of water availability on weathering yields at national level. Given the requirement for extended water- bedrock contact to facilitate the slower dissolution of silicate minerals, a negative correlation between runoff and silicate yield might be anticipated if water availability primarily controlled silicate yield. However, there is no such relationship between these two factors.

Although the link between runoff and silicate and carbonate yields in the UK is unclear (given Figures 6.3 and 6.4), this does not necessarily exclude the possibility of water availability influencing UK weathering. Two alternative approaches are employed to further assess the impact of water availability: (i) examining the potential constraints posed by the calcite saturation index ($SI_{calcite}$) of the river (for the carbonate yields and water) and (ii) considering the relationship between the proportion of solutes from silicates (X_{sil}) and runoff (for silicate weathering and water).

The $SI_{calcite}$ can establish an upper boundary on the quantity of DIC that can be transported by the river, thereby limiting the catchment's weathering yield. In the UK, strong associations between high $SI_{calcite}$ and regions in the southeastern regions characterized by abundant chalk lithology. This suggests that variations in saturation index may be more informative for elucidating factors influencing carbonate yields: and the relevance to silicate yields may be limited. In general, as the calcite saturation index ($SI_{calcite}$) of the river increases, so too does the carbonate yield, leading to a strong, positive correlation between the two variables (Figure 6.5a). However, this trend is only applicable until $SI_{calcite}$ ~0.4, then further increasing the $SI_{calcite}$ decreases the yield (Figure 6.5b). As expected, there is no relationship between $SI_{calcite}$ and silicate yield (Appendices, Figure E1).

A set of catchments with $SI_{calcite} \geq 0.4$ (within the highlighted box of 5(a)) are likely approaching the threshold saturation for carbonate precipitation (termed $SI_{threshold}$; results from Chapter 5 indicate that significant carbonate precipitation is unlikely prior to $SI_{threshold} \geq 1$). In other words, this suggests that these catchments might be approaching their capacity to accommodate additional DIC input, potentially reaching, or already attaining, the limit of DIC transportability through these rivers due to weathering. Increasing the water flow in these catchments could reduce the calcite saturation index, which may potentially lead to carbonate CO_2 yields surpassing those reported in Chapter 4 in these regions. Therefore, results suggest that runoff does play a role in carbonate weathering in the UK. An increase in runoff may enhance UK carbonate weathering in certain catchments that may be water limited.

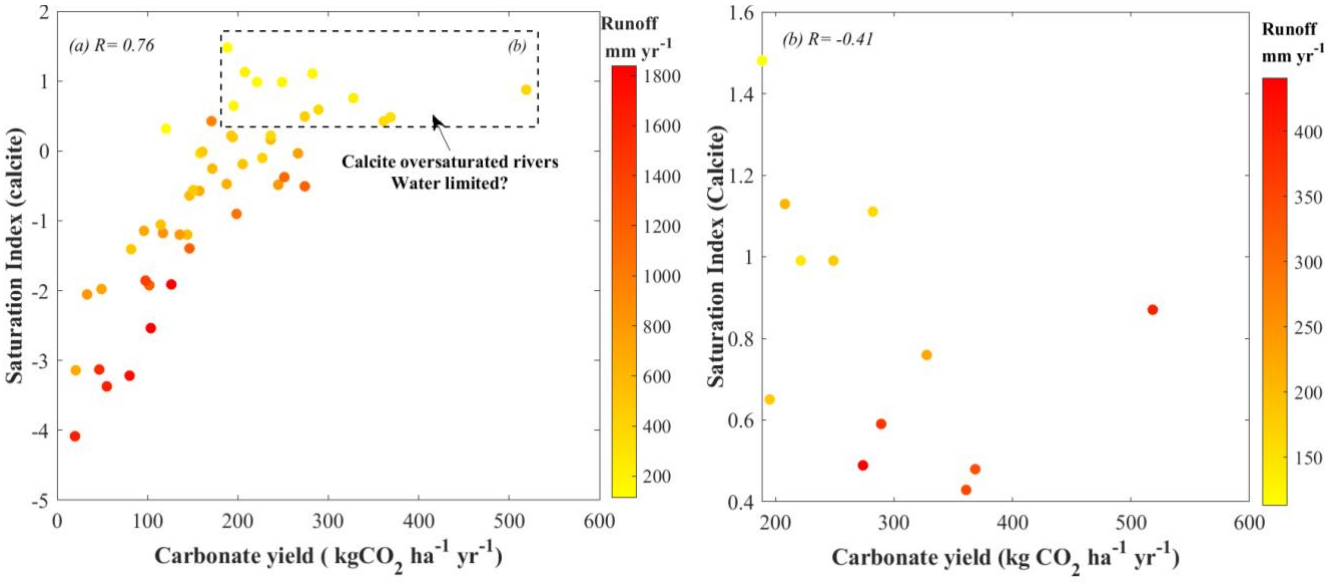

Figure 6.5- The relationship between saturation index in UK rivers and the CO_2 yield due to carbonate weathering. 5(a) is the trend seen in all UK rivers. The highlighted area in Figure 6.5(a) is shown in Figure 6.5(b). In general, 6.5 (a) shows that carbonate yield increases with saturation index until ~SI= 0.4, then any further increase in saturation index tends to drive lower yields. 5(b) shows this negative relationship in the calcite oversaturated rivers. For catchments of similar saturation indexes, increasing the runoff increases yield, suggesting water availability/ runoff does play a role in increasing carbonate yields in UK catchments.

To assess the influence of runoff and water availability on silicate weathering, exploring the relationship between the proportion of major cations (Ca^{2+}, Mg^{2+}, and Na^{+}) from silicates (X_{sil}) and water availability presents an alternative to silicate yield. Previous research has indicated that X_{sil} has been shown to rise with decreased flow rates and prolonged fluid residence times within a catchment (Tipper *et al.*, 2006). Correlating catchment attributes with X_{sil} does not reveal any significant link between annual runoff (mm yr^{-1}), average flow rate (m^3 s^{-1},

Appendices, Figure E.2) and X_{sil}. This implies that at national scale, runoff is not a primary factor of silicate weathering. However, at individual catchment level, temporal variations in X_{sil} occur. Consequently, runoff could play a role in driving temporal variations at a seasonal and sub-catchment level.

The X_{sil} variations at individual catchment level exhibits seasonality. This presents as higher X_{sil} in the summer months, and higher X_{carb} in the winter months (i.e., as shown for a subset of catchments in Figure 6.6), and for 84% of the catchments within the study, the average fraction of solutes from silicates is greater in summer months (i.e. June, July, August, $X_{sil(JJA)}$) than the yearly average ($X_{sil(annual)}$, and i.e. $X_{sil(JJA)} > X_{sil(annual)}$). As such, in Chapter 3, seasonal patterns in X_{sil} and X_{carb} were observed in the Severn and Thames catchments (i.e. Figure 3.7, Chapter 3).

This fluctuation in seasonal X_{sil} may be attributed to temporal temperature changes. Higher X_{sil} in summer months aligns with the established strong positive relationship between temperature and silicate weathering rates (Palandri and Kharaka, 2004). Yet, certain catchments exhibit a more pronounced rise in X_{sil} in summer than others (Figure 6.6). Given the relatively minor (average 1.4 ^{o}C) spatial temperature variations across the UK, it is unlikely that temperature alone explains the variations in the intensity of the summer X_{sil} peaks of Figure 6.6. This interpretation is confirmed by the fact that catchments near to each other, such as the Tweed and Wear (Figure 6.6), have varying peaks in X_{sil} . Therefore, it is likely that other factors, such as lithology and water availability, significantly contribute to these variations.

There are strong negative relationships between the average monthly X_{sil} and average monthly runoff (mm month^{-1}) for some catchments, and therefore some of this seasonal variation is likely, at least in part, due to water availability (Figure 6.7). This trend is clearer for some catchments than others. Some catchments (e.g. Ribble, Lee, Wear, Arun and Trent) show strong negative relationships between average monthly X_{sil} and average monthly runoff (Table 6.2). For these catchments (Termed 'X_{sil} hydrologically influenced' in Table 6.2), water fluctuations appear to influence silicate weathering. In contrast the Tweed, Forth, Ely Ouse, Tay and Tamar catchments lack a relationship between X_{sil} and runoff, indicating that water availability plays a less significant role in regulating silicate weathering in these areas ('non- hydrologically influenced' catchments in Table 6.2).

It is unclear why some catchments have these stronger relationships between silicate weathering and water flow variations. It may simply be that in these 'hydrologically influenced silicate weathering' catchments (a selection of which are given in Table 6.2), other optimal environmental conditions may support silicate weathering, such that specific water conditions stand as the last requirement for reactions to proceed. These 'Hydrologically influenced' catchments have median X_{sil} at least double the average for the catchments in the study and are located within geologically silicate rich areas (i.e. see Chapter 4, Figure 4.2). The lithology within three of the catchments in Table 6.2 is highly permeable- facilitating prolonged water residence times (discussed further in the section below). They typically have lower than average rainfall and runoff (Table 6.2). Additionally, there are large variations in flow rates throughout the year which, combined with other parameters, may attribute to the high seasonality.

In contrast, catchments with no hydrological influence may be less favourable for silicate weathering. Firstly, the Ely Ouse catchment lies within a highly chalk- rich region, making it highly permeable but likely lacking significant silicate lithologies. The Tamar catchment underlies mainly impermeable lithology, and its elevated topographic terrain may hinder water retention within the catchment- even during lower flow conditions. In the case of the Tay and Forth catchments, their exceptionally high runoff and rainfall levels is likely to maintain water availability at a consistently elevated level, potentially limiting the significant influence of water availability on silicate weathering.

In summary, based on the findings presented here, it is evident that whilst water availability may not dictate a catchment's overall X_{sil} or silicate yield, it may help play a role, alongside temperature, in influencing the seasonal variability observed within certain UK catchments.

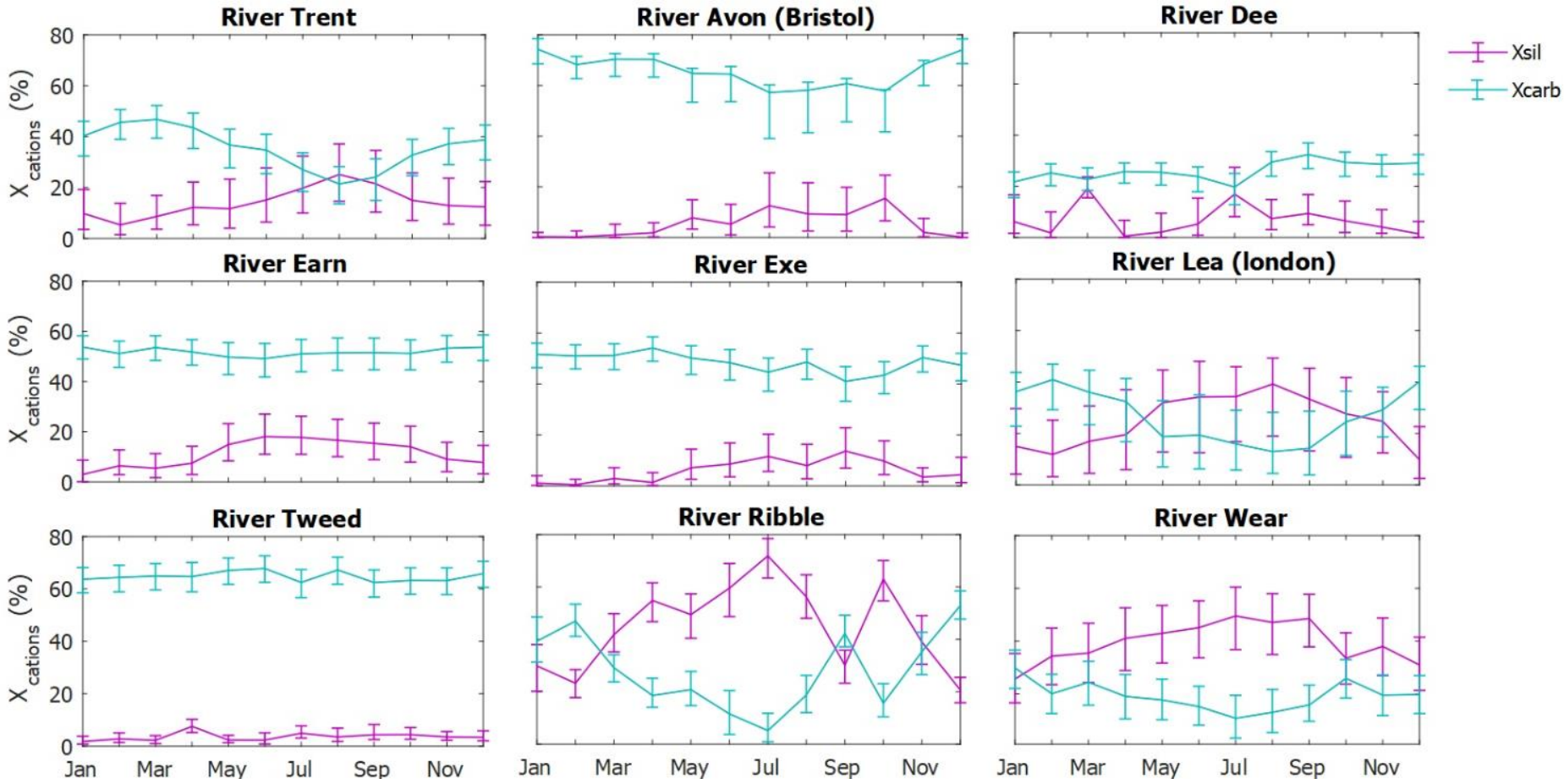

Figure 6.6- Seasonal trend in the portion of solutes from silicates (X_{sil}) and carbonates (X_{carb}) for a selection of UK river. (X_{sil}) and (X_{carb}) were calculated based on the inversion results from Chapter 4 for each datapoint. For each river, data was then collated into months, and the average (X_{sil}) and (X_{carb}) for each month was taken. In the majority of UK catchments, X_{sil} increases in summer months compared to carbonates, however the extent of this variation is heterogeneous across catchments: in rivers such as the River Ribble, large variations are observed, whilst the River Tweed sees comparatively minor seasonal variations.

*Table 6.2- Example catchments split into two groups. In the first group of catchments, termed 'hydrologically influenced' catchments in the table, the variations in X_{sil} appear to be influenced by variations in hydrology. In the second group of catchments, termed 'non- hydrologically influenced', there is no discernible relationship between X_{sil} and hydrology in the table, and other parameters must have a greater influence on silicate weathering. Catchment parameters are compared to the average for the catchments within the study. *Variability in flow rate is the 5-95 percentile range in flow rate over the sampling period for each catchment ($m^3 s^{-1}$). $\boldsymbol{X_{sil-JJA}}$ is the average X_{sil} for summer months, and therefore the ratio $\frac{X_{sil-JJA}}{X_{sil}}$ refers to the seasonal variability in X_{sil} within a catchment. The higher the value, the greater seasonal variability.*

X_{sil} variation	Catchment	X_{sil} (%)	Runoff (mm yr^{-1})	Rainfall (mm yr^{-1})	Variation in flow rate* ($m^3 s^{-1}$)	Permeability (%)	Elevation 50 percentile	SSY (kg ha^{-1} yr^{-1})	$X_{sil-JJA}/X_{sil}$
Hydrologically influenced catchments	Lee	26	130	639	3-17	54	89	130	1.44
	Wear	44	470	884	3-53	44	213	192	1.20
	Trent	14	348	756	27-248	14	636	157	1.42
	Arun	24	467	825	0.3-25	4	55	203	1.54
	Ribble	14	950	1370	1-58	0.63	197	321	1.40
Non-hydrologically influenced	Ely Ouse	0.53	143	603	3-44	80	34	125	0.90
	Tamar	0.01	789	1253	2-67	0	580	322	1.95
	Forth	15	1410	1855	3-112	3.2	181	225	1.40
	Tay	11	1187	1483	50-433	0	395	91	1.30
	Tweed	3	588	1004	12-165	19	255	92	1.0

Average of the catchments in the study	**7**	**717**	**1132**		**19**	**186**	**125**	**1.38**

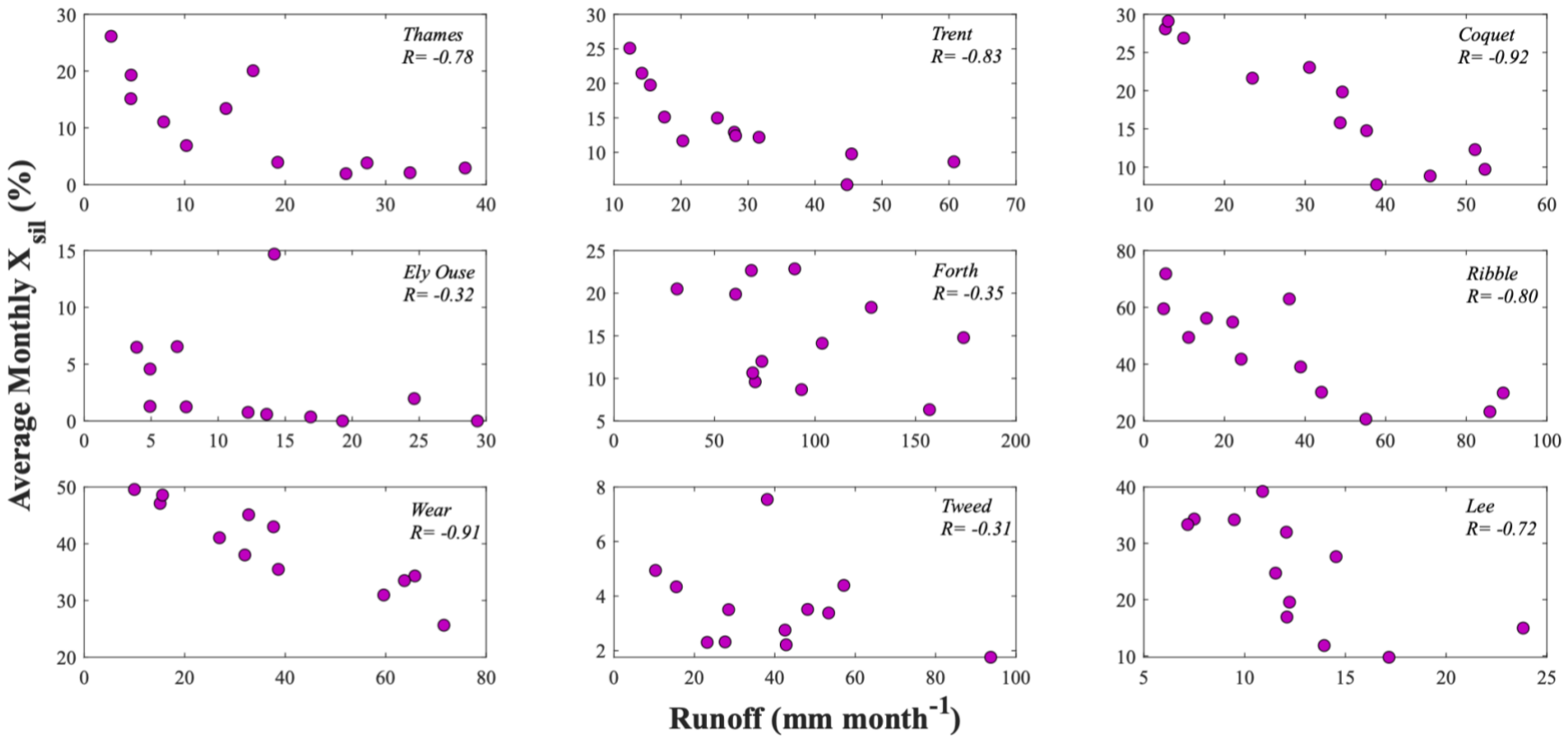

Figure 6.7- Average monthly X_{sil} vs average monthly runoff for a few select catchments. Plot highlights that some rivers (Trent, Ribble, Coquest, Thames, and Wear) have a strong negative correlation between Average monthly X_{sil} vs average monthly runoff, while others (Ely Ouse, Forth, and Tweed) do not have the same trend . (T-tests for these catchments are >0.05 and therefore statistically significant).

6.3.2.2 Permeability

The development of fractures within highly permeable lithologies can enhance water movement through bedrock, and in this way permeability can drive faster dissolution rates by increasing the contact time between minerals and water (Worthington *et al.*, 2016). Indeed, carbonate weathering yields in the UK increase as a function of bedrock permeability (Figure 6.3a), which aligns with this current consensus of how permeability enhances weathering. In contrast, there is no similar relationship between silicate yield and permeability within a catchment (Figure 6.3c), or X_{sil} and permeability (Appendix, Figure 6.9b). This suggests that permeability could serve as good indicator for optimal areas for carbonate weathering, but not silicate weathering, in the UK.

However, the role of permeability in driving the variation in carbonate weathering CO_2 yields across the UK is unclear. Permeability is a function of the mineralogy and lithology, and the rapid dissolution kinetics of carbonate minerals can contribute to increased bedrock permeability (Worthington *et al.*, 2016). Catchments with a greater proportion of carbonate lithologies are therefore expected to exhibit greater permeability, and this feature is observed in UK catchments, particularly towards the southeast (Appendices for Chapter 4, Table C.1). Therefore, the positive relationship between permeability and carbonate CO_2 yield, as seen in (Figure 6.3a), could simply reflect the primary underlying lithological control (i.e., the increased carbonate content) on both these parameters, rather than the direct influence of permeability on yields.

Permeability may not play a leading role in the variation in silicate weathering seen across the UK but, given that water residence times and permeability are interconnected, increased permeability may be associated with more pronounced seasonal variations in X_{sil} in some catchments. During summer, rivers with groundwater sources tend to receive a higher proportion of their overall water from baseflow, whilst in winter months will receive more from direct surficial runoff (Fortner *et al.*, 2012). In particular, previous research has revealed that groundwater flow is important in recharging southeastern UK rivers in summer months (Neal, 2002). This observation may explain why in Chapter 3, a greater seasonal X_{sil} variation was observed in the Thames than the Severn. Examining the relationship between permeability and

the extent of seasonal variability in X_{sil} could therefore be informative in identifying catchments where permeability contributes to enhanced natural silicate weathering.

As introduced in the previous section, the average X_{sil} is typically higher during summer months (June, July and August, termed $X_{sil-JJA}$), and exceeds the total average X_{sil} for 84% of the catchments. The ratio between these two variables ($X_{sil-JJA}/X_{sil}$) describes the extent of seasonal variation within catchments, with a higher ratio indicating greater seasonal variation in X_{sil}. At national scale, there is no correlation between catchments with high seasonal variation and permeability, or silicate yield (Appendices, Figure E.1). This can likely be attributed to the fact that many highly permeable UK catchments primarily consist of carbonate lithologies and have limited silicate content. Consequently, many of the highly permeable UK catchments are unlikely to display substantial variations in X_{sil} due to the minimal occurrence of silicate weathering (such as in the Ely Ouse catchment, Table 6.2). It is likely that permeability only plays an importance in the seasonal variations in X_{sil} when a catchment has enough silicate minerals for substantial reactions to proceed, and the role of water is important in driving reactions (such as in the Thames).

6.3.2.3 Erosion

Weathering rates can be enhanced, or limited, by the supply of minerals through erosional processes. At low erosion rates, silicate weathering can be limited by mineral supply, and therefore increasing erosion may increase weathering rates (West *et al.*, 2005; Brantley *et al.*, 2023). However, the slow kinetics of silicate weathering means that at higher erosion rates, silicate weathering rates do not increase and may even decrease (Bufe *et al.*, 2021). As kinetic limitations are less of a barrier for carbonates, weathering yields often increase with increased erosion (Bufe *et al.*, 2021).

Suspended sediment yield (SSY) can be utilized as a proxy for erosion to assess the influence of erosion on variations in weathering yields across the UK. If erosional processes exerted a first order control over carbonate weathering CO_2 yields, it might be expected that a positive correlation exists between the carbonate weathering yield and SSY across the UK. There are no significant trends between SSY and both carbonate and silicate yield at national scale (Figure 6.8a). This suggests that erosion may not be the primary driver of weathering in the UK. However, erosion may be important for certain UK catchments in which carbonate yields

are primarily limited by mineral supply. For example, for catchments with high runoff (i.e. >1000mm, see Appendices for Chapter 4, Table C.1) carbonate yields generally increase with suspended sediment (i.e., Figure 6.8b). These catchments are typically located in northwestern zones with low carbonate content, and here, the exposure of fresh mineral surfaces by erosional processes is necessary to increase the carbonate yield of a catchment. In the remaining catchments (i.e., runoff <1000 mm yr^{-1}), this relationship is not observed, suggesting other parameters (i.e. lithology, water availability, see respective sections) exert a greater control over carbonate weathering yields.

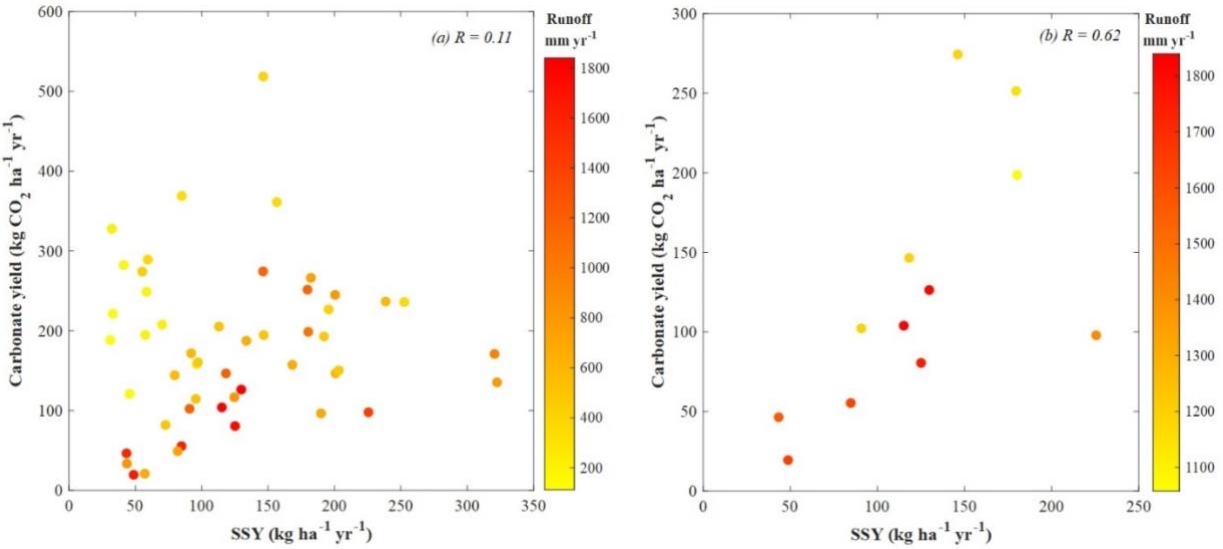

Figure 6.8 (a) Catchment scale annual carbonate derived CO_2 yield vs suspended sediment yield. Suspended sediment data is taken from the Harmonised Monitoring Scheme dataset used within Chapter 3 and 4 (DEFRA, 2013). *Note the lack of correlation (R= 0.11) between carbonate yield and SSY for the catchments in general. Figure 6.8(b) shows SSY and carbonate yield for rivers with high runoff. For these rivers, a medium strength positive relationship (R= 0.62) exists between carbonate yield and SSY (b). These areas are typically have limited carbonate lithology, and this positive relationship may suggest an erosional control to weathering fluxes in these catchments, possibly due to a lack of mineral supply and abundant water supply.*

When assessing at national level, there is no clear relationship between SSY and silicate weathering CO_2 yields (Figure 6.9a). This is unsurprising, given the more complicated impact of erosion on silicate weathering as highlighted above. It might be expected instead that (i) at lower SSY, increasing SSY increases the silicate weathering yield and (ii) at higher SSY, increasing SSY reduces silicate weathering yield. At low erosion rates, defined here as the top ten catchments with the least suspended sediment transfer (SSY < 57 kg ha^{-1} yr^{-1}), there is no relationship between increasing SSY and silicate yields (Figure 6.9b). However, at higher erosion rates, defined as the top ten catchments with the most suspended sediment (SSY > 190

kg ha^{-1} yr^{-1}), there is a weak negative correlation between increasing the SSY and silicate yield. This suggests that low erosion rates may not hinder silicate weathering in the UK, however high erosion rates do.

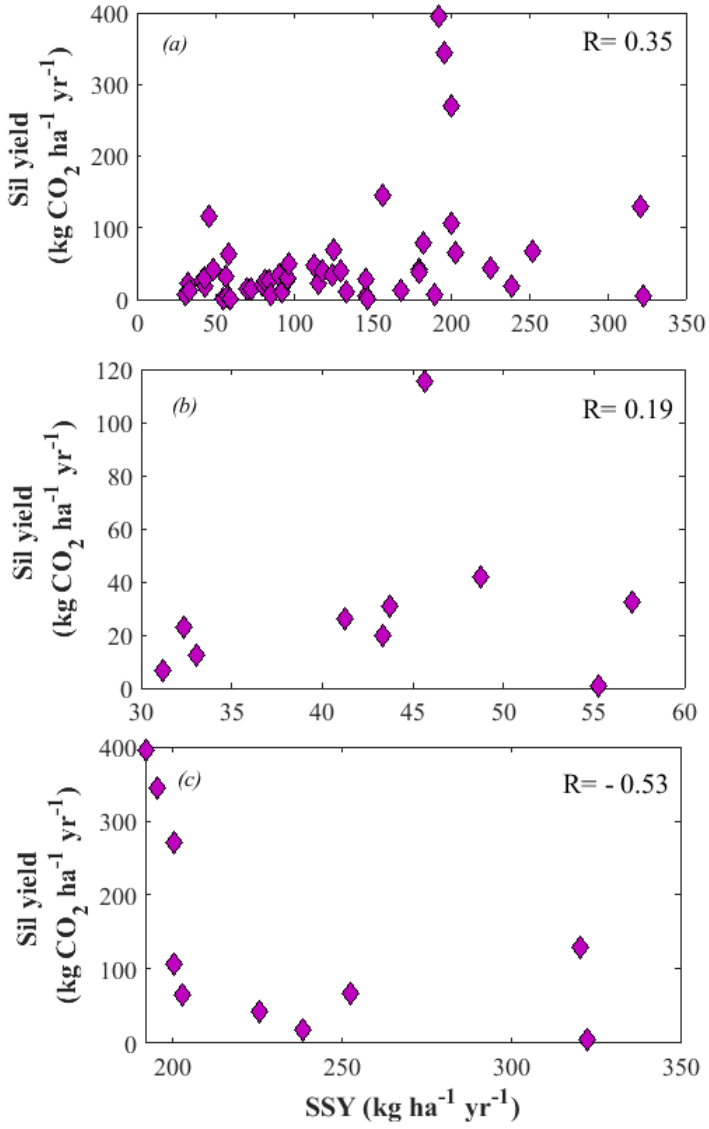

Figure 6.9- No correlation exists between (a) the suspended sediment yield and the silicate yield when assessing all the studied catchments together. (b) 10 catchments with the least suspended sediment yield- plot of the SSY vs silicate yield shows no correlation. (c) The top 10 catchments with the most suspended sediment yield. A weak negative relationship between silicate yield and SSY suggests possibility that high erosion rates decrease silicate yield in certain UK catchments.

6.3.3 Impacts of Anthropogenic land use on UK weathering rates

While it is anticipated that land use exerts an influence on weathering rates within a catchment, the extensive and long-term modification of land in the UK makes it challenging to obtain direct evidence to quantify the specific impact of these modifications. For example, land utilized for agricultural practises varies significantly across the UK (See Chapter 4, Figure 4.4), and therefore relationships between the proportion of arable land within a catchment and its carbonate or silicate CO_2 yields might be expected if this variation were to influence weathering patterns. Statistical analysis demonstrates a positive relationship between the proportion of arable land and the carbonate yield (Figure 6.3a), but no relationship with silicate yield (Figure 6.3c). However, this finding alone does not establish a conclusive link between arable land and carbonate weathering. This is because in the UK, the percentage of arable land increases towards the southeast and towards regions rich in carbonate lithology. These carbonate rich regions present ideal locations for crop growth, as they supply more HCO_3^-/CO_3^{2-} ions, promoting healthy soils by neutralising acidification and inhibiting heavy metal uptake in plants (Wang *et al.*, 2015). Therefore, the specific role of arable land management on carbonate weathering is obscured by co-variation between lithology, land use, and carbonate yield.

Nevertheless, alternative parameters may prove useful when assessing the influence of arable land on weathering CO_2 yields, such as: (i) the variation in erosion with arable land, (ii) the potential alterations in riverine chemistry in response to variations in liming practices in the UK, and (iii) temporal relationships between riverine nitrate concentrations (as a proxy for fertiliser use) and weathering yields within catchments with high arable land.

(i) Land use and erosion

To assess the impact of land-use induced erosion on weathering yields, it is first essential to determine if agricultural practices drive erosion. Erosion may vary across the UK due to multiple factors, including arable land use, as well as variations in runoff and topography (Walling and Webb, 1996; Walling, 1999). Utilizing suspended sediment yield (SSY) again as

a proxy for erosion, the relationship between SSY and arable land, runoff and elevation are assessed.

At a national level, there is a weak negative correlation between arable land and SSY (Figure 6.10a), but no correlations between SSY and maximum elevation (Figure 6.10b) or runoff (Figure 6.10c). This suggests that (i) arable land has limited impact on SSY at national level and, if anything, more arable land corresponds to less erosion, and (ii) multiple factors must be driving SSY variations in the UK simultaneously.

In the UK, arable land increases in low- lying regions (See Chapter 4, Figure 4.3), leading to a strong negative correlation between maximum elevation and arable land (R= -0.84). Therefore, trends between parameters within the 15 lowest-lying catchments (defined as those with maximum elevations < 330m) are considered independently. For these catchments, there is a strong negative correlation between SSY and arable land (Figure 6.10d), while SSY is positively correlated with maximum elevation (Figure 6.10e) and runoff (Figure 6.10f). This suggests that for the low-lying arable catchments, SSY is more likely to be influenced by topography and runoff variations rather than agricultural land use.

Comparing the trends observed in the low-lying catchments to those in highland regions reveals potential differences in the main drivers of erosion in each region. For the 15 most highland catchments (defined here as those with maximum elevations > 850m), there are no correlations between SSY and arable land (Figure 6.10g), or runoff (Figure 6.10i). Furthermore, there is a strong negative correlation between SSY and elevation (Figure 6.10h) which is surprising, given our understanding of the link between increased topography and erosion (Jacobson and Blum, 2003). These results suggest that there could be an additional factor other than runoff and erosion- potentially the erodibility of the bedrock- driving erosional variability in the highlands.

These findings indicate that arable land has a limited impact on SSY in the UK. However, it is possible that such erosion may have played a more important role in the past, particularly during the initial transformation of land from the natural forested state. Additionally, findings show that runoff may be less important in increasing erosion in the highlands compared the lowlands. This is logical, given that the lowland catchments are often water limited, while the highlands catchments are not. Whilst outside the scope of this research, investigating the erosional drivers in highland catchments could yield valuable insights.

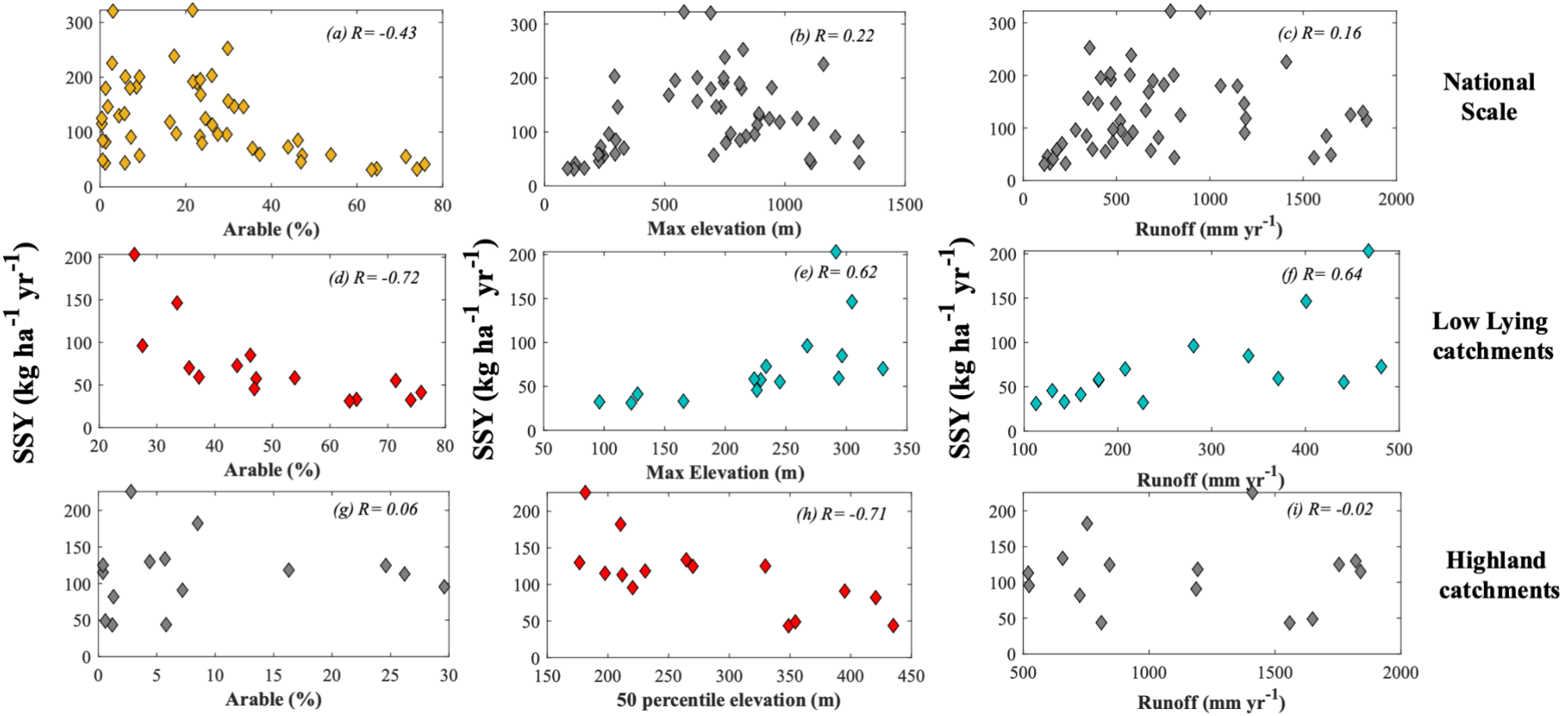

Figure 6.10- Investigating the potential causes of high sediment yield in UK rivers to discover whether arable land may impact erosion. Colours indicate positive (green), negative (red), weak negative (orange) or no (grey) trend. Figures (a- c) represent the relationship between suspended sediment and (a) the percentage of arable land in a catchment, (b) the maximum elevation (metres above sea level) and (c) the average annual runoff (mm yr-1) for the whole 52 catchments studied in Chapter 4. Figures (d-f) are a sub-set of the 15 most low- lying catchments (defined as those with a maximum elevation no greater than 330 m. Figures (g-i) represent the same trends for the top 15 highland catchments (defined here as those with a maximum elevation of greater than 850m.

(ii) Liming impacts on river chemistry

The dissolution of the lime (Agri-lime, $CaCO_3$) applied to fields can increase the supply of DIC and Ca^{2+} to rivers. In 2020, 6.4% of all UK tilled crops and grassland was supplied with $CaCO_3$ (equating to approximately 0.70 Mha, using areas given in Defra, 2022), at an average spreading rate of 4 t ha^{-1} (i.e. Defra, 2022). This equates to 2.78 Mt of $CaCO_3$ applied to UK soils per year (1.1 Mt Ca yr^{-1}). If some of the Ca^{2+} from Agri-lime were to be added to rivers and balanced with DIC (as HCO_3^-), a portion of the estimated annual flux of DIC transported by UK rivers (~8.4 Mt CO_2 yr^{-1}, see Table 4.2 in Chapter 4) may originate from the dissolution of added $CaCO_3$ rather than from weathering of existing soils or bedrock. In a hypothetical maximum scenario where all Ca^{2+} from lime entered rivers (1.1 Mt Ca yr^{-1}) and is entirely balanced by HCO_3^-, then a maximum 2.2 Mt DIC yr^{-1} in rivers may originate from lime rather than natural sources: 26% of the total DIC transported by rivers.

The presence of Ca^{2+} from lime may introduce inaccuracies in the MEANDIR inversion method utilised in Chapters 3 and 4. This occurs because the method will attribute the Ca^{2+} to weathering instead of recognising its origin from lime. The challenge arises because lime exhibits chemical ratios close to carbonates, preventing the inclusion of a distinct agri-lime endmember in the inversion process. Consequently, the methods employed in this thesis do not allow for distinguishing the river chemistry derived from these two sources.

There is some initial evidence to suggest that the CDR calculated in Chapter 4 from carbonates is predominately sourced from the weathering of natural carbonates rather than from lime. Firstly, the observed lithological control on carbonate yield and the positive relationship with percentage arable land means that many of the top yielding catchments are unlikely to be limed (Figure 6.4a, and see Geology of the UK, Figure 4.2, Chapter 4). Secondly, there was a significant decline in lime production and application to UK soils in the UK from 1995, which did not lead to corresponding decreases to the calculated flux of riverine Ca from carbonates in any of the top yielding catchments (Figure 6.11). Diverse lithologies exist in the catchments within Figure 6.11, with varying carbonate content and potential for liming. Despite this, no corresponding decrease occurred, indicating that broadly river chemistry may not have been significant modified following the decline in liming in 1995.

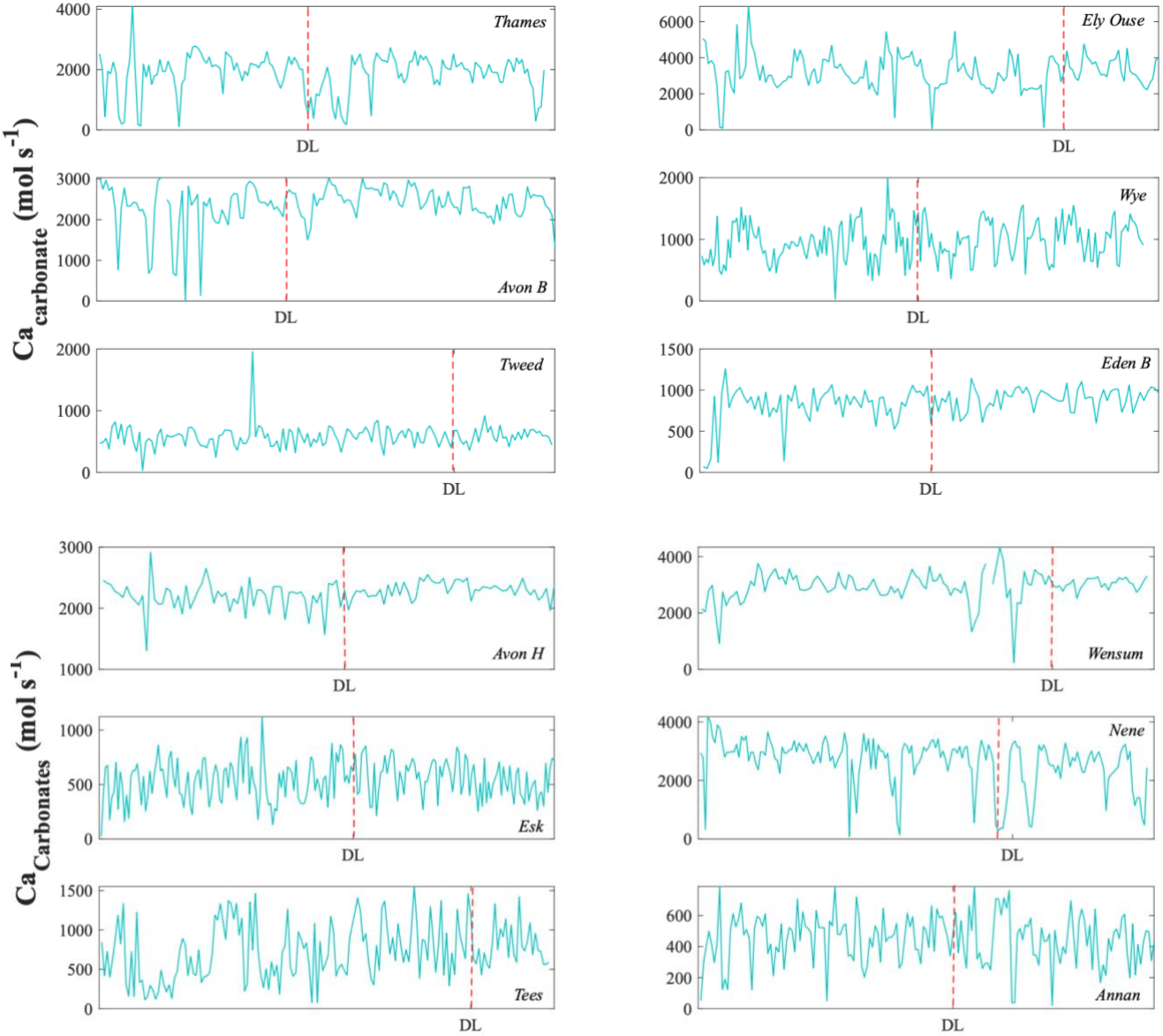

Figure 6.11- Meandir calculated flux weighted Ca^{2+} from carbonates (mol s^{-1}) in a subsection of UK rivers with highest carbonate flux. All the rivers within this study had different starting dates for sampling, and the annual quantity of samples collected was variable- with some rivers having extensive records while others had fewer. Therefore, rather than time, the x-axis for each of these graphs represents individual sampling dates arranged chronologically. DL= Decreased Lime (production) in the UK, which decreased by ~1.5 Mt CaO in 1995. DL is marked on each of the sub-plots as the first sampling date after 01/01/1996. All data points to the right of this line are therefore taken after the decreased lime addition to soils.

Therefore, while the direct quantification of the amount of lime in UK rivers remains challenging, the evidence presented above suggests a minimal impact of lime on the CDR calculated in this study. Nevertheless, further research to validate this evidence is warranted to ensure that the calculated CDR genuinely represents that derived from natural carbonate weathering rather than liming.

(iii) Fertilizer impacts on increasing weathering fluxes

Assessing the top ten catchments with the highest arable land use reveal that there are positive correlations between NO_3^- concentrations and the concentration of cations from carbonates in some catchments (Ely Ouse, Hull, Welland, Appendices, Figure E5). However, in other catchments this correlation is less convincing (Stour, Chelmer, Ugie), whilst others exhibit no correlation (Wensum, Test, Lee). These findings suggest that (i) the impact of fertilizers on weathering may vary considerably across the UK and (ii) future research aiming to assess this further may be more suitable in regions where the correlation between NO_3^- and cations from weathering are strongest.

6.3.4 Summary of main drivers for silicate and carbonate weathering

Deciphering the main drivers of weathering processes at a national scale poses challenges due to the influence of multiple drivers, with varying degrees of importance across different zones of the UK. This study suggests that it is more informative to study UK weathering at individual catchment level to understand reasons for variations in weathering yields within specific catchment zones.

Carbonate weathering in the UK primarily exhibits a lithological control, with weathering yields increasing towards the southeastern carbonate rich catchments. However, certain southeastern catchments may experience calcite saturation index constraints to weathering, caused by water supply. In these catchments, carbonate weathering may be promoted by increasing runoff. Conversely, in some highland Scottish catchments, carbonate weathering may be constrained by mineral supply. These regions have less carbonates and may rely on erosional processes to generate reactive mineral surfaces. Additionally, UK carbonate yields are strongly correlated to the percentage of arable land. This trend tends to co-vary with the lithology and unpicking the contribution of arable land to carbonate weathering is difficult using the available information. Among the assessed arable land processes, the addition of fertiliser induced acid exhibits the highest potential to drive weathering in catchments characterised by high arable land percentages.

Silicate weathering in the UK also seems to be influenced by lithology, although this influence is less apparent compared to that for carbonate weathering. Seasonal variations in X_{sil} imply the presence of an additional, significant driver apart from lithology. This is likely water availability, given that there are strong relationships with average monthly X_{sil} and average monthly runoff in some catchments. The influence of other environmental factors, such as permeability or arable land, is difficult to unpick at national scale, but may have some impact at the catchment level. These other environmental drivers may work to increase the importance of water supply variations in catchments which have strong relationships between runoff and X_{sil}. Lastly, within certain catchments characterised by high erosion, erosion may decrease silicate yields.

6.4 What are the best UK locations for the adoption of EW?

Ideally, the best locations for implementing enhanced rock weathering are those characterised by elevated natural weathering rates, coupled with river waters exhibiting low natural calcite saturation indices. Water plays a pivotal role: catchments should not be water limited, but without an excess in runoff that could impede the silicate weathering reactions or prematurely wash away the undissolved basalt.

6.4.1 Southeastern catchments: Ely Ouse, Welland, Hull, Nene, Test, Stour, Arun, Avon (Bath), Avon (Hampshire), Chelmer

These catchments, characterised by high natural CDR yields (from carbonates), owe this productivity to their carbonate- rich lithologies. With limited natural silicates, their CDR potential from silicate weathering is low. Despite their high CDR productivity, they may not be the optimal choice for EW due to their elevated $SI_{calcite}$ (Table 6.3). Section 6.3.2.1 reveals that these high $SI_{calcite}$ may impose water limitations, suppressing natural weathering rates. Additionally, in Chapter 5 it was observed that due to these high $SI_{calcite}$, if basalt were to be applied to the arable land within the catchment and fully dissolved and transported to the river, a significant proportion of the ERW generated alkalinity would precipitate as $CaCO_3$ (Table 6.3).

Carbon dioxide removal via EW will still occur with carbonate precipitation, albeit less so. In the event of EW implementation in these catchments, it is imperative to exercise careful monitoring of river and soil carbonate precipitation and ensure accurate carbon accounting. Given the substantial arable land in these catchments (for instance, 74% of the Wensum catchment is arable land), it is likely advisable to employ lower spreading rates, targeting only a portion of the available arable land.

6.4.2 Midlands- northeastern catchments: Severn, Trent, Wear, Wharfe, Ouse, Coquet, Tees, Ribble, Mersey, Clyde, Annan, Eden (Kemback)

Chapter 4 findings suggest that the midlands and select northeastern catchments could yield high CDR through natural weathering, often comparable to the southeast (Figure 6.2). Moreover, Chapter 5 indicates that the application of basalt on the arable land in these catchments may lead to less carbonate precipitation than in the southeast (Table 6.3).

These results are closely tied to water availability: these catchments exhibit higher runoff compared to the southeast, although still lower than the average of all catchments studied in Chapter 4 (771 mm yr^{-1}). Consequently, these catchments typically maintain lower average SIs than those in the southeast. Striking a balance, where the natural water supplied to a catchment is sufficient to avoid limiting weathering by carbonate equilibrium, yet not excessive enough to hinder silicate weathering reactions- positions these catchments within an ideal "Goldilocks" zone for optimal natural weathering. Hence, these zones may be ideal for the implementation of EW in the UK.

Therefore, the results of this thesis imply that (i) optimal weathering conditions in these regions may yield significant CDR through EW application, and (ii), the combination of higher runoff and reduced SI means that more basalt could be applied to these catchments, either through higher application rates or the utilisation of more available land (or a mixture of both).

6.4.3 Cornish: Exe, Tamar, Taw; northeastern: Tweed, Tyne; highlands: Don, Tay, Dee

These catchments are significantly undersaturated, indicating their capacity to retain substantial products of EW. Consequently, if EW was to be adopted in these catchments, and

all basalt was to dissolve, the amount of EW derived alkalinity expected to precipitate is low (Table 6.3). This characteristic alone suggests that they may be suitable regions for the adoption of ERW. However, their lower yields per unit area (Figure 6.1), implies that weathering conditions in these catchments are suboptimal. These sub- optimal weathering conditions may impede the weathering reactions of the spread basalt in these catchments.

Additionally, elevated runoff (Table 6.3) introduces the risk that a portion of the basalt applied to these catchments might be washed away before weathering reactions are able to proceed. In contemplating the adoption of EW in these regions, three critical questions to address are: (i) how do we account for this removed portion? (ii) is it significant? and (iii) What is its fate? Should we assume that this portion will dissolve elsewhere, either in the catchment or ocean, and factor it into carbon budgets? If we cannot verify where, or if, this portion dissolves, then it is unlikely that we can include this portion in EW carbon budgets.

Measuring this fraction using established methodologies is challenging yet will be essential for accurate accounting of EW. This is particularly important as new protocols are currently being established to provide transparency in 'Monitoring, Reporting and Verification' in EW to accurately quantify CDR. This ensures that carbon offset companies (currently showing considerable interest in EW) only sell carbon offsets via EW that genuinely reflects the CO_2 removed.

Table 6.3- Comparison of the natural average riverine calcite saturation index (calculated using natural river chemistry from HMS dataset and carbonate equations via PHREEQC. See Chapter 4) for different catchment zones across the UK. HL= Highland, NE= northeastern, C= Cornish. This is compared to the estimated proportion of alkalinity derived from EW (utilising a 20 t ha^{-1} spreading rate and assuming 100% dissolution and complete transfer to the river) expected to precipitate as $CaCO_3$. This is the median calculated using the median pCO_2 in calculations (see Chapter 5 for further information).

	Catchment	Average annual runoff (mm yr^{-1})	Average natural SI(Calc) Chap4	Estimated % of ERW alkalinity precipitated (20 t ha^{-1})
Southeast examples	Ely Ouse	143	0.99	65
	Thames	208	0.80	26
	Wensum	227	0.76	63
	Welland	179	0.65	52
Midlands examples	Severn	356	0.22	7
	Trent	348	0.43	11
	Wear	470	0.22	11
	Ouse	496	0.2	5
	Tees	520	-0.19	10
HL/NE/C examples	Exe	672	-0.57	0
	Tamar	789	-1.2	0
	Taw	695	-1.14	2.6
	Tweed	588	-0.25	1.4
	Tay	1187	-1.92	0
	Don	523	-1.06	0.1

6.5 Future Research Opportunities

Numerous uncertainties remain concerning EW that require resolving before its widespread implementation for CDR in the UK. One of these uncertainties concerns the rate and quantity of transport of EW products from catchments to streams and rivers. This process is likely to be

highly complex and vary according to specific catchment characteristics. Chapter 5 faced data limitations regarding this factor. In the effort to determine the potential precipitation of secondary carbonates in UK rivers resulting from EW application, two scenarios were employed to account for this substantial range of possibilities: from complete transfer of the products of EW to the river, to a severely restricted scenario characterised by minimal catchment weathering due to Si released during dissolution. Ongoing field trials are expected to provide valuable data which could be used to reduce the range of uncertainty in the quantity of possible flux of material to the river. Future work will need to further assess the impact to CDR fluxes, to river chemistry, and to evolution of the soil based on the fate of the products from minerals added to soils for EW.

It was also considered crucial for the overall assessment of the potential CDR via EW in the UK to establish the baseline values for natural weathering in the UK. The values are derived based on a number of assumptions. The first main assumption pertains to the choice of silicate endmember in the MEANDIR inversion, which was employed to estimate the quantity of riverine dissolved solutes originating from silicates. Although the broad range of the silicate endmember used in Chapters 3-4 reflects the degree of uncertainty in this value, reducing the range could reduce the uncertainty in the results and verify the estimates presented here. Considering that endmembers are derived from river chemistry from catchments draining silicate bedrock, the development of a model which was capable of accounting for silicate rock incongruent dissolution, and accurately predicting what river chemistry would look like due to the weathering of typical UK silicate rocks would be advantageous. To achieve this, the availability of a comprehensive database with variations in silicate rock chemistry across the UK would be invaluable.

Additionally, a conclusion drawn in this thesis was that the natural CDR from UK weathering might be substantially reduced by the replacement of carbonic acid for sulphuric acid in weathering reactions. This conclusion was drawn from river sulphate concentrations which were corrected for numerous sources. However, there was one challenging source- determining the fraction of sulphate originating from fertiliser which remained hard to constrain using the methods employed in this thesis. Future studies which could determine this value would aid to refine the overall estimate on reduced CDR resulting from natural weathering in these catchments.

In summary the following would be useful to constrain natural and enhanced CDR in the UK and could be useful topics for future research:

1. A database of the chemical variations of UK silicate rock types
2. A model-based assessment of how this typical UK silicate chemistry may influence river chemistry (and hence silicate endmembers), given typical variations in dissolution rates across silicate minerals (incongruent dissolution)
3. Quantification of the pollutive sulphate in UK rivers
4. Fertilizers (Nitrates) role in facilitating weathering reactions
5. Quantifying the flux of material to rivers from enhanced weathering
6. What happens to Si during EW weathering reactions.

Chapter 7

7 Thesis Conclusions

Enhanced weathering (EW), the application of crushed alkaline silicate rock to agricultural land, shows promise as a method for atmospheric carbon dioxide removal (CDR). However, before it's widespread implementation, it is essential to quantify the CO_2 removed, and account for any potential re-emission of CO_2 during the transportation of EW products from the site of weathering to ocean storage. This thesis seeks to explore two factors within the riverine system crucial for determining this carbon budget: (i) the background CO_2 removal due to natural weathering in the UK and (ii) the potential re-emission resulting from secondary carbonate precipitation in UK rivers.

Geochemical modelling in this study reveals that UK rivers transport up to 6.3 Mt CO_2 yr^{-1} from combined natural silicate and carbonate weathering. Within this total, silicate weathering, vital for long-term carbon removal, contributes up to 1.3 Mt CO_2 yr^{-1}. Normalising the amount of carbon dioxide removed by catchment area reveals significant variability in CDR across the UK, with midlands and southeastern catchments exhibiting the highest natural weathering CO_2 yields. Lithology was thought to be a primary driver to these high weathering rates, however other environmental factors, such as water availability and agricultural land use, may also contribute to enhancing yields in these areas.

These findings suggest that the midlands and southeastern catchments could be optimal locations for enhanced weathering implementation: the favourable environmental conditions for natural weathering may also enhance the reactions of the applied silicates. However, for the southeastern catchments in particular, elevated weathering rates also coincide with high DIC concentrations, leading to rivers exhibiting high calcite saturation indices. This implies that, even without the addition of EW material, the capacity of the rivers within these regions to

transport DIC from weathering is approaching a maximum. I suggest therefore that these rivers would unlikely be able to accommodate the extra flux of material from EW.

The CDR potential expected in some previous literature through widespread adoption of EW in the UK (6-30 $MtCO_2\ yr^{-1}$) exceeds the calculated background weathering derived DIC flux in rivers (6.5 $Mt\ CO_2\ yr^{-1}$). If this anticipated CDR is achieved and uniformly distributed within UK rivers as DIC, the background riverine DIC flux from natural weathering would at least double. However, given the heterogeneous distribution of arable land across the country, an even distribution of DIC flux across UK rivers is unlikely. A primary thesis conclusion is that implementing EW across the UK will yield distinct regional implications for river chemistry, which will mean that some rivers are more likely to be able to accommodate EW products than others. In a scenario that all EW products dissolve at site and enter UK rivers, this study demonstrates that catchments with a high amount of arable land, particularly in the southeast, would experience substantial increases in EW-derived alkalinity, elevating their carbonate saturation indices above the threshold for carbonate precipitation. In contrast, comparatively minor changes would be observed in regions with less available land (such as in Scotland).

I suggest that a standardised 'one size fits all' approach to EW implementation may be unsuitable when contemplating the widespread adoption of EW as a standard CDR method in the UK. In light of these findings, I propose a catchment specific approach, which would involve a meticulous calculation of the potential impact of river chemistry based on the proposed spreading rate and area of arable land. In the UK because much of the arable land occurs in the southeast, it might be that other land types, for instance grassland, may need to be exploited if EW were to achieve the CDR drawdown proposed. This would allow for a more uniform distribution of crushed silicates and potentially mitigate significant alterations in river chemistry resulting from EW material into rivers.

This study offers an assessment of natural weathering in the UK. It sheds light on the potential drivers of weathering, as well as the chemical processes influencing the overall quantity of

atmospheric CO_2 consumed through natural weathering reactions. Additionally, it provides novel scientific perspectives on the practicality of employing EW for CDR in the UK. The findings are valuable for policymakers and future research seeking insights into this area.

References

Amann, T., Hartmann, J., Struyf, E., Garcia, W.D.O., Fischer, E.K. and Janssens, I. (2020) 'Enhanced Weathering and related element fluxes – a cropland mesocosm approach', pp. 103–119.

Barnes, R.T. and Raymond, P.A. (2009) 'The contribution of agricultural and urban activities to inorganic carbon fluxes within temperate watersheds', *Chemical Geology*, 266(3–4), pp. 318–327. Available at: https://doi.org/10.1016/j.chemgeo.2009.06.018.

Beerling, D.J., Kantzas, E.P., Lomas, M.R., Wade, P., Eufrasio, R.M., Renforth, P., Sarkar, B., Andrews, M.G., James, R.H., Pearce, C.R., Mercure, J., Pollitt, H., Holden, P.B. and Edwards, N.R. (2020) 'Potential for large-scale CO 2 removal via enhanced rock weathering with croplands', *Nature*, 583(July). Available at: https://doi.org/10.1038/s41586-020-2448-9.

Beerling, D.J., Leake, J.R., Long, S.P., Scholes, J.D., Ton, J., Nelson, P.N., Bird, M., Kantzas, E., Taylor, L.L., Sarkar, B., Kelland, M., DeLucia, E., Kantola, I., Müller, C., Rau, G.H. and Hansen, J. (2018) 'Farming with crops and rocks to address global climate, food and soil security', *Nature Plants*, 4(6), pp. 392–392. Available at: https://doi.org/10.1038/s41477-018-0162-5.

Bell, V.A., Naden, P.S., Tipping, E., Davies, H.N., Carnell, E., Davies, J.A.C., Dore, A.J., Dragosits, U., Lapworth, D.J., Muhammed, S.E., Quinton, J.N., Stuart, M., Tomlinson, S., Wang, L., Whitmore, A.P. and Wu, L. (2021) 'Long term simulations of macronutrients (C, N and P) in UK freshwaters', *Science of the Total Environment*, 776. Available at: https://doi.org/10.1016/j.scitotenv.2021.145813.

Berner, E. and Berner, R.A. (1996) *Global Environment: Water, Air and Geochemical Cycles*. Prentice Hall, New York.

Berner, R.A., Lasaga, A.C. and Garrels, R.. (1983) 'The carbonate- silicate geochemical cycle and its effect on atmospheric carbon dioxide over the past 100 million years', *American Journal of Science*, 283, pp. 641–683.

BGS (2023a) *BSG Geology 625k Digimap GB*. Available at: https://www.bgs.ac.uk/datasets/bgs-geology-625k (Accessed: 1 October 2021).

BGS (2023b) *Major shales and clays in England and Wales*. Available at: https://www2.bgs.ac.uk/groundwater/shaleGas/aquifersAndShales/maps/shales/home.html (Accessed: 15 June 2023).

BGS (2023c) *The BGS Lexicon of Named Rock Units- Yoredale gp*. Available at: https://webapps.bgs.ac.uk/lexicon/lexicon.cfm?pub=YORE (Accessed: 21 April 2023).

BGS (2023d) *The BGS lexicon of Named Rock Units, Mercia Mudstone*. Available at: https://webapps.bgs.ac.uk/lexicon/lexicon.cfm?pub=MMG (Accessed: 3 June 2023).

Bickle, M.J., Tipper, E., Galy, A., Chapman, H. and Harris, N. (2015) 'On discrimination between carbonate and silicate inputs to Himalayan rivers', *American Journal of Science*, 315(2), pp. 120–166. Available at: https://doi.org/10.2475/02.2015.02.

Bloomfield, J.P., Jackson, C.R. and Stuart, M.E. (2013) 'A climate change report card for water Working Technical Paper 1 . Changes in groundwater levels , temperature and quality in the UK over the 20 th century : an assessment of evidence of impacts from climate change .', pp. 1–14. Available at: http://nora.nerc.ac.uk/503271/).

Bowes, M.J., Armstrong, L.K., Harman, S.A., Wickham, H.D., Nicholls, D.J.E., Scarlett, P.M., Roberts, C., Jarvie, H.P., Old, G.H., Gozzard, E., Bachiller-Jareno, N. and Read, D.S. (2018) 'Weekly water quality monitoring data for the River Thames (UK) and its major tributaries (2009-2013): The Thames Initiative research platform', *Earth System Science Data*, 10(3), pp. 1637–1653. Available at:

https://doi.org/10.5194/essd-10-1637-2018.

Brantley, S.L., Shaughnessy, A., Lebedeva, M.I. and Balashov, V.N. (2023) 'How temperature-dependent silicate weathering acts as Earth's geological thermostat', *Science (New York, N.Y.)*, 379(6630), pp. 382–389. Available at: https://doi.org/10.1126/science.add2922.

Buckingham, F. (2022) *The potential of enhanced weathering as a CO 2 removal technique in UK agricultural soils*.

Buckingham, F., Henderson, G.M., Holdship, P. and Renforth, P. (2022) 'Soil core study indicates limited CO2 removal by enhanced weathering in dry croplands in the UK', *Applied Geochemistry*, 147(October), p. 105482. Available at: https://doi.org/10.1016/j.apgeochem.2022.105482.

Buckingham, F.L., Henderson, G.M. and Renforth, P. (2023) 'Response to Comment from West et al. on, "Soil core study indicates limited CO2 removal by enhanced weathering in dry croplands in the UK"', *Applied Geochemistry*, 152(February). Available at: https://doi.org/10.1016/j.apgeochem.2023.105622.

Bufe, A., Hovius, N., Emberson, R., Rugenstein, J.K.C., Galy, A., Hassenruck-Gudipati, H.J. and Chang, J.M. (2021) 'Co-variation of silicate, carbonate and sulfide weathering drives CO2 release with erosion', *Nature Geoscience*, 14(4), pp. 211–216. Available at: https://doi.org/10.1038/s41561-021-00714-3.

Burke, A., Present, T.M., Paris, G., Rae, E.C.M., Sandilands, B.H., Gaillardet, J., Peucker-Ehrenbrink, B., Fischer, W.W., McClelland, J.W., Spencer, R.G.M., Voss, B.M. and Adkins, J.F. (2018) 'Sulfur isotopes in rivers: Insights into global weathering budgets, pyrite oxidation, and the modern sulfur cycle', *Earth and Planetary Science Letters*, 496, pp. 168–177. Available at: https://doi.org/10.1016/j.epsl.2018.05.022.

Bussi, G., Dadson, S.J., Bowes, M.J. and Whitehead, P.G. (2017) 'Seasonal and Interannual Changes in Sediment Transport Identified through Sediment Rating Curves', *Journal of Hydrologic Engineering*, 22(2), pp. 1–8. Available at: https://doi.org/10.1061/(asce)he.1943-5584.0001466.

Calmels, D. (2007) 'Sustained sulfi de oxidation by physical erosion processes in the Mackenzie River basin : Climatic perspectives', pp. 1003–1006. Available at: https://doi.org/10.1130/G24132A.1.

Campbell, J. *et al.* (2023) 'Measurements in Geochemical Carbon Dioxide Removal', p. 171.

Van Cappellen, P. and Qiu, L. (1997) 'Biogenic silica dissolution in sediments of the Southern Ocean. I. Solubility', *Deep-Sea Research Part II: Topical Studies in Oceanography*, 44(5), pp. 1109–1128. Available at: https://doi.org/10.1016/S0967-0645(96)00113-0.

CCC (2020a) *Land use : Policies for a Net Zero UK*.

CCC (2020b) 'The Sixth Carbon Budget The UK 's path to Net Zero'.

CEH (2014) *Hydrometric areas for Great Britian and Northern Ireland. NERC- Environmental Information Data Centre*. Available at: https://doi.org/10.5285/1957166d-7523-44f4-b279-aa5314163237.

Cerling, T.., Pederson, B.L. and Von Damm, K.L. (1989) 'Sodium-calcium ion exchange in the weathering of shales: Implications for global weathering budgets', *Geology*, 18(2), pp. 190–191. Available at: https://doi.org/10.1130/0091-7613(1990)018<0190:CAROSC>2.3.CO;2.

Chen, B.B., Li, S.L., Pogge von Strandmann, P.A.E., Wilson, D.J., Zhong, J., Sun, J. and Liu, C.Q. (2022) 'Calcium isotopes tracing secondary mineral formation in the high-relief Yalong River Basin, Southeast Tibetan Plateau', *Science of the Total Environment*, 827, p. 154315. Available at: https://doi.org/10.1016/j.scitotenv.2022.154315.

Chetelat, B., Liu, C.Q., Zhao, Z.Q., Wang, Q.L., Li, S.L., Li, J. and Wang, B.L. (2008) 'Geochemistry

of the dissolved load of the Changjiang Basin rivers: Anthropogenic impacts and chemical weathering', *Geochimica et Cosmochimica Acta*, 72(17), pp. 4254–4277. Available at: https://doi.org/10.1016/j.gca.2008.06.013.

Cornelis, J.T., Delvaux, B., Cardinal, D., André, L., Ranger, J. and Opfergelt, S. (2010) 'Tracing mechanisms controlling the release of dissolved silicon in forest soil solutions using Si isotopes and Ge/Si ratios', *Geochimica et Cosmochimica Acta*, 74(14), pp. 3913–3924. Available at: https://doi.org/10.1016/j.gca.2010.04.056.

Das, A.D., Krishnaswami, S., Sarin, M.M. and Pande, K. (2005) 'Chemical weathering in the Krishna Basin and Western Ghats of the Deccan Traps , India ':, 69(8), pp. 2067–2084. Available at: https://doi.org/10.1016/j.gca.2004.10.014.

Defra (2022) *The British Survey of fertilizer practise: Fertilizer Use on Farm Crops for Crop year 2021*.

DEFRA (2013) *Historic UK Water Quality Sampling Harmonised Monitoring Scheme Detailed data*. Available at: https://data.gov.uk/dataset/bda4e065-41e5-4b78-b405-41c1d3606225/historic-uk-water-quality-sampling-harmonised-monitoring-scheme-summary-data (Accessed: 1 August 2022).

DEFRA (2015) *The British Survey of Fertiliser Practise*.

DEFRA (2022a) *Agriculture in the UK Evidence Pack, September 2022 Update*. Available at: https://assets.publishing.service.gov.uk/government/uploads/system/uploads/attachment_data/file/1106562/AUK_Evidence_Pack_2021_Sept22.pdf (Accessed: 30 August 2023).

DEFRA (2022b) *LIDAR Composite 10m DTM 2022*. Available at: https://environment.data.gov.uk/dataset/ce8fe7e7-bed0-4889-8825-19b042e128d2 (Accessed: 1 May 2023).

DEFRA (2022c) *National Statistics Agriculture in the United Kingdom 2021*.

DEFRA (2022d) *Water Quality Archive*. Available at: https://www.nationalarchives.gov.uk/doc/open-government-licence/version/3/ (Accessed: 1 August 2022).

DESNZ (2023) *2022 UK greenhouse gas emissions, provisional figures, National Statistics*.

Dessert, C., Dupré, B., François, L.M., Schott, J., Gaillardet, J., Chakrapani, G. and Bajpai, S. (2001) 'Erosion of Deccan Traps determined by river geochemistry: Impact on the global climate and the 87 Sr/ 86 Sr ratio of seawater', *Earth and Planetary Science Letters*, 188(3–4), pp. 459–474. Available at: https://doi.org/10.1016/S0012-821X(01)00317-X.

Drever, J.I. (1997) *The Geochemistry of Natural Waters- Surface and Groundwater Environments*.

ECN (2015) *UK Environmental Change Network (ECN) precipitation chemistry data: 1992-2015. NERC Environmental Information Data Centre. (Dataset).* Available at: https://doi.org/https://doi.org/10.5285/18b7c387-037d-4949-98bc-e8db5ef4264c.

Environmental Agency (2019) *2021 River Basin Management Plan, Environment Agency*.

Environmental Agency (2021) *Nitrates: Challenges for the water environment*. Available at: https://www.gov.uk/government/publications/nitrate-challenges-for-the-water-environment.

Erlanger, E.D., Rugenstein, J.K.C., Bufe, A., Picotti, V. and Willett, S.D. (2021) 'Controls on Physical and Chemical Denudation in a Mixed Carbonate-Siliciclastic Orogen', *Journal of Geophysical Research: Earth Surface*, 126(8), pp. 1–24. Available at: https://doi.org/10.1029/2021JF006064.

Fohrer, N., Haverkamp, S., Eckhardt, K. and Frede, H.G. (2001) 'Hydrologic response to land use changes on the catchment scale', *Physics and Chemistry of the Earth, Part B: Hydrology, Oceans and Atmosphere*, 26(7–8), pp. 577–582. Available at: https://doi.org/10.1016/S1464-1909(01)00052-1.

Fortner, S.K., Lyons, W.B., Carey, A.E., Shipitalo, M.J., Welch, S.A. and Welch, K.A. (2012) 'Silicate weathering and CO2 consumption within agricultural landscapes, the Ohio-Tennessee River Basin, USA', *Biogeosciences*, 9(3), pp. 941–955. Available at: https://doi.org/10.5194/bg-9-941-2012.

Fretzdorff, S. and Haase, K.M. (2002) 'Geochemistry and petrology of lavas from the submarine flanks of Réunion Island (western Indian Ocean): Implications for magma genesis and the mantle source', *Mineralogy and Petrology*, 75(3–4), pp. 153–184. Available at: https://doi.org/10.1007/s007100200022.

Friedlingstein, P. *et al.* (2022) 'Global Carbon Budget 2022', *Earth System Science Data*, 14(11), pp. 4811–4900. Available at: https://doi.org/10.5194/essd-14-4811-2022.

Fuhr, M., Geilert, S., Schmidt, M., Liebetrau, V., Christoph, V., Ledwig, B. and Wallmann, K. (2021) 'Kinetics of olivine weathering in seawater: an experimental study', *Frontiers in Climate*, 4(March), pp. 1–20. Available at: https://doi.org/10.7185/gold2021.7375.

Fuss, S., Lamb, W.F., Callaghan, M.W., Hilaire, J., Creutzig, F., Amann, T., Beringer, T., De Oliveira Garcia, W., Hartmann, J., Khanna, T., Luderer, G., Nemet, G.F., Rogelj, J., Smith, P., Vicente, J.V., Wilcox, J., Del Mar Zamora Dominguez, M. and Minx, J.C. (2018) 'Negative emissions - Part 2: Costs, potentials and side effects', *Environmental Research Letters*, 13(6), pp. 2016–2050. Available at: https://doi.org/10.1088/1748-9326/aabf9f.

Gaillardet, J., Calmels, D., Romero-Mujalli, G., Zakharova, E. and Hartmann, J. (2019) 'Global climate control on carbonate weathering intensity', *Chemical Geology*, 527(November 2017), p. 118762. Available at: https://doi.org/10.1016/j.chemgeo.2018.05.009.

Gaillardet, J., Dupré, B., Louvat, P. and Allègre, C.J. (1999) 'Global silicate weathering and CO2 consumption rates deduced from the chemistry of large rivers', *Chemical Geology*, 159(1–4), pp. 3–30. Available at: https://doi.org/10.1016/S0009-2541(99)00031-5.

Galy, A. and France-Lanord, C. (2001) 'Higher erosion rates in the Himalaya: Geochemical constraints on riverine fluxes', *Geology*, 29(1), pp. 23–26. Available at: https://doi.org/10.1130/0091-7613(2001)029<0023:HERITH>2.0.CO;2.

Gandois, L., Perrin, A.S. and Probst, A. (2011) 'Impact of nitrogenous fertiliser-induced proton release on cultivated soils with contrasting carbonate contents: A column experiment', *Geochimica et Cosmochimica Acta*, 75(5), pp. 1185–1198. Available at: https://doi.org/10.1016/j.gca.2010.11.025.

Georg, R.B., Reynolds, B.C., West, A.J., Burton, K.W. and Halliday, A.N. (2007) 'Silicon isotope variations accompanying basalt weathering in Iceland', 261, pp. 476–490. Available at: https://doi.org/10.1016/j.epsl.2007.07.004.

Gleeson, T., Befus, K.M., Jasechko, S., Luijendijk, E. and Cardenas, M.B. (2016) 'The global volume and distribution of modern groundwater', *Nature Geoscience*, 9(2), pp. 161–164. Available at: https://doi.org/10.1038/ngeo2590.

Goldich, S. (1938) 'A Study in Rock-Weathering', *The Journal of Geology*, 46(1), pp. 17–58.

Goll, D.S., Ciais, P., Amann, T., Buermann, W., Chang, J., Eker, S., Hartmann, J., Janssens, I., Li, W., Obersteiner, M., Penuelas, J., Tanaka, K. and Vicca, S. (2021) 'Potential CO2 removal from enhanced weathering by ecosystem responses to powdered rock', *Nature Geoscience*, 14(8), pp. 545–549. Available at: https://doi.org/10.1038/s41561-021-00798-x.

Grace, J. (2004) 'Understanding and managing the global carbon cycle', *Journal of Ecology*, 92, pp. 189–202.

Gruber, N. and Galloway, J.N. (2008) 'An Earth-system perspective of the global nitrogen cycle', *Nature*, 451(7176), pp. 293–296. Available at: https://doi.org/10.1038/nature06592.

Hangx, S.J.T. and Spiers, C.J. (2009) 'International Journal of Greenhouse Gas Control Coastal

spreading of olivine to control atmospheric CO 2 concentrations : A critical analysis of viability', 3, pp. 757–767. Available at: https://doi.org/10.1016/j.ijggc.2009.07.001.

Harrington, K.J., Hilton, R.G. and Henderson, G.M. (2023) 'Implications of the Riverine Response to Enhanced Weathering for CO2 removal in the UK', *Applied Geochemistry*, 152(March), p. 105643. Available at: https://doi.org/10.1016/j.apgeochem.2023.105643.

Hartmann, J., Lauerwald, R. and Moosdorf, N. (2019) *GLORICH- Global river chemistry database, PANGAEA*. Available at: https://doi.org/https://doi.org/10.1594/PANGAEA.902360.

Hartmann, J., West, J., Renforth, P., Köhler, P., La De Rocha, C.L., Wolf-Gladrow, D.A., Dürr, H. and Scheffran, J. (2013) 'Enhanced Chemical Weathering as a Geoengineering Strategy to Reduce Atmospheric Carbon Dioxide, a Nutrient Source and to Mitigate Ocean Acidification: (accepted article)', *Philosophical Transactions of the Royal Society*, (2012), pp. 113–150. Available at: https://doi.org/10.1002/rog.20004.

Henderson, P. and Henderson, G.M. (2009) *The Cambridge Handbook of Earth Science Data*.

Henley, R.W. (1983) 'pH and silica scaling control in geothermal field development', *Geothermics*, 12(4), pp. 307–321. Available at: https://doi.org/10.1016/0375-6505(83)90004-4.

Hilton, R.G. and West, A.J. (2020) 'Mountains, erosion and the carbon cycle', *Nature Reviews Earth and Environment*, 1(6), pp. 284–299. Available at: https://doi.org/10.1038/s43017-020-0058-6.

Holland, J.E., Bennett, A.E., Newton, A.C., White, P.J., Mckenzie, B.M., George, T.S., Pakeman, R.J., Bailey, J.S., Fornara, D.A. and Hayes, R.C. (2018) 'Science of the Total Environment Liming impacts on soils , crops and biodiversity in the UK : A review', *Science of the Total Environment*, 610–611, pp. 316–332. Available at: https://doi.org/10.1016/j.scitotenv.2017.08.020.

Howard, A.S., Warrington, G., Ambrose, K. and Rees, J.G. (2008) 'A formational framework for the Mercia Mudstone Group (Triassic) of England and Wales'.

IPCC (2018) 'Summary for Policymakers. In: Global Warming of 1.5°C. An IPCC Special Report on the impacts of global warming of 1.5°C above pre-industrial levels and related global greenhouse gas emission pathways, in the context of strengthening the global response to'.

IPCC (2023) 'Summary for Policy Makers. IN: Climate Change 2023: Synthesis Report. Contribution of Working Groups I, II, and III to the Sixth Assessment Report of the Intergovernmental Panel on Climate Change'. Available at: https://doi.org/10.59327/IPCC/ARC-9789291691647.001.

Jacobson, A.D. and Blum, J.D. (2003) 'Relationship between mechanical erosion and atmospheric CO2 consumption in the New Zealand Southern Alps', *Geology*, 31(10), pp. 865–868. Available at: https://doi.org/10.1130/G19662.1.

Jarvie, H.P., King, S.M. and Neal, C. (2017) 'Inorganic carbon dominates total dissolved carbon concentrations and fluxes in British rivers: Application of the THINCARB model – Thermodynamic modelling of inorganic carbon in freshwaters', *Science of the Total Environment*, 575, pp. 496–512. Available at: https://doi.org/10.1016/j.scitotenv.2016.08.201.

Jones, N. (2023) 'When will global warming actually hit the landmark 1 . 5 ° C limit ?', *Nature*, 618, p. 5.

Jonkers, A.R.T. and Sharkey, K.J. (2016) 'The differential warming response of Britain's rivers (1982-2011)', *PLoS ONE*, 11(11), pp. 1–23. Available at: https://doi.org/10.1371/journal.pone.0166247.

Kantzas, E.P. *et al.* (2022) 'Substantial carbon drawdown potential from enhanced rock weathering in the United Kingdom', *Nature Geoscience*, 15(5), pp. 382–389. Available at: https://doi.org/10.1038/s41561-022-00925-2.

Katz, J.L., Reick, M.R., Herzog, R.E. and Parsiegla, K.I. (1993) 'Calcite Growth Inhibition by Iron',

Langmuir, 9(5), pp. 1423–1430. Available at: https://doi.org/10.1021/la00029a043.

Kay, A.L., Bell, V.A., Blyth, E.M., Crooks, S.M., Davies, H.N. and Reynard, N.S. (2013) 'A hydrological perspective on evaporation: Historical trends and future projections in Britain', *Journal of Water and Climate Change*, 4(3), pp. 193–208. Available at: https://doi.org/10.2166/wcc.2013.014.

Keeping, M.G. (2017) 'Uptake of silicon by sugarcane from applied sources may not reflect plant-available soil silicon and total silicon content of sources', *Frontiers in Plant Science*, 8(May), pp. 1–14. Available at: https://doi.org/10.3389/fpls.2017.00760.

Kelemen, P.B., McQueen, N., Wilcox, J., Renforth, P., Dipple, G. and Vankeuren, A.P. (2020) 'Engineered carbon mineralization in ultramafic rocks for CO2 removal from air: Review and new insights', *Chemical Geology*, 550(May), p. 119628. Available at: https://doi.org/10.1016/j.chemgeo.2020.119628.

Kelland, M.E., Wade, P.W., Lewis, A.L., Taylor, L.L., Sarkar, B., Andrews, M.G., Lomas, M.R., Cotton, T.E.A., Kemp, S.J., James, R.H., Pearce, C.R., Hartley, S.E., Hodson, M.E., Leake, J.R., Banwart, S.A. and Beerling, D.J. (2020) 'Increased yield and CO2 sequestration potential with the C4 cereal Sorghum bicolor cultivated in basaltic rock dust-amended agricultural soil', *Global Change Biology*, 26(6), pp. 3658–3676. Available at: https://doi.org/10.1111/gcb.15089.

Kemeny, P.C., Lopez, G.I., Dalleska, N.F., Torres, M., Burke, A., Bhatt, M.P., West, A.J., Hartmann, J. and Adkins, J.F. (2021) 'Sulfate sulfur isotopes and major ion chemistry reveal that pyrite oxidation counteracts CO2 drawdown from silicate weathering in the Langtang-Trisuli-Narayani River system, Nepal Himalaya', *Geochimica et Cosmochimica Acta*, 294, pp. 43–69. Available at: https://doi.org/10.1016/j.gca.2020.11.009.

Kemeny, P.C. and Torres, M.A. (2021) 'PRESENTATION AND APPLICATIONS OF MIXING ELEMENTS AND DISSOLVED ISOTOPES IN RIVERS (MEANDIR), A CUSTOMIZABLE MATLAB MODEL FOR MONTE CARLO INVERSION OF DISSOLVED RIVER CHEMISTRY', pp. 579–642. Available at: https://doi.org/10.2475/05.2021.03.

Kirchner, J.W., Neal, C. and Robson, A.J. (2004) 'The fine structure of water-quality dynamics : the (high-frequency) wave of the future', 1359(August 2003), pp. 1353–1359. Available at: https://doi.org/10.1002/hyp.5537.

Klemme, A., Rixen, T., Müller, M., Notholt, J. and Warneke, T. (2022) 'Destabilization of carbon in tropical peatlands by enhanced weathering', *Nature communications*, pp. 1–9. Available at: https://doi.org/10.1038/s43247-022-00544-0.

Knapp, W.J. and Tipper, E.T. (2022) 'The efficacy of enhancing carbonate weathering for carbon dioxide sequestration', *Frontiers in Climate* [Preprint]. Available at: https://doi.org/10.3389/fclim.2022.928215.

Köhler, P., Hartmann, J. and Wolf-gladrow, D.A. (2010) 'Geoengineering potential of artificially enhanced silicate weathering of olivine', *Proceedings of the National Academy of Sciences of the United States of America*, 107(47), pp. 20228–20233. Available at: https://doi.org/10.1073/pnas.1000545107.

Lasaga, A.C. (1984) 'Chemical kinetics of water-rock interactions', 89(4), pp. 4009–4025.

Lasaga, A.C. (2018) 'Fundamental approaches in describing mineral dissolution and precipitation rates', *CHEMICAL WEATHERING RATES OF SILICATE MINERALS*, 31, pp. 23–86. Available at: https://doi.org/10.1515/9781501509650-004.

Lasaga, A.C., Soler, J.M., Ganor, J., Burch, T.E. and Nagy, K.L. (1994) 'Chemical weathering rate laws and global geochemical cycles', *Geochimica et Cosmochimica Acta*, 58(10), pp. 2361–2386. Available at: https://doi.org/10.1016/0016-7037(94)90016-7.

Lefebvre, D., Goglio, P., Williams, A., Manning, D.A.C., de Azevedo, A.C., Bergmann, M.,

Meersmans, J. and Smith, P. (2019) ‘Assessing the potential of soil carbonation and enhanced weathering through Life Cycle Assessment: A case study for Sao Paulo State, Brazil’, *Journal of Cleaner Production*, 233, pp. 468–481. Available at: https://doi.org/10.1016/j.jclepro.2019.06.099.

Lezaun, J., Healey, P., Kruger, T. and Smith, S.M. (2021) ‘Governing Carbon Dioxide Removal in the UK: Lessons Learned and Challenges Ahead’, *Frontiers in Climate*, 3(August), pp. 1–5. Available at: https://doi.org/10.3389/fclim.2021.673859.

Lin. Y. and Singer. P. (2005) 'Inhibition of calcite growth, by polyphosphates, *Water Research*, 39, 4835- 4843. Available at: https://doi.org/10.1016/j.watres.2005.10.003.

Louvat, P. and Allègre, C.J. (1997) ‘Present denudation rates on the Island of Reunion determined by river geochemistry: Basalt weathering and mass budget between chemical and mechanical erosions’, *Geochimica et Cosmochimica Acta*, 61(17).

Lupker, M., France-Lanord, C. and Lartiges, B. (2016) ‘Impact of sediment–seawater cation exchange on Himalayan chemical weathering fluxes’, *Earth Surface Dynamics*, 4(3), pp. 675–684. Available at: https://doi.org/10.5194/esurf-4-675-2016.

Maher, K. (2010) ‘The dependence of chemical weathering rates on fluid residence time’, *Earth and Planetary Science Letters*, 294(1–2), pp. 101–110. Available at: https://doi.org/10.1016/j.epsl.2010.03.010.

Maher, K. (2011) ‘The role of fluid residence time and topographic scales in determining chemical fluxes from landscapes’, *Earth and Planetary Science Letters*, 312(1–2), pp. 48–58. Available at: https://doi.org/10.1016/j.epsl.2011.09.040.

Maher, K. and Chamberlain, C.P. (2014) ‘Hydrologic regulation of chemical weathering and the geologic carbon cycle’, *Science*, 343(6178), pp. 1502–1504. Available at: https://doi.org/10.1126/science.1250770.

Manabe, S. and Wetherald, R.T. (1967) ‘Thermal Equilibrium of the Atmosphere with a Given Distribution of Relative Humidity’, *Journal of the Atmospheric Sciences*, pp. 241–259. Available at: https://doi.org/10.1175/1520-0469(1967)024<0241:teotaw>2.0.co;2.

Manning, D.A.C. (2022) ‘Mineral stabilities in soils: how minerals can feed the world and mitigate climate change’, *Clay Minerals*, pp. 1–10. Available at: https://doi.org/10.1180/clm.2022.17.

Marc, V. and Robinson, M. (2007) ‘The long-term water balance (1972-2004) of upland forestry and grassland at Plynlimon, mid-Wales’, *Hydrology and Earth System Sciences*, 11(1), pp. 44–60. Available at: https://doi.org/10.5194/hess-11-44-2007.

Marsh, T., Sanderson, F. and Swain, O. (2015) ‘Derivation of the UK national and regional runoff series’. Available at: http://nora.nerc.ac.uk/id/eprint/510580.

Marston, C., Rowland, C.., O’Neil, A.. and Morton, R.. (2022) *Land Cover Map 2021 (10m classified pixels, GB).*, *NERC EDS Environmental Data Centre*. Available at: https://doi.org/https://doi.org/10.5285/a22baa7c-5809-4a02-87e0-3cf87d4e223a.

MET (2023) *UK temperature, rainfall and sunshine time series*. Available at: https://www.metoffice.gov.uk/research/climate/maps-and-data/uk-temperature-rainfall-and-sunshine-time-series (Accessed: 9 December 2023).

Meybeck, M. (1983) ‘Atmospheric inputs and river transport of dissolved substances.’, *Dissolved loads of rivers and surface water quantity/quality relationships. Proc. Hamburg symposium, 1983*, (141), pp. 173–192.

Meybeck, M. (2003) ‘Global analysis of river systems: From Earth system controls to Anthropocene syndromes’, *Philosophical Transactions of the Royal Society B: Biological Sciences*, 358(1440), pp. 1935–1955. Available at: https://doi.org/10.1098/rstb.2003.1379.

Montserrat, F., Renforth, P., Hartmann, J., Leermakers, M., Knops, P. and Meysman, F.J.R. (2017) 'Olivine Dissolution in Seawater: Implications for CO2 Sequestration through Enhanced Weathering in Coastal Environments', *Environmental Science and Technology*, 51(7), pp. 3960–3972. Available at: https://doi.org/10.1021/acs.est.6b05942.

Moon, S., Chamberlain, C.P. and Hilley, G.E. (2014) 'New estimates of silicate weathering rates and their uncertainties in global rivers', *Geochimica et Cosmochimica Acta*, 134, pp. 257–274. Available at: https://doi.org/10.1016/j.gca.2014.02.033.

Moosdorf, N., Hartmann, J., Du, H.H., Meybeck, M., Kempe, S., Curie, M., Vi, P., Lithological, Á. and Major, Á. (2012) 'The geochemical composition of the terrestrial surface (without soils) and comparison with the upper continental crust', pp. 365–376. Available at: https://doi.org/10.1007/s00531-010-0635-x.

Morris, D.G. and Flavin, R.W. (1990) *A digital Terrain Model for Hydrology*, *4th Symposium on Spatial Data Handling. Zurich*.

Mucci, A. (1983) 'The Solubility of Calcite and Aragonite in Seawater at Various Salinities, temperatures, and one atmosphere total pressure', *American Journal of Science*, 283, pp. 780–799.

Neal, C. (2002) 'Calcite saturation in eastern UK rivers'.

Neal, C., Bowes, M., Jarvie, H.P., Scholefield, P., Leeks, G., Neal, M., Rowland, P., Wickham, H., Harman, S., Armstrong, L., Sleep, D., Lawlor, A. and Davies, C.E. (2012) 'Lowland river water quality: A new UK data resource for process and environmental management analysis', *Hydrological Processes*, 26(6), pp. 949–960. Available at: https://doi.org/10.1002/hyp.8344.

Neal, C., Harrow, M. and Williams, R.J. (1998) 'Dissolved carbon dioxide and oxygen in the River Thames: Spring-summer 1997', *The Science of the Total Environment*, pp. 205–217.

Neal, C., Jarvie, H.P., Neal, M., Hill, L. and Wickham, H. (2006) 'Nitrate concentrations in river waters of the upper Thames and its tributaries', *Science of the Total Environment*, 365(1–3), pp. 15–32. Available at: https://doi.org/10.1016/j.scitotenv.2006.02.031.

Neal, C., Neal, M., Leeks, G.J.L., Old, G., Hill, L. and Wickham, H. (2006) 'Suspended sediment and particulate phosphorus in surface waters of the upper Thames Basin, UK', *Journal of Hydrology*, 330(1–2), pp. 142–154. Available at: https://doi.org/10.1016/j.jhydrol.2006.04.016.

Neal, C., Reynolds, B., Norris, D., Kirchner, J.W., Neal, M., Rowland, P., Wickham, H., Harman, S., Armstrong, L., Sleep, D., Lawlor, A., Woods, C., Williams, B., Fry, M., Newton, G. and Wright, D. (2011) 'Three decades of water quality measurements from the Upper Severn experimental catchments at Plynlimon, Wales: An openly accessible data resource for research, modelling, environmental management and education', *Hydrological Processes*, 25(24), pp. 3818–3830. Available at: https://doi.org/10.1002/hyp.8191.

Negrel, P., Allegre, C.J., Dupre, B. and Lewin, E. (1993) 'Erosion sources determined by inversion of major and trace element ratios and strontium isotopic ratios in river water : The Congo Basin case', 120, pp. 59–76.

Neilsen, M.R., Sand, K.K., Rodriguez- Blanco, J.D., Bovel, N., Generosi, J., Dalby,K.N., Stipp, S.L.S (2016) 'Inhibition of calcite growth: Combined effects of Mg^{2+} and $SO2^{-4'}$, Crystal Growth and Design, 16, 6199- 6207.

Neubauer, E., Köhler, S.J., Von Der Kammer, F., Laudon, H. and Hofmann, T. (2013) 'Effect of pH and stream order on iron and arsenic speciation in boreal catchments', *Environmental Science and Technology*, 47(13), pp. 7120–7128. Available at: https://doi.org/10.1021/es401193j.

Newell, A.J. (2018) 'Rifts, rivers and climate recovery: A new model for the Triassic of England', *Proceedings of the Geologists' Association*, 129(3), pp. 352–371. Available at: https://doi.org/10.1016/j.pgeola.2017.04.001.

Nielsen, M.R., Sand, K.K., Rodriguez-Blanco, J.D., Bovet, N., Generosi, J., Dalby, K.N. and Stipp, S.L.S. (2016) 'Inhibition of Calcite Growth: Combined Effects of Mg2+ and SO42-', *Crystal Growth and Design*, 16(11), pp. 6199–6207. Available at: https://doi.org/10.1021/acs.cgd.6b00536.

NRFA (2023) *https://nrfa.ceh.ac.uk*.

Oh, N. and Raymond, P.A. (2006) 'Contribution of agricultural liming to riverine bicarbonate export and CO 2 sequestration in the Ohio River basin', 20(June 2005), pp. 1–17. Available at: https://doi.org/10.1029/2005GB002565.

Ohrui, K. and Mitchell, M.J. (1999) 'Hydrological ¯ ow paths controlling stream chemistry in Japanese forested watersheds', 888(January 1998), pp. 877–888.

Palandri, J.L. and Kharaka, Y.K. (2004) *A COMPILATION OF RATE PARAMETERS OF WATER-MINERAL INTERACTION KINETICS FOR APPLICATION TO O PEN FILE REPORT 2004-1068 N / A A Compilation of Rate Parameters of Water-Mineral Interaction Kinetics, USGS*.

Parkhurst, D.. and Appelo, C.A.. (2013) 'Description of input and examples for PHREEQC version 3—A computer program for speciation, batch-reaction, one-dimensional transport, and inverse geochemical calculations: U.S. Geological Survey Techniques and Methods'. Available at: https://doi.org/https://doi.org/10.3133/tm6A43.

Perrin, A.S., Probst, A. and Probst, J.L. (2008) 'Impact of nitrogenous fertilizers on carbonate dissolution in small agricultural catchments: Implications for weathering CO2 uptake at regional and global scales', *Geochimica et Cosmochimica Acta*, 72(13), pp. 3105–3123. Available at: https://doi.org/10.1016/j.gca.2008.04.011.

Peters, S.C., Blum, J.D., Driscoll, C.T. and Likens, G.E. (2004) 'Dissolution of wollastonite during the experimental manipulation of Hubbard Brook Watershed', *Biogeochemistry*, 67(3), pp. 309–329. Available at: https://doi.org/10.1023/B:BIOG.0000015787.44175.3f.

Plummer. L.N, Wigley, T.M.L, and Parkhurst, D.L. (1978) The kinetics of calcite dissolution in CO2-water systems st 5C to 60C and 0.0- 1.0 atm CO2, American Journal of Science, 278, 179-216.

Pogge von Strandmann, P.A.E., Tooley, C., Mulders, J.J.P.A. and Renforth, P. (2022) 'The Dissolution of Olivine Added to Soil at 4°C: Implications for Enhanced Weathering in Cold Regions', *Frontiers in Climate*, 4(February), pp. 1–11. Available at: https://doi.org/10.3389/fclim.2022.827698.

Rademacher, L.K., Clark, J.F., Hudson, G.B., Erman, D.C. and Erman, N.A. (2001) 'Chemical evolution of shallow groundwater as recorded by springs , Sagehen basin ; Nevada County , California'.

Raymo, M.E. and Ruddiman, W.F. (1992) 'Tectonic forcing of late Cenozoic climate', *Nature*, 359(6391), pp. 117–122. Available at: https://doi.org/10.1038/359117a0.

Raymond, P.A. and Cole, J.J. (2003) 'Increase in the export of alkalinity from North America's largest river', *Science*, 301(5629), pp. 88–91. Available at: https://doi.org/10.1126/science.1083788.

Raymond, P.A. and Hamilton, S.K. (2018) 'Anthropogenic influences on riverine fluxes of dissolved inorganic carbon to the oceans', *Limnology and Oceanography Letters*, 3(3), pp. 143–155. Available at: https://doi.org/10.1002/lol2.10069.

Raymond, P.A. and Oh, N.H. (2009) 'Long term changes of chemical weathering products in rivers heavily impacted from acid mine drainage: Insights on the impact of coal mining on regional and global carbon and sulfur budgets', *Earth and Planetary Science Letters*, 284(1–2), pp. 50–56. Available at: https://doi.org/10.1016/j.epsl.2009.04.006.

Regnier, P. *et al.* (2013) 'Anthropogenic perturbation of the carbon fluxes from land to ocean', *Nature Geoscience*, 6(8), pp. 597–607. Available at: https://doi.org/10.1038/ngeo1830.

Relph, K.E., Stevenson, E.I., Turchyn, A. V., Antler, G., Bickle, M.J., Baronas, J.J., Darby, S.E.,

Parsons, D.R. and Tipper, E.T. (2021) ‘Partitioning riverine sulfate sources using oxygen and sulfur isotopes: Implications for carbon budgets of large rivers’, *Earth and Planetary Science Letters*, 567. Available at: https://doi.org/10.1016/j.epsl.2021.116957.

Renforth, P. (2012) ‘The potential of enhanced weathering in the UK’, *International Journal of Greenhouse Gas Control*, 10, pp. 229–243. Available at: https://doi.org/10.1016/j.ijggc.2012.06.011.

Renforth, P. (2019) ‘The negative emission potential of alkaline materials’, *Nature Communications*, 10(1). Available at: https://doi.org/10.1038/s41467-019-09475-5.

Renforth, P. and Henderson, G.M. (2017) ‘Assessing ocean alkalinity for carbon sequestration’, *Reviews of Geophysics*, 55(3), pp. 636–674. Available at: https://doi.org/10.1002/2016RG000533.

Renforth, P., Manning, D.A.C. and Lopez-capel, E. (2009) ‘Carbonate precipitation in artificial soils as a sink for atmospheric carbon dioxide’, *APPLIED GEOCHEMISTRY*, 24(9), pp. 1757–1764. Available at: https://doi.org/10.1016/j.apgeochem.2009.05.005.

Renforth, P., Pogge von Strandmann, P.A.E. and Henderson, G.M. (2015) ‘The dissolution of olivine added to soil: Implications for enhanced weathering’, *Applied Geochemistry*, 61, pp. 109–118. Available at: https://doi.org/10.1016/j.apgeochem.2015.05.016.

Renforth, P., Washbourne, C.L., Taylder, J. and Manning, D.A.C.C. (2011) ‘Silicate production and availability for mineral carbonation’, *Environmental Science and Technology*, 45(6), pp. 2035–2041. Available at: https://doi.org/10.1021/es103241w.

Royal Society (2018) *Greenhouse Gas Removal*.

Schaller, J., Puppe, D., Kaczorek, D., Ellerbrock, R. and Sommer, M. (2021) ‘Silicon cycling in soils revisited’, *Plants*, 10(2), pp. 1–36. Available at: https://doi.org/10.3390/plants10020295.

Schuiling, R.D., Wilson, S.A. and Power, L.M. (2011) ‘Enhanced silicate weathering is not limited by silicic acid saturation’, *Proceedings of the National Academy of Sciences of the United States of America*, 108(12), p. 2011. Available at: https://doi.org/10.1073/pnas.1019024108.

Semhi, K., Amiotte Suchet, P., Clauer, N. and Probst, J.L. (2000) ‘Impact of nitrogen fertilizers on the natural weathering-erosion processes and fluvial transport in the Garonne basin’, *Applied Geochemistry*, 15(6), pp. 865–878. Available at: https://doi.org/10.1016/S0883-2927(99)00076-1.

Shand, P., Darbyshire, D.P.F., Gooddy, D. and Haria, A.H. (2007) ‘87Sr / 86Sr as an indicator of flowpaths and weathering rates in the’, 236, pp. 247–265. Available at: https://doi.org/10.1016/j.chemgeo.2006.09.012.

Shao, S., Driscoll, C.T., Johnson, C.E., Fahey, T.J., Battles, J.J. and Blum, J.D. (2016) ‘Long-Term responses in soil solution and stream-water chemistry at Hubbard Brook after experimental addition of wollastonite’, *Environmental Chemistry*, 13(3), pp. 528–540. Available at: https://doi.org/https://doi.org/10.1071/EN15113.

Smith, S.M. *et al.* (2023) ‘The State of Carbon Dioxide Removal- 1st Edition’, *The State of Carbon Dioxide Removal*, p. 114. Available at: https://www.stateofcdr.org/resources.

Spears, D.A. (1997) ‘Environmental impact of minerals in UK coals’, *Geological Society Special Publication*, 125(125), pp. 287–295. Available at: https://doi.org/10.1144/GSL.SP.1997.125.01.25.

Spears, D.A. (2015) ‘The geochemistry and mineralogy of high-S coals, with examples mainly from the East Pennines Coalfield in Yorkshire and Nottinghamshire, UK: An overview’, *Proceedings of the Yorkshire Geological Society*, 60(3), pp. 204–226. Available at: https://doi.org/10.1144/pygs2015-356.

Spears, D.A., Rippon, J.H. and Cavender, P.F. (1999) ‘Geological controls on the sulphur distribution in British carboniferous coals: A review and reappraisal’, *International Journal of Coal Geology*, 40(1), pp. 59–81. Available at: https://doi.org/10.1016/S0166-5162(98)00057-3.

Strefler, J., Amann, T., Bauer, N., Kriegler, E. and Hartmann, J. (2018) 'Potential and costs of carbon dioxide removal by enhanced weathering of rocks', *Environmental Research Letters*, 13(3). Available at: https://doi.org/10.1088/1748-9326/aaa9c4.

Stumm, W. and Morgan, J.. (1996) *Aquatic Chemistry*.

Tipper, Edward T., Bickle, M.J., Galy, A., West, A.J., Pomiès, C. and Chapman, H.J. (2006) 'The short term climatic sensitivity of carbonate and silicate weathering fluxes: Insight from seasonal variations in river chemistry', *Geochimica et Cosmochimica Acta*, 70(11), pp. 2737–2754. Available at: https://doi.org/10.1016/j.gca.2006.03.005.

Tipper, E.T., Gaillardet, J., Galy, A., Louvat, P., Bickle, M.J. and Capmas, F. (2010) 'Calcium isotope ratios in the world ' s largest rivers : A constraint on the maximum imbalance of oceanic calcium fluxes', 24. Available at: https://doi.org/10.1029/2009GB003574.

Tipper, E. T., Galy, A., Gaillardet, J., Bickle, M.J., Elderfield, H. and Carder, E.A. (2006) 'The magnesium isotope budget of the modern ocean: Constraints from riverine magnesium isotope ratios', *Earth and Planetary Science Letters*, 250(1–2), pp. 241–253. Available at: https://doi.org/10.1016/j.epsl.2006.07.037.

Tipper, E.T., Stevenson, E.I., Alcock, V., Knight, A.C.G., Baronas, J.J., Hilton, R.G., Bickle, M.J., Larkin, C.S., Feng, L., Relph, K.E. and Hughes, G. (2020) 'Global silicate weathering flux overestimated because of sediment-water cation exchange', *Proceedings of the National Academy of Sciences of the United States of America*, 118(1). Available at: https://doi.org/10.1073/pnas.2016430118.

Torres, M.A., West, A.J., Clark, K.E., Paris, G., Bouchez, J., Ponton, C., Feakins, S.J., Galy, V. and Adkins, J.F. (2016) 'The acid and alkalinity budgets of weathering in the Andes–Amazon system: Insights into the erosional control of global biogeochemical cycles', *Earth and Planetary Science Letters*, 450, pp. 381–391. Available at: https://doi.org/10.1016/j.epsl.2016.06.012.

Torres, M.A., West, A.J. and Li, G. (2014) 'Sulphide oxidation and carbonate dissolution as a source of CO2 over geological timescales', *Nature*, 507(7492), pp. 346–349. Available at: https://doi.org/10.1038/nature13030.

Tucker, M.E. (1991) 'Sequence stratigraphy of carbonate-evaporite basins: Models and application to the Upper Permian (Zechstein) of northeast England and adjoining North Sea', *Journal of the Geological Society*, 148(6), pp. 1019–1036. Available at: https://doi.org/10.1144/gsjgs.148.6.1019.

Tye, A.M. *et al.* (2022) 'Dissolved inorganic carbon export from rivers of Great Britain: Spatial distribution and potential catchment-scale controls', *Journal of Hydrology*, 615(PA), p. 128677. Available at: https://doi.org/10.1016/j.jhydrol.2022.128677.

Vicca, S., Goll, D.S., Hagens, M., Hartmann, J., Janssens, I.A., Neubeck, A., Peñuelas, J., Poblador, S., Rijnders, J., Sardans, J., Struyf, E., Swoboda, P., van Groenigen, J.W., Vienne, A. and Verbruggen, E. (2022) 'Is the climate change mitigation effect of enhanced silicate weathering governed by biological processes?', *Global Change Biology*, 28(3), pp. 711–726. Available at: https://doi.org/10.1111/gcb.15993.

Vincent, C.J., Rowley, W.J. and Monaghan, A.A. (2010) 'Thermal and burial history modelling in the Midlothian-Leven syncline in the Midland Valley of Scotland using BasinMod and HotPot', *Scottish Journal of Geology*, 46(2), pp. 125–142. Available at: https://doi.org/10.1144/0036-9276/01-376.

Walling, D.E. (1999) 'Linking land use, erosion and sediment yields in river basins', *Hydrobiologia*, 410, pp. 223–240. Available at: https://doi.org/10.1023/A:1003825813091.

Walling, D.E. and Webb, B.W. (1996) 'Erosion and sediment yield: A global overview', *IAHS-AISH Publication*, 236(236), pp. 3–19.

Wang, C., Li, W., Yang, Z., Chen, Y., Shao, W. and Ji, J. (2015) 'An invisible soil acidification :

Critical role of soil carbonate and its impact on heavy metal bioavailability', *Nature Publishing Group*, (November 2014), pp. 1–9. Available at: https://doi.org/10.1038/srep12735.

West, A.J., Galy, A. and Bickle, M. (2005) 'Tectonic and climatic controls on silicate weathering', *Earth and Planetary Science Letters*, 235(1–2), pp. 211–228. Available at: https://doi.org/10.1016/j.epsl.2005.03.020.

West, L.J., Banwart, S.A., Val, M., Kantzas, E. and Beerling, D.J. (2023) 'Applied Geochemistry Making mistakes in estimating the CO 2 sequestration potential of UK croplands with enhanced weathering', *Applied Geochemistry*, 151(December 2022), p. 105591. Available at: https://doi.org/10.1016/j.apgeochem.2023.105591.

White, A.F. and Blum, A.E. (1995) 'Effects of climate on chemical weathering in watersheds', *Water-rock interaction. Proc. symposium, Vladivostok, 1995*, 59(9), pp. 57–60. Available at: https://doi.org/10.1201/9780203734049-13.

Whitehead, P.G., Hill, T.J. and Neal, C. (2004) 'Impacts of forestry on nitrogen in upland and lowland catchments: a comparison of the River Severn at Plynlimon in mid-Wales and the Bedford Ouse in south-east England using the INCA Model', *Hydrology and Earth System Sciences*, 8(3), pp. 533–544. Available at: https://doi.org/10.5194/hess-8-533-2004.

Woodward, J. and Foster, I. (1997) 'Erosion and Suspended Sediment Transfer in river Catchments: Environmental controls, processes and problems', *Geography: Journal of the Geographical Association*, 82(Oct).

Worrall, F., Howden, N.J.K. and Burt, T.P. (2014) 'A method of estimating in-stream residence time of water in rivers', *Journal of Hydrology*, 512, pp. 274–284. Available at: https://doi.org/10.1016/j.jhydrol.2014.02.050.

Worrall, F., Howden, N.J.K., Burt, T.P. and Hannah, D.M. (2022) 'River water temperature demonstrates resistance to long-term air temperature change', *Hydrological Processes*, 36(11), pp. 1–14. Available at: https://doi.org/10.1002/hyp.14732.

Worthington, S.R.H., Davies, G.J. and Alexander, E.C. (2016) 'Enhancement of bedrock permeability by weathering', *Earth-Science Reviews*, 160, pp. 188–202. Available at: https://doi.org/10.1016/j.earscirev.2016.07.002.

Xu, S., Li, S., Su, J., Yue, F., Zhong, J. and Chen, S. (2021) 'Oxidation of pyrite and reducing nitrogen fertilizer enhanced the carbon cycle by driving terrestrial chemical weathering', *Science of the Total Environment*, 768, p. 144343. Available at: https://doi.org/10.1016/j.scitotenv.2020.144343.

Zavadlav, S., Rožic, B., Dolenec, M. and Lojen, S. (2017) 'Stable isotopic and elemental characteristics of recent tufa from a karstic Krka River (south-east Slovenia): Useful environmental proxies?', *Sedimentology*, 64(3), pp. 808–831. Available at: https://doi.org/10.1111/sed.12328.

Zeebe, R.E. and Wolf-Gladrow, D.A. (2001) *CO2 in Seawater: Equilibrium, Kinetics, Isotopes, Elsevier Oceanography Series Book*.

Zeng, S., Liu, Z. and Kaufmann, G. (2019) 'Sensitivity of the global carbonate weathering carbon-sink flux to climate and land-use changes', *Nature Communications*, 10(1), pp. 1–10. Available at: https://doi.org/10.1038/s41467-019-13772-4.

Zhang, S., Planavsky, N.J., Katchinoff, J., Raymond, P.A., Kanzaki, Y., Reershemius, T. and Reinhard, C.T. (2022) 'River chemistry constraints on the carbon capture potential of surficial enhanced rock weathering', *Limnology and Oceanography*, 67(S2). Available at: https://doi.org/10.1002/lno.12244.

8 Appendices

8.1 Appendix A- Appendices for Chapter 2

8.1.1 Auto titrator Precision Testing

Table A.1: Precision test for auto titrator, using CRM material ($CaCO_3$ 500 mg L^{-1})

Standard number	Alkalinity Mmol/L	% Difference
Std 1	10.1	0.25
Std 2	10.06	0.15
Std 3	9.93	0.18
Std 4	9.9	0.25
Std 5	10	0
Std 6	10.04	0.10
Std 7	10	0
Std 8	9.85	0.38
Std 9	9.96	0.1
Std 10	10.04	0.1
Std 11	9.9	0.25
Std 12	9.95	0.13
Std 13	9.88	0.38
Std 14	10.1	0.3
Std 15	9.85	0.25
Average		**0.19**

8.1.2 The volume of concentrated alkalinity added to Thames River water (for carbonate precipitation experiments)

Table A.2- The volume of concentrated alkalinity added to Thames beakers. Solution A is concentrated $CaCl_2/MgCl_2$, and solution B is concentrated Na_2CO_3/K_2CO_3. Scenarios 1 and 2 are discussed in the main text of Chapter 5 but refer to the potential for the complete release of cations from basalt (scenario 1) or the potential that basalt dissolution is limited by silica saturation.

	Solution A (mL)	Solution B (mL)	Total volume (mL)
Beaker A (Control)	0	0	500
Beaker B (Scenario 2)	2.44	4.31	506.75
Beaker C (10 t ha^{-1}; scenario 1)	8.85	15.59	524.44
Beaker D (10 t ha^{-1}; scenario 1)	18.59	32.79	551.38
Beaker E (50 t ha^{-1}; scenario 1)	54.96	96.90	651.86

8.1.3 The volume of concentrated alkalinity added to the Severn River

Table A.3: The volume of alkalinity added to the Severn beakers.

	Solution A (mL)	Solution B (mL)	Total Volume (mL)
Beaker A (Control)	0	0	500
Beaker B (Scenario 2)	0.09	1.55	501.62
Beaker C (10 t ha^{-1}; scenario 1)	3.088	5.45	508.54
Beaker D (10 t ha^{-1}; scenario 1)	6.282	11.10	517.38
Beaker E (50 t ha^{-1}; scenario 1)	16.61	29.26	545.87

8.2 Appendix B- Appendices for Chapter 3

8.2.1 Flow rate histograms for the two catchments

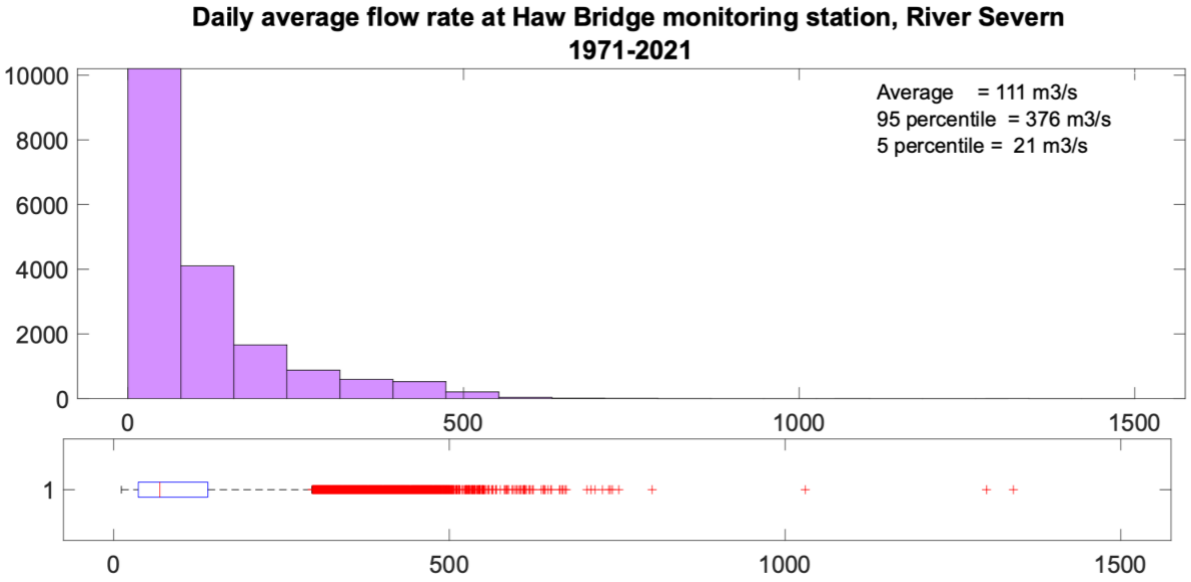

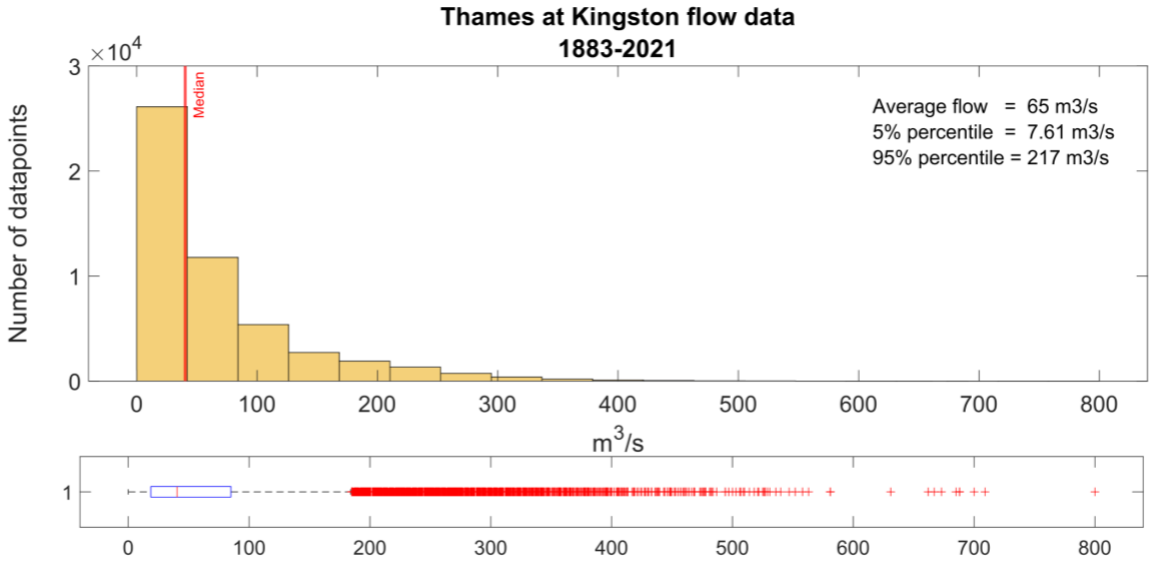

Figure B.1 - Flow rate data at Kingston (Thames) and Haw Bridge (Severn) with statistical information for the 5-95% percentiles.

8.2.2 Historical DIC concentration and flux in the Severn and Thames Catchments

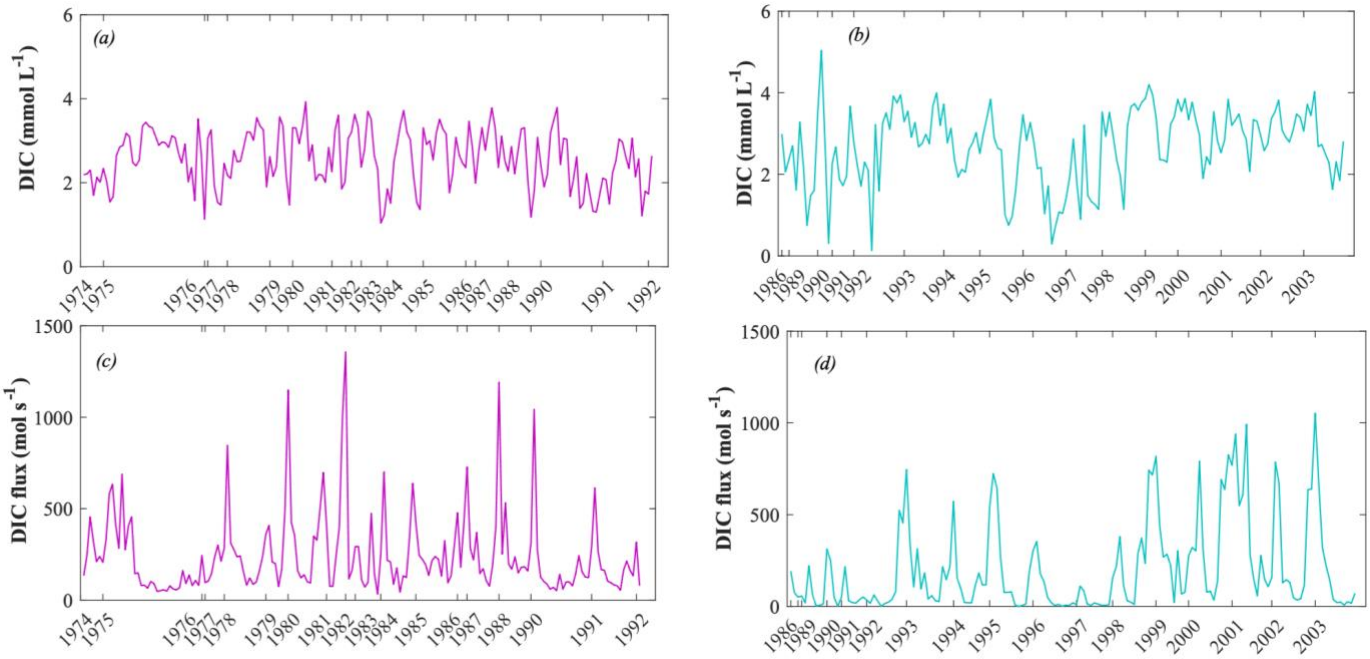

Figure B.2- Historic DIC calculated from alkalinity, pH and temperature in PHREEQC. (a) DIC concentrations in the River Severn, (b) DIC concentrations in the River Thames, (c) flow-weighted flux (mol s^{-1}) in the River Severn, and (d) in the Thames.

8.2.3 Historic chemical variations implying changes in source endmembers.

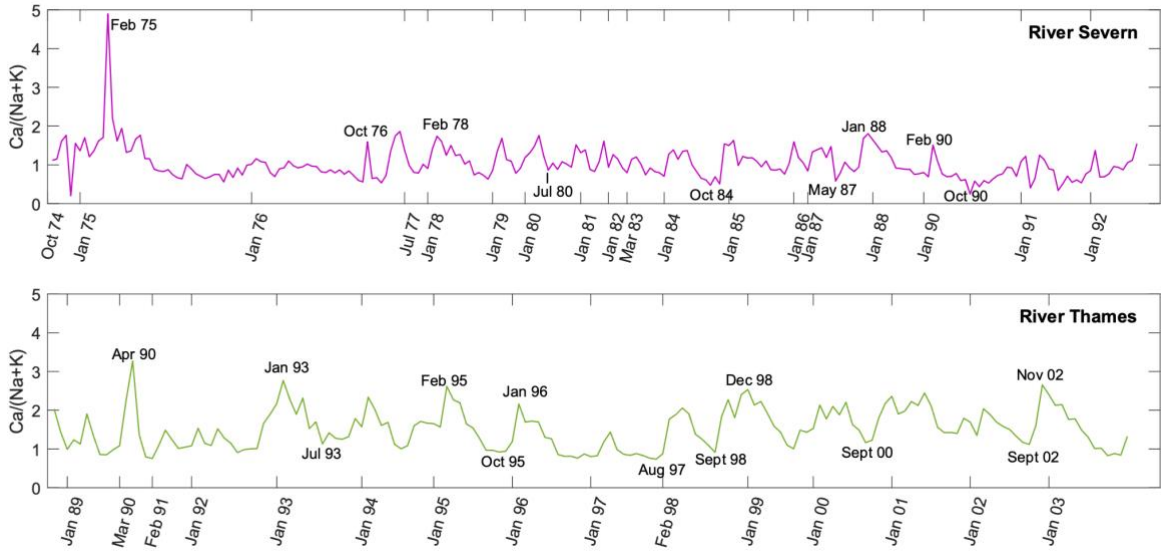

Figure B.3- Temporal variations in the magnitude of major cations to rivers may indicate a possible connection between weathering and season.

8.2.4 Variations in the fraction of solutes from each endmember (MEANDIR results)

Table B.1- Inversion results. The 25th and 75th percentile range in the fraction of total major cations from each source endmember over the measurement period for each river. S= Severn, T= Thames

	f_{sil} (%)		f_{carb} (%)		f_{evap}		f_{cyclic}	
	S	**T**	**S**	**T**	**S**	**T**	**S**	**T**
Median	11.3	11.0	45.5	50.5	36.7	29.8	6.5	8.7
25 percentile Range	0.5	1.5	35.9	41.3	30.1	24.5	4.6	7.7
75 percentile range	15.9	11.3	55.3	61.3	42.0	34.5	7.6	8.9

8.2.5 Variation in source of solutes across the River Severn

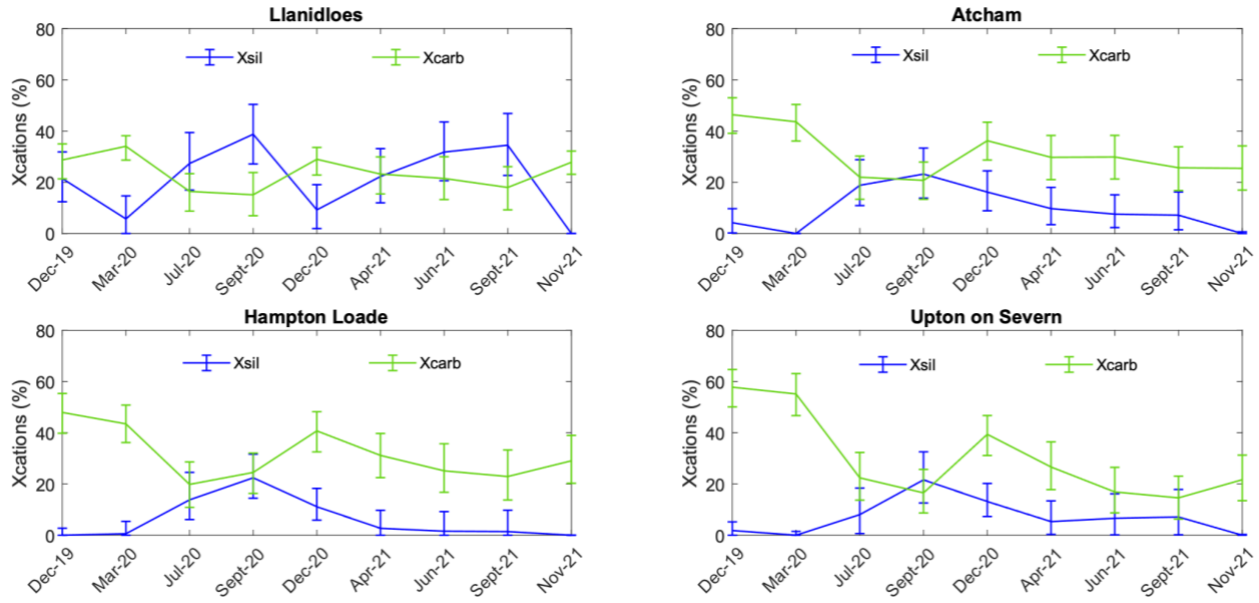

Figure B.8.1- Percentage of total dissolved major cations (Ca^{2+}, Mg^{2+}, Na^{+}) from silicate and carbonate weathering (X_{sil}, Xcarb) at four sampling locations within the River Severn over the time series sampling period. Error bars represent the range in Xsil and Xcarb calculated using 25th and 75th percentile inversion results. Llanidloes has more pronounced peaks in X_{sil}, possibly due to the combination of silicate rich lithology, as well as a minimal contribution from other inputs. (Distance downstream)

8.2.6 Longer term changes in Qsil and Qcarb in the Severn and Thames catchments

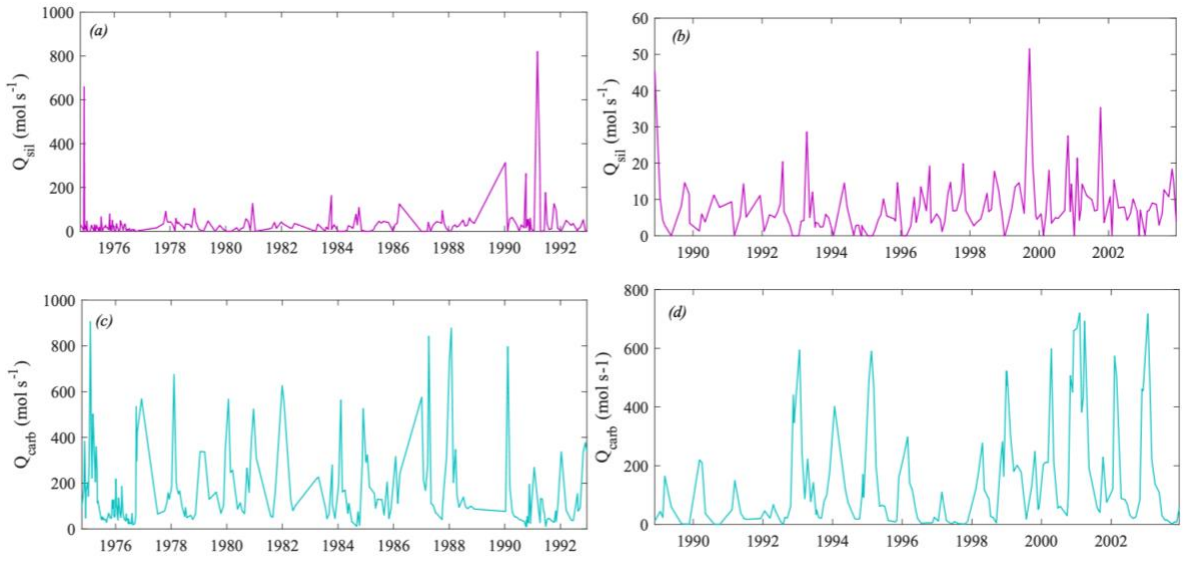

Figure B.8.2- Longer- term variations in the flux of silicate ions and carbonate ions in the Rivers Severn and Thames.

8.2.7 Historic SI_{calc}

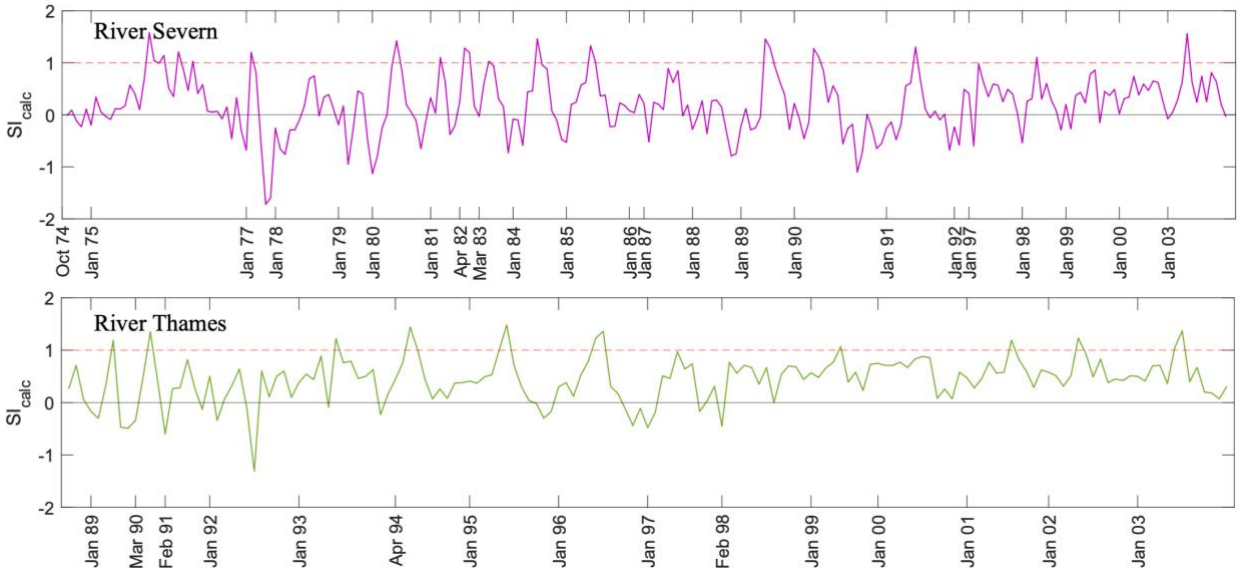

Figure B.8.3- Historic saturation indexes for the Thames (at Teddington Lock) and the Severn (at Haw Bridge) Catchments. Median SI for the Thames = 0.5, and Severn= 0.2. Solid lines mark SI= 0 which is the saturation index necessary for carbonate precipitation under ideal conditions. SI= 1 is also marked which is the threshold value used in this study to account for the suppression of precipitation due to inhibiting ions in solution.

8.2.8 Historic sulphate trends

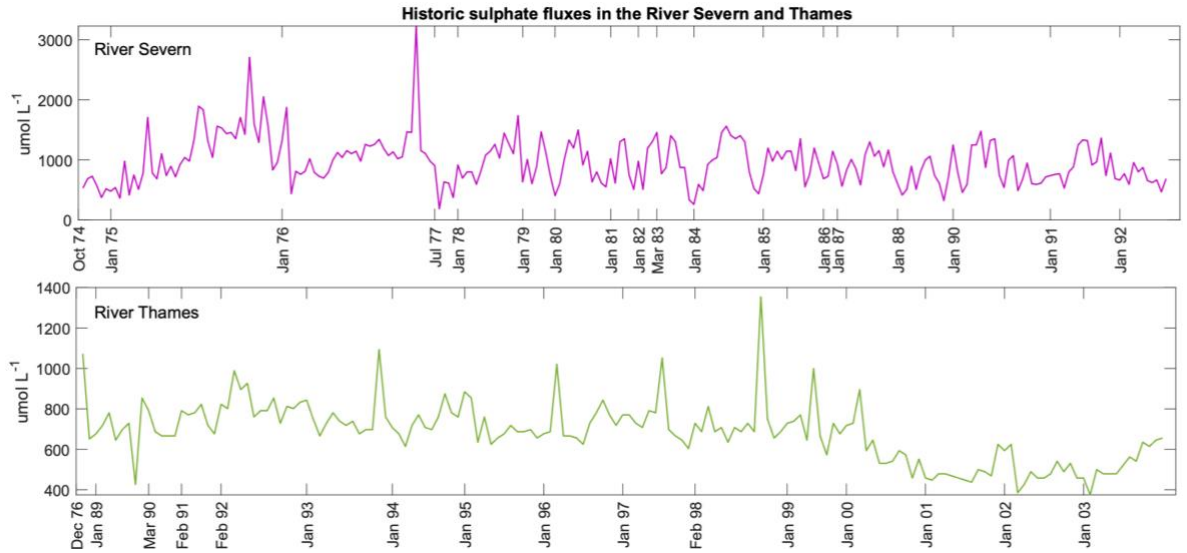

Figure B.8.4: Historic sulphate concentrations in the River Severn and The Thames. Data from: Harmonized Monitoring Scheme (HMS) dataset, Environment Agency. The River Thames SO4 concentrations decrease in the early 2000s, which imply a possibility that some sulphate pre-2000 was from anthropogenic sources.

8.2.9 Changes to overall fertilizer application in the UK (NO_3^-, PO_4^{3-}, K^+)

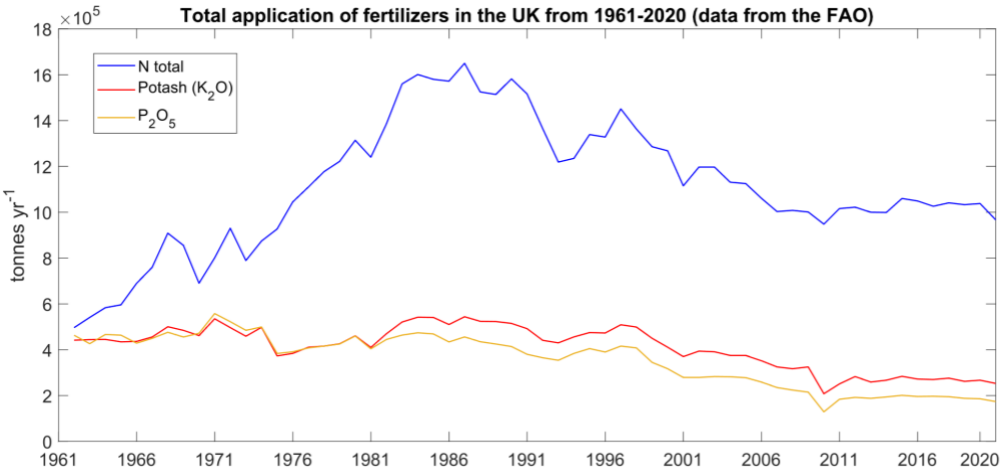

Figure B.8.5: average fertilizer use in the UK from the FAO

8.2.10 Spatial NO_3/Cl varations across the Thames and Severn Catchments

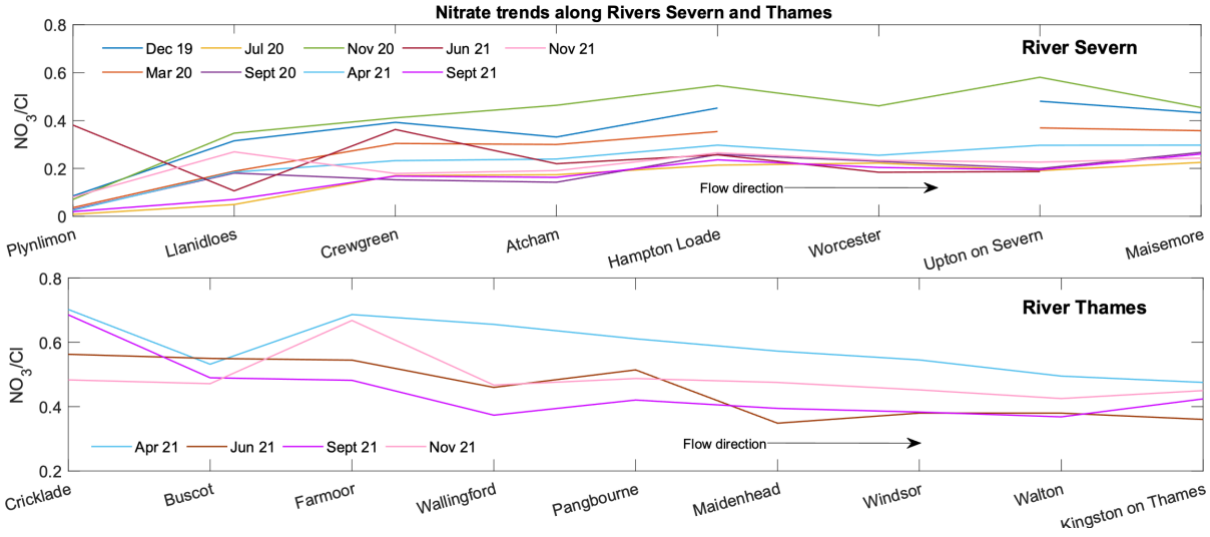

Figure B.8.6: River NO_3/Cl trends along the river Thames and Severn during the sampling period of this study.

8.3 Appendix C- Appendices for Chapter 4

8.3.1 Catchment characteristics

Catchment	% Arable	% Grassland	Mean rainfall (mm yr^{-1})	Elevation (m) 50 percentile	Max Elevation (m)	% High Permeability Bedrock	% Low permeability bedrock	PROP_Wet	BFIHOST	SSY kg ha^{-1} yr^{-1}	runoff mm yr^{-1}
Annan	7.0	58.8	1395.3	204.9	820.0	19.4	80.5	0.62	0.49	180.3	1057.7
Arun	26.1	33.6	825.5	55.1	291.4	4.4	83.9	0.35	0.39	203.2	467.4
Avon Bristol	33.5	46.0	843.7	104.6	304.6	46.6	32.7	0.34	0.57	146.4	400.8
Avon Hampshire	37.3	39.8	840.1	119.9	293.7	72.5	1.0	0.34	0.86	59.4	371.1
Chelmer	63.4	16.2	628.2	64.6	122.4	1.8	0.0	0.29	0.40	31.2	112.7
Clyde	9.2	54.9	1194.4	251.9	745.2	24.3	43.2	0.59	0.41	200.6	806.4
Conon	0.6	11.3	1818.9	354.4	1103.4	0.0	98.4	0.75	0.36	48.8	1649.0
Conwy	0.4	65.2	2169.6	329.7	1050.6	0.0	100.0	0.70	0.36	125.1	1754.4
Coquet	17.8	52.8	876.6	192.8	774.5	0.0	26.4	0.44	0.39	97.1	481.5
Dee Aberdeenshire	5.8	13.8	1132.3	435.1	1308.9	0.0	95.0	0.58	0.51	43.7	810.3
DeeGlenlochar	0.6	51.6	1873.7	237.3	813.3	0.0	100.0	0.65	0.37	84.8	1624.5
Deveron	23.8	34.7	953.3	209.5	754.2	0.0	94.7	0.46	0.51	79.6	558.1

Don Aberdeenshire	29.6	28.9	902.2	220.4	873.9	0.3	98.0	0.54	0.58	95.6	523.3
Don Ouse	23.4	29.0	1157.8	124.2	543.4	2.3	0.0	0.34	0.49	195.6	415.0
Earn	16.3	38.7	1482.9	230.7	978.6	0.0	53.0	0.59	0.51	118.3	1193.0
Eden Beaumont	8.5	72.2	1227.2	210.4	945.4	17.3	15.7	0.64	0.49	182.3	753.9
Ely Ouse	64.6	17.5	602.7	34.4	165.5	80.3	11.5	0.25	0.73	33.1	142.9
Esk Canonbie	1.3	52.1	1526.7	277.9	691.7	17.5	81.1	0.61	0.41	179.7	1148.2
Exe	23.5	57.2	1114.0	171.3	516.8	2.6	61.6	0.44	0.56	168.3	672.1
Forth	2.8	44.8	1855.5	181.4	1160.3	3.2	56.1			225.6	1410.1
Hull	71.4	21.2	715.9	68.6	245.1	100.0	0.0	0.31	0.81	55.2	441.0
LeeLondon	46.9	18.8	639.2	89.1	226.1	53.8	0.0	0.29	0.51	45.7	130.0
LevenHaitherwaite	4.4	62.8	2257.2	176.6	893.2	0.0	100.0	0.71	0.44	129.8	1820.5
Levenrenton	0.4	47.4	2133.1	197.6	1120.0	22.4	62.8	0.71	0.44	115.2	1839.9
Lune	1.8	80.9	1559.6	264.4	734.4	0.0	29.8	0.64	0.40	146.2	1184.1
Medway	27.5	36.6	767.0	67.9	267.7	11.0	39.7	0.35	0.44	96.2	280.8
MerseyHW	5.9	42.8	1077.5	130.3	635.5	20.4	0.0	0.47	0.44	200.8	571.6
Nene	53.9	26.0	635.5	90.1	223.9	2.2	44.5	0.26	0.53	58.4	179.5
Ness	1.2	13.3	1866.4	348.8	1109.6	0.0	90.2	0.71	0.42	43.4	1558.2
NthEsk	24.6	18.0	1125.0	270.0	935.7	0.0	61.6	0.55	0.52	124.6	842.9
Ouse	31.3	43.9	931.4	118.0	714.3	33.6	5.8	0.37	0.44	146.7	496.3

Ribble	3.0	70.9	1369.7	197.2	691.4	0.6	1.4	0.56	0.37	320.6	950.2
Severn	29.8	47.6	810.9	110.0	826.2	15.8	53.0	0.32	0.51	252.6	356.0
Spey	1.3	15.6	1157.8	420.6	1306.1	0.0	96.4	0.63	0.48	81.9	724.6
Stour	75.8	13.0	591.7	74.8	127.6	76.2	0.0	0.25	0.51	41.3	160.4
Tamar	21.6	63.3	1252.8	144.9	580.3	0.0	100.0	0.49	0.48	322.5	789.1
Taw	22.6	60.2	1176.1	168.4	811.4	0.0	97.2	0.48	0.47	189.9	695.3
Tay	7.2	24.7	1482.9	395.1	1210.0	0.0	82.9	0.58	0.48	90.8	1186.8
Tees	26.2	39.7	986.2	211.8	884.8	28.5	0.0	0.40	0.37	113.0	519.9
Test	46.2	30.8	821.8	100.4	296.4	91.4	0.0	0.34	0.90	85.0	339.3
Thames	35.6	32.2	719.5	99.4	330.2	43.2	22.0	0.30	0.65	70.1	207.8
Trent	29.9	41.8	756.1	112.7	635.5	13.9	11.7	0.30	0.50	156.7	347.8
Tweed	23.3	44.9	1004.4	255.0	838.0	18.9	69.7	0.49	0.49	92.1	588.2
Tyne	5.7	53.8	1048.3	264.5	891.9	0.5	0.6	0.51	0.32	133.6	656.6
Ugie	43.9	34.6	843.7	84.1	233.7	0.0	97.6	0.40	0.52	72.8	480.9
Wear	21.7	48.3	883.9	213.0	745.3	5.9	0.0	0.40	0.35	192.1	470.1
Welland	47.2	34.5	650.1	102.6	229.3	21.1	71.8	0.29	0.49	57.4	179.4
Wensum	74.0	13.6	694.0	50.0	96.1	93.4	0.0	0.30	0.69	32.4	226.9
Wharfe	9.2	59.1	1157.8	239.9	703.7	7.2	0.0	0.41	0.42	57.1	683.9
Wye	17.3	61.1	1044.6	199.0	750.0	0.0	95.6	0.38	0.54	238.6	578.8

8.3.2 Sulphate variability across UK catchments

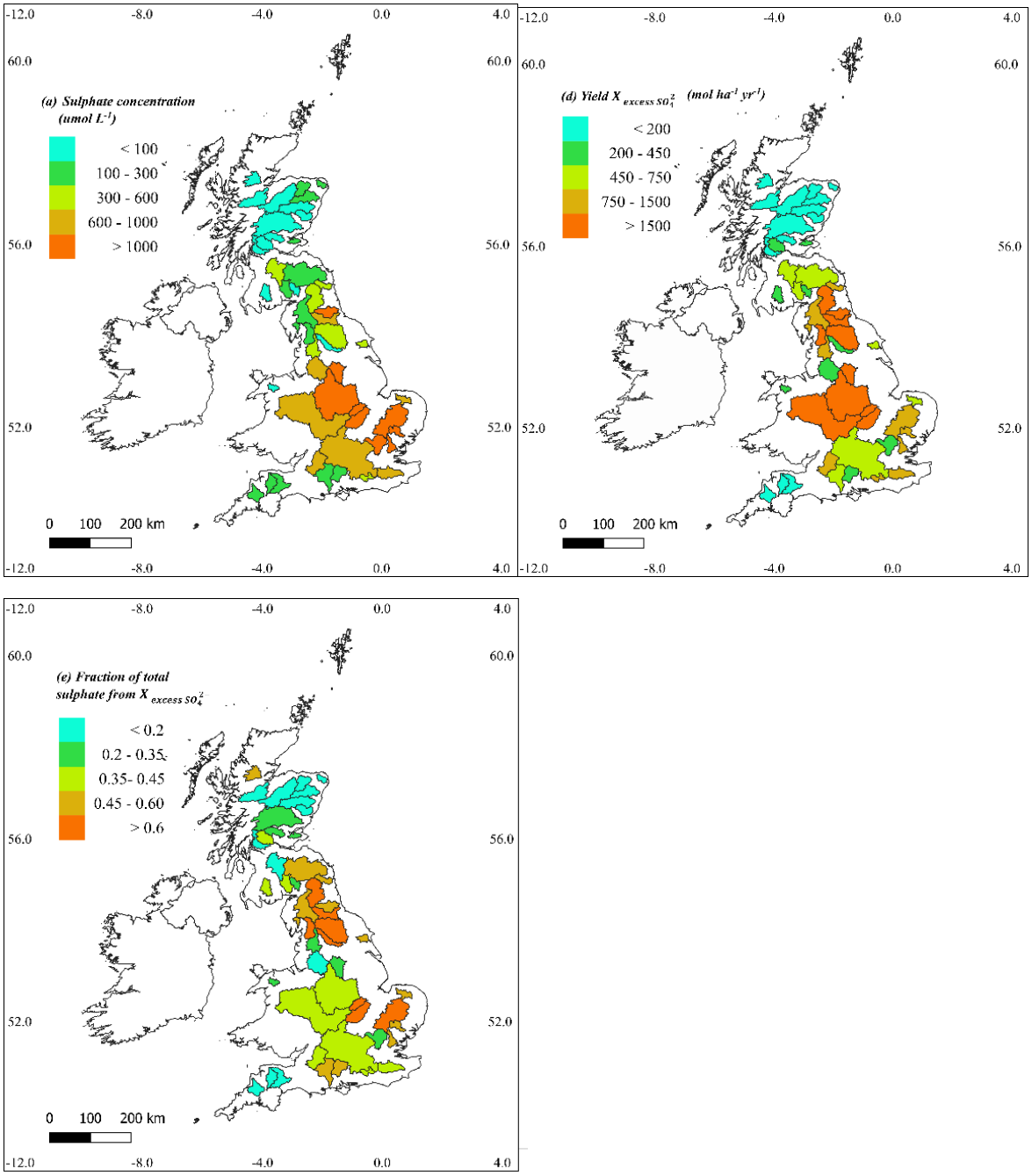

Figure C.1 - Variation in catchment (a) sulphate concentrations (umol L^{-1}), (b) excess sulphate yield (mol ha^{-1} yr^{-1}) and (c) the fraction of riverine SO_4^{2-} from excess sources (SO_4^{2-} which is not derived from evaporites or from non- sulphide silicates.

8.3.3 Percentage reduction in CDR due to nitrate from fertiliser

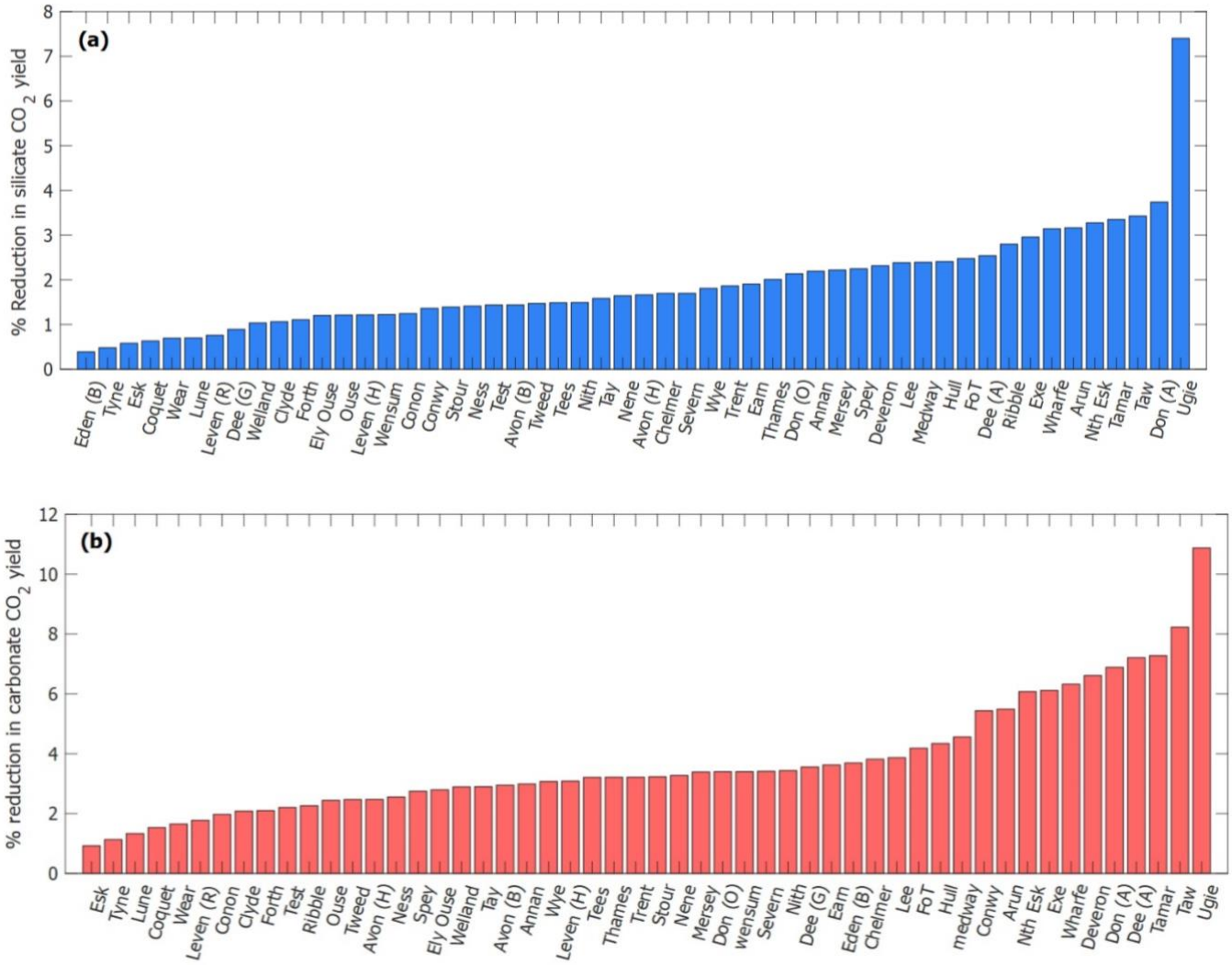

Figure C.2- The percentage reduction in the CO_2 yield for (a) silicate and (b) carbonate weathering from the maximum in each of the catchments in the study due to nitric acid weathering. Leven (R)= Leven, Renton, Avon (H)= Avon Hampshire, Avon (B)= Avon Bristol, Don (O)= Don Ouse, Dee (G)= Dee, Glenlochar, Eden (B)= Eden Beaumont, Don (A)= Don Aberdeenshire, Dee (A)= Dee Aberdeenshire.

8.4 Appendix D- Appendices for Chapter 5

8.4.1 Arable land and annual discharge in each catchment

For each catchment, the total catchment area was defined in QGIS, and the proportion of arable land was found using the National River Flow Archive (NRFA), from the Centre of Ecology and Hydrology (https://nrfa.ceh.ac.uk).

Total discharge was also obtained from the NRFA. Average flow rate was collated for each river that flowed to the ocean within each catchment (if more than 1). This was then converted to annual discharge (L/yr).

Table D.4-UK catchment information. Total Discharge accounts for all rivers in the catchment which discharge to the ocean. River column refers to the river where the natural chemical data was obtained.

Catchment	Catchment Area (10^5Ha)	% Arable Land	Annual Discharge (10^{10}L/yr)
Avon (Bristol)	2.2	33.5	78.1
Hull	2.1	71.4	16.5
Wear	1.8	21.7	46.7
Exe	2.3	23.5	105
Lee (London)	1.4	46.9	25.1
Ouse	11.4	31.3	445
Alchome	2.0	72.4	8.18
Avon and Stour	3.0	41.9	113
Essex Rivers	3.2	67.5	26.4
Somerset Rivers	2.9	40.1	40.9
Stour (Essex and Suffolk)	1.0	75.4	9.77
Sussex Rivers	3.1	25.7	44.9
Tamar	1.8	21.6	120
Taw and Torridge	2.2	24.2	115
Tay	5.1	7.2	543
Tees	2.2	26.2	72.6
Welland	1.6	47.2	17.5
Witham and Steeping	3.4	73.8	19.1
Ythan	1.4	50.8	41.3
Firth of Tay	1.1	49.0	20.6
Frome	1.3	49.0	32.3
Hampshire Rivers	2.7	39.9	68.4
Kent Rivers	4.8	29.3	66.6
Nene	2.3	53.9	29.3
Norfolk Rivers	3.7	73.8	38.3
Deveron	1.6	38.8	62.9
Don (Aberdeenshire)	1.3	29.6	66.4
East Suffolk Rivers	1.6	76.1	15.1

Cheshire Rivers	1.9	23.2	44.2
Coquet	2.1	19.7	24.8
Severn	11.4	29.8	338
Thames	16.2	35.6	206
Trent	10.4	26.9	268
Tweed	5.3	23.3	257
Wye	4.2	17.3	230
Great Ouse	8.6	64.6	54.2

8.4.2 UK baseline river chemical data

Table D.5: Natural median chemistry of UK rivers, obtained from the HMS and the EA datasets Data from the Environmental Agency WIMS dataset Open WIMS data and the Harmonized Monitoring Scheme (HMS) dataset ENV-16 Harmonised Monitoring Scheme datasets - GOV.UK (www.gov.uk)

**Chemistry is taken from median values in above datasets and used as the baseline composition in enhanced weathering calculations.*

Catchment Name	River Name	Sampling Site	Alkalinity mmol/L	pH	Ca^{2+}	Mg^{2+}	Na^{+}	K^{+}	Cl^{-}	SO_4^{2-}	TP	NO_3^{-}	Silica
Hull	Hull	Hempholme Lock	1.9783	8.0	2.333	0.143	0.683	0.052	0.776	0.286	0.005	0.134	0.092
Alcholme	Alcholme	Horkstow Top	2.0282	8.2	4.591	0.815	1.888	0.200	2.017	2.821	0.007	0.171	0.003
Witham and Steeping	Witham	Langrick bridge	2.0282	8.1	3.843	0.667	1.566	0.164	2.144	2.019	0.007	0.256	
Norfolk Rivers Group	Wensum	Costessey Mill	2.4479	8.3	3.219	0.197	1.174	0.120	1.467	0.614	0.003	0.083	0.103
Kent Rivers Group	Medway	Upstream Allington Sluices	1.0491	7.8	1.190	0.224	1.701	0.175	1.329	0.503	0.017	0.095	0.028
Essex Group	Chelmer	Chelmer Langford Intake	1.7884	8.1	3.294	0.400	1.196	0.114	1.455	1.041	0.006	0.300	0.136
Nene	Nene	Dog in A Doublet Sluice	1.9383	8.2	2.745	0.321	1.305	0.151	1.247	0.958	0.015	0.143	0.123
Avon and Stour	Avon	Knapp Mill	2.1282	8.1	2.570	0.085	0.405	0.045	0.539	0.239	0.002	0.103	0.079
East Suffolk Rivers	Waveney	Waveney River Centre	2.8225	8.0	6.238	0.302	1.522	no_info	1.977	3.269	0.002	0.121	no_info

Somerset Rivers	Parrett	West Over Bridge	2.4978	8.0	2.869	0.297	1.005	0.146	0.928	0.500	0.014	0.071	0.155
Hampshire Rivers	Test	Testwood	2.2680	8.1	2.595	0.081	0.478	0.049	0.601	0.171	0.001	0.106	
Sussex Rivers	Arun	Pallingham Manor	1.0090	7.5	1.193	0.245	2.123	0.246	1.317	0.583	0.096	0.141	0.161
Stour (Essex and Suffolk)	Stour	Langham	2.9674	8.1	2.820	0.576	2.653	0.210	2.426	0.937	0.026	0.009	0.181
Welland	Welland	Crowland	1.8784	8.2	3.269	0.428	1.814	0.166	1.785	1.093	0.007	0.206	0.166
Avon (Bristol)	Avon	Keynsham	2.2480	8.1	2.994	0.277	1.100	0.154	1.010	0.500	0.006	0.102	0.125
Ythan	Ugie	InverUgie	0.3347	7.3	0.402	0.223	0.770	0.083	1.128	0.207	0.003	0.080	0.238
Frome Group	Frome	Holme Bridge	2.0782	8.1	2.520	0.111	0.548	0.048	0.697	0.185	0.001	0.117	0.123
Deveron	Deveron	Bridge of Alvah	0.3407	7.7	0.382	0.207	0.666	0.059	0.883	0.122	0.054	0.071	0.221
Don (Aberdeenshire)	Don	Grandholm Bridge	0.5096	7.5	0.358	0.165	0.519	0.042	0.733	0.167	0.003	0.048	0.170
Tay	Tay	Perth (Queens Bridge)	0.1988	7.4	0.216	0.074	0.261	0.023	0.280	0.043	0.001	0.015	0.062
Thames	Thames	Kingston	4.3750	8.0	2.923	0.230	1.255	0.160	1.240	0.747	0.019	0.568	
Severn	Severn	Haw Bridge	2.3700	7.8	1.321	0.386	0.711	0.106	0.717	0.403	0.008	0.310	0.098
Ouse	Ouse	Skelton	3.1740	7.9	1.668	0.490	0.809	0.091	0.839	0.568	0.002	0.059	
Trent	Trent		3.6601	8.0	2.490	0.877	2.825	0.241	2.634	1.661	0.015	0.140	
Tweed	Tweed	Norham	1.3680	8.0	0.582	0.300	0.437	0.032	0.502	0.138	0.003	0.103	0.003
Wye	Wye		1.0790	7.7	1.026	0.274	0.331	0.064	0.166	0.332	0.001	0.065	
Tees	Tees	Low Worsall	0.9517	7.9	0.646	0.359	1.174	0.080	1.343	0.198	0.010	0.037	0.072
Exe Group	Exe	Trews Weir	0.4996	7.8	0.524	0.253	0.448	0.061	0.453	0.500	0.001	0.060	0.075
Taw and Torridge	Taw	Chapelton Bridge	0.3697	7.7	0.357	0.187	0.478	0.092	0.480	0.104	0.001	0.043	0.094
Firth of Tay	Eden	Kemback	1.0990	7.9	1.033	0.568	0.570	0.080	0.615	0.221	0.005	0.077	0.190
Tamar	Tamar	Gunnislake	0.3597	7.6	0.399	0.165	0.652	0.079	0.677	0.135	0.001	0.047	0.048

Coquet	Coquet	Warkworth Dam	0.7194	8.0	0.649	0.243	0.405	0.061	0.395	0.125	0.001	0.016	0.089
Wear	Wear	Lamb bridge	1.2989	7.9	1.432	0.823	1.235	0.143	1.171	0.920	0.006	0.059	0.121
Lee (London)	Lee	Carpenter's rd	2.3380	7.6	2.919	0.436	3.758	0.399	3.018	1.041	0.071	0.181	0.260
Great Ouse	Ely Ouse	Denver Sluice	2.9974	8.2	3.543	0.313	1.457	0.185	1.642	1.176	0.012	0.125	0.150

8.4.3 Composition of basalt used for the EW calculations.

Table D.6- Average composition of basalt, taken from The Cambridge Handbook of Earth Science Data, Henderson and Henderson (2009).

Element	Wt%
CaO	9.47%
MgO	6.73%
Na_2O	2.91%
K_2O	1.1%
SiO_2	49.20%
Al_2O_3	15.74%
FeO	7.13%
Fe_2O_3	3.79%
P_2O_5	0.35%

8.4.4 Ranges of natural pCO2 in UK rivers

*Table D.7: Natural variation of pCO_2 in rivers studied. Used to find the error associated with keeping pCO2 constant in EW calculations. *Taken from natural river chemistry- HMS and WIMS datasets. The median, 95 and 5 percentiles were used in the enhanced weathering calculations to account for the range in pCO_2 seen.*

River name	median	min	max	Q1	Q3	mean	STD	95% percentile	5% percentile
Hull	1333.1	79.3	9415.3	989.0	2009.6	1664.2	1120	3731.1	609.3
Alcholme	706.0	63.4	7377.7	373.8	1137.0	899.6	959.0	2384.9	133.0
Witham	540.4	10.1	3655.8	200.9	838.3	594.1	507.9	1263.4	59.0
Norfolk Group (Wensum)	1120.8	70.7	9691	748.5	1732	1466.2	2354.1	3586.2	445.3
Kent Rivers (Medway)	1083.9	20.1	14775.9	741.5	1561.1	1306.6	1110.6	3112.9	134.7
Essex Group (Chelmer)	804.5	130.8	7842.3	520.4	1100.7	950.8	805.7	1983.7	201.6
Nene	674.2	63.8	3786.4	452.8	945.7	791.2	545.4	1776.0	183.0
Avon	878.4	212.4	5868.1	715.6	1260.7	1097.0	735.7	2125.3	445.2
East Suffolk (Waveney)	2240.0	448.2	15939.6	1747.4	2924.5	2868.5	2499.6	7490.4	762.6
Somerset Rivers (Parrett)	1197.0	48.0	8371.5	930.8	1597.8	1460.1	1098.3	3481.7	306.6
Hampshire rivers (Test)	940.4	249.5	6511.4	752.8	1296.9	1174.2	876.1	2498.0	452.3
Sussex (Arun)	1291.9	15.9	20590.5	864.1	1972.9	1679.7	1602.1	4319.4	270.3
Stour	875.4	32.0	8335.2	586.4	1276.4	1023.2	791.5	2246.7	173.7
Welland	584.7	11.5	7131.8	290.3	903.2	713.5	677.1	1640.4	110.8
Avon (Bristol)	866.4	126.6	8329.1	737.3	1233.3	1082.1	839.2	2156.0	398.2
Ythan (Ugie)	890.9	72.2	25832.5	511.5	1563.1	1766.9	2903.5	6538.2	220.8
Frome	868.8	263.8	9703.1	683.2	1134.3	1009.1	707.4	1927.1	428.1
Deveron	456.7	7.0	23023.5	263.6	921.3	1195.1	2820.7	4797.1	91.5
Don (Aberdeenshire)	722.8	61.8	35480.0	412.6	1667.6	1848.3	3460.1	8054.2	227.3
Tay	470.8	5.5	5761.9	333.2	692.6	715.3	790.5	2528.6	124.7
Thames	2445.7	115.9	4944.6	1974.2	2848.0	2377.4	723.0	3333.0	1178.9
Severn	907.3	49.5	7410.9	585.4	1284.3	1054.0	781.6	2381.3	213.5
Ouse	1061.1	1.2	7209.8	747.2	1503.7	1212.4	743.7	2504.9	409.7
Trent	1242.6	101.6	8068.8	857.4	1760.2	1473.5	1006.6	3266.6	467.0

Wye	560.5	14.1	4996.2	316.1	837.5	660.7	541.0	1533.8	103.7
Tweed	400.3	1.0	16137.7	156.9	693.1	618.0	1086.9	1699.5	24.7
Tees	710.6	56.3	8321.9	509.5	1087.7	864.4	686.2	1829.1	183.4
Exe	592.2	19.5	17937.7	431.6	835.9	811.6	1124.6	1680.9	261.9
Taw	443.7	4.3	38677.5	296.8	743.6	799.6	2256.5	1929.4	80.9
Firth of Tay	767.6	62.3	34510.7	595.7	1017.5	1031.2	1853.6	2037.8	356.8
Tamar	620.4	13.1	12713.0	406.8	986.4	856.0	918.2	2173.7	220.9
Coquet	501.8	30.1	55455.2	319.8	784.1	764.2	2265.4	1665.2	172.6
Wear	1011.1	96.6	91775.4	724.2	1507.4	1549.4	4522.0	3178.1	463.9
Lee (London)	2460.2	279.5	49158.3	1746.6	3688.7	3275.3	3394.0	7269.6	1042.9
Ely Ouse	933.2	68.7	20597.4	606.5	1450.1	1133.9	1005.2	2562.2	243.6
Cheshire	1711	67.4	8163	1076	2346	1848	1170	4019.7	436.9

8.4.5 Temperature and pressure dependence on the saturation concentration of silica (Deriving the saturation concentration of silica in UK soils)

The temperature dependence of Silica solubility is defined by (Eq D.1)(Henley, 1983):

$$logC = -\frac{731}{T(K)} + 4.52 \quad (D.9)$$

Where C is the solubility of silica for a given T. Here we use a temperature of 10˚C (283.15K) which is the approximate average UK temperature of freshwater (9.8ºC). C= 1.444108 mmol/L

C is then used in equation 2 to find the pH and temperature combined dependence on silica saturation concentration (Si_{sol}):

$$Si_{sol} = C * (1 + \frac{10^{pH}+K_1}{\gamma_{H_4SiO_4}}) \quad (D.10)$$

We use a soil water pH of 6 and a $K_1 = 1.2593x10^{-10}$ as defined by Drever 1997(Drever, 1997). $\gamma_{H_4SiO_4}$ is equated using the Davies equation (for solutions of higher ionic strength, such as soil porewaters)(Stumm and Morgan, 1996):

$$-log\gamma = Az_i^2 * [\frac{\sqrt{u}}{1+\sqrt{u}} - 0.2u] \ (D.11)$$

Where Z is the charge of $\gamma_{H_4SiO_4}$, A= 0.509 (at 25 °C), and u is the ionic strength. We use a soil water ionic strength of 0.005, based on the mean ionic strength of soil porewarer from New Zealand (Black and Campbell, 1982). Inputting known variables into equation 3 gives a $\gamma_{H_4SiO_4}$ of 0.9266

And then using this activity co-efficient in 2 gives a $Si_{sol} = 1.4443$ mmol/L.

We thus use a silica saturation concentration of 1.4 mmol/L in this study which is comparable to that derived in (Van Cappellen and Qui 1997)

8.4.6 Sampling localities for beaker experiments

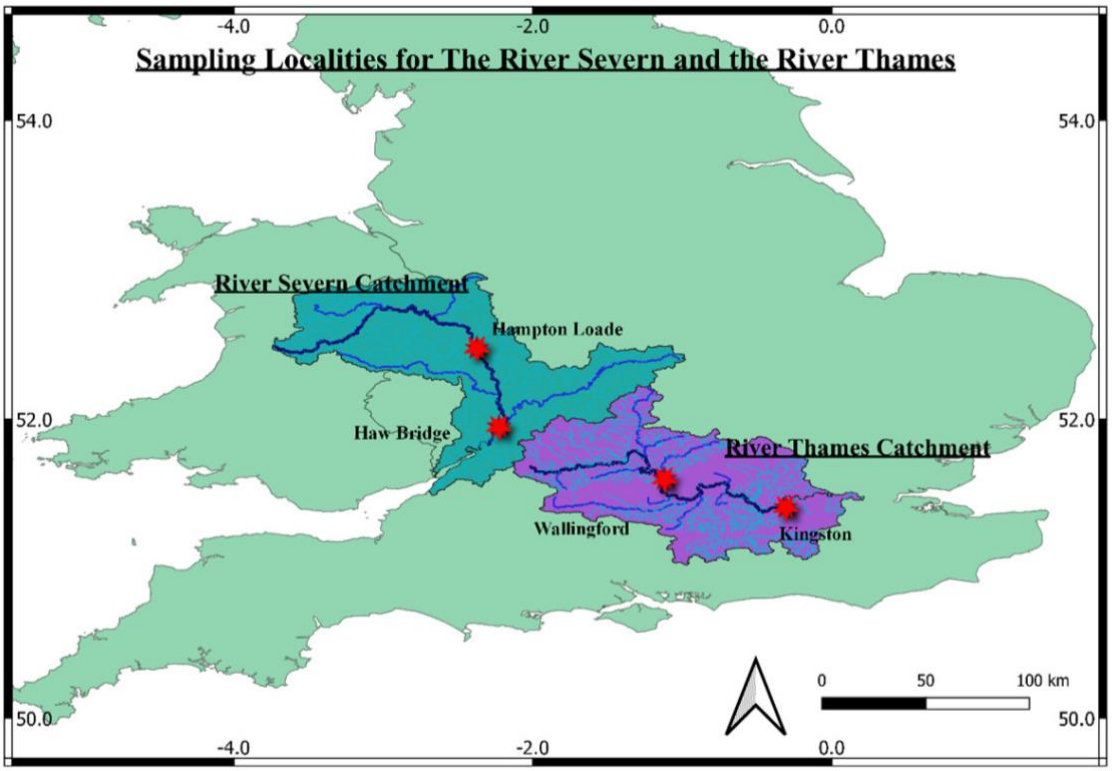

Figure D.1: The Severn and the Thames Catchments. Water was collected from Hampton Loade (Severn) and Wallingford (Thames). Flow stations used in the calculations were also included: Haw Bridge (Severn) and Kingston (Thames) were the closest flow monitoring stations to the estuary. The tidal reach in both rivers is just downstream of these stations.

8.4.7 Experimental methodology

Approximately 10L of unfiltered water was collected from an accessible but flowing area of the River Severn and the River Thames (Figure D1). The pH and the temperature of water were immediately tested when sampled. Aliquots of the river water were filtered to 0.2 µm to test natural alkalinity (using a metrohm autotitrator) and baseline cation and anion concentrations (using inductively coupled plasma mass spectroscopy, ICP-MS and Ion Chromatography respectively). The collected water was then stored in cold conditions for 1-2 weeks (~4°C) until the commencement of the experiments.

The collected unfiltered river water was then distributed into 5x 500ml conical beakers, which were placed on a magnetic multi-stir plate to represent flowing river conditions.

Alkalinity was added to the beakers to represent the addition of basalt derived alkalinity to river water under the two scenarios (1- maximum alkalinity from full release of cations, 2- minimum

alkalinity release from silica limitations). The alkalinity was added as two concentrated solutions (given in Table D.5), which were made separately to ensure that the calcium and carbonate ions did not precipitate before the start of the experiment.

Table D.5: Composition of the concentrated solutions added to the beakers

Solution A	Concentration mmol/L	Solution B	Concentration mmol/L
$CaCl_2$	50	**Na_2CO_3**	70
$MgCl_2$	49.4	**K_2CO_3**	2.1

The water was then left on the multi-stir plate for 4 days (Severn) and 5 days (Thames), a duration which Worral et al. (2016) calculated as the mean residence time for water within the two rivers (Worrall *et al.*, 2014). During this period, alkalinity and pH were tested daily. At the end of this period, a final sample was filtered for cation analysis, and the remaining 450ml of water was filtered to collect any accumulated precipitate. The sediments were oven dried at 40˚C, and then weighed on a microbalance.

To analyse the composition of the precipitate, the sediment was rescued from the filter and placed in a centrifuge tube to homogenise the sample, dissolved using concentrated nitric acid, and then the acid diluted with MQ water. The diluted acidified sample was then filtered to remove any silicate material present and then analysed with ICP-MS to determine the concentration of cations present in the sample. X-ray diffraction (XRD) was also undertaken on an aliquot of the accumulated sediment to investigate which phase of carbonate formed during the experiments.

8.4.8 Composition of the precipitate collected from the beaker experiments.

Table D.8- XRD analysis of the suspended sediment. Beakers are numbered by the scenario and application rate they represent. Scenario 1- the maximum alkalinity addition due to complete release of basalt alkalinity to the river and therefore SI-10= 10 t/ha; S1-20=20 t/ha, S1-50= 50 t/ha for scenario 1. Scenario 2- is the minimum alkalinity addition due to silica limitation (S2-min). The table shows various forms of carbonate formed in each beaker, and numbers indicate the % of the total sediment.

	Beaker	Calcite	Aragonite	Mg bearing carbonate*	Hydrated carbonate	Quartz	Other (suspended sed)	*Chemical formulae
Severn	**S1-10**	96				4	small	
Sep-21	**S1-20**	87	13					
	S1-50		97				3	
Thames	**S2-min**	98				2		
	S1-10	98				2		
	S1-20		14	86				$Ca(0.9)Mg(0.1)CO_3$
	S1-50				100			$CaCO_3(H_2O)$
Severn 2	**S1-10**	96				5		
Nov-21	**S1-20**	98				2		
	S1-50		10	90				$Ca(0.9)Mg(0.1)CO_3$

8.4.9 Chemistry changes during beaker precipitation experiments.

Table D.9- ICP-MS results from the Severn and the Thames Beaker Experiments (in mmol/L). Beaker A= silica saturation, S1-10= 10 t/ha, S1-20= 20 t/ha, S1-50= 50 t/ha. Added= extra concentrations of cations added to represent the expected median increase due to scenario 2- silica saturation minimum, and scenario 1 (maximum) for application rates- 10, 20 and 50t/ha. End concentrations- samples taken on day 4-5 of the experiment.

		Severn					Thames				
		Ca	**Mg**	**Na**	**K**	**Alk (mEq)**	**Ca**	**Mg**	**Na**	**K**	**Alk (mEq)**
	Natural	0.87	0.29	1.71	0.12	1.46	2.84	0.25	1.75	0.21	4.29
Added + Natural	**S2-min**	1.11	0.53	2.81	0.16	2.61	3.51	0.92	4.81	0.31	7.44
	S1-10	1.72	1.13	5.57	0.24	5.46	5.20	2.58	12.45	0.54	15.31
	S1-20	2.6	1.97	9.43	2.48	9.56	7.46	4.92	23.16	0.87	26.15
	S1-50	5.13	4.50	21.01	0.71	21.37	14.6	11.9	55.25	1.85	59.42
End	**S2-min**	1.09	0.50	2.71	0.15	2.40	1.32	0.85	4.47	0.30	2.57
	S1-10	0.55	1.27	4.66	0.23	2.47	0.40	2.24	11.35	0.48	3.87
	S1-20	0.14	1.75	8.53	0.65	3.51	0.06	3.88	23.67	0.77	9.69
	S1-50	0.04	3.82	19.52	0.63	8.27	0.10	11.2	57.26	1.59	30.73
% Remain-ing	**S2-min**	98.2	93.8	96.5	97.4	92.0	37.6	92.9	92.8	96.4	34.6
	S1-10	31.7	112.7	83.7	94.6	45.3	7.72	86.6	91.2	89.2	25.3
	S1-20	5.3	88.8	90.4	26.2	30.3	0.80	78.9	102.2	88.9	37.1
	S1-50	0.8	84.9	92.9	89.3	38.7	0.66	94.3	103.6	86.3	51.7

8.4.10 PHREEQC predicted the proportion of Ca removed in secondary carbonates in all catchments in the study under scenario 1.

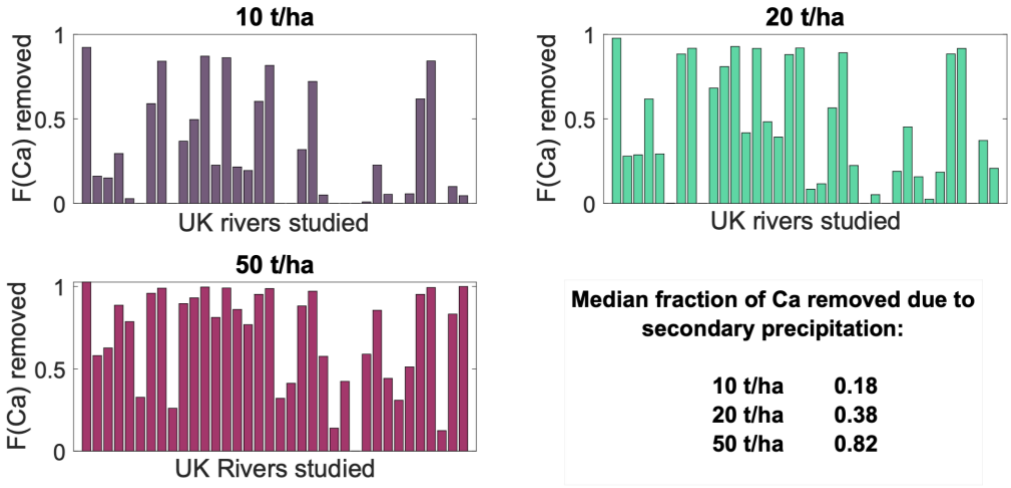

Figure D.13: fraction of EW derived Ca^{2+} initially added to UK rivers which was removed due to carbonate precipitation in UK rivers studied, under a scenario where 10 t ha^{-1}, (a), 20 t ha^{-1} (b) and 50 t ha^{-1} (c) basalt is applied to the arable land in each catchment, and all the basalt dissolves in a one-year period.

8.5 Appendix E- Appendices for Chapter 6

8.5.1 Silicate yield vs calcite saturation index

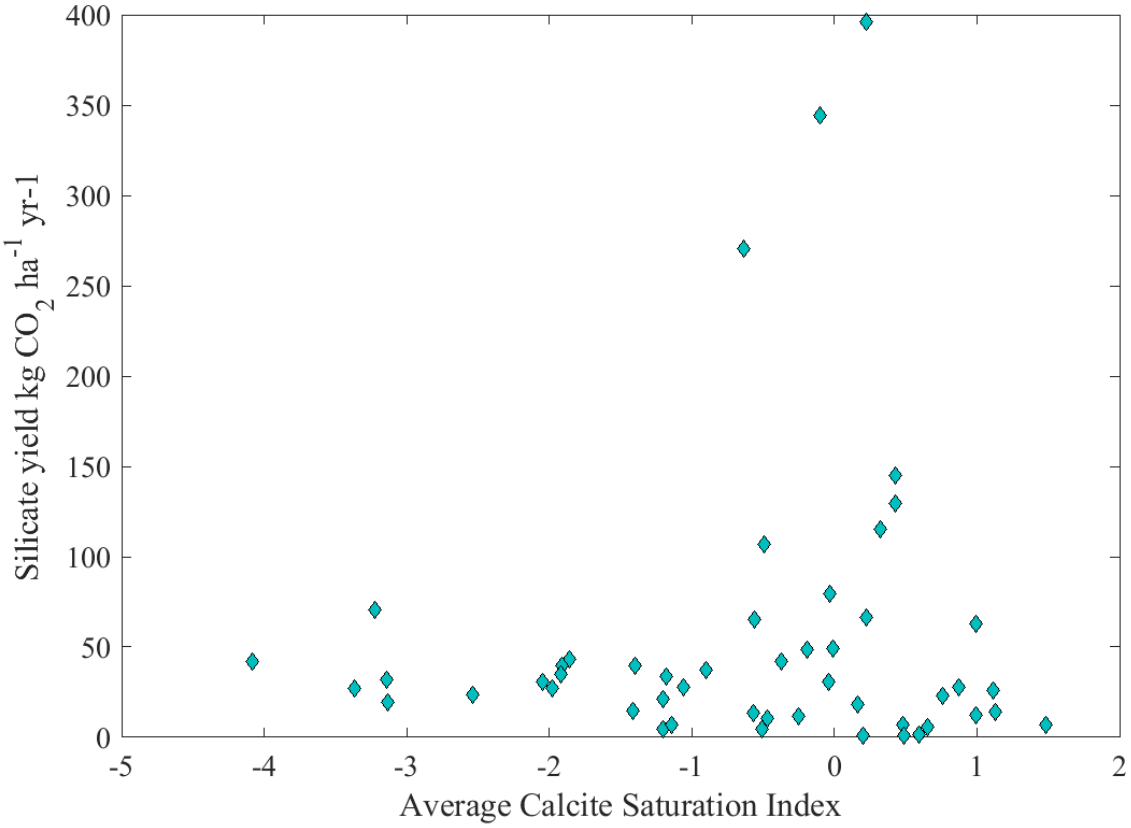

Figure E.1- No observable relationship between the average calcite saturation index of the UK rivers in Chapter 4, and the silicate yield.

8.5.2 X_{sil} and average flow and permeability

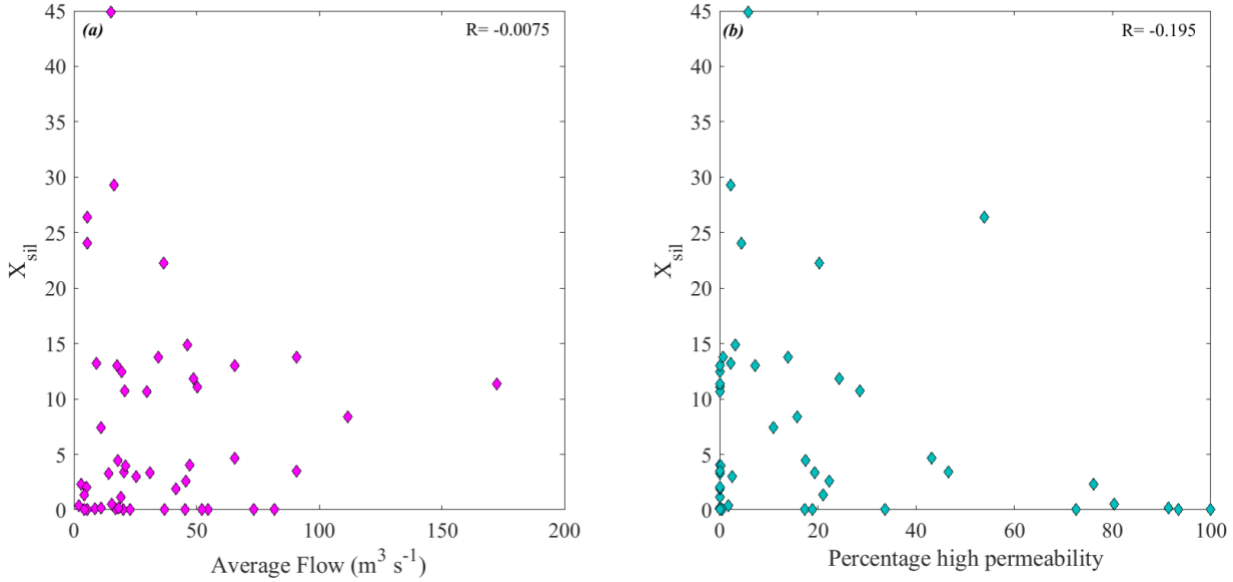

Figure E.2- Relationship between the average X_{sil} of a catchment and the average flow rate (a) and permeability (b). Assessed at national scale, each point represents an individual catchment in the study.

8.5.3 The degree of seasonal variability in X_{sil} and permeability and silicate yield

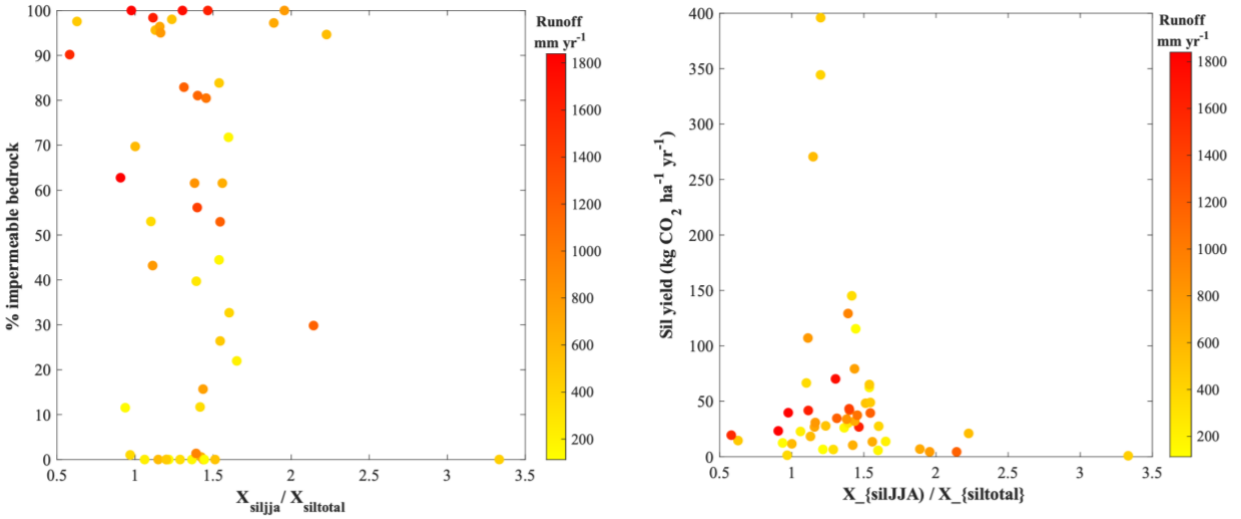

Figure E.3: Lack of correlation is observed between catchments with high summer Xsil and the amount of permeable bedrock.

8.5.4 Suspended sediment yield and %arable and runoff

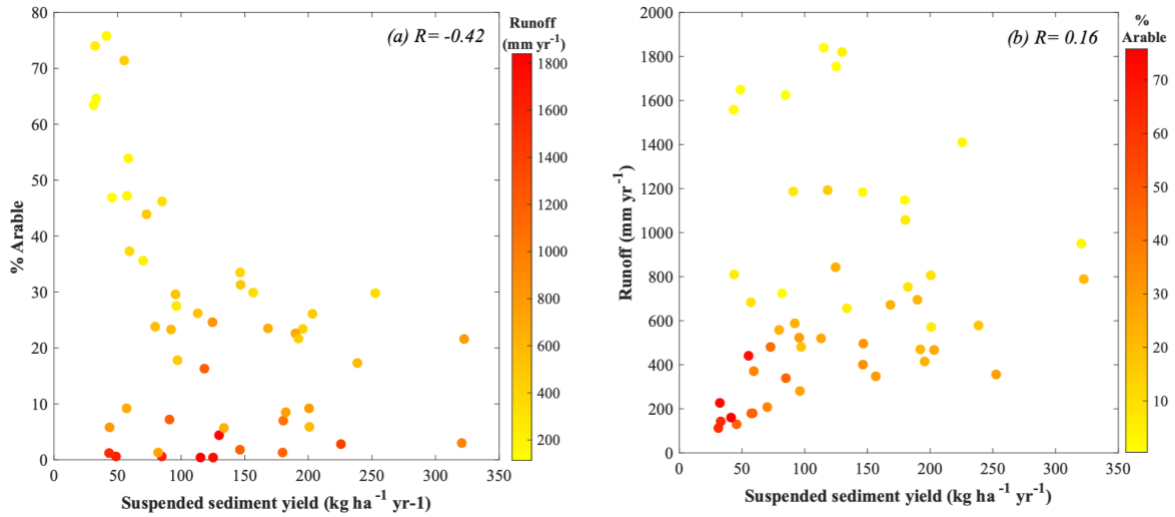

Figure E.4: Investigating the potential connection between land- use and erosion in the catchments within Chapter 4. (a) a weak negative relationship is observed at national scale between SSY and %arable land. (b) no relationship is observed between runoff and suspended sediment yield at national scale.

8.5.5 Relationship between riverine nitrate concentration and the concentration of cations from carbonates

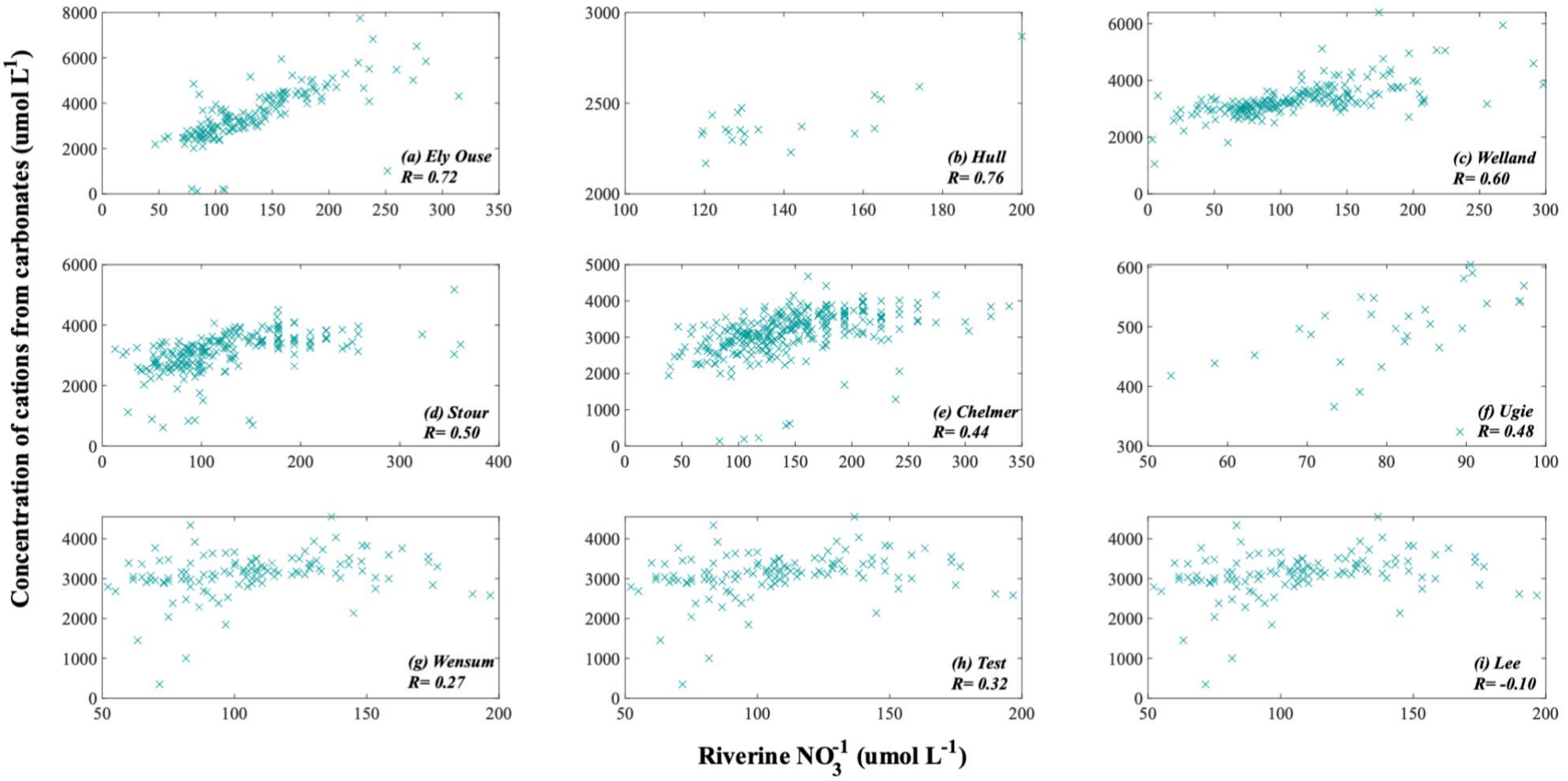

Figure E.5- The relationship between the concentration of cations sourced from carbonates (estimated using MEANDIR as discussed in Chapter 4), and the concentration of riverine nitrate. Catchments selected for the figure are the catchments with the most arable land out of the 52 catchments in the study (Chapter 4). The strength of the relationship between the two variables is variable- suggesting that the influence of nitric acid on carbonate weathering is catchment specific.